Characterization of the Ground Thermal Response to Heating by a Deep Vertical Borehole Heat Exchanger

by

Maeir Zalman Olfman

A Thesis submitted to the Faculty of Graduate Studies of
The University of Manitoba
in partial fulfilment of the requirements of the degree of

MASTER OF SCIENCE

Department of Mechanical and Manufacturing Engineering
University of Manitoba
Winnipeg

Abstract

This thesis presents an experiment and an analysis that evaluates some of the long-standing assumptions in deep vertical borehole ground heat exchanger (GHX) theory. These assumptions neglect ground heterogeneity and depth variations in GHX output and the ground temperature response (GTR). This thesis describes an apparatus and an experiment that measured the GTR at several depths, times, and at two different horizontal distances from a GHX both during and immediately after its operation. This thesis also reports the temperature response data, which may not be available from other sources in such detail. The experiment showed that the GTR can be highly depth dependant. The analysis involved a parametric study to characterize the GTR by developing an effective computer simulation of the experiment. The analysis showed that ground heterogeneity significantly affected the GTR and the GHX output in this study. Furthermore, this GHX output showed depth and time, dependence.

Acknowledgments

I would like to thank Manitoba Hydro, especially Peter Kidd and Rob Andrushuk of Manitoba Hydro, and the Natural Sciences and Engineering Research Council of Canada (NSERC) for their financial support. I would like to thank Kerry Lynch for his assistance with the equipment set-up. Lastly, I would like to thank my advisors, Dr. Allan Woodbury, Dr. Jonathan Bartley, and the late Dr. Daniel Fraser for their support and guidance over the years.

Dedication

I dedicate this thesis to my family, grandmother, grandfather, and uncle for their love and support all of these years, which made this thesis possible. To my whole family, I appreciate your patience and warmth, and the fact that you are always so much fun.

Contents

Abstract i
Acknowledgments ii
Dedication iii
List of Tables viii
List of Figures x
Chapter 1 Introduction 1
1.1 General Overview 1
1.2 Overview of Heat Pumps 1
1.3 Overview of Geothermal Heat Pumps 4
1.4 Literature Review 8
1.4.1 Computational Methods 8
1.4.2 Semi-Analytical Methods 18
1.4.3 Analytical Methods 21
1.4.4 Supplementary Material 29
1.5 Problem Description 31
Chapter 2 Experimental Facility and Methods 35
2.1 Experimental Facility and Equipment 35
2.1.1 Description of the Heat Transfer Equipment 35
2.1.2 Description of the Heat Transfer Rate Monitoring Equipment 39
2.1.3 Description of the Ground Temperature Monitoring Equipment 40
2.1.4 Description of the Control Systems 42
2.2 Experimental Procedures 49
2.2.1 Heat Pump Mode Selection 49
2.2.2 Portable Temperature Probe Compatibility Check 50
2.2.3 Preparations and Settings 51
2.2.4 Experimentation Schedule 52

2.2.5 Detailed Temperature Measurement Procedures 54
2.2.6 Improvement of the Method 57
2.2.7 Improvement of the Apparatus 57
Chapter 3 Modeling 58
3.1 Introduction 58
3.2 Conceptual Model Development 64
3.3 Computer Model Definition 69
3.4 Material Properties 74
3.5 Parametric Study Procedure 82
3.6 Summary 91
Chapter 4 Results and Discussion 93
4.1 Preliminary Findings 93
4.1.1 Near Surface Range 94
4.1.2 Deep Range 113
4.1.3 Analysis of the Heat Output of the Heat Pump Unit 114
4.1.4 Implications of the Preliminary Findings on the Model Definition 118
4.2 Parametric Study Results 119
4.2.1 Depth Varying Borehole Wall Temperature Case 119
4.2.2 Depth Varying Borehole Wall Heat Flux Case 136
4.2.3 The Effect of Vertical Heat Conduction 150
4.3 Alternate Modelling Scenarios 161
4.3.1 Alternate Models of the Ground Heat Exchanger 161
4.3.2 Regarding the Possibility of Underground Convection 163
4.4 More Advanced Modelling Scenarios 170
4.4.1 Staggered Start Hypothesis 171
4.4.2 U-Loop Natural Convection Hypothesis 177

4.5 Chapter 4 Nomenclature 195

Chapter 5 Discussion and Conclusions 197

5.1 Summary 197

5.2 Speculations Regarding Ground Heat Exchanger Design and Modelling 199

5.3 Future Work 203

5.4 Conclusion 205

Appendix A Introduction 207

A.1 Introduction 207

A.2 Conceptual Model 208

A.3 The Infinite-length Line and Cylindrical Source Solutions 210

A.3.1 Comparing the Infinite-Length Line Source and Cylindrical Source Theories: 213

A.4 Theory for the Property Estimation Method 215

A.4.1. Parametric Study Complement of the Simplified Investigation of the Appendix 222

A.5 Property Estimation Methodology 224

A.6 Results 226

A.7 Conclusion 237

A.8 Appendix A Nomenclature 241

Appendix B Experimental Data 245

Table 16 Nearer Well Temperature Data, Experiment 1 246

Table 17 Further Well Temperature Data, Experiment 1 259

Table 18 Nearer Well Temperature Data, Experiment 2 273

Table 19 Farther Well Temperature Data, Experiment 2 281

Heat Pump Shutdown Times 288

References 289

List of Tables

Chapter 3

Table 1 Composite Property Relations 74

Table 2 Definitions of the symbols in Table 1 75

Table 3 Value Table for Property Range Calculations (Values in Red Appear in Table 4, also see Figure 4) 84

Table 4 Material Property Combinations under Study (see Figure 11 and Table 3) 89

Table 5 Material Property Values under Study (see Figure 11 and Table 3) 90

Chapter 4

Table 6 Initial Test Matrix for the Depth Varying Borehole Wall Temperature study 120

Table 7 Final Test Matrix for the Depth Varying Borehole wall Temperature Case 121

Table 8 Summary of The Depth Varying Borehole-Wall Temperature Calibration. Minimum RMS Error values are shaded in orange 123

Table 9 Test Matrices for the Depth Varying Borehole Flux study 136

Table 10 Summary of the Depth Varying Borehole Wall Heat-Flux Calibration. Minimum RMS Error values are shaded in orange 140

Table 11 Table of definitions for the Rayleigh Number and their associated values, in this study. 165

Table 12 Comparison Between the Time Invariant and Transient Borehole Wall Heat Flux Models of the Ground Heat Exchanger Output 185

Table 13 Transient Boundary Conditions Used in the More Advanced Modelling. 185

Appendix A Introduction

Table 14 Comparison of material property estimates from the thesis body (Combination H) and the Appendix 226

Table 15 Comparison of thermal flux estimations from the thesis body (Combination H) and the Appendix 227

Appendix B Experimental Data

Table 16 Nearer Well Temperature Data, Experiment 1 246

Table 17 Further Well Temperature Data, Experiment 1 259

Table 18 Nearer Well Temperature Data, Experiment 2 273

Table 19 Farther Well Temperature Data, Experiment 2 281

List of Figures

Chapter 2

Figure 1 Exterior of the research field site. 36

Figure 2 Interior of the research field site. 37

Figure 3 Diagram of the GHX 38

Figure 4 Data from 107BAM Room Temperature Monitoring Probe during the July 2008 test... 45

Figure 5 Block diagram of the control systems. 46

Figure 6 Block diagram of the control systems showing constant output mode 47

Figure 7 Air Diversion Valve and Room Temperature Monitoring Probe 48

Chapter 3

Figure 8 Comparison of analytical model and experiment at r=1.4m during heating phase 62

Figure 9 Comparison of analytical model and experiment at r=2.8m during heating phase 63

Figure 10 Example of Flux Boundary Condition Imposed on the Cylinder r=0.05m, 5m≤z≤61m 67

Figure 11 Diagram of the Computer Model 70

Figure 12 Direct Porosity Measurements from G. A. G. Ferguson (personal communications, July 16, 2009) 80

Figure 13 Direct Density Measurements from G. A. G. Ferguson (personal communications, July 16, 2009) 80

Figure 14 Direct Thermal Conductivity Measurements at the University of Manitoba from G. A. G. Ferguson (personal communications, July 16, 2009) 81

Figure 15 Diagram of the Thermal Properties Under Study - Dry Condition. 86

Figure 16 Diagram of the Thermal Properties Under Study - Saturated Condition. 87

Chapter 4

Figure 17 Ground temperature profile over time for the nearer observation well during the heating portion of the test. 96

Figure 18 Reduced scale of Figure 17 to show detail. 97

Figure 19 Reduced scale of Figure 17 to show detail. Note that increased temperature corresponds to increased time. 98

Figure 20 Natural ground temperature recovery phase in the nearer observation well. 99

Figure 21 Reduced scale of Figure 20 to show detail. Note the continued temperature rise. 100

Figure 22 Reduced scale of Figure 20 to show detail. Note that the leftmost line in the mid-range is the rightmost line elsewhere. This is the 10-Aug line. 101

Figure 23 Ground temperature profile over time for the Farther observation well during the heating portion of the test. 102

Figure 24 Reduced scale of Figure 23 to show detail. 103

Figure 25 Reduced scale of Figure 23 to show detail. Note that increased temperature corresponds to increased time. 104

Figure 26 Measurements from the further observation well in the natural ground recovery phase. 105

Figure 27 Reduced scale of Figure 26 to show detail. 106

Figure 28 Reduced scale of Figure 26 to show detail. 107

Figure 29 Measured temperature change (present temperature – initial temperature) at both the nearer and further observation wells at 10m depth. 108

Figure 30 Measured temperature change (present temperature – initial temperature) at both the nearer and further observation wells at 20m depth. 109

Figure 31 Measured temperature change (present temperature – initial temperature) at both the nearer and further observation wells at 40m depth. 110

Figure 32 Measured temperature change (present temperature – initial temperature) at both the nearer and further observation wells at 60m depth. 111

Figure 33 Temperature change at 2m depth that strongly shows both the oscillatory behaviour and continued temperature rise of the near surface region. 112

Figure 34 Entering and Exiting Heat Transfer Fluid Temperature difference Measured at the Heat Pump Unit for the July 2008 Test 115

Figure 35 Calibration Graph for material combination H in the constant borehole wall temperature series. 122

Figure 36 Overall Ground Heat Exchanger Output for the Depth Varying (Time Invariant) Borehole Wall-Temperature Case..... 125

Figure 37 Results for Material Combination H. Best Calibration Results for the Depth Varying Borehole Wall Temperature Case in the Upper Portion of the Domain During the Ground-Heating Phase for the Nearer Observation Well..... 128

Figure 38 Results for Material Combination H. Best Calibration Results for the Depth Varying Borehole Wall Temperature Case in the Lower Portion of the Domain During the Ground-Heating Phase for the Nearer Observation Well. 129

Figure 39 Results for Material Combination H. Best Calibration Results for the Depth Varying Borehole Wall Temperature Case in the Upper Portion of the Domain During the Natural Ground-Temperature Recovery Phase for the Nearer Observation Well. 130

Figure 40 Results for Material Combination H. Best Calibration Results for the Depth Varying Borehole Wall Temperature Case in the Lower Portion of the Domain During the Natural Ground-Temperature Recovery Phase for the Nearer Observation Well. 131

Figure 41 Results for Material Combination H. Best Calibration Results for the Depth Varying Borehole Wall Temperature Case in the Upper Portion of the Domain During the Ground-Heating Phase for the Further Observation Well..... 132

Figure 42 Results for Material Combination H. Best Calibration Results for the Depth Varying Borehole Wall Temperature Case in the Lower Portion of the Domain During the Ground-Heating Phase for the Further Observation Well. 133

Figure 43 Results for Material Combination H. Best Calibration Results for the Depth Varying Borehole Wall Temperature Case in the Upper Portion of the Domain During the Natural Ground-Temperature Recovery Phase for the Further Observation Well..... 134

Figure 44 Results for Material Combination H. Best Calibration Results for the Depth Varying Borehole Wall Temperature Case in the Lower Portion of the Domain During the Natural Ground-Temperature Recovery Phase for the Further Observation Well..... 135

Figure 45 Calibrated Material Model..... 139

Figure 46 Results for Material Combination H. Best Calibration Results for the Depth Varying Borehole Wall Heat-Flux Case in the Upper Portion of the Domain During the Ground-Heating Phase for the Nearer Observation Well..... 142

Figure 47 Results for Material Combination H. Best Calibration Results for the Depth Varying Borehole Wall Heat-Flux Case in the Lower Portion of the Domain During the Ground-Heating Phase for the Nearer Observation Well..... 143

Figure 48 Results for Material Combination H. Best Calibration Results for the Depth Varying Borehole Wall Heat-Flux Case in the Upper Portion of the Domain During the Natural Ground-Temperature Recovery Phase for the Further Observation Well. 144

Figure 49 Results for Material Combination H. Best Calibration Results for the Depth Varying Borehole Wall Heat-Flux Case in the Lower Portion of the Domain During the Natural Ground-Temperature Recovery Phase for the Nearer Observation Well..... 145

Figure 50 Results for Material Combination H. Best Calibration Results for the Depth Varying Borehole Wall Heat-Flux Case in the Upper Portion of the Domain During the Ground-Heating Phase for the Further Observation Well..... 146

Figure 51 Results for Material Combination H. Best Calibration Results for the Depth Varying Borehole Wall Heat-Flux Case in the Lower Portion of the Domain During the Ground-Heating Phase for the Further Observation Well..... 147

Figure 52 Results for Material Combination H. Best Calibration Results for the Depth Varying Borehole Wall Heat-Flux Case in the Upper Portion of the Domain During the Natural Ground-Temperature Recovery Phase for the Further Observation Well. 148

Figure 53 Results for Material Combination H. Best Calibration Results for the Depth Varying Borehole Wall Heat-Flux Case in the Lower Portion of the Domain During the Natural Ground-Temperature Recovery Phase for the Further Observation Well. 149

Figure 54 Effect of Vertical Heat Conduction on Computer Modelling for R=1.4m, July 2008 Test 05-35m - Heating Phase. 153

Figure 55 Effect of Vertical Heat Conduction on Computer Modelling for R=1.4m, July 2008 Test 05-35m - Recovery Phase. 154

Figure 56 Effect of Vertical Heat Conduction on Computer Modelling for R=1.4m, July 2008 Test 36-61m - Heating Phase. 155

Figure 57 Effect of Vertical Heat Conduction on Computer Modelling for R=1.4m, July 2008 Test 36-61m - Recovery Phase. 156

Figure 58 Effect of Vertical Heat Conduction on Computer Modelling for R=2.8m, July 2008 Test 05-35m - Heating Phase. 157

Figure 59 Effect of Vertical Heat Conduction on Computer Modelling for R=2.8m, July 2008 Test 05-35m - Recovery Phase. 158

Figure 60 Effect of Vertical Heat Conduction on Computer Modelling for R=2.8m, July 2008 Test 36-61m - Heating Phase. 159

Figure 61 Effect of Vertical Heat Conduction on Computer Modelling for R=2.8m, July 2008 Test 36-61m - Recovery Phase. 160

Figure 62 Comparisons Between The Three Depth Dependant Borehole Wall Heat Flux Models and The Experimental Results at R=1.4m and 37m Depth. 173

Figure 63 Comparisons Between The Three Depth Dependant Borehole Wall Heat Flux Models and The Experimental Results at R=1.4m and 40m Depth. 174

Figure 64 Comparisons Between The Three Depth Dependant Borehole Wall Heat Flux Models and The Experimental Results at R=1.4m and 44m Depth. 175

Figure 65 Comparisons Between The Three Depth Dependant Borehole Wall Heat Flux Models and The Experimental Results at R=1.4m and 53m Depth. 176

Figure 66 Comparisons Between The Three Depth Dependant Borehole Wall Heat Flux Models and The Experimental Results at R=1.4m and 11m Depth. 179

Figure 67 Comparisons Between The Three Depth Dependant Borehole Wall Heat Flux Models and The Experimental Results at R=1.4m and 19m Depth. 180

Figure 68 Comparisons Between The Three Depth Dependant Borehole Wall Heat Flux Models and The Experimental Results at R=1.4m and 25m Depth. 181

Figure 69 Comparisons Between The Three Depth Dependant Borehole Wall Heat Flux Models and The Experimental Results at R=1.4m and 32m Depth. 182

Figure 70 Overall Heat Transfer Rate versus Time Throughout the More Advanced Model 186

Figure 71 Results for Material Combination H Using Depth and Time Varying Borehole Wall Heat-Flux in the Upper Portion of the Domain During the Ground-Heating Phase for the Nearer Observation Well. 187

Figure 72 Results for Material Combination H Using Depth and Time Varying Borehole Wall Heat-Flux in the Lower Portion of the Domain During the Ground-Heating Phase for the Nearer Observation Well. 188

Figure 73 Results for Material Combination H Using Depth and Time Varying Borehole Wall Heat-Flux in the Upper Portion of the Domain During the Natural Ground-Temperature Recovery Phase for the Nearer Observation Well..... 189

Figure 74 Results for Material Combination H Using Depth and Time Varying Borehole Wall Heat-Flux in the Lower Portion of the Domain During the Natural Ground-Temperature Recovery Phase for the Nearer Observation Well..... 190

Figure 75 Results for Material Combination H Using Depth and Time Varying Borehole Wall Heat-Flux in the Upper Portion of the Domain During the Ground-Heating Phase for the Further Observation Well. 191

Figure 76 Results for Material Combination H. Best Calibration Results Using Depth and Time Varying Borehole Wall Heat-Flux in the Lower Portion of the Domain During the Ground-Heating Phase for the Further Observation Well. 192

Figure 77 Results for Material Combination H Using Depth and Time Varying Borehole Wall Heat-Flux in the Upper Portion of the Domain During the Natural Ground-Temperature Recovery Phase for the Further Observation Well..... 193

Figure 78 Results for Material Combination H. Best Calibration Results Using Depth and Time Varying Borehole Wall Heat-Flux in the Lower Portion of the Domain During the Natural Ground-Temperature Recovery Phase for the Further Observation Well..... 194

Appendix A Introduction

Figure 79 Example of a match between measured and simulated data after completing the parameter estimation method of this appendix for 11m depth..... 228

Figure 80 Example of a match between measured and simulated data after completing the parameter estimation method of this appendix for 19m depth..... 229

Figure 81 Example of a match between measured and simulated data after completing the parameter estimation method of this appendix for 32m depth..... 230

Figure 82 Example of a match between measured and simulated data after completing the parameter estimation method of this appendix for 44m depth. 231

Figure 83 Example of a match between measured and simulated data after completing the parameter estimation method of this appendix for 53m depth. 232

Figure 84 Example of a match between measurement and experiment using the staggered start and continued natural convective heating hypothesis with fixed diffusivity. 236

Appendix B Experimental Data

Figure 85 Measurements from the 3-Wire RTD adjacent to the HPU – July 2008 Experiment.. 272

Chapter 1 Introduction

1.1 General Overview

Research into the thermal response of the ground to heating or cooling by a heat exchanger has been ongoing for some time. Authors such as Yavuzturk (1999) and Yang et al. (2010) credit (Kelvin, 1882) as the earliest mathematical model that could approximate the ground temperature response to heat exchange with an infinitely long, and very narrow heat exchanger. Texts such as Carslaw (1921), Ingersoll (1954), and Carslaw and Jaeger (1959) give additional theoretical treatments, with the later two texts directly discussing ground heat exchange. Carslaw and Jaeger (1959) also give a theoretical treatment of an infinitely long, cylindrical heat source with a finite radius using Laplace transforms. Many contemporary studies have continued to refine the science of geothermal heat transfer, perhaps due to growing demand for these systems around the world (see section 1.4). The American Society of Heating, Refrigerating and Air Conditioning Engineers include a chapter on geothermal applications in their quadrennial ASHRAE Applications manual, such as ASHRAE (2007). This is not surprising, given that regions as diverse as Manitoba (Ferguson & Woodbury, 2005) and Switzerland (Spitler, 2005) have made at least some use of some form of geothermal heat transfer applications for the last century.

1.2 Overview of Heat Pumps

The Engineering text by Çengel and Boles (2002) describes heat pumps and their associated calculations. In summary, a heat pump is any device that transports heat from one environment to another environment. To elaborate, the name likely derives from an

analogy to fluid pumps. Much as a fluid pump moves fluid from one location to another location, a heat pump moves thermal energy in the form of heat from one location to another location. Heat will flow spontaneously from one location to a second location if the second location is colder than the first location. However, the reverse operation requires a heat pump.

Perhaps the two most common examples of heat pumps are refrigerators and air-conditioners. Both of these devices transport heat from a cooler region to a warmer region. This operation requires a heat pump. A refrigerator maintains the temperature inside of its compartment below the air-temperature of the room that contains the refrigerator by transporting heat from inside of the refrigerator compartment to the air of the room housing the refrigerator. Similarly, an air conditioner maintains the indoor air-temperature of a room, or larger structure below the temperature of the outdoor air by transporting heat from the indoor air to the outdoors through its machinery. If one were to operate an air-conditioner in reverse, the device would to transport heat from outdoors to the inside of a room or larger structure and heat the indoor space. In the application of space heating, rather than space cooling, a heat pump goes by its own name.

In a heat pump used for space heating, the majority of the heat provided to the warm space comes from an outdoor environment. Heat producing devices such as electric heaters and furnaces convert electrical energy or chemical energy into heat. This process could never deliver more heat to the user than the energy content of the electric power-source or fuel. However, it is possible to move heat from one location to another. In fact, a heat pump must deliver the energy it consumes in the act of pumping the heat, as well as any energy it absorbs from the environment it cools to the environment it heats

(Çengel & Boles, 2002). Consequently, space heating with heat pumps has the potential to use much less energy to provide the same amount of heat as the most efficient furnace or an electric heater because a heat pump provides the majority of the heat to the warm space by extracting it from a separate, outside environment.

A heat pump begins the refrigeration cycle by pressurizing a vapour in a compressor in order to increases the vapour's temperature. This allows the vapour to exchange heat with an external environment through a heat exchanger. The vapour cools in the heat exchanger until it completely condenses. The condensed liquid then passes through an expansion valve, where the cross-sectional area of the tube containing the liquid abruptly increases. The instantaneous expansion of the tube is sufficient to cause the pressure of the liquid to decrease below the saturation pressure. This process results in partial vaporization of the liquid and a lowering of the resulting fluid's temperature. The fluid enters a second heat exchanger, where it absorbs heat from a second environment. After the fluid has fully vaporized, it completes the cycle by re-entering the compressor.

The amount of work a compressor does increases with greater difference between the thermodynamic state of the fluid at its inlet and exit (Çengel & Boles, 2002). Therefore, the compressor must do more work to raise the temperature of the fluid from the cool heat exchanger, at the inlet of the compressor, to the temperature required for the fluid in the warm heat exchanger, at the exit of the compressor, when this temperature difference increases. As stated above, one of the primary advantages of using a heat pump for space heating is its potential to use much less energy to provide the same amount of heat as a furnace or an electric heater. However, the fluid in the heat exchanger in the cool environment must be even colder than the cool environment to absorb heat from it.

Furthermore, the fluid in the heat exchanger in the warm environment must be warmer than the warm environment in order to expel heat to it. Therefore, the compressor power largely depends on the environmental temperature of both the warm and cool environments. However, the air-temperature of a heated space should usually be stable at "room temperature", for the occupants' comfort. Thus, the power used to operate a heat pump for indoor heating depends strongly on the temperature of the cooler outdoor environment.

1.3 Overview of Geothermal Heat Pumps

A geothermal heat pump is a special application of heat pump technology wherein a heat pump operates between an artificially conditioned indoor space and the ground. A heat pump requires two separate temperature regions in order to move a net amount of heat (Çengel & Boles, 2002). The net amount of heat either heats or cools those regions. Obviously, the conditioned space comprises one of those regions in space conditioning. The options for the other region are the air, the ground (geothermal), or a separate body of water (hydrothermal).

Geothermal heat pumps have thermodynamic advantages over other heat pump configurations. The ground temperature is often more stable than the ambient air temperature. This temperature may be much warmer than the outside air temperature during the heating seasons and much colder than the outside air temperature during the cooling seasons (Yang, Cui, & Fang, 2010). This means a heat pump operating between a conditioned space and the ground will consume less energy to provide the same amount of conditioning as a heat pump that uses the outside air. Although the seasonal temperature fluctuations of bodies of water also have lower amplitudes than the air,

bodies of water are not always present or available for heat transfer. Therefore, geothermal heat pumps have the potential to be much more effective and practical than other heat pump configurations in many geographic regions.

Ground heat exchangers communicate heat with the ground by either direct mass or heat transfer. Mass transfer refers to open loop systems, which pump groundwater used to exchange heat with either the input or output of the refrigeration cycle. This corresponds to space heating and cooling, respectively. The other option is a closed loop system, which pumps a heat transfer fluid into and out of the heat exchange well or wells through a continuous series of supply and return pipes. The heat transfer fluid from a closed loop system also exchanges heat with the heat pump on either the input or output of the refrigeration cycle.

Open loop systems require sufficient groundwater to supply their heat pump. Clearly, this affects the hydraulic head in an aquifer or the height of the water table. These systems either replace the groundwater to the aquifer or exhaust it to wastewater (Ferguson & Woodbury, 2005). If they reinject the water to the aquifer, they maintain the water budget at zero and only affect the head or water table level near the pumping and reinjection wells. One potential advantage of a properly designed open loop systems is that they always draw groundwater at ambient temperature. Since they remove the groundwater from the ground before they exchange heat with it, the operation of an open loop heat system would only effect the water inlet temperature if the groundwater replenishment occurs sufficiently close upstream of the supply well to thermally contaminate it.

Thermal interference between supply and return wells refers to the situation where the supply line draws exhaust groundwater from the return line. Space heating requires absorbing energy from the groundwater, thus cooling the groundwater. The heat pump transports the heat it absorbs from the groundwater to heat the indoor space. Space cooling involves the same process, except that the heat pump absorbs the heat from the occupied space and delivers it to the groundwater, thus raising its temperature. Systems that reinject groundwater to the aquifer have the potential to cause interference.

Interference between supply and return wells may increase the power requirements of the heat pump system. In space heating mode, interference results in the intake of groundwater that the heat pump had previously cooled. In space cooling mode, interference results in the intake of groundwater that the heat pump had previously warmed. Either way, this increases the difference between the warm and cool environments of the refrigeration cycle. This has the effect of increasing the heat pump power requirements. Interestingly, aquifer thermal energy storage (ATES) systems seek to take advantage of the change in ground temperature by operating bidirectional supply and return pumping so that the colder water pumped into the ground during heating season provides cooling in the cooling season and vice versa (Doughty, Hellström, Tzang, and Claesson (1982), Dickinson, Buik, Matthews, and Snijders (2009)). Clearly, this is only advantageous without significant interference.

Closed loop systems do not require a supply of groundwater because they have their own reservoir of heat transfer fluid that circulates through a closed loop of piping. The closed loop means that they do not need to exhaust any heat transfer fluid as part of system operation. Much like ATES systems, closed loop systems use the ground as a thermal

storage reservoir for extraction and replenishment of energy and benefit from their own effect on ground temperature from one season to the next. However, closed loop systems only require one well to accomplish this and do not pump any groundwater. Therefore, they may experience continuously varying loop fluid temperatures as part of normal operation. Clearly, this could have the same effect as interference in an open loop system.

Closed loop systems can also have less loop fouling and corrosion than open loop systems. Open loop systems use naturally occurring groundwater directly in the system. This may include minerals and other components that foul or corrode the system. In contrast, closed loop systems use a manufactured fluid made of clean water and a commercial anti-freezing agents to extract heat from the ground in the closed loop. (This could even include anti-corrosive agents if the customer were so inclined.) Therefore, the closed loop separates the system from environmental contaminants.

Closed loop systems may consume less power in pumping their heat transfer fluid. Firstly, the heat transfer fluid of a closed loop system circulates through manufactured pipes rather than the ground itself. Secondly, the heat transfer fluid can be an antifreeze solution. A heat exchanger may be able to cool an antifreeze solution more than groundwater because of the lower freezing point. The rate of energy extraction is proportional to flow rate and the temperature change of the fluid. Therefore, a closed loop system could operate a higher temperature drop than an open loop system for the same flow rate. This could represent a reduction in fluid pumping power. However, any closed loop system may also reach a point where the heat pump itself would require more power to extract heat from a continuously decreasing temperature source than it saved in fluid pumping costs.

1.4 Literature Review

As indicated in the introduction, researchers have studied heat transfer related to the modelling of a deep vertical borehole heat exchanger for quite some time. Numerous authors from North America, Europe, and Asia have contributed to the advancement of the understanding of heat transfer from a deep (and relatively thin) vertical borehole heat exchanger. These models include analytical solutions, numerical solutions, and semi-analytical models. They range in complexity from a one-dimensional (radial) analytical model with a line source (Kelvin (1882), Ingersoll (1954), etc.) to a fully three-dimensional model of the subsurface and the ground heat exchanger, in complete detail that includes the ground surface conditions and the convective heat transfer within the U-Loop itself (Nam, Ooka, & Hwang, 2008). Note that, most investigators characterize the ground as a homogeneous medium of infinite radial extent. Investigations that account for vertical variations usually do so in order to obtain what their authors believe is a better estimate of the true average of the variation.

1.4.1 Computational Methods

Rottmayer et al. (1997) developed a finite difference numerical model of a ground heat exchanger. This model considers the most of the actual geometry of the heat exchanger. The model includes both the supply and return lines of the u-loop and the convection therein. Rottmayer et al. (1997) represents the loops themselves as wedge shaped *pie sectors* as an approximation of the more complicated actual loop geometry. They modified the pie sectors' wall elements' properties and dimensions to equivocate the actual, circular geometry, as well as a shape factor to account for the discrepancy between the approximate and actual geometries. This model does not consider axial heat

flow in the depth (z) direction, which Rottmayer et al. (1997) justify by noting the large distances between axial nodes relative to their temperature differences. However, apart from this the model is three-dimensional model, capable of representing spatial ground property variations and interference of other heat exchangers.

Rottmayer et al. (1997) verified their model by comparison to another numerical model, FEHT (Klien et al., 1997). They used what "simple conditions", which included ground homogeneity. Rottmayer et al. (1997) suggested that incorporating ground stratification or other more realistic conditions would be more useful in real-world situations. However, there is no reference to him having tried this in the literature. Work that expanded on this tended to focus on depth-averaged versions of this method, and eventually also abandoned the pie sector model entirely (Yavuzturk and Spitler (1999), and Yavuzturk and Spitler (2001)), etc. In the opinion of this author, the most likely reason for using methods other than the pie sector method of Rottmayer et al. (1997) may be the need to employ a "geometric factor" to correct for the approximate geometry of the pie sector model.

Austin (1998) conducted a study wherein he developed a method for determining ground thermal properties based on an in situ property measurement test. Austin developed a test rig containing heat exchange and measurement equipment for conducting the ground thermal property measurement experiments. Austin analysed his data using three different mathematical models to process his data and obtain ground thermal properties. Austin considered the line source model (Ingersoll, 1954), the cylindrical source model (Carslaw & Jaeger, 1959), and a numerical model that Yavazturk (1999) developed based on Rottmayer et al. (1997) as part of his 1999 Ph.D. thesis.

Austin (1998) concluded that both the line source and cylindrical source theories were inadequate to model the ground thermal response. Austin (1998) suggested that this inadequacy stemmed from approximating the ground heat exchanger, which is actually a U-Loop, as either a line or cylindrical source. In the case of the line source, Austin (1998) found difficulties in interpreting the data. This model predicted different values of thermal conductivity when evaluated over different time intervals. These predicted values oscillated in such a manner that Austin (1998) found it difficult to obtain a property estimate from the scattered results. Other authors, such as Gehlin (1998), simply fit the line source solution to the entire dataset. However, it appears that Austin (1998) was trying to highlight the uncertainty with using this method. Austin (1998) found similar difficulty with the cylindrical source model. However, in the case of the cylindrical source model, he also found that the estimated conductivity value slightly increased with time. Austin (1998) concluded that the thermal conductivity results from Yavuzturk's (1999) numerical model were more reliable than the results from the analytical solutions he investigated.

In order to use Yavazturk's (1999) model, Austin (1998) needed to make a number of assumptions. Firstly, the model itself approximates the individual pipes of the U-Loop as wedge-like *pie sectors*. Secondly, Austin (1998) arbitrarily assumes that the ground heat exchanger dissipates two thirds of its heat in the supply line and the remainder in the return line. Obviously, this neglects thermal short-circuiting between the two lines because it does not account for the heat transfer between the supply and return path. In addition, this neglects a situation that appears to be present in investigations carried out in the present thesis. There is the possibility that the supply line equilibrates with its

underground surroundings long before reaching the end of the ground heat exchanger. In this case, there would be minimal heat transfer from the lower portions of the loop, and the return path would primarily oppose the supply line as the return fluid starts at the same temperature as the ground. Finally, although the model (Austin, 1998) accounts for circumferential variations, it neglects vertical temperature effects.

Austin (1998) used parameter estimation to determine the ground and borehole grout thermal conductivities. Austin (1998) initially attempted to perform his parameter estimation on the ground thermal properties, neglecting other parameters. However, he found that a small error in loop spacing could result in significant error in the thermal property estimation. He also noted that the exact value of this spacing and orientation is unknown because the U-Loop deforms on installation. In order to correct for this, Austin (1998) decided to estimate parameters for both the ground and the borehole grout. Austin (1998) concluded that this was the superior method.

Austin (1998) noticed a trend in the results for the estimates of the two independent parameters that he obtained from his two-parameter method. The two-parameter method tended to predict higher ground thermal conductivity values that corresponded to lower borehole grout thermal conductivity values, and vice versa. This suggests that the estimate of one material's thermal conductivity depended strongly on the material's thermal conductivity in Austin's (1998) method. However, the thermal conductivity of the ground and the thermal conductivity of the borehole grout are actually independent parameters because these are different and separate materials. The thermal conductivity of one material does not depend on the thermal conductivity of another, separate material. Finally, Austin (1998) noted that the borehole grout thermal conductivity estimates from

his two-parameter method differed from known values. Therefore, it may have been better to vary one or more of the geometrical parameters of the ground loop model, rather than to estimate the known value of grout thermal conductivity.

Gehlin (1998) conducted in-situ ground thermal property measurement experiments using a test rig developed at the Luleå University of Technology, Sweden. She analysed her data using the line source method. Unlike Austin (1998), she fitted her test curves through all of the data in spite of the fact that the results did not perfectly fit the mathematical model. The fit that she obtained appeared reasonable, even though the imperfections in the data should produce the same difficulties that Austin (1998) reported. However, Gehlin (1998) did not investigate how the property predictions varied over time.

Gehlin (1998) also considered a thermosyphon effect in boreholes for cases where the borehole fills with groundwater because it does not contain grout to hold the U-Loop in place. A thermosyphon effect is where natural convection occurs inside of a buried tube, for example, and draws heat from one location to another location connected to that pipe. Natural convection is heat transferred via a moving fluid that flows because of the density variations associated with uneven fluid heating. In contrast, forced convection results when a fan, pump, or other artificial driver forces fluid to flow. Gehlin (1998) concluded that there would be no thermosyphon effect in grouted boreholes. However, the research in this thesis shows that there may actually be a thermosyphon effect within the inactive legs of the U-loop beginning immediately after periods of heat pump activity, when the heat pump and heat-transfer-fluid circulation pump are not active.

Yavuzturk (1999) developed a two-dimensional numerical model to simulate vertical U-Loop borehole heat exchanger operation using the fully implicit finite-volume method. His method is a two dimensional simplification of Rottmayer's (1997) numerical model. Yavuzturk (1999) modified this model for use in depth averaged property ground thermal property evaluations. In order to conduct a short-term ground property evaluation, one needs an accurate model of the initial temperature response to vertical borehole heating. Yavuzturk (1999) felt that the simplifying assumptions in other models made them inaccurate for the first days, or longer, of ground heat exchanger operation. This is the method used by Austin (1998) in his thesis.

Yavuzturk (1999) applies his numerical model to different pipe and borehole sizes, as well as shank spacing using an automatically generated grid. This allows for the solution of a range of borehole and U-tube configurations from a small set of geometric parameters. The purpose of this paper was to verify the effectiveness of the numerical method. Yavuzturk (1999) verified his model by comparing it to the analytical solution of a cylindrical source in a finite homogeneous medium from Carslaw and Jaeger (1959). In the comparison, Yavuzturk (1999) used only one loop path and constant properties throughout his modelling domain. He uses the solution for a finite domain in place of the solution for an infinite medium because the numerical model has a finite radial extent. However, the model domain is sufficiently large that there is no temperature change or heat flux at the radial limit. Therefore, this approximates an infinite domain.

The model by Yavuzturk (1999) uses the pie sectors of the numerical model in Rottmayer et al. (1997). However, (Yavuzturk, 1999) uses a two dimensional model which averages the vertical temperature and thermal property distributions. As Rottmayer et al. (1997)

found, the pie sector model proved quite effective when compared to the analytical solution. Yavuzturk (1999) does not directly consider the convective heat transfer. Rather, he implements it as a boundary flux in the inner surface of the U-Loop. However, because he does not consider this effect, Yavuzturk (1999) instead arbitrarily assigns 60% of the heat transfer to one loop path and the balance to the other. Yavuzturk (1999) justifies this with a sensitivity analysis wherein he shows that there is little difference in the average borehole temperature regardless of the percentage of the power output assigned to either part of the U-loop. He conducted the sensitivity on a range of 100%/0% to 50%/50%, where he found little difference. Thus, it would appear that modelling both U-loop paths is unnecessary in his formulation. This model represents the net power output of the individual loops. Consequently, this represents a limitation of this model, as it is not able to predict the thermal short circuit between loop paths.

Yavuzturk and Spitler (1999) test the computer model that Yavuzturk (1999) reported. The method extends work by Hellström (1991) and Eskelson (1987). Yavuzturk and Spitler (1999) developed time response factors to evaluate performance over long-term heat pump service. Time response factors are function values for ground temperature response. Yavuzturk's (1999) method refines the approaches of Hellström (1991) and Eskilson (1987) as by giving hourly energy consumption data. Yavuzturk and Spitler's (1999) paper presents an example of using this approach. The paper also presents a simplification to the problem.

In Yavuzturk (1999), additional function evaluations result from each change in ground heat exchanger load. Therefore, particularly when the simulation accepts hourly variations, long-term predictions can involve an unreasonable number of computations.

The number of computations may be unreasonable because Yavuzturk and Spitler (1999) show that it is possible to lump the majority of the earlier steps into an average response. Fortunately, the number of steps that one may lump into a single, average response increases with time so that the computation does not become any more complicated after sufficient time that lumping becomes possible. This keeps the simulation manageable. Where Yavuzturk and Spitler (1999) needed information about borehole resistance and thermal short-circuiting effects, they used the results of Paul (1996), rather than Rottmayer et al (1997).

Shonder and Beck (2000) developed a method for modelling the ground heat exchanger as a composite infinite medium. They take an equivalent radius to approximate the U-Loop as a coaxial pipe, and consider three layers. They assume a thin film to represent the contents of the U-Loop, a thicker layer representing the grout, and an infinite layer representing the surrounding earth. They use the Crank-Nicholson method to solve this problem numerically and a parameter estimation to determine the unknowns of their system. This method has good accuracy in the short term. They incorporated their method into a software package called GPM. They only consider radial heat flow and explicitly average the individual properties and temperature distributions with depth. They verify their model by using test data from an experimental setup containing sand with a known thermal conductivity and a school in Nebraska that already had a year of data from operating bore fields. In each of these checks, the model and experiment showed excellent agreement.

Yavuzturk and Spitler (2001) tested their short time-step numerical model using field data from a school in Nebraska. Their simulation followed the experimental data quite

well. The greatest errors occurred when the experimental data contained flow rate discontinuities due to intermittent system operation. However, the energy calculations based on the simulated data were within at most 5% of the actual energy measurements in the worst scenario and within 1% when the simulation matched better with the data. However, the modelling technique appears to have abandoned the pie sector approximation for the U-loop paths of Rottmayer, Beckman, and Mitchell (1997) in favour of Paul (1996). In addition, by 2006 the group at Oklahoma State University seems to have adopted a one-dimensional model Xu and Spitler (2006).

Xu and Spitler (2006) modify the methods of Yavuzturk and Spitler (1999) and Yavuzturk and Spitler (2001). These modifications include a theoretical simplification to one variable as well as the addition of the effect of variable U-loop convection. The rationale behind the simplification to a one variable model is computational efficiency as well as their efforts to ensure equivalence between their one variable, axisymmetric model and more physically realistic models that include both U-loop paths. The convective properties of the antifreeze typically used as the heat transfer fluid in U-loop heat exchangers may change dramatically with temperature. Therefore, including variable convective behaviour is more accurate than assuming it is constant. They model the convective heat transfer as an equivalent conductive layer. They use a combination of their own formulations and Bennet, Claesson, and Hellström (1987) to obtain all of the thermal resistance and capacitance values used in their model.

Nam, Ooka, and Hwang (2008) used the commercially available advanced simulation software FEFLOW to model heat conduction, groundwater advection, surface radiation, and mass transport around a set of ground heat exchangers. This model considers spatial

ground property variations. This model uses the Kasubuch (1984) method to estimate thermal properties, and formulas by Hazen, Terzaghi, Zunker, and Kozeny to obtain the hydraulic properties. Nam et al. (2008) use these formulae to calculate ground thermal properties instead of determining them directly from field measurements. In a subsequent study, Nam and Ooka (2010) performed a similar analysis with an open loop.

Nam, Ooka, and Hwang (2008) verified their model by taking measurements of the physical system. This apparatus was a full scale geothermal heat exchange system constructed at the Chiba Experimental Station of the University of Tokyo's Institute of Industrial Science. The experiment consisted of a heating period, a cooling period, and intermittent periods of neither. Each period lasted for 3 months with space conditioning simulation occurring between 09:00 and 18:00, from Monday to Friday. The loads and cycles were commensurate with what they defined as typical for an office building.

The ground heat exchanger that Nam et al. (2008) analysed consisted of two 20m deep, 1.5m diameter cast-in-place concrete piles with eight u-loop ground heat exchangers evenly distributed around each pile. The supply lines were 5mm thick, with a 45mm outer diameter. Nam et al. (2008) compared their modelling results to experimental temperature measurements at 10m and 19m depths, at points 1.25m and 2.75m from the centre of one of the piles. Although they located both of the measurement points proximate to one of the piles, they selected the location of the measurement points such that they should be able detected effects from both piles. They located their measurement points on a line that makes a 135° angle with the line formed by the two piles.

The simulated data compared well with the experimental data. Therefore, Nam et al. concluded that the model was successful. There was a small, consistent bias in the simulation data presented in the paper. The simulation results were about 1°C above the measurement for most of the simulation. The success of this model is obvious from the comparison between simulation and experiment. However, Nam et al. did not conduct a sensitivity analysis to determine if the bias resulted from inaccuracies in the experimental correlations he used for ground property values. In addition, they did not compare these property values to any measurements.

1.4.2 Semi-Analytical Methods

Eskilson and Claesson (1988) give a detailed explanation of a fully three dimensional, semi-analytical method for calculating the temperature response to multiple borehole heat exchangers. They begin with a brief overview of theory and proceed to solve the quasi-3D, quasi-steady-state problem of the temperature of the heat transfer fluid within both borehole paths as a function of depth and time. The method is quasi-3D because they neglect vertical heat flow in the grout and u-loop paths. The result is quasi-steady-state because they treat the heat exchanger as a thermal resistance network, and neglect the heat capacity of the grout and u-loop paths. Recently, Lamarche, Kajl, and Beauchamp (2010) have shown that the three thermal resistance model that Eskilson and Claesson (1988) and Hellström (Hellström, 1991) used can predict heat flow from the cooler U-Loop path to the warmer one. Therefore, these authors favour a four-resistance model that they proposed (Lamarche, Kajl, & Beauchamp, 2010), although they do not indicate how to calculate these resistances.

Eskilson and Claesson (1988) detail their numerical method for solving the 3D transient heat conduction equation, outside the borehole using a finite difference method and implicit forward differences in time. They claim that their solution is valid as long as the time steps are more than either two or three hours. The reason for this time factor is the quasi-steady state, quasi-3D model of the ground heat exchanger and the assumption of uniform temperature at the well bore wall. This work also discussed their superposition technique for multiple boreholes and boreholes drilled at an angle from vertical. They also give examples and appendices for further clarification on their superposition process.

Eskilson and Claesson (1988) give a detailed account of their work on ground heat exchanger modelling. They discuss the heat transfer at the ground surface, which they conclude is negligible after a few metres. This finding agrees with data collected in this Thesis. They discuss the importance of groundwater movement and provide an equation for the minimum homogenous Darcy velocity that causes groundwater flow effects to manifest. They their model of conductive heat transfer from a finite length ground heat exchanger in a homogenous medium for the case of a uniformly distributed heat flux. They give methods for analysing non-uniform heat excitation by means of pulses. Borehole thermal resistance for three possible U-loop path placements and a list of significant and insignificant parameters comprise the majority of the remainder of the discussion.

Of particular interest is their claim of the insignificance of vertical thermal conductivity variations, and heat exchanger output. They provide an equation for the heat exchange from a deep vertical borehole heat exchanger emitting a spatially constant heat flux into a homogenous and radially uniform domain. This discussion also appears in Zeng, Diao,

and Fang (2002) and follows the method that sources such as Carslaw and Jaeger (1959) and Exhert and Drake (1972) describe (see section 1.4.3 of this thesis). The prediction indicates that the temperature response should be essentially depth invariant (except near the ends of the heat exchanger) for several years. The experiment conducted in this thesis will be the only known direct experimental comparison with this equation.

Remund (1999) gives an overview of the work done by Paul (1996) and himself. This work is an empirical analysis of the effect of grout thermal conductivity, and the ratio between loop-pipe and borehole diameter on the thermal resistance of the ground heat exchanger. These experiments considered three different borehole configurations. All of the configurations located both u-loop paths along the borehole centreline. One configuration had the individual loop pipes touching at the centre of the borehole, another configuration had the loop pipes touching the inner surface of the borehole, and the third configuration was between the two – with the space between the individual pipes being equal to the space between the pipes and the borehole. (This corresponds to configurations A, C, and B in the paper.)

The laboratory experiments yielded an empirical formula for the thermal resistance of the borehole Paul (1996). The experiments considered three different placements of the U-Loops within the borehole. They obtained one set of constants for each of the three configurations. They tested the field utility of this formula by running ground thermal property experiments in areas with known subsurface material properties. They found that in nearly all of the cases, the measured value for the borehole thermal resistance lay between the prediction for configuration B and C. However, Remund (1999) suggests using configuration B as an input for design purposes.

Sutton et al. (2002) describe how they have applied the results of Hellström (1991) to borehole analysis. This comprises work on multiple borehole fields and stratified geologic regimes. The work includes formulae for thermal resistance between interacting boreholes in close proximity to one-another. They provide an analysis method for incorporating the effects of variable heating output. However, these primarily lead up to their approach for dealing with stratified geologic regimes.

Sutton et al. (2002) subdivide the geology into multiple horizontal layers with different thermal properties. They use the formulae from Hellström (1991) to evaluate the heat transfer on each level. This discounts the effect of vertical heat transfer. Sutton et al. (2002) justify this by indicating the prevalence of infinitely long models in the literature that neglect vertical heat transfer, and typically very large ratio of length to diameter in typical ground heat exchanger applications. Unfortunately, they are only able to verify their model qualitatively.

1.4.3 Analytical Methods

Deerman and Kavanaugh (1991) give an overview of methods for augmenting the solution from Carslaw and Jaeger (1959) or a cylindrical heat source in an infinite, homogeneous material to develop a better representation of the heat transfer from a deep vertical borehole heat exchanger. The solution from Carslaw and Jaeger f (1959) gives the temperature distribution within an infinite solid that experiences constant and uniform heating from a cylindrical cavity that extends along a central axis within that solid. These conditions could conceivably approximate a number of heat transfer situations. Therefore, Deerman and Kavanaugh (1991) sought to include information regarding the physical processes that result in the heat transfer to the ground so that the infinite

cylindrical heat source solution would represent the heat transfer from a deep vertical borehole heat exchanger. These details include the thermal resistance of the borehole, the convective resistance within the u-loop, and the thermal short-circuit between the u-loop paths.

Deerman and Kavanaugh (1991) used a combination of analytical treatments and experimental correlations to incorporate the u-loop and grout into the cylindrical source solution. In addition, they present a method of dealing with heating loads that are not constant in time. Later works, such as Yavuzturk and Spitler (1999), and Bernier (2001) refer to this strategy as the "load aggregation" technique. Deerman and Kavanaugh (1991) tested their model using a ground thermal property test to measure properties, followed by a longer ground-heat-transfer test. The results of these tests compared well with the simulation values based on their model. However, they conducted their initial thermal property test for six hours, which later authors such as Austin (1998), Gehlin (1998), and Kavanaugh (2010), have said is too short for sufficient confidence in the thermal property test results.

Bernier (2001) gives a method for simulating the ground thermal response to a deep vertical borehole heat exchanger. He uses analytical solutions that originated in Carslaw and Jaeger f (1959) and Ingersoll (1954), and the "load aggregation" technique of Yavuzturk and Spitler (1999). His method is, as he intended, relatively easy to use. However, it requires averaging ground heat exchanger performance and ground thermal properties over the ground heat exchanger depth. This neglects any variation in ground temperature response with depth.

Zeng et al. (2002) reported an analytical solution for the temperature change around a vertical borehole ground heat exchanger as a function of radial position, depth, and time. The solution technique appears in texts such as Carslaw and Jaeger (1959) and Eckert and Drake (1972). Zeng et al. (2002) use the form from Carslaw and Jaeger (1959) because they believe that the form in Eckert and Drake (1972) resulted from an error in derivation. Zeng et al. (2002) follow the same procedure as Carslaw and Jaeger (1959). This solution also appears in Eskilson (1987).

The derivation of the finite-length line source solution proceeds from the point source solution that texts such as Carslaw and Jaeger (1959) give. The point source solution is the solution of the heat conduction equation subject to the following conditions. An infinite, three-dimensional, homogeneous medium with an initially uniform temperature experiences heat transfer (e.g. W/m^2) from an arbitrary point at time greater than zero. The heat transfer at the arbitrary point continues uniformly from zero to infinite time. The derivation proceeds by taking a superposition of point sources in order approximately to form the geometry of a vertical ground heat exchanger.

With the solution for a point heat source, one may assemble other heat source geometries by superposing the effect of many point sources. In the case of the finite-length line source, the derivation proceeds by assembling the point sources into a continuous vertical line that starts at zero and ends at a finite depth. Each point source will emit heat and contribute to the temperature distribution around the line they form. Selecting an arbitrary point away from the line and integrating the contribution to the temperature field of each point source gives the effect of a finite-length line source.

The boundary condition for the finite-length line source model that authors such as Zeng, Diao, and Fang (2002), Eskilson (1987), Carslaw and Jaeger (1959), etc. chose for the ground surface was zero temperature change. In three dimensions, this means that there is no temperature change on the plane described by the equation given in words as height equals zero. To achieve this, they added a second line of point sources that extended from zero to a finite altitude equal to the depth of the original line. This line formed the mirror image of the first line. To achieve zero temperature change at zero depth, the heat transfer from the mirror-line was the negative of the heat transfer from the first line. Therefore, the superposition of the original finite-length line source and the mirror-image finite-length line sink of equal strength caused the formation of an isothermal plane orthogonal to both lines located at the average position of those lines, at zero depth. Claesson and Eskilson (1988) extended this idea to include a source and a mirror-image sink that touch at zero depth and make an angle other than π to simulate boreholes drilled diagonally into the ground.

Diao et. al. (2004) give an overview of their work on ground heat exchanger theory. In this work, they propose analytical solutions for both the heat transfer inside and outside of the borehole. The solution for the temperature field outside the borehole is that given in Zeng et al. (2002) and previously in Eskilson (1987). The solution for heat transfer inside the borehole is a quasi-3D model that considers the borehole as a thermal resistance network. This development also appears in Claesson and Eskilson (1988). Diao et. al. (2004) apply the method of Hellström (1991) to determine the resistances for the thermal resistance network. They also provide methods to determine the borehole efficiency, and short circuit. They rely on a number of simplifying assumptions for their

borehole model, such as a depth invariant borehole temperature. Their results improve over other borehole analyses, wherein the variation with depth is not considered. However, they use these mode advanced theoretical treatments to obtain better estimates of the various depth-averaged temperatures typically used in heat pump analysis. As in Zeng, Diao, and Fang (2002), and the subsequent work by Lamarche and Beauchamp (2007a), Diao et al. (2004) contend that the use of analytical solutions is superior to the numerical methods proposed in Eskilson (1987) because of their greater flexibility and computational speed.

Lamarche and Beauchamp (2007a) developed an analytical solution for the temperature distribution in the grout layer separating the ground and the outer radius of a concentric tube heat exchanger. This is also approximately the temperature distribution between the ground and the equivalent radius of the U-Loop. They solved for a composite infinite medium with a cylindrical source. They solved this for cases of imposed heat flux and convection. The Laplace transform technique solves their model in the form of a depth invariant analytical solution. The solution to the transformed system involves rational functions that contain Bessel functions in both the numerator and denominator. An analytical solution to the Inverse Laplace Transform would require an antiderivative for that function, which Lamarche and Beauchamp (2007a) do not believe exists. Therefore, they use numerical methods to complete the inverse transform and complete the solution.

Lamarche and Beauchamp (2007a) tested their model by comparison to a number of other solutions. They compared their analytical solution to a numerical computer model that they constructed using the finite element software Comsol. They also compared their solution to Carslaw and Jaeger's (1959) solution to a uniform cylindrical heat source in an

infinite medium, and the method of Sutton et al. (2002). For the comparison between their analytical solution and Sutton et al. (2002), Lamarche and Beauchamp (2007a) used the thermal resistance proposed by Hellström (1991). The results all compared well. However, the comparison was best between the numerical computer model in Comsol and the analytical solution that Lamarche and Beauchamp (2007a) proposed.

Lamarche and Beauchamp (2007b) provide an improved method of evaluating the finite-length line source solution that both Eskilson (1987) and Zeng, Diao, and Fang (2002) give. Lamarche and Beauchamp (2007b) observe that, although Eskilson (1987) derives an analytical solution, he uses a numerical approach for the problem of obtaining the ground temperature response. Lamarche and Beauchamp (2007b) speculate that this is a result of the difficulties associated with evaluating the analytical solution, as proposed by Eskilson (1987). They go on to explain that the numerical method Eskilson (1987) used instead of the analytical solution requires a time-consuming numerical evaluation. Therefore, Eskilson (1987) provided a table of values for evaluating the numerical method under various conditions. Zeng et al. (2002) suggest using the analytical solution because of the obvious improved flexibility associated with an analytical solution as compared to a table of values. Lamarche and Beauchamp (2007b) offer an improvement over the method of evaluating the analytical solution proposed by Zeng et al. (2002).

Lamarche and Beauchamp (2007b) observed that the finite-length line source solution involved a definite double integral. Zeng et al. (2002) evaluated the definite double integral with a double-iterated numerical integration because no analytical solution exists. However, Lamarche and Beauchamp (2007b) were able to obtain a partial analytical solution. The partial solution replaces the double integral with analytical expressions and

a single definite integration that had no analytical solution. Therefore, Lamarche and Beauchamp (2007b) evaluate the remaining single-integration by a numerical method. Lamarche and Beauchamp (2007b) conclude that their method of evaluating the finite-length line source solution is superior to the prior studies because of the increased computational efficiency. They also cite difficulties with the treatment given by Zeng et al. (2002)

Lamarche and Beauchamp (2007b) verified their method by comparing it to the numerical results of Eskilson (1987) with success. There are some slight numerical discrepancies, which may have resulted from the minor differences between the derivation of the analytical and numerical solutions. For example, evaluation of the analytical solution involves assuming a constant temperature for the borehole wall. They also show the improvement that their method provides over previous approaches by comparing the computer time to evaluate the double integral and their simplified formulation. They provide a number of examples where the evaluation time of their method is between 5.8 and 3555.6 time faster than the double integral on the same computer with primarily the same software.

Wang et al. (2010) implements the result of Lamarche and Beauchamp (2007b) in the data analysis of a ground thermal property test. In addition, they seek to improve on the in-situ ground thermal property measurement test methods by using a constant temperature-fluid temperature test. The purpose of using a constant fluid-temperature test is to reduce testing time. Indeed, they observed that injecting a heat transfer fluid at a constant temperature resulted in steady state conditions faster than in constant heat rate test. They report that they are able to obtain stable results after between 24 and 30 hours,

as opposed to the 50 hours associated with constant heat rate tests, as proposed by Austin (1998). Wang et al. (2010) compared their thermal property results and obtained reasonable good agreement – favouring their own results.

Kavanaugh (2010) presents a method for measuring the borehole thermal resistance directly. This is an entirely different approach from most authors, who are interested in calculating it from borehole geometry. He suggests that this can be difficult, as the exact location of the U-loop paths within the borehole are unknowable. He uses the typical thermal property test, recording the inlet and outlet temperatures of a single U-loop GHX for up to 48 hrs. This method is relevant to this thesis, as it is a novel example of a contemporary method employing the line and cylindrical source theories of Carslaw and Jaeger (1959), and Ingersoll (1954), respectively.

Kavanaugh (2010) makes use of line source theory to compute the overall resistance and cylindrical source theory to determine the resistance of the ground around the borehole. The ground resistance value comes from the Fourier G-factor method used by Carslaw and Jaeger (1959). Kavanaugh (2010) suggests using heat capacity and density values from tabulated values or lab tests of the material removed from the drilling. Kavanaugh (2010) notes that as long as the test apparatus is able to maintain a sufficiently stable heat transfer rate, the constant property tests will work. Kavanaugh (2010) suggests calculating the values at numerous times to ensure that there is not too much scatter after eight to twelve hour. He suggests eight to twelve hours as a typical start-up time where the solutions would not give a stable result.

The investigation of Kavanaugh (2010) compared reasonably well with direct methods of borehole resistance calculation developed by Hellström (1991) and Remund (1999). The results he obtained fell between these estimates. Kavanaugh (2010) cites the difficulty with locating the U-loop paths within the borehole as an explanation for the discrepancies. However, Kavanaugh (2010) clearly prefers the method that he used in this paper because he suggests that experiments comparing direct methods to his could improve the accuracy of correlations used in system design. However, Kavanaugh (2010) cautions that the borehole resistance is only between 15% and 25% of the total ground-heat-exchange system, with the bulk of the resistance coming from the ground itself. Therefore, he sees little benefit from attempting to decrease borehole thermal resistance.

1.4.4 Supplementary Material

The thirty-second chapter of the ASHRAE's quadrenial HVAC Applications (ASHRAE, 2007) publication is on Geothermal Energy. Their most recent edition, 2007, cites numerous authors' methods for determining the average ground thermal property values. These methods include many of the line-source, cylindrical-source, and numerical computer methods covered in this review and some others. All of these methods are of the typical thermal property test, where one records the inlet and outlet temperatures of a single U-loop GHX for a brief period of operation. They also provide various formulae for calculating average thermal resistance, and for borehole depth sizing. They provide typical property value tables, ground temperature contour maps and tables for the USA, pointers for ground thermal property tests, and a graph of the Fourier/G-factor method recommended by Kavanaugh (2010). The chapter gives a wealth of other information about geothermal energy, in addition to their details on thermal ground property testing.

Yang et al. (2010) gives a detailed review of ground heat exchanger literature. They divide this paper into simulation models for inside the borehole, and models for the temperature response outside of the borehole. The review covers line, and cylindrical source methods, analytical and numerical procedures, and comparisons of different ground heat exchanger modelling programs. The review notes some multidimensional methods. However, like the literature itself, it focuses on methods that model the ground as a homogenous continuum. The final part of the review covers hybrid systems where some of the heat transfer for the heat pump system occurs with an environment other than the ground. Yang end et al. (2010) this paper with his conclusions and recommendations for future work.

Gehlin and Hellström (2003) compared four different models for analysing ground thermal property measurement tests. The comparison includes Carlsaw and Jaeger's line source model (Carslaw & Jaeger, 1959, p. 261). Note that this line source theory is equivalent to the solutions in Ingersoll (1954) and the solution that Carslaw gave in Carslaw (1921) and Carslaw and Jaeger (1959). Gehlin and Hellström (2003) also evaluate a simplification that a number of authors, such as Eskilson (1987), Helström (1991), have used. Carslaw and Jaeger's Cylindrical Source model (Carslaw & Jaeger, 1959, p. 354) and the authors own model round out the comparison. Gehlin and Hellström's model (Gehlin & Hellström, 2003) is a numerical model that approximates the U-Loop of the ground heat exchanger as a coaxial pipe using an explicit one dimensional finite difference formulation.

Gehlin and Hellström (2003) made their comparisons by using each approach to analyse an experimental data set. They used parameter estimation wherein they varied ground

thermal conductivity and borehole thermal resistance as unknown parameters. They do not know true values of the material properties at their site. Therefore, their review only compares model characteristics. The line source and numerical models compared well, while the cylindrical source models predicted higher conductivity values. When calculating in the forward direction, the line source model agreed best with the temperature data and proved to be the fastest and simplest. The numerical model proved to be the slowest. However, Gehlin and Hellström note that it is the easiest to use with a variable heat rate.

1.5 Problem Description

The reviewed publications in the sections above show that researchers investigating the thermal response to a deep vertical ground heat exchanger prefer to view the ground as a homogeneous medium. There are two likely sources for this preference. On the analytical front, there is all of the work done by Kelvin (1882), Carslaw and Jaeger (1959), Ingersoll (1954), etc. On the more recent, numerical front, there is the work of Eskilson and Claesson (1988). They presented a numerical modelling basis for neglecting ground thermal property variations.

Eskilson and Claesson (1988) have compared a full numerical model of a ground heat exchanger in a stratified medium and an equivalent homogenous medium (Claesson & Eskilson, 1988). They took two models. One model represented the ground as two layers. The top and bottom layers were identical except that they had different thermal conductivity values. In the other model, there was only one layer. This layer was identical to the two layers in the two-layer model except that the homogenous layer covered the

entire domain and used the arithmetic average of the two thermal conductivity values used in the other model.

Eskilson and Claesson (1988) found that the two models predicted the fluid exiting temperature nearly identically for a given entering fluid temperature. The discrepancy amounted to 0.04°C in their example. They conclude that this shows that ground stratification is not significant for their ground-heat-exchanger calculation applications. However, what this really shows is that the temperature histories of the inlet and outlet of a ground heat exchanger cannot reveal any effects associated with ground stratification. The inlet and outlet temperatures only give the net effect of the ground-heat-exchanger. They do not give any information about the inner workings the system.

Investigations such as Nam et al. (2008), Nam et al. (2010) and Rottmayer et al. (1997) have made computers models that consider ground stratification. However, neither Nam et al. (2008) nor Nam et al. (2010) reported on the vertical effects. Indeed, they only measure temperatures at two different depths. This is not sufficient to evaluate the vertical ground temperature profile. No one has ever used the model that Rottmayer et al. (1997) proposed to its full potential in evaluating the ground temperature response to heating by a deep vertical borehole heat exchanger. Other investigations, such as Austin (1998), Yavuzturk (1999), Yavuzturk and Spitler (1999), Yavuzturk and Spitler (1999), etc. have expanded on the research from Rottmayer et al. (1997). However, they only used the pie-sector approximation to the heat exchanger cross section. They did not use it to consider vertical effects.

Many of the reviewed investigations have shown great success in predicting heat exchanger performance, despite neglecting vertical variations in properties and temperature response. However, the duration of these studies were at least an order of magnitude less than the expected lifetime of a heating system. Furthermore, they could not evaluate the possibility of improvements to modelling or design by considering vertical property and temperature variations. Therefore, there is both an academic and practical need to determine the validity of the assumption that ground stratification and other vertical variations are irrelevant to ground heat exchanger calculations. Academically, there is always a need to evaluate the validity of assumptions. Such evaluations can translate into practical applications from the resultant improvement in understanding.

The only way to determine if there are significant effects caused by stratification or other vertical variations is to conduct an experiment that measures the vertical temperature profile in a stratified medium for comparison with models that neglect stratification. This thesis seeks to investigate the depth dependency of the ground thermal response to heat exchange with a deep vertical borehole heat exchanger. This study includes the augmentation of an already existing experimental site with heat transfer, measurement, and control equipment. The field site includes a commercially available heat pump intended for residential use, a deep borehole heat exchanger, and both near and far field monitoring wells located at various distances from the GHX. These monitoring wells allow measurement of the ground temperature with at various depths and times. The vertical ground temperature profiles will allow for comparison between theoretical predictions for vertical temperature profiles that assume a homogenous ground and

uniform thermal disturbance at the ground heat exchanger such as Eskilson (1987) and Zeng, Diao, and Fang (2002).

This study does uncover noticeable differences between this study's experimental results and the models based on homogenous media and an evenly distributed thermal disturbance along the length of the ground heat exchanger. Therefore, this thesis will model the experiment in order to elucidate the depth dependency of the observed ground thermal response and heat exchanger output. This experiment was a field investigation that measured the effect on the temperature field from operating a geothermal heat pump with a deep vertical borehole ground heat exchanger in a stratified geologic regime. This thesis includes a parametric study of the interrelationship between ground thermal properties and temperature response using advanced software to model heterogeneous layering in the ground and various heat transfer modes. This analysis is necessary because the true values of effective ground thermal properties are unknown at the outset. The analysis will also focus on finding an effective method of approximating the depth dependence of the heat transfer from the GHX because this is another unknown of the system.

Chapter 2 Experimental Facility and Methods

This chapter describes the experimental site and methods for characterizing the ground thermal response to heating by a 61m deep vertical borehole heat exchanger. The chapter discusses the experimental site, and methods in two separate sections. The first section details the augmentation of the research facility for the present study and the operation of this new heat-transfer, measurement, and control equipment. The second section describes the experimental methods used in the field portion of the present research. The chapter concludes with discussions of possible improvements on the equipment and methods.

2.1 Experimental Facility and Equipment

2.1.1 Description of the Heat Transfer Equipment

The heat transfer equipment consists of a heat pump unit (HPU) and a ground heat exchanger (GHX). The unit is a 230V Florida Heat Pumps' Energy Miser series EM015, designed for home heating and air conditioning. As in a home, the HPU provides either heating or cooling to the conditioned space. In this experiment, the conditioned space is the inside of the trailer that houses the HPU at the research field station (see Figure 1 and Figure 2). To provide heating to the trailer, the HPU absorbs heat (primarily) from the ground through the GHX (see Figure 3) and delivers it to the trailer. To provide air-conditioning, the HPU absorbs heat from the trailer and exhausts this heat (primarily) to the ground through the GHX. Thus, trailer-heating mode results in ground heat extraction, and air-conditioning mode results in ground heat addition.

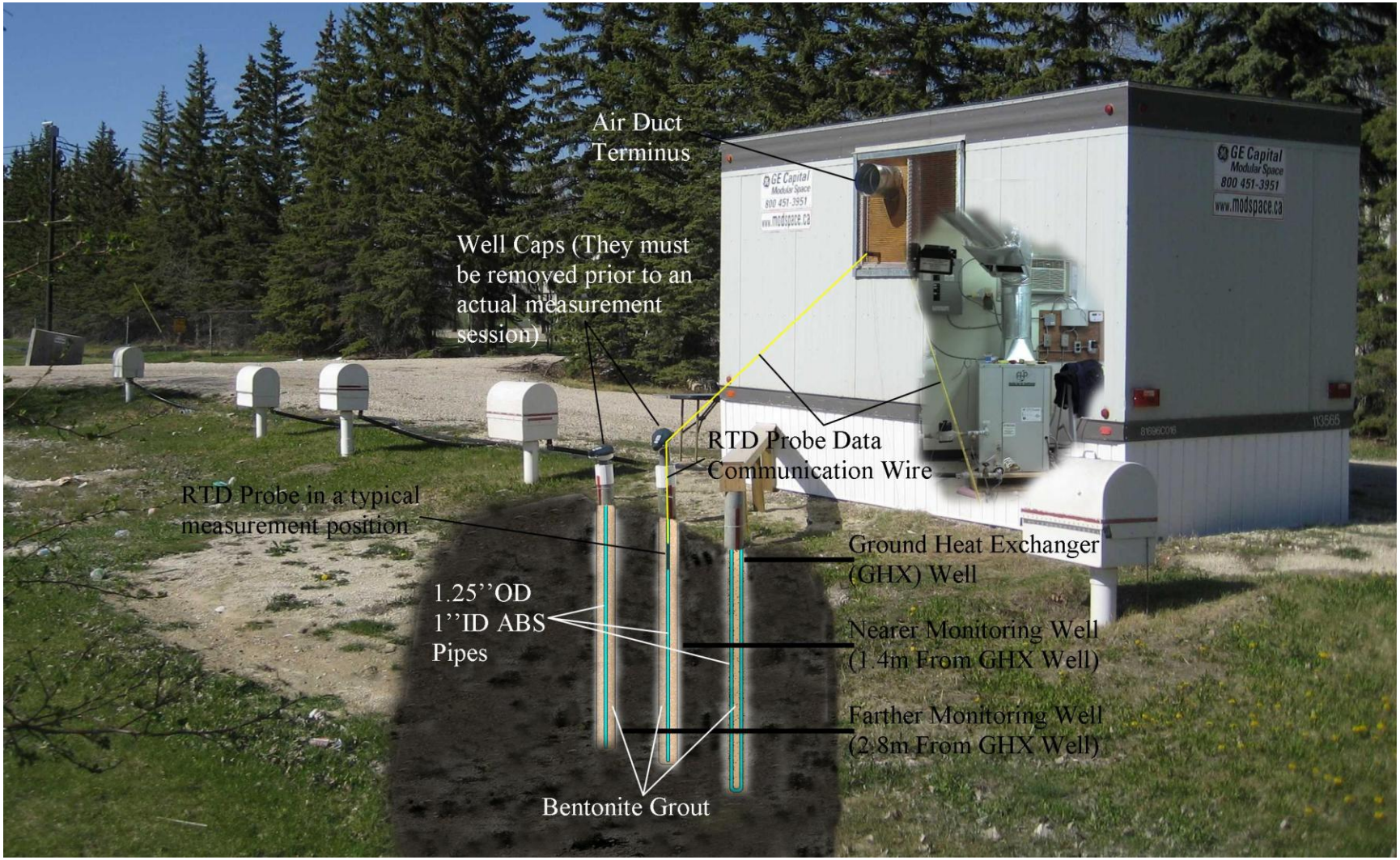

Figure 1 Exterior of the research field site.

Figure 2 Interior of the research field site.

The ground loop of the GHX (Figure 3) consists of one supply and one return pipe connected with a U-bend at the bottom of a vertical borehole. These pipes transport a heat transfer fluid from the ground surface to the bottom of the well and back. The heat transfer fluid also circulates inside the heat pump unit in an additional heat exchanger that transfers heat between the GHX and the refrigerant used in the heat pump. Both lines are straight sections of 2.54cm ABS piping with a 0.3048cm thickness connected at the bottom of a 61m deep 10cm diameter borehole. A 50/50 mixture of sand and bentonite

clay grouts the loop in place. The heat transfer fluid is a 20/80 methanol and water antifreeze mixture. For modelling purposes, the ground heat exchanger includes the cylinder of sand and clay grout that fills the cylindrical borehole and surrounds the supply and return lines of the ground loop. This allows for the simplification of axisymmetric modelling, as the heat exchanger is a right circular cylinder, in this model.

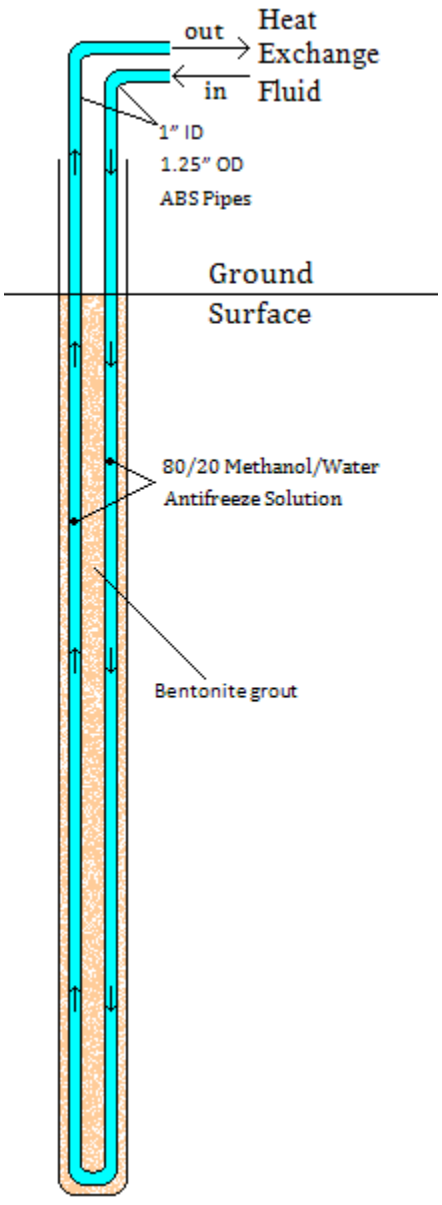

Figure 3 Diagram of the GHX

2.1.2 Description of the Heat Transfer Rate Monitoring Equipment

Two fixed three-wire platinum Resistance Temperature Detectors or RTDs measure the temperature change across the GHX (Figure 2). The temperature difference between the supply and return lines of the GHX combined with the flow rate and properties of the heat transfer fluid indicate the heat transfer rate to the GHX. A Campbell Scientific CR10X datalogger records the RTDs' output once per minute. An Elster Amco water meter sends a pulse to the datalogger every time 10L of heat-transfer-fluid flows through the ground loop. The logger counts and times the pulses to obtain the volume flow rate in the loop.

The fixed three-wire RTDs adjacent to the HPU measure the inlet and outlet temperatures of the heat-transfer-fluid at the pipe centerline. They measure temperatures adjacent to the HPU, inside the trailer. A short length of uninsulated pipes exists within the trailer and insulated tubing carries the heat transfer fluid between the trailer and the ground, outside the trailer. Therefore, heat transfer between the heat transfer fluid and its surroundings in transit between the HPU and GHX is assumed negligible.

A Campbell Scientific 107BAM thermistor (see Figure 7) measures a representative value of the air temperature inside the trailer every minute and the Campbell Scientific CR10X datalogger records this data. The 107BAM is installed about 30cm to the side of the ducting and outside of direct sunlight. The measurement end of the thermistor rests approximately 30cm from the duct surface, in a shaded part of the trailer. This position should prevent direct sunlight or radiated heat from the duct biasing thermistor readings. Of course, one temperature probe is not sufficient to characterize the air inside the trailer.

Instead, the probe acts as a passive observer of the trailer environmental conditions. This data is useful for troubleshooting issues that arise when the trailer is unoccupied.

2.1.3 Description of the Ground Temperature Monitoring Equipment

The ground temperature measuring equipment (see Figure 1) consists of a four-wire Platinum RTD temperature probe on a spool of electrical wire, a cable counter, two monitoring wells spaced 1.4m in series, and 20 Campbell Scientific 107BAM thermistors. A digital temperature read-out box displays the temperature measured by the RTD probe. Lowering the temperature probe down one of the monitoring wells allows measurement of the ground temperature at any desired depth. The cable counter (see Figure 2) indicates the depth of the reading by measuring the length of wire fed to the well. This system allows temperature measurements at virtually any time, in addition to any depth within the well. Section 2.2 discusses the practical limitations on how often one can take temperature measurements due to the unavoidable mixing of fluid in the measurement tube caused by the passage of the probe.

There are two 61m deep near field monitoring wells used to monitor ground temperature, located in line with the GHX. The wells are 10cm in diameter and located 1.4m and 2.8m from the heat exchanger well, respectively. Each monitoring well contains a single 2.54cm inner diameter, 0.3048cm thick ABS temperature measurement tube, grouted in place with a 50/50 sand and bentonite clay mixture. The temperature measurement tubes contain a different fluid from the GHX tubes. The fluid in the temperature measurement tubes is a 50/50 antifreeze mixture of Ethylene Glycol and Water to ensure good thermal communication between the probe and the surrounding ground. The tubes are open at ground level to allow passage of the temperature probe and sealed at the bottom to

prevent fluid loss. A hose fitting in the sides of the temperature measurement tubes located between 5cm and 10cm from the top is useful to recover the fluid that the probe and wire displace during temperature readings.

The initial use of this equipment resulted in an unexpected problem that may be of interest to future investigators. The initial temperature readings fluctuated randomly on a range of ± 0.10°C for more than ten minutes. This occurred despite the fact that the probe's accuracy is actually ± 0.01°C and that the probe responded nearly instantly in tests and other uses. After investigating the problem, it would appear that the probe housing prevented the fluid within the measurement tubes from flowing freely through the unit. If the probe housing drags fluid with it on its way down the measurement tube, then it would not be able to give an accurate reading due to the mixing of fluid from the new measurement depth and the fluid carried by the probe housing from other levels of the measurement tube. Therefore, the probe housing must expose the probe tip and allow fluid to flow past the unit freely as it progresses through the temperature measurement tube. Most likely, this problem only occurs when the outer diameter of the probe housing and the inner diameter of the measurement tube are similar because this probe has given accurate readings in previous use with larger diameter measurement wells.

Twenty installed thermistors provide far-field temperature monitoring points appropriate for future work such as long-term-testing. An example of a long-term test would be a yearlong domestic simulation using the cyclic control mode. A datalogger records the far field thermistors' output daily and the thermistors provide temperature measurement at depths of 15m, 18.75m, 22.5m, 26.25m, and 30m. The site has four such sets of thermistors located in separate wells. These wells are 5m, 8m, 11m, and 14m from the

ground heat exchanger. Unfortunately, the thermistor located 11m from the ground heat exchanger and 26.25m depth does not record any temperature readings, apparently damaged on installation. The present study though does not make use of the far field sensors.

2.1.4 Description of the Control Systems

The Geothermal Research Site has both constant heat pump output and cyclic heat pump output modes. These modes allow investigators to perform a variety of ground-heat-exchange experiments. In constant operation mode, the heat pump unit (HPU) either provides or extracts a constant rate of heat (e.g. Watts) from the ground heat exchanger (GHX). In cyclic operating mode, the HPU turns on and off on a predetermined cycle. In cyclic output mode, a control system activates and deactivates the heat pump system at predetermined intervals. This allows the site to simulate domestic operation of a heat pump, as domestic operation would involve on and off cycles, except perhaps during extreme weather.

Two control systems allow the HPU to function in either constant or cyclic output mode (see Figure 5 and Figure 6). One control system seeks to maintain the trailer air temperature at a constant value, while the other system dictates the durations of the on and off cycles of the HPU. Initial performance monitoring showed that a steady air temperature inside the trailer results in a steady heat transfer rate between the HPU and the GHX. Cycling the heat pump on and off on a predetermined schedule allows the equipment to simulate the on and off cycles of domestic operation. Both of these systems are user-programmable. Together, these systems allow investigators to perform both ground thermal property investigations and domestic usage studies. Both of these systems

are necessary to simulate domestic operation because the trailer lacks the level of insulation of a typical Manitoba residence and cannot approximate its heat transfer characteristics or behaviour without these systems.

A Temperature Control Timer regulates the trailer air temperature. However, it is a timer in name only as it only functions as a plug-in thermostat. The Temperature Control Timer operates from a conventional 120V 60Hz wall plug, which it switches and uses for its own power. Like any hard-wired thermostat, the plug-in thermostat activates the circuit it controls when it detects that the environmental temperature is beyond a user-defined value. The plug-in thermostat has both heating and cooling modes.

A programmable timer controls the cycle timing for operating the HPU on an on-and-off cycle. The timer controls a relay that switches the heat pump at 230V and 60Hz despite using conventional 120V 60Hz wall electricity for a control signal. The timer provides the 120V 60Hz relay control signal from a standard three-pronged outlet, according to a user-defined program. These units' design makes it is possible to sequence them if one wishes to increase the number of programs beyond the capacity of a single unit. To run the heat pump continuously, the operator simply connects the relay control plug to a continuous power supply, in place of the programmable timer.

The air-temperature control system employs two plug-in thermostats. One of these thermostats controls the interior trailer air temperature by controlling an air valve in the heat pump ducting and one of two auxiliary room temperature control devices – an electric heater for winter operation and (primarily) an air conditioner for summer operation, as described below. Together, these thermostats and their associated

equipment maintain the trailer air temperature within ±2.5°C of a user-defined value (e.g. Figure 4) regardless of the type of experiment, and under reasonable day-to-day variations in outside weather conditions for a specific season. However, the outside weather does affect the mean value of this temperature range, thus necessitating periodic equipment adjustment. Without the control system, the trailer room-air-temperature varied by about ±10°C about a mean temperature that changed daily, based upon the outside weather.

One of the plug-in thermostats controls an air valve in the ducting system that diverts the air from the HPU to the outside when the trailer air temperature has already reached its set point. This allows the HPU to complete its on-cycle despite the temperature inside the trailer. This plug-in thermostat is on a different circuit from the HPU. Therefore, it can provide power to one auxiliary room temperature control device while the HPU operates without exceeding the trailer's overall electrical capacity. This provides auxiliary conditioning air in continuous operation mode.

Cyclic operation mode requires the use of the second plug-in thermostat. In cyclic mode, the heat pump cycle control relay provides power alternately to the HPU and an auxiliary room temperature control device. The auxiliary device supplements the HPU during cyclic operation when the on-cycle is too short to provide enough conditioning air to maintain the set trailer temperature. The second plug-in thermostat controls the auxiliary temperature control device. The cycle control relay alternates between the HPU and auxiliary control device to ensure that the heat pump and the auxiliary systems do not overload the circuit by running simultaneously.

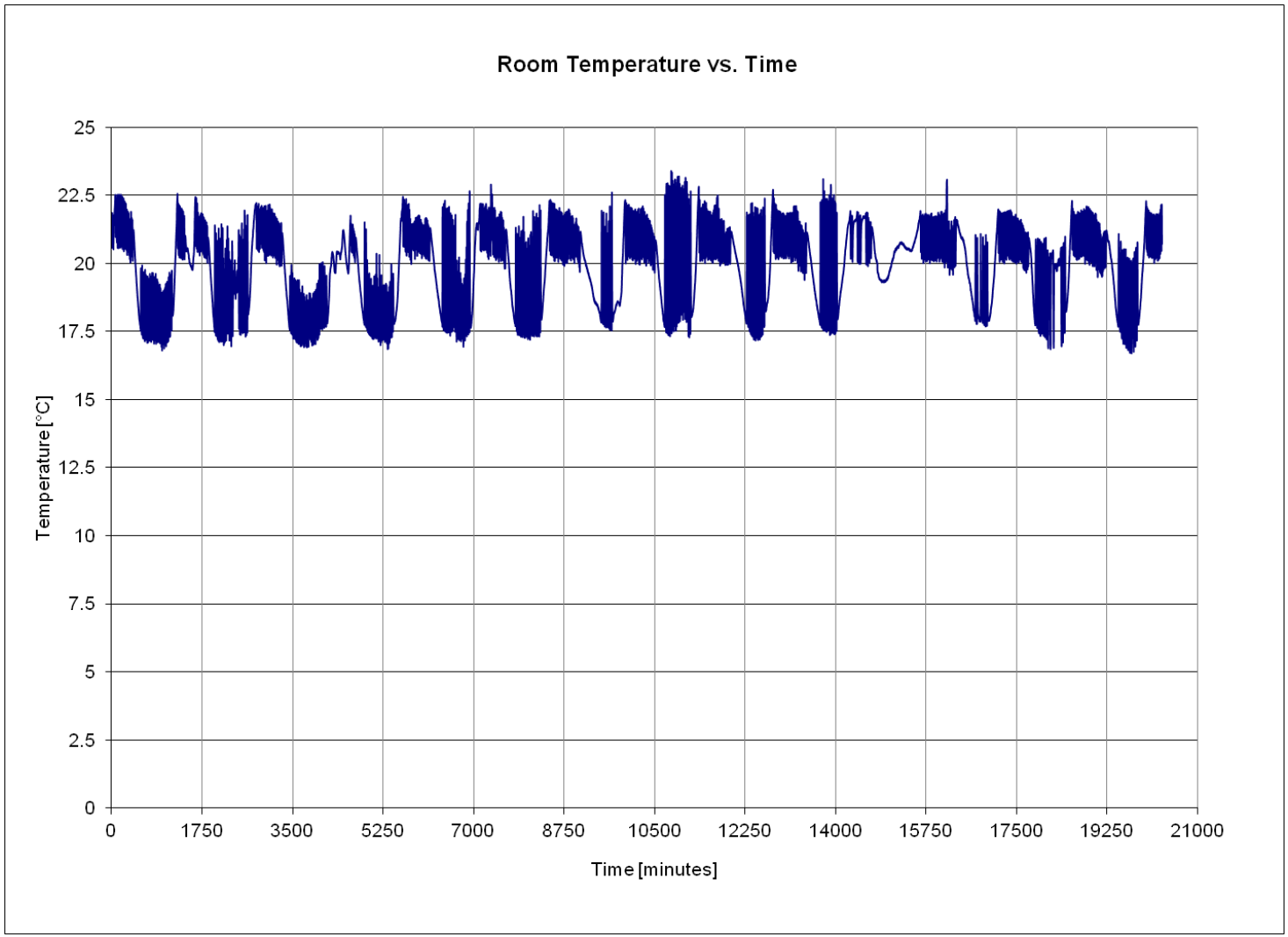

Figure 4 Data from 107BAM Room Temperature Monitoring Probe during the July 2008 test.

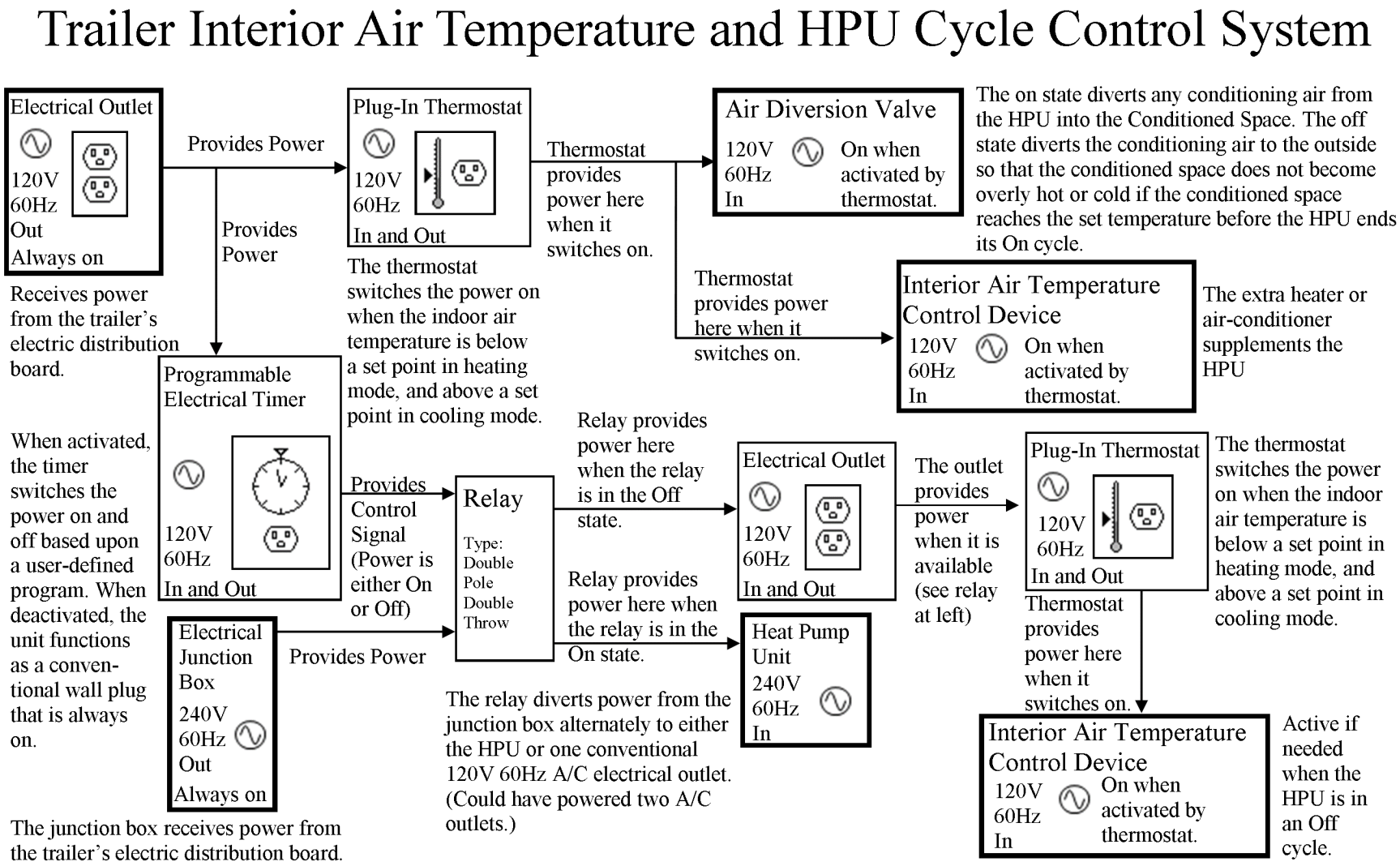

Figure 5 Block diagram of the control systems.

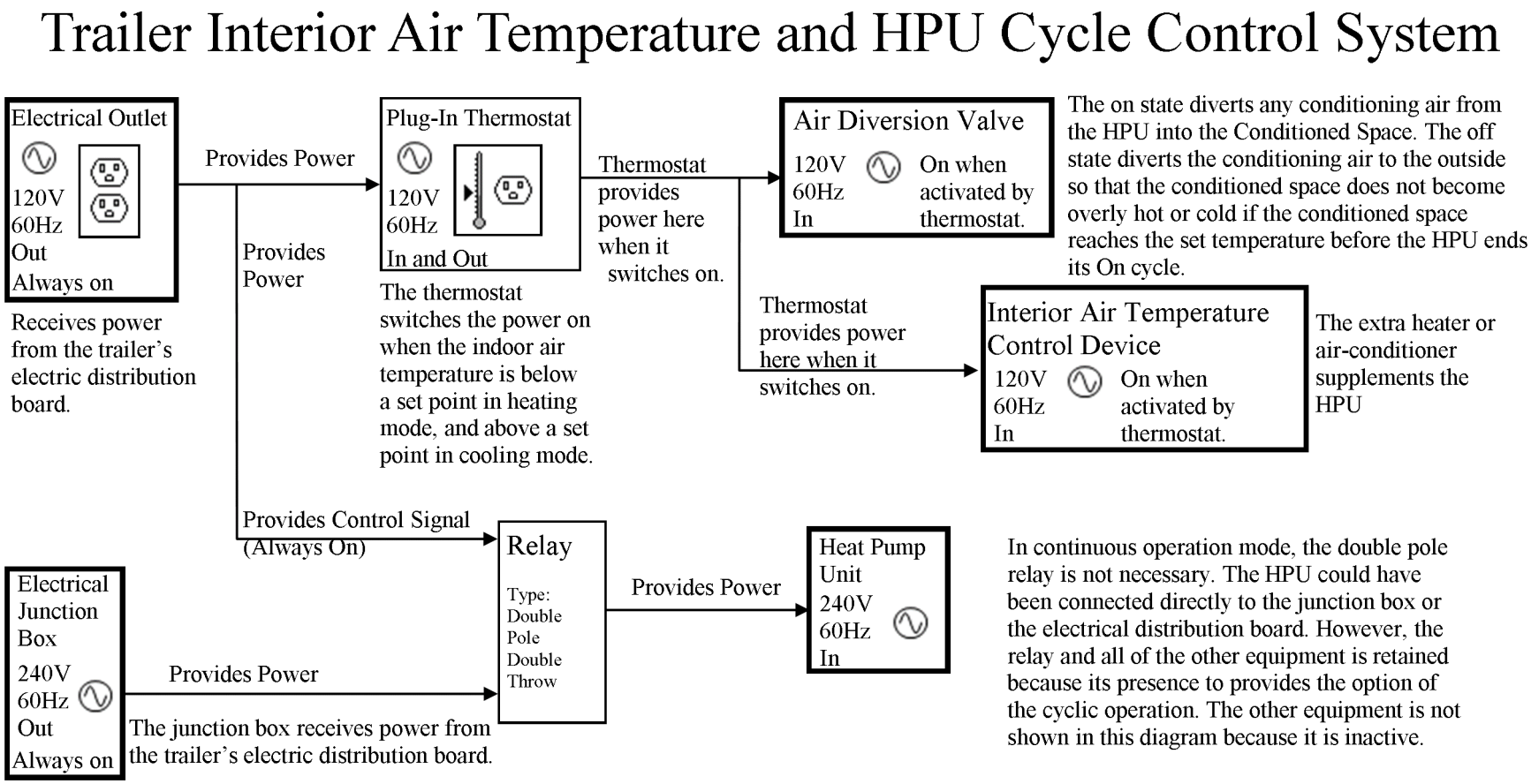

Figure 6 Block diagram of the control systems showing constant output mode.

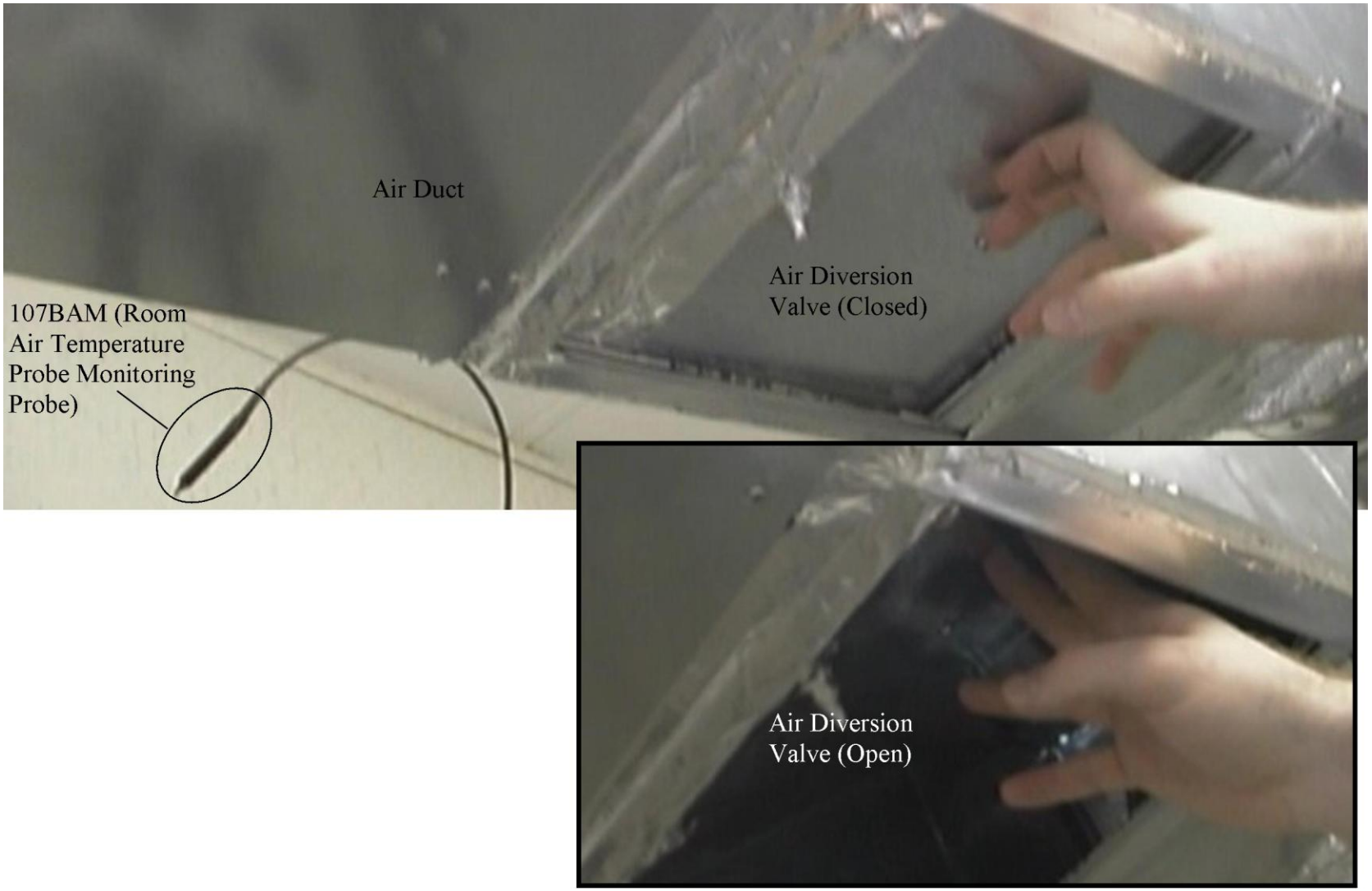

Figure 7 Air Diversion Valve and Room Temperature Monitoring Probe

Summertime operation occasionally requires heating at night because the outside temperature can be low enough that the trailer air temperature drops below the daytime set value. A lower daytime value is not always possible because the outside daytime temperature may also be sufficiently hot that the HPU could not maintain a sufficiently low temperature inside the trailer during the day. In this case, the second plug-in thermostat may control an auxiliary heater through the same circuit as air duct valve and the auxiliary air-conditioner. Setting the heater control temperature below the air-conditioning control temperature ensures that the two auxiliary devices do not overload the circuit by operating simultaneously.

A wooden plate provides a mounting for all of the equipment that communicates between the inside and outside of the trailer, other than the ground loop. The plate replaces the window screen on the side of the trailer that faces the GHX and the measurement wells. The plate provides a mount for the cable counter, a conduit for the four-wire probe, and a support for the ducting that exits the trailer. Locating the cable counter, probe-wire spool, and readout box inside the trailer permits an investigator to take ground temperature measurements from inside the trailer.

2.2 Experimental Procedures

2.2.1 Heat Pump Mode Selection

Ground heat addition is ideal for this study because it avoids the possibility of ground freezing. Avoiding ground freezing avoids the significant increase in the analytical complexity associated with the establishment of a phase change front, where groundwater turns to ice. As the frozen region expands and the liquid water becomes solid, the

properties at one location will change from one day to the next as the water at this location freezes. Modelling this requires considering the change in properties as a function of time and space, the effect of latent heat, the local porosity, as well as the time varying geometry of the frozen region. These phenomena are all topics that are beyond the scope of this thesis. Therefore, ground heat addition is ideal for the experiments of this study.

2.2.2 Portable Temperature Probe Compatibility Check

To check for the fluid entrapment problem discussed in section 2.1.3, one inserts the probe into a measurement tube exposed to an underground temperature region that is (approximately) constant in time and rapidly changing with depth. One such region is likely the first few metres of depth below the ground surface. One then watches the probe readout to see how long it takes to stabilize at a particular depth. In this study, when the probe was functioning properly, near surface temperature readings settled down to the readout noise of ±0.01°C within one minute. For deeper readings, where the ground temperature changed more slowly with depth, it took less than fifteen seconds. With fluid entrapment, the readout continued to fluctuate by ±0.10°C for more than ten minutes without any sign of abating.

The most likely causes of prolonged readout fluctuations are a malfunctioning sensor or electrical connection and insufficient freedom of fluid movement around the probe tip. Re-testing the probe in a vigorously stirred calibration bath, using the field readout equipment, can determine if the sensor or electrical connection is malfunctioning. If the probe and probe-reader function properly, then the probe design likely prevents proper fluid circulation. In this study, correcting the problem simply required removing the

probe shroud, which was not necessary to use in the measurement tubes at the Geothermal Research Trailer.

2.2.3 Preparations and Settings

The following checks are necessary at least two days before the scheduled test start-date. The fluid level in the temperature measurement tubes may drop over time. Any new fluid will need at least a day to equilibrate with the ground temperature before measurements are possible. Checking that the portable equipment is both present in the trailer and operational is also advisable before the testing start-date. This equipment includes the four-wire RTD probe and spool, the probe-reader and its power supply, tools, and other miscellaneous materials.

The following tests simply confirm that previously verified equipment remains operational and that the equipment is set correctly. Of course, the data acquisition equipment must function properly in order to collect the data. The datalogger program 20PT records the data for the present tests. After loading this program, it is advisable to check that all of the probes read correctly. If a probe fails to read, the electrical contact between the probe and the datalogger is probably loose. Therefore, tightening the electrical contact screws on the data acquisition board is advisable periodically, throughout the test.

Additional tests reconfirming equipment include checking the HPU. Running the HPU for about twenty minutes should indicate if there is any air in the ground loop. If future experiments require a much longer ground loop or a much lower flow rate, then this test may take longer. The flow measurement equipment should show flow in the ground loop

and the appropriate change in temperature should show on the readout from the data acquisition system. Of course, there should be airflow in the duct system and the flap should open when activated by the thermostat plug. The water meter can verify that the heat-transfer-fluid is flowing through the ground loop.

Further checks before beginning an experiment, in any mode, include the main room temperature control systems. In air-conditioning mode, as in this study, the HPU's thermostat was set to its minimum to prevent erroneous shutdown because the plug-in thermostat, rather than the heat pump's thermostat, controls the room temperature. Conversely, the maximum temperature setting is necessary in room-heating mode. One of the plug-in thermostats should control both the air-valve and the air-conditioner or auxiliary heater. This thermostat should be on, set to a seasonally appropriate temperature, and control mode. Our testing occurred in the warmer Winnipeg summer months, thus 20°C was appropriate. During the cooler part of the summer, the auxiliary heater control was set to 17°C to provide nighttime temperature control that did not conflict with the air-conditioner.

2.2.4 Experimentation Schedule

The experiments occurred in two stages: ground heating and natural recovery. The ground heating stage lasted two weeks, beginning on day zero and ending on day fourteen. The natural recovery stage began on day fourteen, when the HPU was deactivated, and ends on day twenty-eight with the cessation of temperature readings. The room temperature control system may continue during recovery using only the auxiliary equipment to maintain the room conditions at a comfortable level. However, all

that is necessary for recovery is deactivation of the HPU and heat transfer fluid circulation pump.

Readings for this experiment took place in the early afternoon from Sunday to Friday inclusive for the duration of each test. There are twenty-five sets of readings per well, beginning on July 13 2008. These twenty-five sets comprise six measurements per week for four weeks plus an additional measurement on the fifth Sunday. Measurements of the ground-heating period began on day zero, the first Sunday, concurrently with heat pump activation. The first period ends the same day the second period begins, on day fourteen – which is the third Sunday. Measurements of the recovery period end on day twenty-eight or the fifth Sunday. However, the ground temperature remained elevated above ambient levels for over two months.

A daily limitation on temperature reading frequency arises because the probe and cable displace the liquid in the monitoring well with each temperature measurement. This arises because the solid probe, probe housing, and probe wire must push past the fluid in the flooded measurement tube in order to proceed down the measurement tube to take temperature readings. It is assumed that limiting the measurement frequency to one measurement session per well per day would allow the fluid in each well time to equilibrate with its subsurface surroundings. Measurements proceeded down the well in each session so that successive readings only measured from undisturbed or equilibrated fluid. Periodic checks of temperature measurements while rewinding the probe indicated little or no change in the readings observed at random and decreasing depths as the temperature probe rose back toward the surface, despite the disturbance of that fluid. (The low speed of the probe and the narrow annulus separating the probe housing and the

measurement tube likely resulted in primarily laminar flow.) Therefore, disturbing the measurement fluid did not adversely affect the temperature measurements.

2.2.5 Detailed Temperature Measurement Procedures

The preliminary stage in every temperature measurement is setting the fluid recovery equipment. As described before, there is a hose fitting in the measurement tubes. Plugging one end of a rubber hose into that fitting allows the fluid displaced by the four-wire RDT and the wire spool to a fluid recovery vessel. A pan beneath the spool collects the heat transfer fluid that tends to drip from the wire spool. Monthly replenishment of fluid was necessary with the reading scheme of this study because some fluid loss was unavoidable. Without fluid recovery, four-wire-RTD and the 61m length of roughly 0.6cm diameter wire will displace about 2L of fluid from the measurement tubes. This results in draining the first few meters of depth in the temperature measurement tubes and wastes fluid.

After setting-up the fluid recovery equipment and passing the four-wire RTD probe through its opening in the trailer, it is possible to insert the probe into the measurement tubes. Holding and pulling on the wire instead of the probe should prevent damage to the probe when drawing it to the measurement wells. Removal of any detachable part of the probe housing that may entrap fluid precedes insertion of the probe into the measurement tube. In this study, readings began in the measurement tube nearest the GHX.

The probe tip should penetrate the measurement tube until it reaches ground level. Zeroing the cable counter at this time maintains a consistent reference level for all of the depth measurements. Proper maintenance of measurement fluid levels should have

resulted in the probe being submerged at this depth. The probe will not make accurate ground temperature readings unsubmerged. Therefore, in the event that the probe is not submerged at zero depth, the investigator must lower the probe until it reaches fluid after zeroing the cable counter.

The temperature reading from the four-wire RTD probe readout will fluctuate for a brief period before recording it is possible. Fortunately, this should not take more than a minute near the ground surface. If this does not occur, the probe may suffer from the fluid entrapment problem discussed in 2.2.2. At greater depths, where there is less change in temperature with depth, the reading should stabilize in less than fifteen seconds. The wire spool must maintain traction with the pulley wheel on the cable counter in order for it to make an accurate depth reading. Therefore, it may be necessary to turn the pulley by-hand. Each temperature measurement recording includes the depth of the measurement.

There were two measurement densities for the temperature readings made for this experiment. Temperature recordings occurred once per third of a metre in the first ten meters (i.e. at depth of 0.00m, 0.33m … 9.67m, 10m). Once per metre readings occurred for the remainder of the depth (i.e. at depths of 11m, 12m … 61m). Thus, there are eighty-one readings per well, per session. Thirty-one readings are from 0m to 10m depth and fifty are from 11m to 61m.

The average of the first and last measurement time in each measurement well represents the approximate temperature recording time. Recording the exact time of each temperature reading is not necessary because the total time for one measurement session in each well is about one hour. Therefore, the measurement time has an error of ±0.5h.

The first measureable temperature increase occurred after about 48 hours. This means that the maximum uncertainty in the measurement time is about 1%, and decreases with time.

An alternate view of the error introduced by using the average measurement time for all measurements is the error in the temperature measurement. The maximum and average day-over-day temperature changes are 0.29°C and 0.034°C, respectively. Over a twenty-four hour period, those numbers indicate that the maximum and average rates of temperature change are approximately 0.012°C/h and 0.0014°C/h, respectively. Multiplying those rates by the 0.5h error in the time measurement gives the respective maximum and average temperature errors as ±0.006°C and ±0.0007°C. However, as the maximum temperature changes used in this study actually occur roughly half way through the measurement, the maximum error in temperature measurement is probably much closer to the average error. In addition, either of those temperature error values is smaller than the error of the probe itself.

The final stage of a measurement is to return the fluid displaced from the temperature measurement tube. The temperature probe cannot be in the measurement tube during the replacement. Hand removal of the probe from the temperature measurement tubes should prevent damage to the probe. A funnel makes it easier to pour the recovered fluid from the recovery vessel back into the measurement tubes. One ensures the return of the fluid to the measurement tube by holding the free end of the fluid recovery hose above the mouth of the funnel. A check of the fluid level finalizes the recovery procedure.

2.2.6 Improvement of the Method

Future experiments may need to record higher spatial resolution in the areas of greatest temperature change. Locating these regions should be possible at the beginning of the test because, in this study, the regions whose rate of temperature change was largest were the first to show temperature change. Therefore, these points become apparent very soon after the beginning of testing. Consequently, it is possible to increase the sampling density near these points for the remainder of the test. These extra measurements would not take very much time because they occur in the deeper region, where the temperature measurements stabilize in less than fifteen seconds.

2.2.7 Improvement of the Apparatus

A limitation of this study is that there are no sensors in the GHX to measure its performance. Therefore, the actual thermal boundary condition at the grout/loop interface and the GHX/underground interface are unknown. Thus, any model of the underground surrounding the GHX results in an unbounded system because of the unknown thermal behaviour inside or on the surface of the GHX. Consequently, this research includes a parametric study to estimate the boundary condition that approximates the GHX heat transfer activities. Therefore, future experiments may wish to instrument their GHX with temperature probes or other thermal sensors in order to remove the unknown boundary condition from the analysis.

Chapter 3 Modeling

3.1 Introduction

Most investigations into the effect of heating the ground by a deep vertical borehole heat exchanger make similar assumptions about the nature of underground heat flow. Usually, this means that the conceptual model of the ground is a homogenous medium that experiences spatially uniform heat flux along the length of an infinitely long ground heat exchanger (see Chapter 1.4). These models are depth invariant because of these assumptions. Both the infinite-length cylindrical source (Carslaw & Jaeger, 1959) and the infinite-length line source theories (Ingersoll, 1954), are prevalent in the literature. However, the detailed depth-dependant measurements made during the experiment conducted for this thesis permits less restrictive analyses.

The depth-varying ground temperature measurements from the experiment for this thesis provide the motivation for more complicated analyses. Depth invariant models have been quite successful, e.g. Eskilson (1987), Austin (1998), Yavuzturk and Spitler (2001), etc. Therefore, the search for a conceptual model began with a review of the main assumptions that result in a depth invariant model. These assumptions include thermal property homogeneity, zero ground-surface heat flux, infinite heat exchanger length, zero vertical heat flow, and uniform heat transfer from the GHX. Fortunately, a mathematical model with fewer assumptions exists in the literature.

Both Eskilson (1987) and Zeng et al. (2002) report a mathematical model that closely resembles the physical system. They each arrived at their solutions by solving the same

mathematical system. The solution is significant because it discards some of the simplifications of the infinite-length source theory that dominates deep vertical ground heat exchanger literature. Their finite-length line source theory approximates the ground heat exchanger as an infinitely thin line that penetrates to a finite depth in a homogeneous ground that extends from zero to infinite depth. The model also approximates the ground-surface boundary condition as a constant temperature.

The finite-length line source theory is very similar to the physical system. The solution to the finite-length line source theory results in a temperature distribution that depends on depth as well as radial position and time. This is more realistic than either the infinite-length line or cylindrical source theories because these theories do not depend on depth. Conceptually, it is more realistic than these other theories because it incorporates the finite length of the ground heat exchanger directly into the model. Finally, it assumes a constant ground surface temperature, rather than zero heat flux at the ground surface. The constant temperature boundary condition is more like the physical system because the complement of meteorological effects at the ground surface makes it unlikely that the ground heat exchanger could significantly affect the ground surface temperature. Eskilson and Claesson (1988) reported this as one of the results of their simulations. Finally, this model predicts that the ground temperature will reach a steady state, while the infinite length line source theory does not predict a steady state because it tends to infinity as time goes to infinity.

The finite-length source theory retains some of the assumptions of the infinite-length theories. This model assumes thermal property homogeneity, and uniform heat flux along

the ground heat exchanger. However, conceptually, it is significantly more similar to the physical system than the infinite-length theories. Therefore, it is a prime candidate for the conceptual model to approximate the experimental results of this thesis. Comparison between this model and the experimental data will confirm its usefulness for simulating the experiment.

The graphs in Figure 8 and Figure 9 show comparisons between the temperature profiles observed in the field experiment and the finite-length line source solution for a ground heat exchanger in a homogeneous, semi-infinite domain. The finite-length line source theory requires constant ground thermal properties and a depth-averaged heat exchange rate. Direct measurements do not exist for most of this information. A parametric study to determine these quantities, as well as to characterize the heat transfer from a deep vertical ground heat exchanger follows the current section. Therefore, the comparison between the finite-length line source theory and the experiment of this thesis uses the averages of the values from the parametric study. These averages gave depth-averaged thermal conductivity as λ=2.225W/m·K, depth-averaged volumetric heat capacity as VHC=3.3245MJ/m^3·K, and depth averaged heat transfer rate Q/L=31.5W/m. The finite-length line source solution is:

$$\mathrm{T}(r,z,t) = \mathrm{T}_0 + \frac{Q}{4\pi \mathrm{L}\lambda}\int_0^1 \left\{ \frac{erfc\left(\frac{1}{2}\sqrt{U_1/F_O}\right)}{\sqrt{U_1}} - \frac{erfc\left(\frac{1}{2}\sqrt{U_2/F_O}\right)}{\sqrt{U_2}} \right\} du \qquad \textbf{[1]}$$

$$U_1 = \frac{r^2 + (z-u)^2}{\mathrm{L}^2} \qquad \textbf{[2]}$$

$$U_2 = \frac{r^2 + (z+u)^2}{\mathrm{L}^2} \quad \textbf{[3]}$$

$$\mathrm{F_o} = \frac{\lambda}{VHC}\frac{t}{\mathrm{L}^2} \quad \textbf{[4]}$$

In the above equations, $\mathrm{T}(r, z, t)$ is the temperature at position (r, z) and time, (t). The initial temperature ($\mathrm{T_0}$), is the temperature field (approximately or exactly uniform) at zero time. The variables r and z are the radial position and depth, respectively, and L is the total depth of the ground heat exchanger (61m in this case). This equation defines a Fourier number ($\mathrm{F_o}$). For consistency with the quantities defined above, position is in metres and time is in seconds.

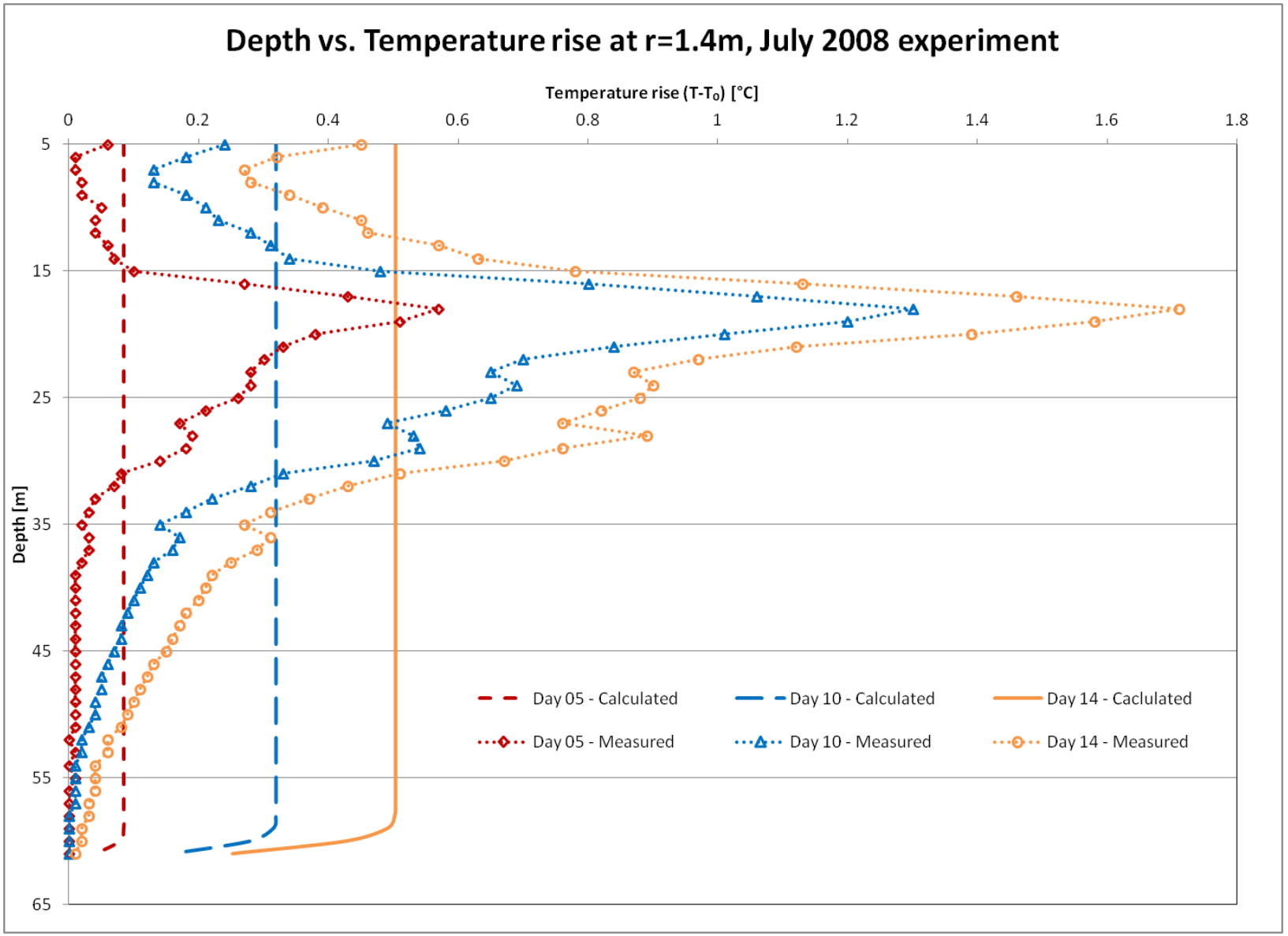

Figure 8 Comparison of analytical model and experiment at r=1.4m during heating phase

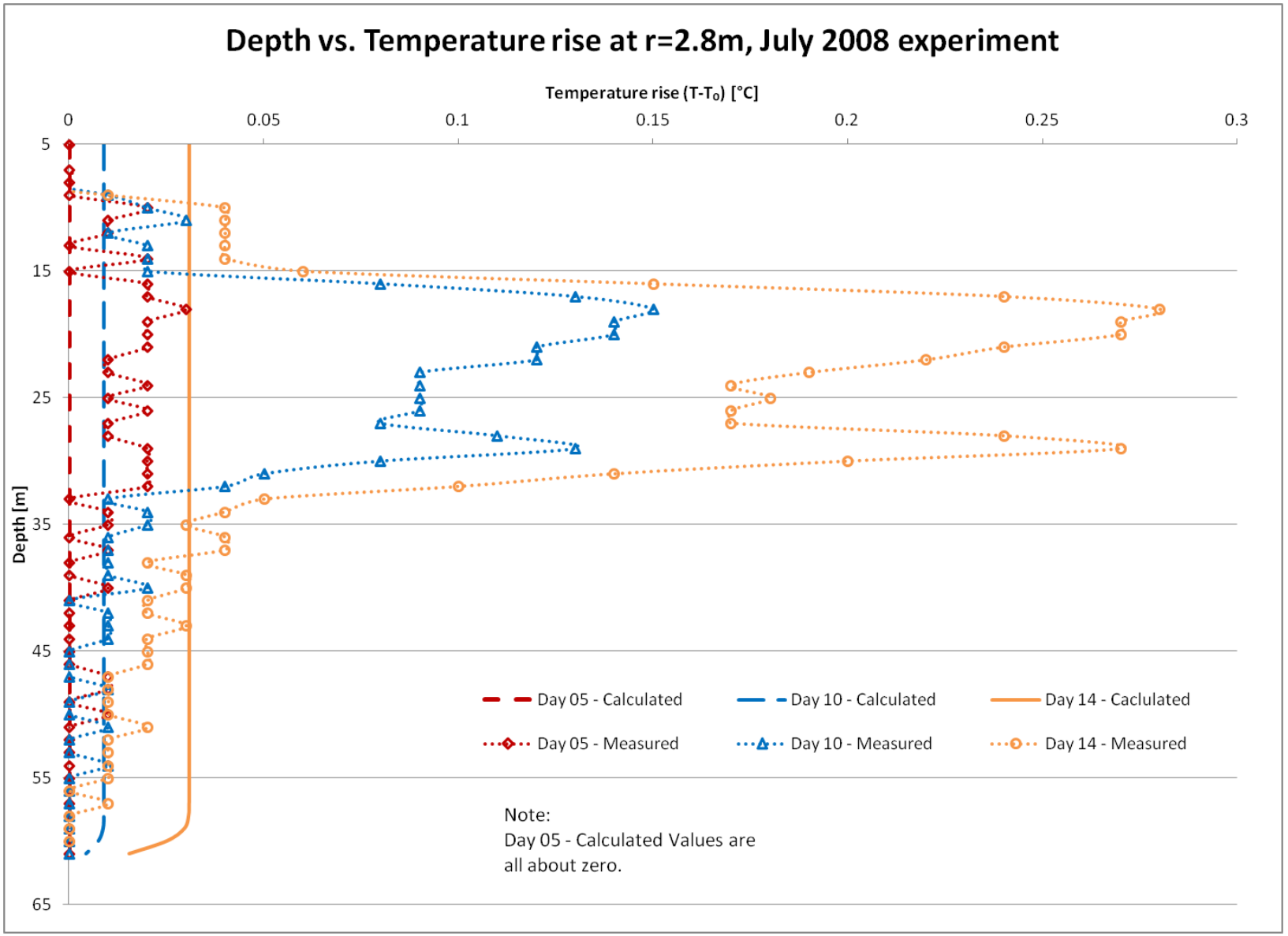

Figure 9 Comparison of analytical model and experiment at r=2.8m during heating phase

The graphs in the previous figures clearly show the discrepancy between the finite-length line source solution and the experimental results. Choosing different material properties or flux values for the finite-length line source solution does not improve the level of detail. The graph of the finite-length line source solution remains much simpler than the experimental results. In fact, the maximum temperature response from the experiment is 3.4 times the value that the finite-length line source solution predicts for day 14 at a radius of 1.4m. This maximum value is also four times the average experimental value. This shows that the finite-length line source solution may not predict the average ground temperature either. Consequently, either one or both of the assumptions of depth invariant heat flux and depth invariant properties are not appropriate. Therefore, the computer modelling must investigate if and how depth variations in thermal properties and input heat flux affects the ground temperature distribution.

3.2 Conceptual Model Development

The goal of the conceptual model is to develop a basis for a computer model to uncover the effect of assuming space-varying thermal properties and heat exchanger output on the match between experiment and simulation. Where possible, the development of the conceptual model will follow the conventions established in the literature. These consistencies include assuming axisymmetry, purely conductive heat transfer, and horizontally layered strata. The model development will also seek to uncover the most parsimonious system to simulate the experimental results. Hopefully, the decision to focus on these two factors will make it easier for future researchers to incorporate the findings of this study into their own work.

The assumptions for the interior of the modelling domain for the remainder of the analysis are as follows. The conceptual model will assume that the heat transfer is purely conductive. The low regional groundwater flow rates at the experimental site (Ferguson G. , 2004) justify this assumption. This assumption is also consistent with most models in the literature. The conceptual model will represent the ground heterogeneity as a vertical stack of different material types to represent each of the geological layers, as in Sutton et al. (2002).

The items outside of the modelling domain that the conceptual model will neglect are as follows. The conceptual model will neglect the behaviour near the ground surface and instead focus on the majority of the ground temperature distribution. This way, the analysis will focus on effects resulting exclusively from heating by a deep vertical borehole heat exchanger, rather than daily-weather effects or the combination of these two effects. The conceptual model will also neglect any circumferential variation in ground heat exchanger output. The distance between the borehole and the measurement points should cause temperature field asymmetries resulting from the presence of two U-loop paths to vanish. Furthermore, the exact internal geometry of the ground heat exchanger is unknowable (Austin (1998) and Kavanaugh (2010)). This will allow the investigation to focus on the ground temperature response, rather than directly modelling inner-workings of the ground heat exchanger.

The concept for the model of the ground heat exchanger is a boundary condition on a cylindrical cavity at the centre of the model of the ground. The cylindrical cavity represents the borehole. A step function will represent the depth variation in the thermal

disturbance of the ground heat exchanger because a step function is the simplest depth-dependant function. The graph of Figure 10 shows an example of this (also see Figure 11). In addition, the computer modelling software that will represent the conceptual model is not able to simulate any more complicated functions. This description intentionally uses the generic term "thermal disturbance" to describe the function of the ground heat exchanger because the parametric study investigates a variety of possible boundary condition types and scenarios.

The parametric study seeks to evaluate the validity of assuming that there is no variation in heat exchanger output with depth. Therefore, the conceptual model must include depth variations in the heat exchanger's thermal disturbance. The model of the thermal variation divides the length of the ground heat exchanger into a series of steps. The strength of the thermal disturbance on each of those steps varies in each trial run of the parametric study. However, the model only considers spatial variation. Therefore, the value of the disturbance remains constant on each vertical division throughout each trial run of the parametric study.

The conceptual model that this section describes shares some similarities with the one that Sutton et al. (2002) used. The similarities include vertical stratification of the underground materials into a "stack", as they describe it, and the assumption of purely conductive heat transfer. However, Sutton et al. (2002) neglected vertical heat transfer, which is not necessary with the computer modelling software that this study will employ. Sutton et al. (2002) consider only one depth-variation step per material layer. However, the conceptual model for this thesis also differs on this point.

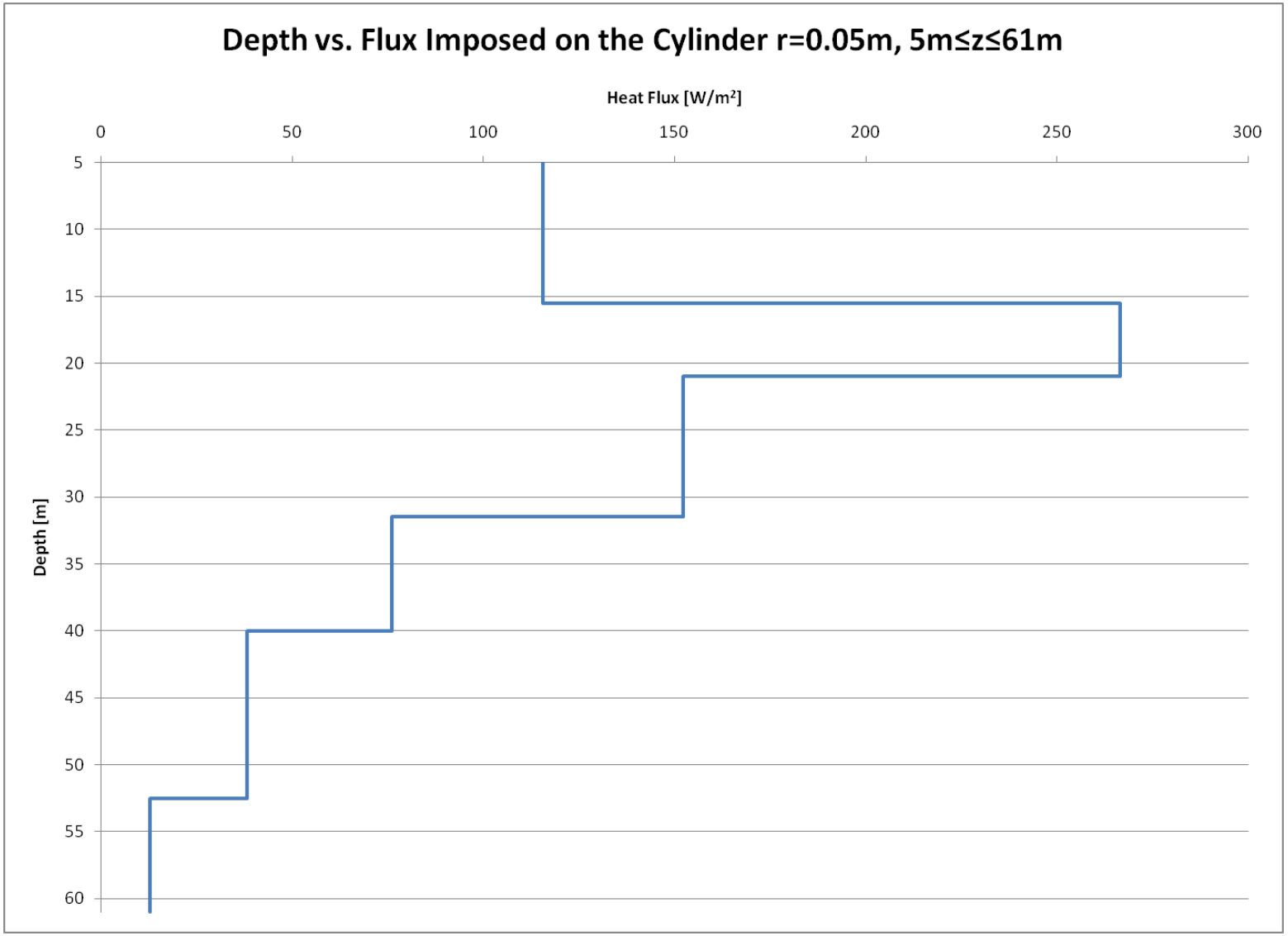

Figure 10 Example of Flux Boundary Condition Imposed on the Cylinder r=0.05m, 5m≤z≤61m

The results of the present investigation show that the ground temperature response is actually more complicated than one boundary condition step per material layer could describe. In fact, the results of this study show that there may be a significant temperature variation within a geologic unit. This is a novel result of the present investigation, as the literature review (chapter 1.4) shows. After observing this fact, the conceptual model for this study considers that the end points of the depth intervals that correspond to the material layers may or may not correspond to the depth intervals of the boundary condition steps (see Figure 11). Therefore, a single material layer may have more than one boundary condition step, as in M_2 and M_3 in Figure 11, and a boundary condition step may overlap a material layer, as in L_3 in Figure 11. This is actually an advantage over Sutton et al. (2002) because their model assumes one boundary condition step per material layer.

The more relaxed conceptual model of this thesis results in fewer parameters than that of Sutton et al. (2002) because it allows the modeller to add boundary condition steps without increasing the number of material layers beyond what is actually present in nature. Preliminary computer modelling attempts showed that the six boundary condition steps that Figure 11 illustrates is the minimum number of boundary condition steps that will effectively simulate the experimental observations. The conceptual model of Sutton et al. (2002) ties the boundary condition step to the material layer. This would require six material property layers to achieve the six boundary condition steps when the physical system only actually has three material layers. Each additional material layer adds three parameters in the form a boundary condition and the two thermal properties that define a material. These properties that define a material are any two of the thermal conductivity,

the thermal diffusivity, and the volumetric heat capacity. However, many of these parameters would be redundant because the system really has only three material layers. Therefore, the freedom that the conceptual model of this thesis gives to add additional boundary condition steps without adding additional material layers results in a significant savings in the number of modelling parameters.

3.3 Computer Model Definition

The computer modelling used the program Temp/W (GEO-SLOPE International, Ltd., 2007). Typical applications of Temp/W software are to model applications of ground heat exchange for a variety of scenarios (Thermal Modeling with TEMP/W 2007, An Engineering Methodology, 2008). The numerical model solves the transient heat conduction equation based on user defined geometry, material properties, initial, and boundary conditions. This computer code will solve the transient heat conduction equation in either two or three dimensions. However, the three dimensional mode is limited to axisymmetric cases, such as the analysis in the present thesis.

There are four material layers divisions in the computer model, M_1, M_2, M_3, and M_∞. The actual geologic stratification of the region from Ferguson (2004) forms the basis for these divisions. The top three layers produced all of the experimental data; consequently, they comprise the layers under study in this analysis. The parametric study seeks to determine appropriate numerical values for the effective properties within the top three layers. Consequently, this section only includes a qualitative description of the material layers. The next section details the development of the numerical values.

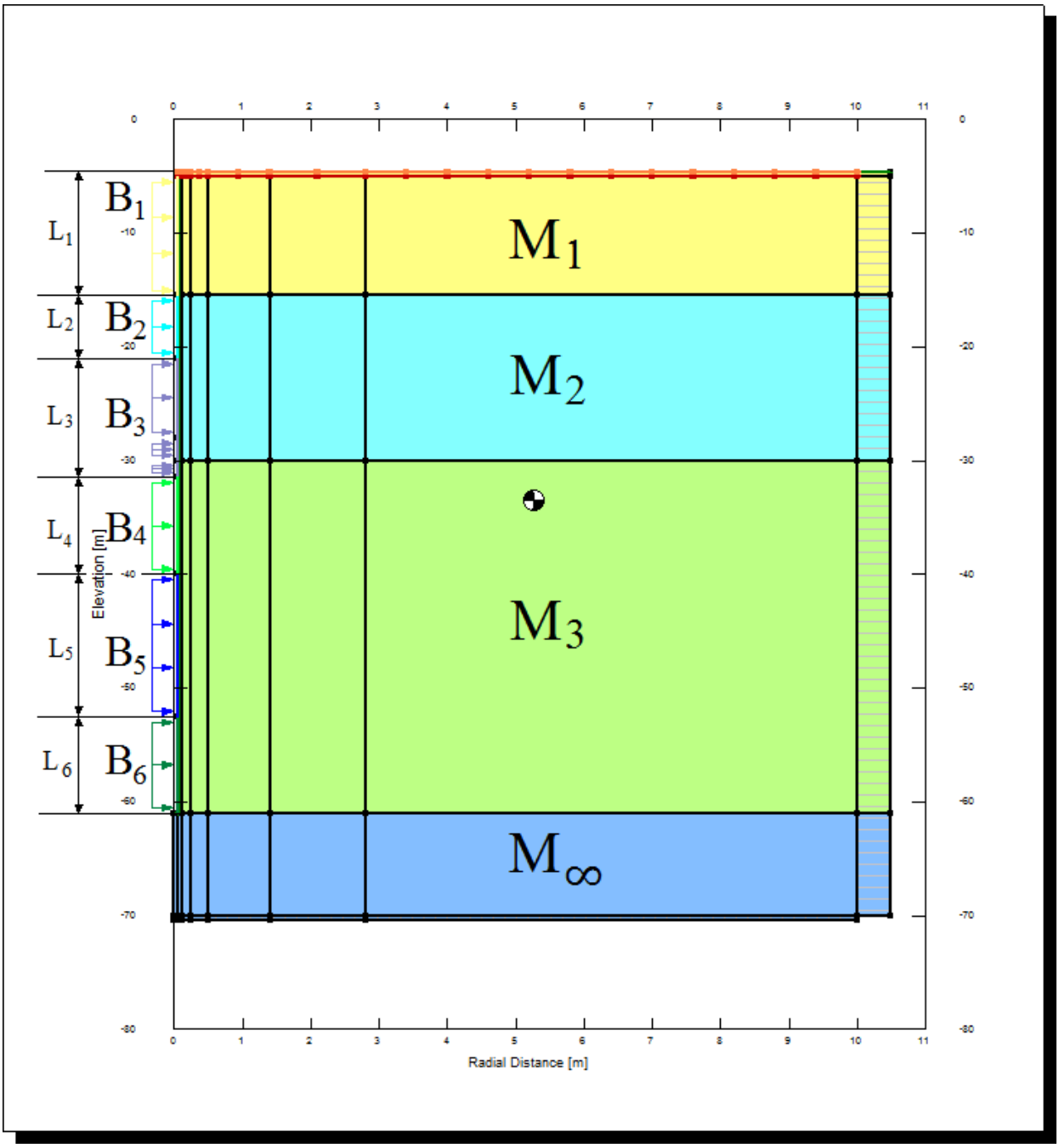

Figure 11 Diagram of the Computer Model

The first material layer, M_1, is clay. The second, third, and infinity layers M_2, M_3, and M_∞, are limestone. Consequently, the properties of these layers correspond to those materials, respectively. The second layer corresponds to the upper carbonate aquifer, and

the third and infinity layers correspond to the lower carbonate aquifer. The difference between the upper and lower carbonate aquifers comes from thermal property investigations by Ferguson (2004). He showed that the thermal conductivity of the limestone in the upper carbonate aquifer is higher than in the lower carbonate aquifer.

The physical system includes a layer of till near the border between the layers M_1 and M_2, likely near the top of M_2. The computer model neglects this layer. The glacial till layer may be more than a metre thick. However, this is small by comparison to the 56m thick problem domain, as well as compared to the thickness of either of the M_1 or M_2 layers. The primary reason for neglecting this relatively thin layer is that the preliminary modelling showed that a three-layer Temp/W model (as in Figure 11) could effectively reproduce the experimental results near 16m depth without an additional, till layer.

The primary motivation for neglecting the till layer was that including it would have doubled the modelling effort. Each material layer takes on one of two property values for every material property combination. Thus, each additional layer doubles the number of possible material property combinations. This doubles the number of modelling runs because the parametric study proceeds by optimizing every material combination type (see sections 3.4 and 3.5). For Four material layers, there would have been $2^4+1=17$ combinations instead of the $2^3+9=17$ combinations that the study actually uses. Furthermore, the temperature measurement spacing near the till layer was one metre. Thus, there may have been only one or two measurements actually in the till. Doubling the modelling effort for the benefit of one or two out of 56 data-points would not have been justified, given that the model (see Figure 11) worked well without this extra effort.

There are other reasons why the computer model neglected the till layer. As noted above, the preliminary computer modelling showed that a three-layer model (as in Figure 11) could reasonably simulate the experiment. Neglecting the till layer may result in an error in the estimate of the second boundary condition step magnitude, B_2 (see Figure 11 and Figure 10). However, this value, B_2, applies over the depth range from 15.5m to 21m, which is only 9.8% of the total depth range – and the till layer is only a fraction of that range. (A library search did not reveal a conclusive source with information on the depth and thickness of the till layer.) Therefore, the error associated with neglecting the till layer would have to be extremely large to effect the overall results or the value of B_2.

The parametric study will consider the effect of variations in material properties in the top three modelling layers. It will establish value ranges to investigate based on the material types within those layers. A compilation of data from a number of sources will provide the limits of these ranges because no single source tabulates all of the required information. However, this only applies to the layers where there is thermal response data. Consequently, the properties of the M_∞ layer will remain constant throughout this study.

The reason for excluding the effect of thermal property variations in the M_∞ layer is the lack of data in or near that layer. There is no data below the boundary of the third layer. In addition, there is little or no temperature response within 10m of the bottom of the measurement depth. Consequently, this study cannot investigate the effect of thermal property variations bellow the measurement domain. The model includes the M_∞ layer as

a representation of the continuity of ground below the experimental domain for the continuity of the model.

The initial and boundary conditions come primarily from the experiment and the physical domain. Where they do not, the parametric study will estimate them. The initial condition comes from measured temperature data. The condition on the bottom and right hand sides of the model is that the domain extends to infinity. Heat cannot transfer infinitely far from its source in a finite amount of time, through a medium of finite diffusivity. Therefore, Temp/W uses special shape functions in the mesh of the infinite elements to approximate this condition (Bettess, 1992). The boundary condition on the top comes from experimental data at 4.67m depth and 5m depth (orange and red lines in Figure 11) to account for any heat transfer occurring with the earth above 5m depth.

The left boundary condition is unknown. Determining this boundary condition forms part of the parametric study of the present computer modelling investigation. The model uses the stepwise distribution described in the conceptual model descriptions to represent the spatial variation in the boundary condition. The symbols B_1 to B_6 (see Figure 11) represent the values of the each of the boundary condition steps. Temp/W allows the user to apply a boundary condition in a number of ways. This model applies the boundary conditions, B_1 to B_6, to line segments, L_1 to L_6, which represent divisions of the inner modelling surface. The vertical divisions occur at 5m, 15.5m, 21m, 31.5m, 40m,52.5m, and 61m (see Figure 10 and Figure 11).The B values represent the strength of the thermal disturbance acting on the corresponding depth range line, L.

3.4 Material Properties

The thermal property information for the parametric study comes from a synthesis of the data from many sources with varying degrees of connection to the experimental site. Some property information came from direct thermal property investigations in the same geologic unit as the present study, within 1Km of the present experimental site. This study (Ferguson G. , 2004) included divided bar thermal conductivity measurement experiments of core samples. In other cases, the data came from standard tables, e.g. (ASHRAE, 2007). These sources provide the information for what constitutes typical ranges for the thermal properties the model requires. Water content is significant for the properties of underground, porous materials. Porosity measurements made either on campus (Ferguson G. , 2004), or in Southern Manitoba (Domenico & Schwartz, 1998) complete the material information. This study accounts for moisture content in the ground materials with the equations in Table 1.

Table 1 Composite Property Relations

$\lambda_{C,max} = \lambda_{S,max}(1-\eta_{S,min}) + \lambda_W \eta_{S,min}$ $\lambda_{C,med} = \lambda_{S,med}(1-\eta_{S,med}) + \lambda_W \eta_{S,med}$ $\lambda_{C,min} = \lambda_{S,min}(1-\eta_{S,max}) + \lambda_W \eta_{S,max}$
$\mathrm{VHC}_{C,min} = \mathrm{VHC}_{S,max}(1-\eta_{S,min}) + \mathrm{VHC}_W \eta_{S,min}$ $\mathrm{VHC}_{C,med} = \mathrm{VHC}_{S,med}(1-\eta_{S,med}) + \mathrm{VHC}_W \eta_{S,med}$ $\mathrm{VHC}_{C,max} = \mathrm{VHC}_{S,min}(1-\eta_{S,max}) + \mathrm{VHC}_W \eta_{S,max}$
$\alpha_{C,max} = \lambda_{C,max}/\mathrm{VHC}_{C,min}$ $\alpha_{C,med} = \lambda_{C,med}/\mathrm{VHC}_{C,med}$ $\alpha_{C,max} = \lambda_{C,min}/\mathrm{VHC}_{C,max}$

Table 2 Definitions of the symbols in Table 1

Symbols for the Properties of Pure Water	
λ_W	Thermal conductivity of pure water.
VHC_W	Volumetric heat capacity of pure water.
Symbols for the Solid Constituent Properties	
$\lambda_{S,min}$	Thermal conductivity of the solid constituent (clay, upper limestone, or lower limestone) – minimum value on the range of reasonable thermal conductivity values.
$\lambda_{S,med}$	Thermal conductivity of the solid constituent (clay, upper limestone, or lower limestone) – medium (average of min and max) value on the range of reasonable thermal conductivity values.
$\lambda_{S,max}$	Thermal conductivity of the solid constituent (clay, upper limestone, or lower limestone) – maximum value on the range of reasonable thermal conductivity values.
$\mathrm{VHC}_{S,min}$	Volumetric heat capacity (VHC) of the solid constituent (clay, upper limestone, or lower limestone) – minimum value on the range of reasonable VHC values.
$\mathrm{VHC}_{S,med}$	Volumetric heat capacity (VHC) of the solid constituent (clay, upper limestone, or lower limestone) – medium (average of min and max) value on the range of reasonable VHC values.
$\mathrm{VHC}_{S,max}$	Volumetric heat capacity (VHC) of the solid constituent (clay, upper limestone, or lower limestone) – maximum value on the range of reasonable VHC values.
$\eta_{S,min}$	Porosity of the solid constituent (clay, upper limestone, or lower limestone) – minimum value on the range of reasonable porosity values.
$\eta_{S,med}$	Porosity of the solid constituent (clay, upper limestone, or lower limestone) – medium (average of min and max) value on the range of reasonable porosity values.
$\eta_{S,max}$	Porosity of the solid constituent (clay, upper limestone, or lower limestone) – maximum value on the range of reasonable porosity values.

Symbols for the Composite Properties	
$\lambda_{C,min}$	Thermal conductivity of the composite (water plus clay, upper limestone, or lower limestone) – minimum value on the range of reasonable thermal conductivity values.
$\lambda_{C,med}$	Thermal conductivity of the composite (water plus clay, upper limestone, or lower limestone) – medium (average of min and max) value on the range of reasonable thermal conductivity values.
$\lambda_{C,max}$	Thermal conductivity of the composite (water plus clay, upper limestone, or lower limestone) – maximum value on the range of reasonable thermal conductivity values.
$\mathrm{VHC}_{C,min}$	Volumetric heat capacity (VHC) of the composite (water plus clay, upper limestone, or lower limestone) – minimum value on the range of reasonable VHC values.
$\mathrm{VHC}_{C,med}$	Volumetric heat capacity (VHC) of the composite (water plus clay, upper limestone, or lower limestone) – medium (average of min and max) value on the range of reasonable VHC values.
$\mathrm{VHC}_{C,max}$	Volumetric heat capacity (VHC) of the composite (water plus clay, upper limestone, or lower limestone) – maximum value on the range of reasonable VHC values.
$\alpha_{C,min}$	Thermal diffusivity of the composite (water plus clay, upper limestone, or lower limestone) – minimum value on the range of reasonable thermal diffusivity values.
$\alpha_{C,med}$	Thermal diffusivity of the composite (water plus clay, upper limestone, or lower limestone) – medium (average of min and max) value on the range of reasonable thermal diffusivity values.
$\alpha_{C,max}$	Thermal diffusivity of the composite (water plus clay, upper limestone, or lower limestone) – maximum value on the range of reasonable thermal diffusivity values.

The equations in Table 1 relate the properties of the composite material (C) to its solid (S) and Water (W) constituents. This study assumes that the moisture content is pure

water. As the properties of underground materials typically range from a minimum to a maximum value, the equations in Table 1 indicate how to calculate the minimum, maximum, and medium composite properties. These equations take into account the fact that water has the lowest thermal conductivity and the highest volumetric heat capacity of the underground materials. Measurements at the experimental site indicated that the water table was at 7.5m deep. This only affects the top 2.5m of the 56m domain from 5m to 61m depth. In addition, the effect is minimal because the bottom 2.5m of the semi-saturated region between 5m and 7.5m depth would be mostly saturated. Therefore, the formulae in Table 1 assume that the ground material is fully saturated throughout the domain.

The weighting factor (η_s) is the porosity of the solid material. Every unit of volume in a porous material contains a certain fraction of void space called porosity. Some fluid occupies these voids in the absence of a vacuum. Dry unsaturated ground materials have a gas, typically air, in the void space. When a ground material becomes saturated, a liquid, typically water, completely replaces the gas in the void spaces of ground materials.

The equations are general. The term λ_S represents the dry, unsaturated thermal conductivity of any one of the solid materials. Similarly, the symbol VHC_S represents the volumetric heat capacity of any one of the solid materials. The additional subscripts, max, med, and min denote the minimum, medium, and maximum values that research showed any one of the dry, unsaturated solid materials can have. The dry, unsaturated materials are clay, upper limestone, and lower limestone.

This thesis takes all of the materials as saturated because the majority of the depth under study is below the water table at 7.5m depth, and the small remaining portion is near this depth. The properties of the saturated materials are a composite of the properties of the solid, porous material and its water content. This investigation assumes that pure water occupies the voids of the solid, porous materials. The composite value of the thermal conductivity of any one of the materials is λ_C. Similarly, the composite value of volumetric heat capacity and thermal diffusivity are VHC_C, and α_C, respectively. The additional terms in the composite property equations are the thermal conductivity of stagnant pure water, λ_w, the volumetric heat capacity of pure water, VHC_W, and the porosity of the particular solid material, η_S. As before, the extra subscripts, max, med, and min denote the minimum, medium, and maximum reasonable values of the composite materials' property ranges.

The parametric study varies the value of the thermal properties within a set of ranges. This allows the parametric study to estimate the true value of each property because the results of the study will show which property combination results in the most accurate computer simulation of the experiment. According to Anderson and Woesner (1992), a parametric study that evaluates more than one material property is most effective when the study considers inter-combinations of the maximum and minimum of the extremes, as well as the medium case. Therefore, the material property test-matrix consists of combinations of the minimum and maximum thermal property values in the three layers where the study varies thermal properties. The material property combinations are described in Table 3Table 4, and given numerically in Table 5.

Some property information is more readily available than others. In some cases, there are direct measurements of relevant ground properties, such as thermal conductivity, porosity, and density made on-campus at the University of Manitoba, or throughout Southern Manitoba. Domenico and Shwartz (1998) give the porosity range and a single value for the thermal conductivity of Lake Agasiz clay, and Ferguson (2004) and G. A. G. Ferguson (personal communication, July 16, 2009) gives the porosity of the upper limestone aquifer, as well as the thermal conductivity at various depths within and beyond the range of this experiment. However, the other properties come from the closest matches given in ASHRAE applications (2007) (in Table 5 of their Chapter 32) and table 4-2 in the (GEO-SLOPE International, Ltd., 2008).

Table 3 gives all of the values used to derive Table 5, the property range table. The notes at the bottom of Table 3 indicate how all of the property values were derived. Figure 12, Figure 13, and Figure 14 show the relevant property measurements from G. A. G. Ferguson (personal communication, July 16, 2009). Value ranges were always preferred over single values for M_1, M_2, and M_3, except in the cases of water. The property value derivations assumed pure water. Properties for the fourth layer, M_∞, came from a combination of the averages of the values used in the other limestone layers and the direct measurements from G. A. G. Ferguson (personal communication, July 16, 2009).

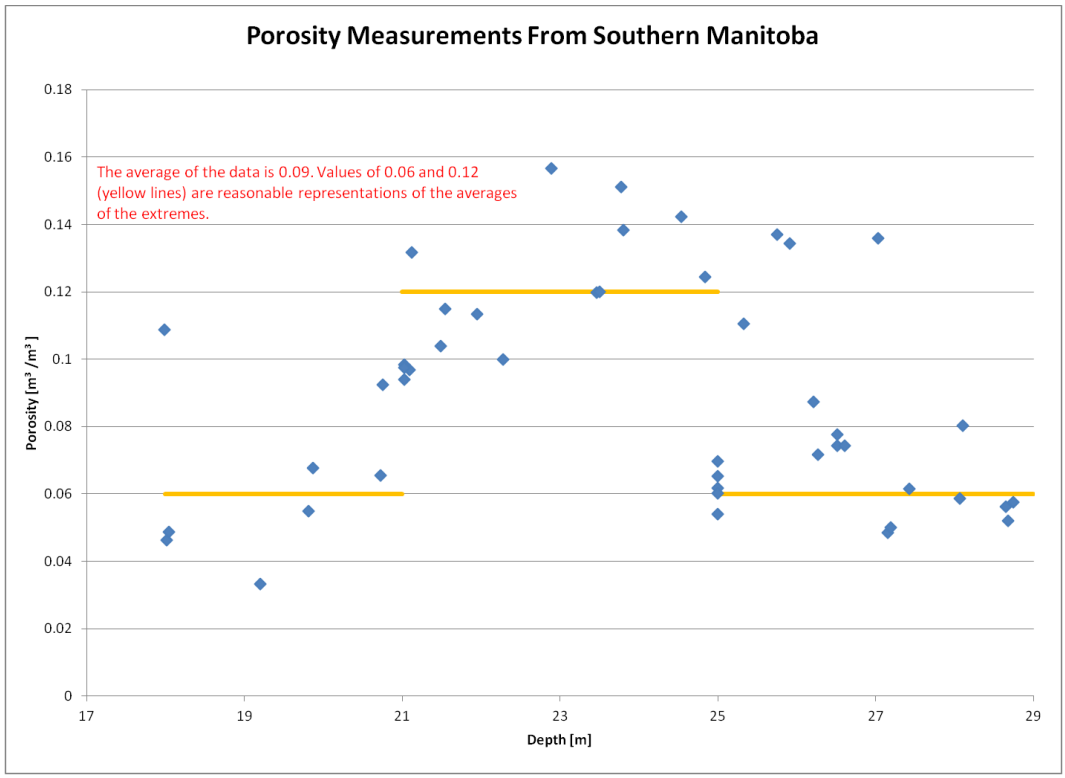

Figure 12 Direct Porosity Measurements from G. A. G. Ferguson (personal communications, July 16, 2009)

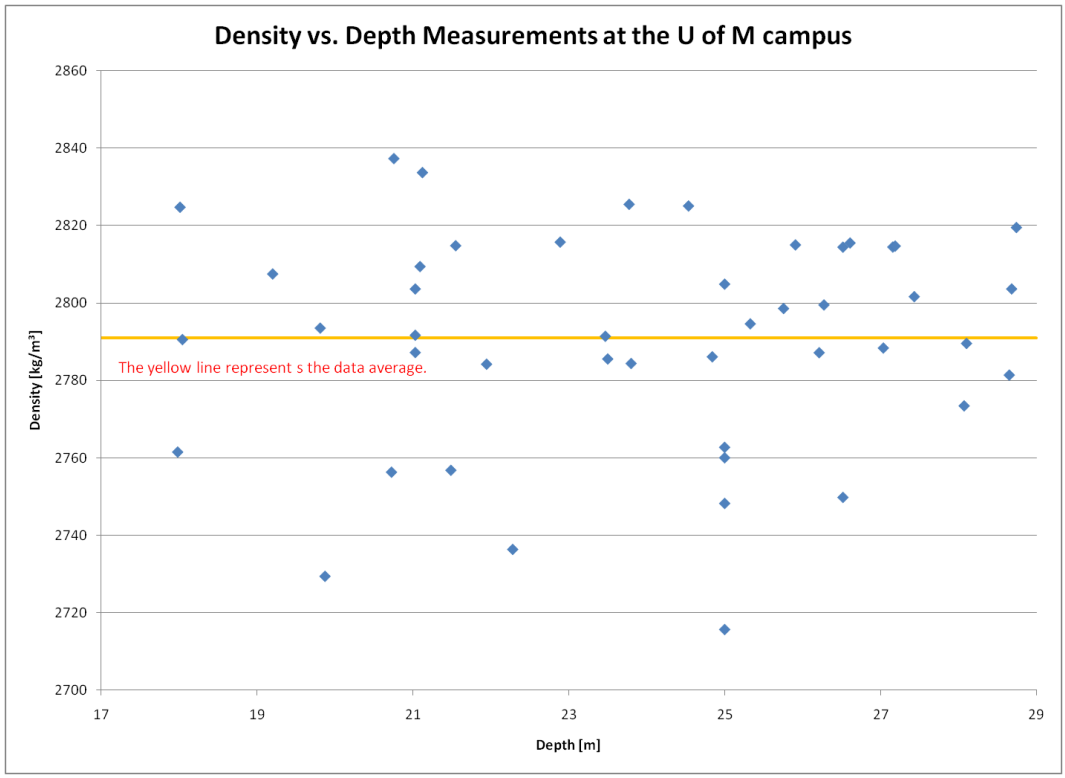

Figure 13 Direct Density Measurements from G. A. G. Ferguson (personal communications, July 16, 2009)

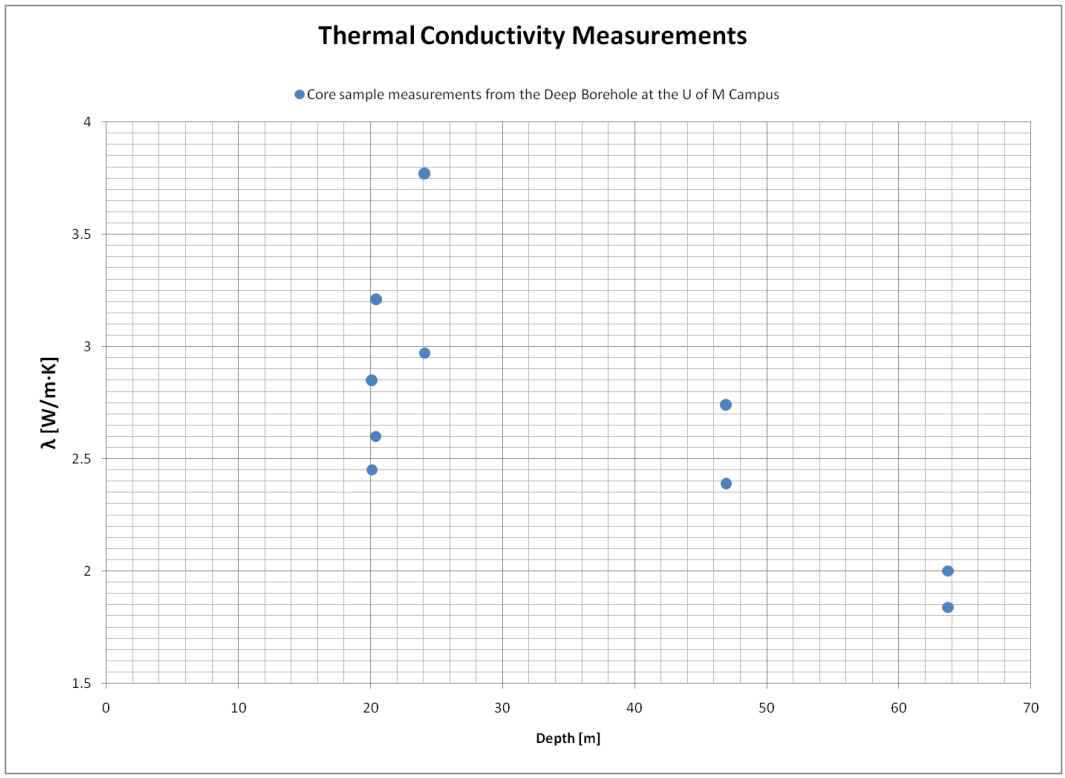

Figure 14 Direct Thermal Conductivity Measurements at the University of Manitoba from G. A. G. Ferguson (personal communications, July 16, 2009)

Constructing the value table required a number of assumptions. The property compilation assumed that the properties ASHRAE gives for heavy clay at 15% water content can be extrapolated to the 55% to 60% range found in the geologic region of the experimental site given in Domenico and Schwartz (1998). The 15% range from ASHRAE is used because the local thermal conductivity value of 1.2W/m·K falls within it, after correcting for water content. The density of limestone for the upper carbonate aquifer uses the full range given in ASHRAE (2007). The measurements from G. A. G. Ferguson (personal communication, July 16, 2009) fall within the range given in ASHRAE (2007). However, they were all so close together that their use would not have resulted in a property range for volumetric heat capacity. Thus, the effect of varying that property would not have been studied using the data from G. A. G. Ferguson (personal communication, July 16,

2009). In addition, this study assumed that the porosity measurements from G. A. G. Ferguson (personal communication, July 16, 2009) are applicable over all limestone in the analysis because his measurements did not include depths below 29m.

The following table (Table 3) summarises all of the property information from all of the various sources. This table includes both dry and saturated property values. The dry values come from a variety of sources, as indicated in the footnotes. The saturated values come from the formulae for composite properties from Table 1. The values in red are the final values that the parametric study uses in the series of models that determine the best property values for each layer. The tables in the next section reference these values, and Table 5 summarizes these directly.

3.5 Parametric Study Procedure

The parametric study focuses on two boundary condition types in two series of analyses. Both series represent vertical variation in the boundary condition as a step function, using the same depth intervals (L_1 to L_6). These steps only depend on depth. In the first series of tests, the step function represents a depth varying and time invariant heat flux (e.g. W/m^2). In the second series of tests, the step function represents a depth varying and time invariant temperature distribution. The value of the heat flux (in series 1) or the temperature (in series 2) varies from interval to interval and from test to test. The set of values of the boundary condition on line segments L_1 to L_6 are B_1 to B_6, respectively (see Figure 11). Chapter 4 section 2 tabulates these values, and the results of the parametric study.

The computer model only applies the thermal disturbance (flux or temperature) during the heating phase. The computer model simulates the natural recovery phase by applying a no-flux boundary condition on the inner surface of the domain, at the borehole surface. This assumption is consistent with the literature. The discussion covers a number of other possible models that were discarded and why they were discarded. The discussion also presents a third model that attempts to explain the shortcomings of the first two model-types with time varying B values for the duration of the model.

Table 3 Value Table for Property Range Calculations (Values in Red Appear in Table 4, also see Figure 4)

Material	Location	Name of Property Range	State	Minimum Value	Medium Value	Maximum Value	Units
Limestone	Common to all Limestone in the model	Porosity[3]	N/A	0.06	0.09	0.12	None
		Specific Heat Capacity	Dry[7]	1200			J/Kg·K
		Density	Dry[8]	2405	2605.51	2806	Kg/m^3
		Volumetric Heat Capacity	Dry[9]	2.89	3.131	3.37	$MJ/m^3 \cdot K$
			Satuated[2]	2.96	3.221	3.47	
	M_2 (Upper Aquifer)	Thermal Conductivity	Dry[3]	2.45	3.111	3.77	W/m·K
			Saturated[2]	2.23	2.88	3.58	
		Thermal Diffusivity	Saturated[4]	0.269	0.319	0.375	mm^2/s
	M_3 (Lower Aquifer)	Thermal Conductivity	Dry[3]	2.05	2.601	3.15	W/m·K
			Satuated[2]	1.87	2.420	3.00	
		Thermal Diffusivity	Satuated[4]	0.541	0.750	1.01	mm^2/s
	M_∞ (Lower Aquifer)	Thermal Conductivity	Dry[3]	1.92[10]			W/m·K
			Satuated[2]	1.80[11]			
		Thermal Diffusivity	Satuated[4]	0.558[11]			mm^2/s

Water	All	Thermal Conductivity	Saturated[12] Liquid @ 280K	0.582			W/m·K
		Volumetric Heat Capacity		4.198			$MJ/m^3 \cdot K$
		Thermal Diffusivity		0.139			mm^2/s
Clay	M_1	Porosity5	N/A	0.550	0.5751	0.600	None
		Thermal Conductivity	Dry6	1.526	1.832	2.137	W/m·K
			Satuated2	0.960	1.113	1.282	
		Volumetric Heat Capacity	Dry6	2.47	2.551	2.63	$MJ/m^3 \cdot K$
			Satuated2	3.42	3.491	3.57	
		Thermal Diffusivity	Satuated4	0.269	0.319	0.375	mm^2/s

1 Average of neighbouring values.
2 Using dry values and porosities indicated here.
3 G. A. G. Ferguson (personal com., July 16, 2009).
4 The ratio of thermal conductivity and volumetric heat capacity values in this table, by definition.
5 (Domenico & Schwartz, 1998).
6 Derived from (ASHRAE, 2007), Table 5, Heavy clay at 15%WC.
7 (GEO-SLOPE International, Ltd., 2008), Table 4-2.
8 From (ASHRAE, 2007), Table 5.
9 Derived from the product of density and specific heat capacity, by definition.
10 Average of values at 63.7m depth from G. A. G. Ferguson (personal communication, July 16, 2009).
11 Uses the medium value in a range.
12 (Incropera & DeWitt, 2002), Table A.6.

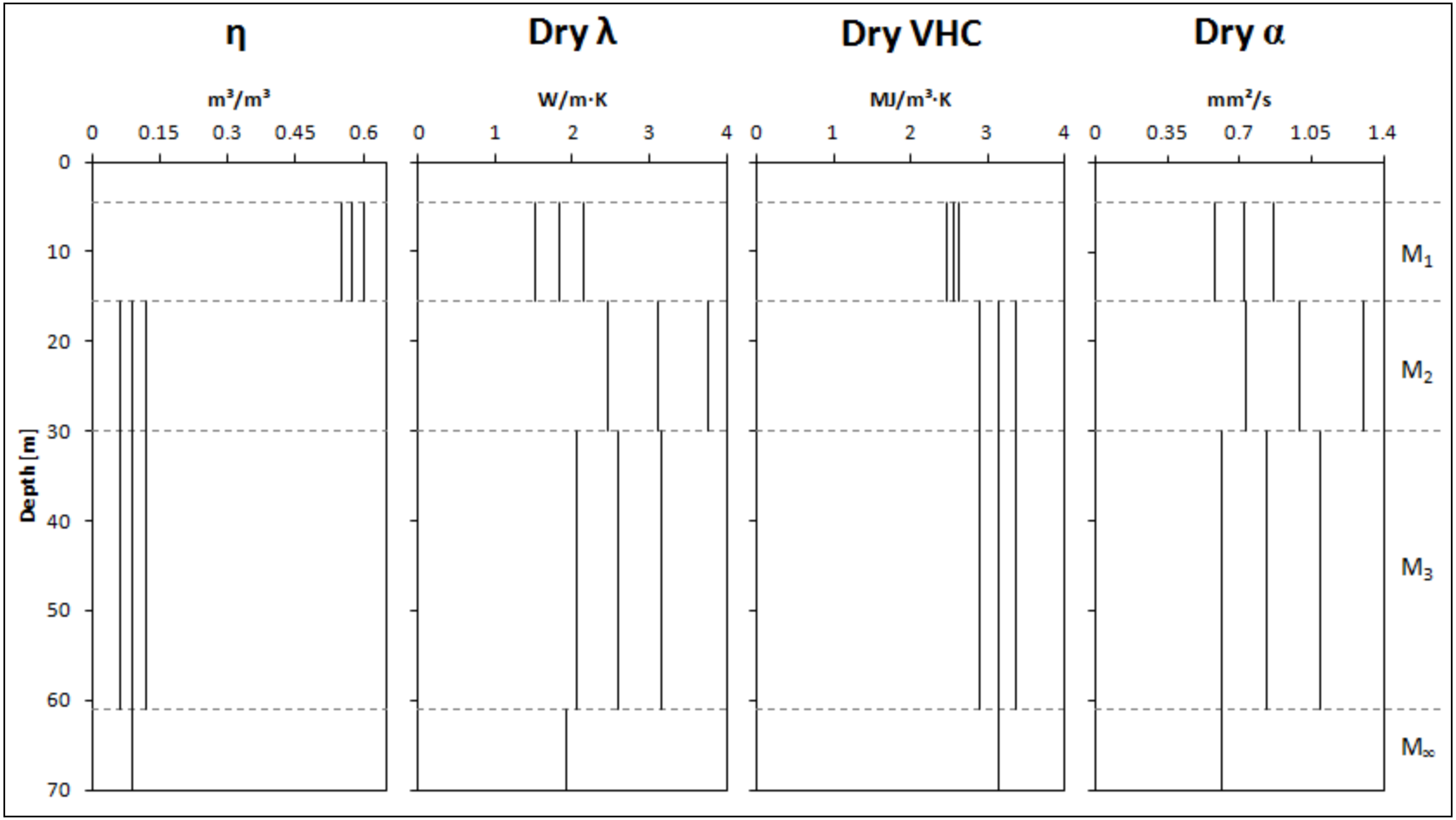

Figure 15 Diagram of the Thermal Properties Under Study - Dry Condition.

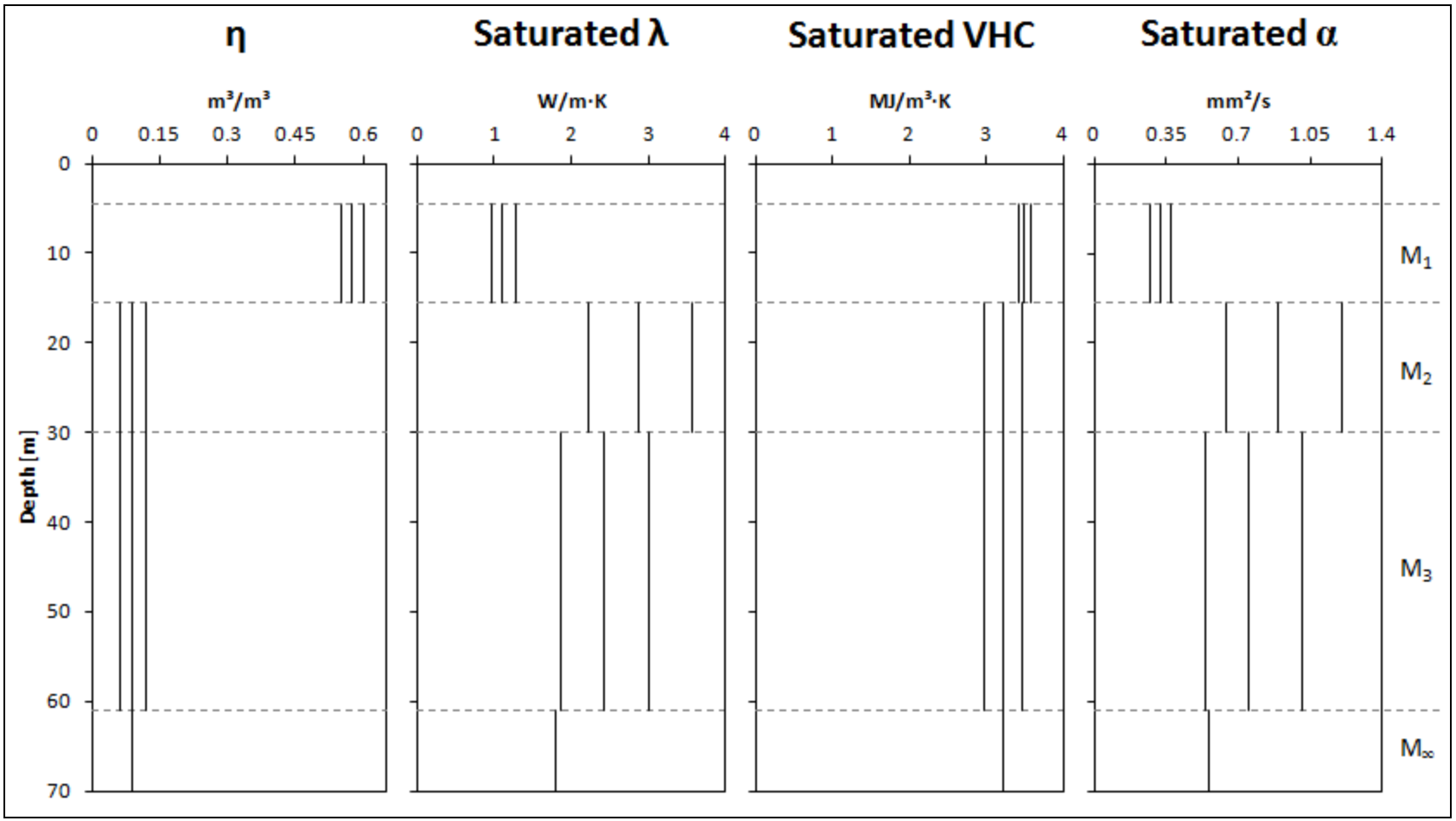

Figure 16 Diagram of the Thermal Properties Under Study - Saturated Condition.

The structure of the parametric study is the same for both model types. The model starts with one of the material property combinations from Table 5 and proceeds to optimize the boundary condition values, B1 to B6, on each of the boundary condition line segments, L_1 to L_6. The optimization procedure is repeated until all of the material property combinations have been tried. Finally, the optimized models are compared to determine select the overall best model. The discussion contains these results as well as a conclusion regarding which boundary condition type is preferred.

The variation in the boundary condition values used in the optimization comes from a set of calibration coefficients, as recommended by Anderson and Woesner (1992). The calibration coefficient is a multiplier applied to the initial value used in an optimization. These multipliers form a test matrix for the optimization variable, which is the set of boundary condition values. The calibration coefficients themselves form a dimensionless independent variable for use in the minimization. This gives a common way of comparing results from various boundary condition types. Chapter 4, section 2 presents the detailed procedure for both the flux and temperature boundary condition types.

Table 4 Material Property Combinations under Study (see Figure 11 and Table 3)

Combination	Thermal Conductivity (λ) Values by Material				Volumetric Heat Capacity (VHC) Values by Material				Thermal Diffusivity (α) by Material			
	M_1	M_2	M_3	M_∞	M_1	M_2	M_3	M_∞	M_1	M_2	M_3	M_∞
A	med	med	med	med	med	med	med	med	med	med	med	med
B	min	min	min		max	max	max		min	min	min	
C	min	min	max		max	max	min		min	min	max	
D	min	max	min		max	min	max		min	max	min	
E	min	max	max		max	min	min		min	max	max	
F	max	min	min		min	max	max		max	min	min	
G	max	min	max		min	max	min		max	min	max	
H	max	max	min		min	min	max		max	max	min	
I	max	max	max		min	min	min		max	max	max	

Table 5 Material Property Values under Study (see Figure 11 and Table 3)

Combination	Thermal Conductivity (λ) Values by Material				Volumetric Heat Capacity (VHC) Values by Material				Thermal Diffusivity (α) by Material			
	M_1	M_2	M_3	M_∞	M_1	M_2	M_3	M_∞	M_1	M_2	M_3	M_∞
A	1.113	2.88	2.42	1.800	3.49	3.22	3.22	3.22	0.319	0.894	0.750	0.558
B	0.960	2.23	1.874		3.57	3.47	3.47		0.269	0.642	0.541	
C	0.960	2.23	3.00		3.57	3.47	2.96		0.269	0.642	1.011	
D	0.960	3.58	1.874		3.57	2.96	3.47		0.269	1.207	0.541	
E	0.960	3.58	3.00		3.57	2.96	2.96		0.269	1.207	1.011	
F	1.282	2.23	1.874		3.42	3.47	3.47		0.375	0.642	0.541	
G	1.282	2.23	3.00		3.42	3.47	2.96		0.375	0.642	1.011	
H	1.282	3.58	1.874		3.42	2.96	3.47		0.375	1.207	0.541	
I	1.282	3.58	3.00		3.42	2.96	2.96		0.375	1.207	1.011	

3.6 Summary

In summary, this chapter recapped the motivation for investigating the effect of vertical variations in material properties and temperature the ground temperature response. It provided experimental evidence for questioning the assumptions of uniform ground temperature response, constant ground thermal properties, and spatially uniform ground heat exchanger performance. The experimental results showed the difficulty with the assumption of uniform ground temperature response. These results were also noticeably different from an analytical solution to a realistic mathematical model of the assumptions of constant ground thermal properties and spatially uniform ground heat exchanger performance from Eskilson (1987) and Zeng, Diao, and Fang (2002). Therefore, the conceptual model for this thesis would have to relieve those assumptions and consider ground heterogeneity and depth variations in ground heat exchanger output. This defined the problem this thesis as characterizing the ground thermal response to heating by a deep vertical borehole heat exchanger.

With a conceptual model in hand, the next step was to obtain a solution framework. As an analytical solution would likely be intractable, computer modelling in Temp/W (GEO-SLOPE International, Ltd., 2007) provided the first part of the solution framework. However, the computer model required values for material properties for the materials within the modelling domain. These were only known within a range based on the material properties and porosity values within the various layers at the site. Furthermore, the exact nature of the heat exchanger output, as well as the depth-dependant magnitudes of this output, was also unknown. Therefore, the solution to the mathematical model

required a parametric study to obtain a good model of the experimental results. The results of this parametric study and the associated discussion comprise the next chapter.

Chapter 4 Results and Discussion

This chapter presents and discussed the results of the experiment (see Chapter 2) and the parametric study (see Chapter 3). This chapter begins by presenting the ground heating experiment and discussing the experimental observations. These are significant for evaluating the validity of the assumption of uniform ground temperature response to heating by a deep vertical borehole ground heat exchanger and for interpreting and evaluating the modelling of this thesis. The next section details the results of the parametric study. This includes a discussion of observations associated with this modelling. The chapter also considers alternative modelling scenarios. The final part of the chapter explores one of these more advanced alternatives. This alternative proves a more effective simulation of the experiment.

4.1 Preliminary Findings

One can make a number of observations from examining the temperature response data. The most prominent feature is the strong depth dependence of the temperature response, as in Figure 17, Figure 18, and Figure 19. A closer examination also reveals another interesting feature of the temperature response. The temporal behaviour of the temperature response varies throughout the depth. The time to measure the first temperature effect, the time to the maximum temperature, and, for the nearer observation well, the existence of either a distinct temperature peak or a flatter, plateau-like maximum are all features that vary with depth. Examining the data also shows that the temperature response depends strongly on radial distance from the heat exchanger, as one would expect. To visualize these phenomena, compare Figure 29, Figure 30, Figure 31, and Figure 32. However, the broadest vertical division in the temperature distribution is

between the majority of the depths that appear to experience temperature change strictly from heat pump operation, and those near the surface that appear also to feel solar heating and other meteorological effects.

4.1.1 Near Surface Range

Defining characteristics of the temperature response near the ground surface include a sharp decline in temperature (see Figure 18), and other effects that seem to result from solar heating and other meteorological phenomena. The temperature readings all occurred in the afternoon, during sunshine. The values at the ground surface ranged between 19°C and 34°C over the course of the measurement period. However, the range of minimum daily low and maximum daily high atmospheric temperatures for the same period was from 9.3°C to 29.4°C (Environment Canada, 2011). The monitoring wells are on the south side of the Geothermal Research Trailer, and in direct sunlight for much of the day. Therefore, the temperature measurement in the monitoring wells near the ground surface likely resulted from a combination of meteorological effects.

The present study recorded a temperature measurement at each of the measurement points to establish a base-line before activating the heat pump system. The initial temperature values in this study at 3m depth were 5.74°C in the nearer well and 5.51°C in the further well. These temperatures rose steadily throughout both the periods of ground heat exchanger operation and inactivity to a maximum of 7.86°C and 7.04°C in the respective wells at the end of the test. The temperatures at 3m depth at the beginning of the test for this study are very close to the arithmetic average of the undisturbed baseline ground temperature measured at the beginning of the test. The value of the average

baseline ground temperature is 6.00°C. The measurements from 0m to 3m depth are also the only range to show noticeable oscillatory behaviour. Therefore, 3m depth is one possible cut-off point where meteorological effects may no longer be significant on the timescale of this test.

However, the ground thermal behaviour that this study observed indicated that 5m depth is a more appropriate cut-off for the penetration of meteorological phenomena in the present experiment. The 3m cut-off depth is too shallow because there is another unique feature of the near-surface depth range that persists to 5m depth. This feature is continual temperature rise throughout the experiment. The graph in Figure 33 clearly shows both of these effects. Every depth range below 5m depth experiences a combination of at least two distinct temperature change phases. These include temperature increase, temperature decrease, and either a peak-like temperature maximum or a plateau-like maximum characterized by little temperature change (see section 4.1.2). Therefore, the first five metres of soil forms a definable, weather-affected zone relative to this study.

For completeness, this thesis also notes the subtle rise-and-fall of the undisturbed ground temperature throughout all of the sampled depths (see Figure 17). This might suggest that seasonal meteorological fluctuations eventually penetrate at lease as deeply as the measurements of this study. This study does not consider larger timescales. However, the computer modelling does use the actual measured data for the undisturbed ground temperature as the initial condition, rather than an average temperature. Therefore, the computer modelling will account for any minor contribution of this effect.

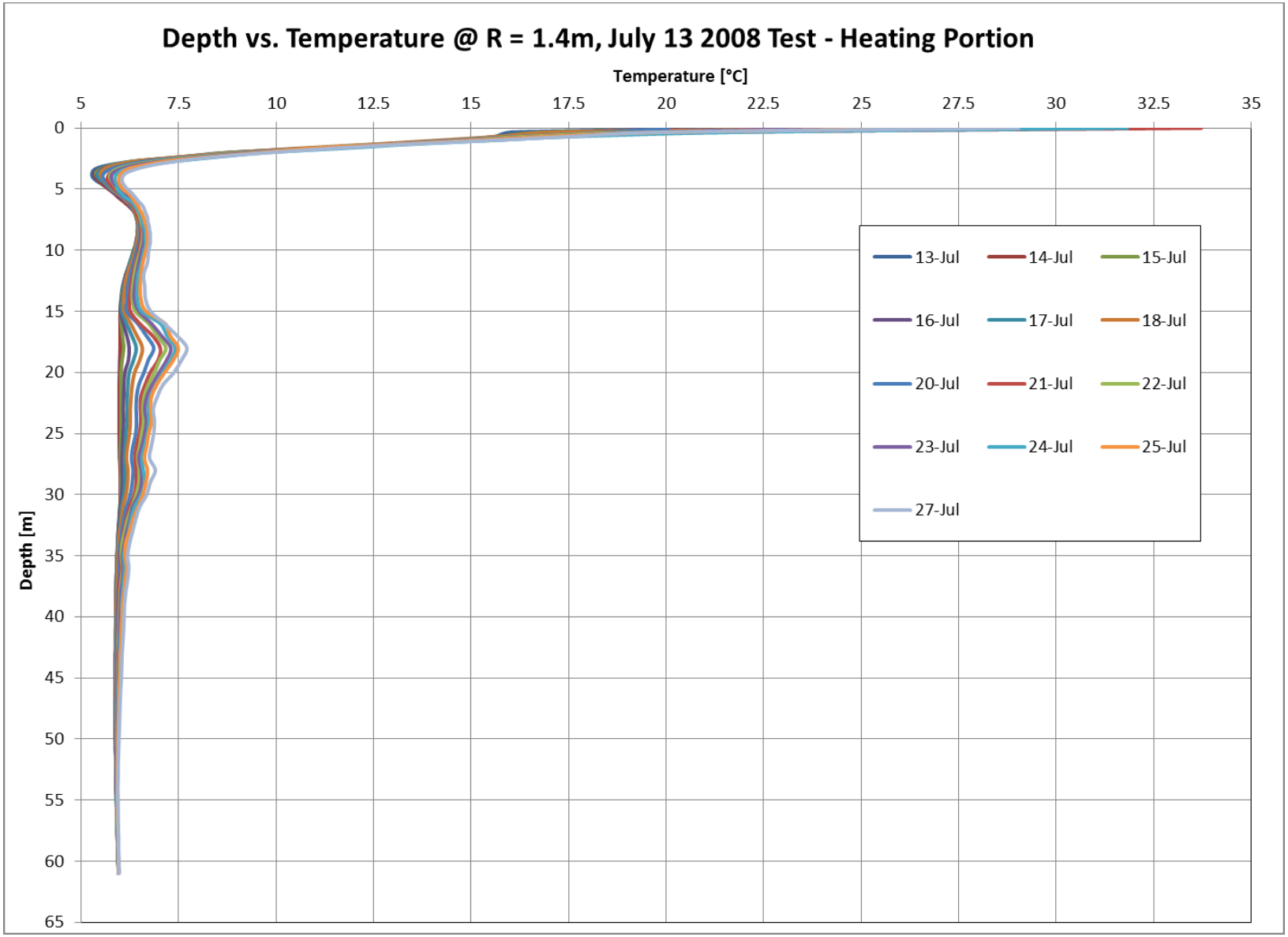

Figure 17 Ground temperature profile over time for the nearer observation well during the heating portion of the test.

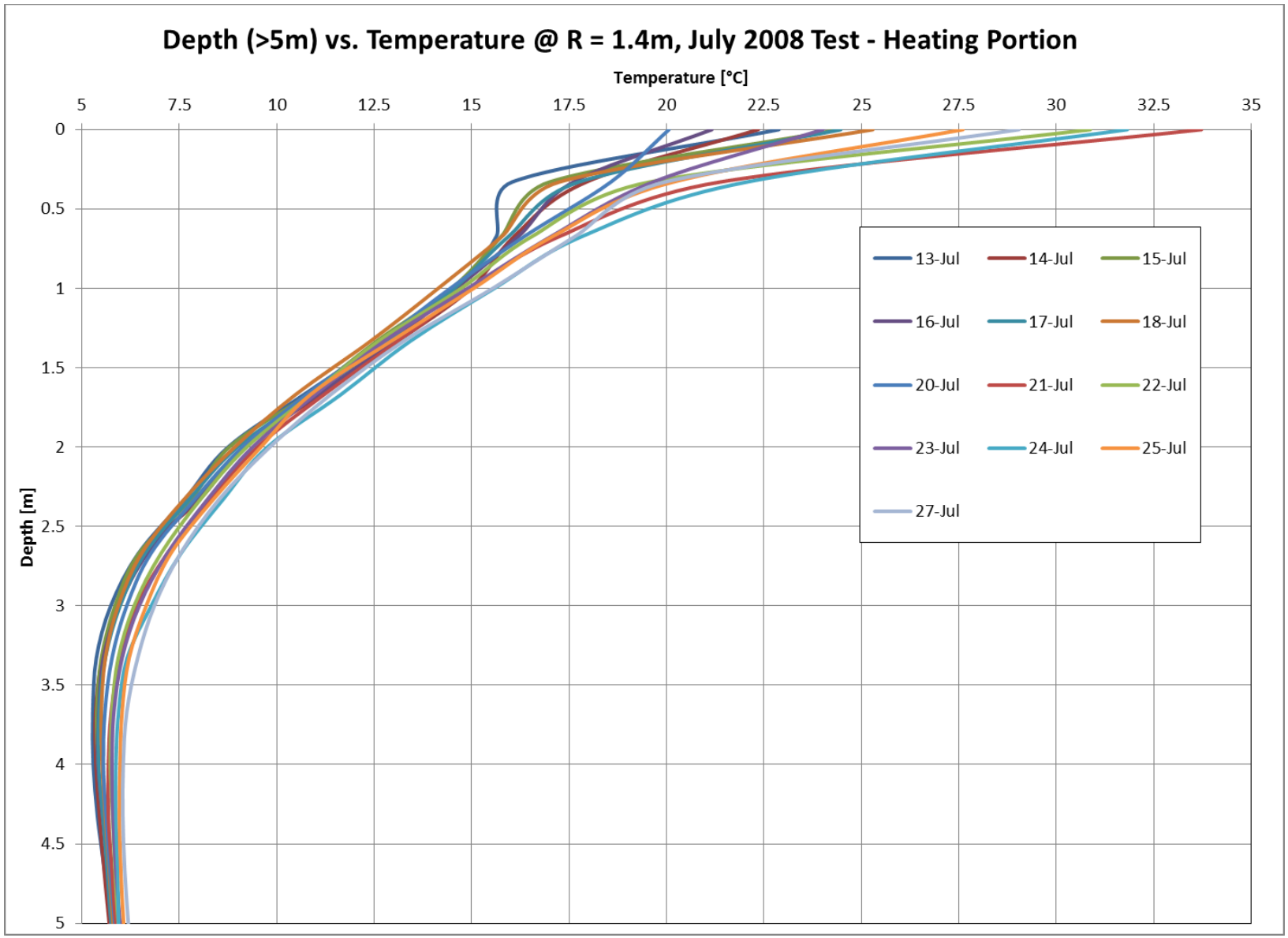

Figure 18 Reduced scale of Figure 17 to show detail.

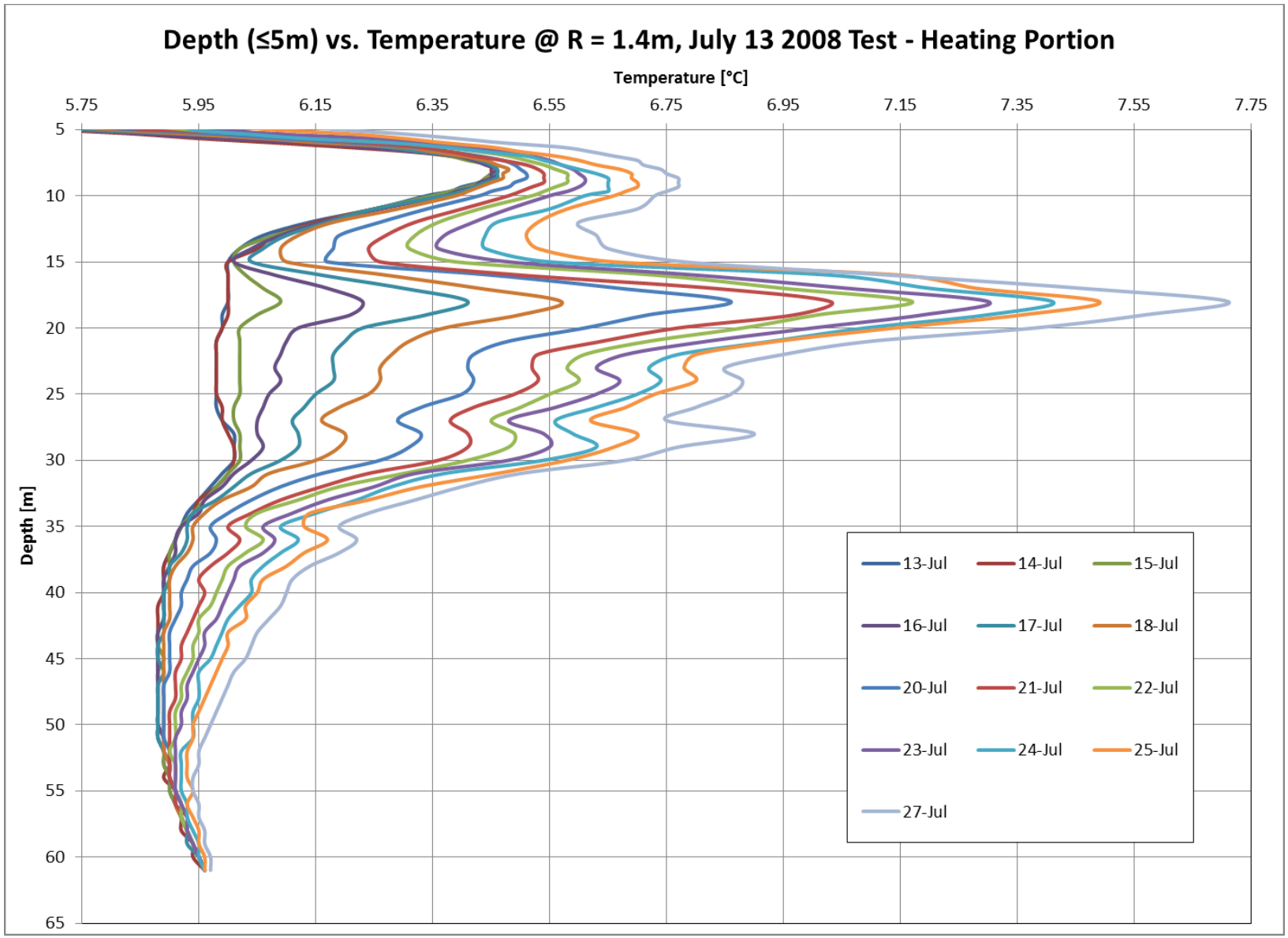

Figure 19 Reduced scale of Figure 17 to show detail. Note that increased temperature corresponds to increased time.

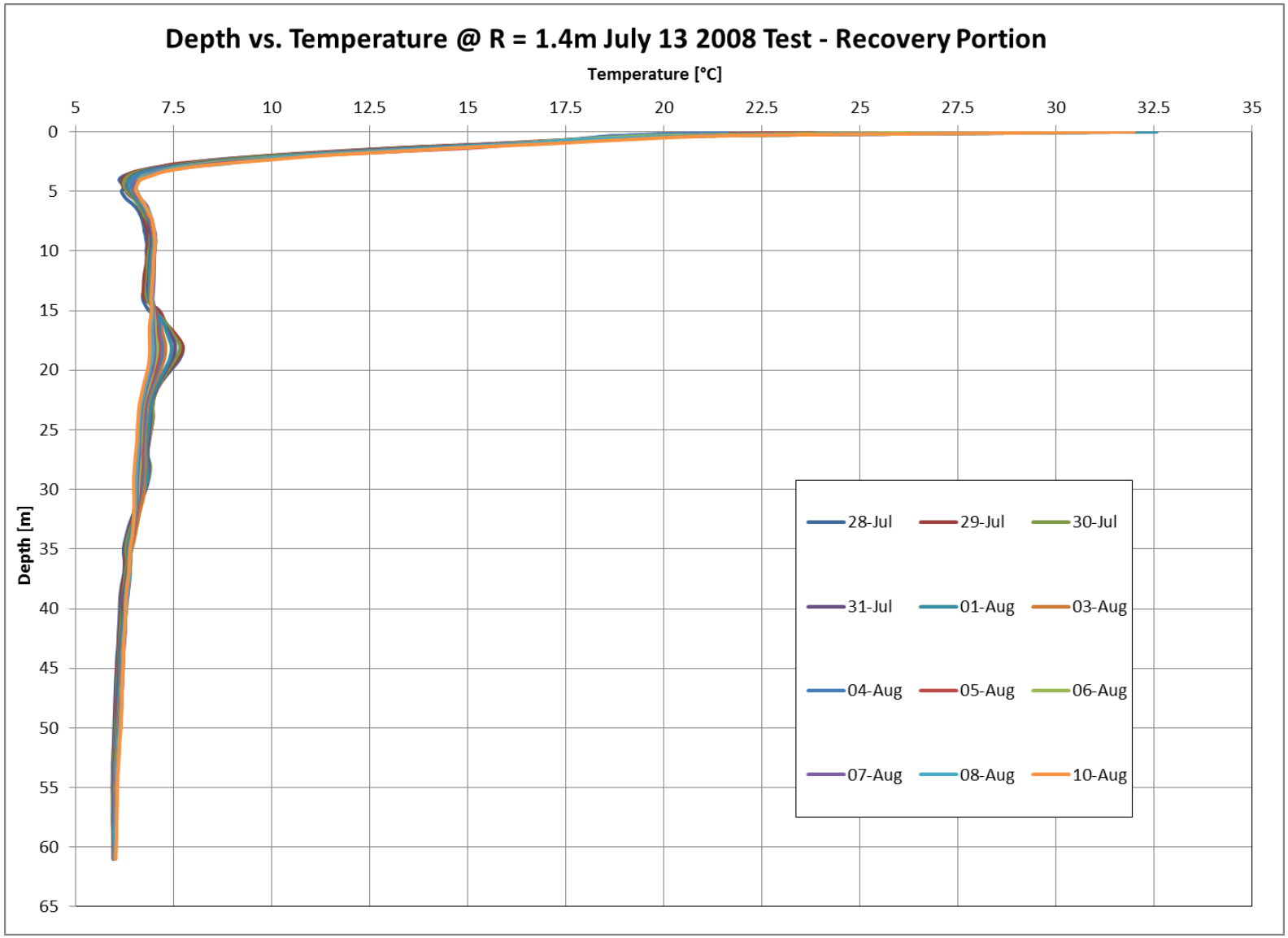

Figure 20 Natural ground temperature recovery phase in the nearer observation well.

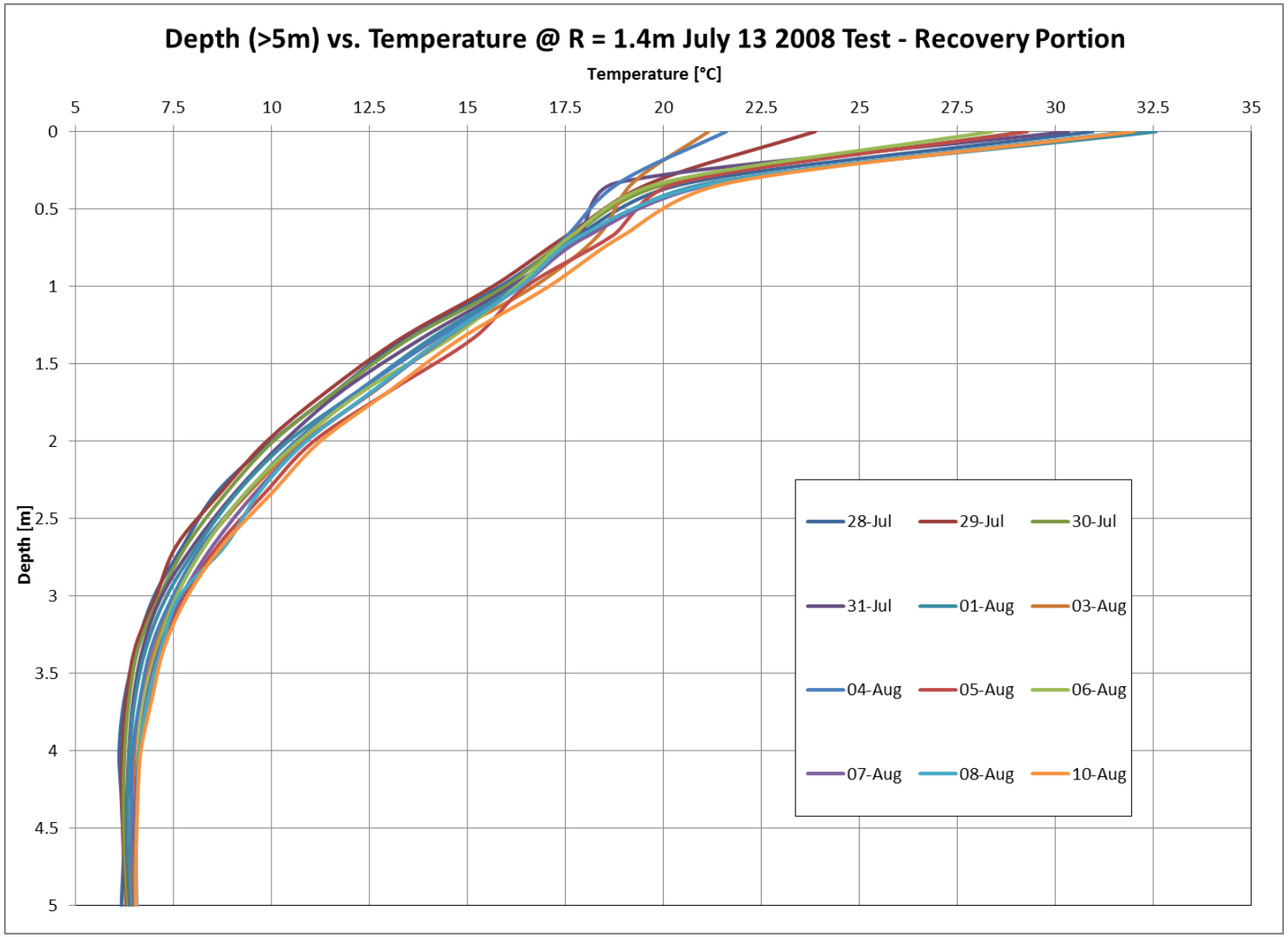

Figure 21 Reduced scale of Figure 20 to show detail. Note the continued temperature rise.

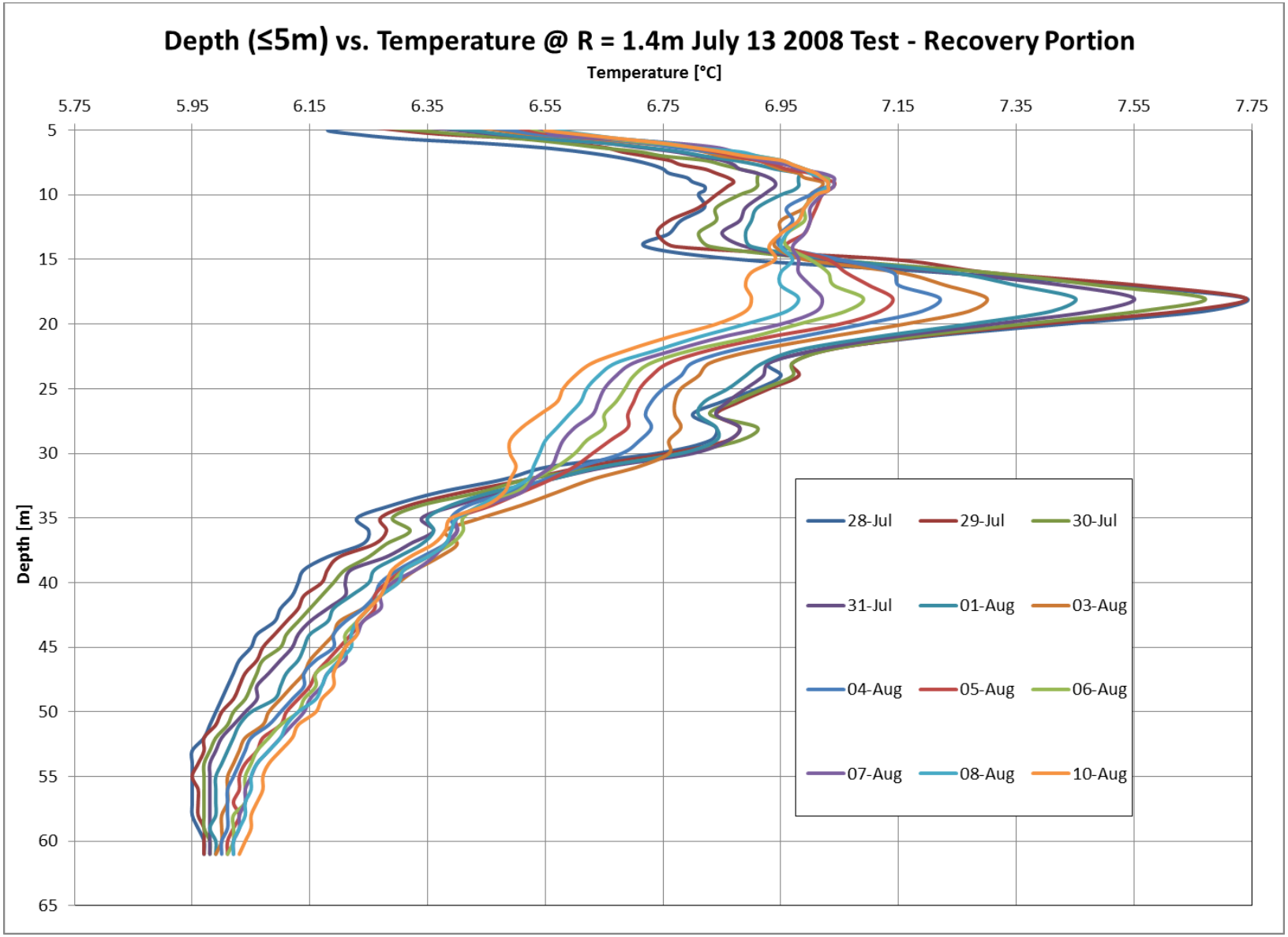

Figure 22 Reduced scale of Figure 20 to show detail. Note that the leftmost line in the mid-range is the rightmost line elsewhere. This is the 10-Aug line.

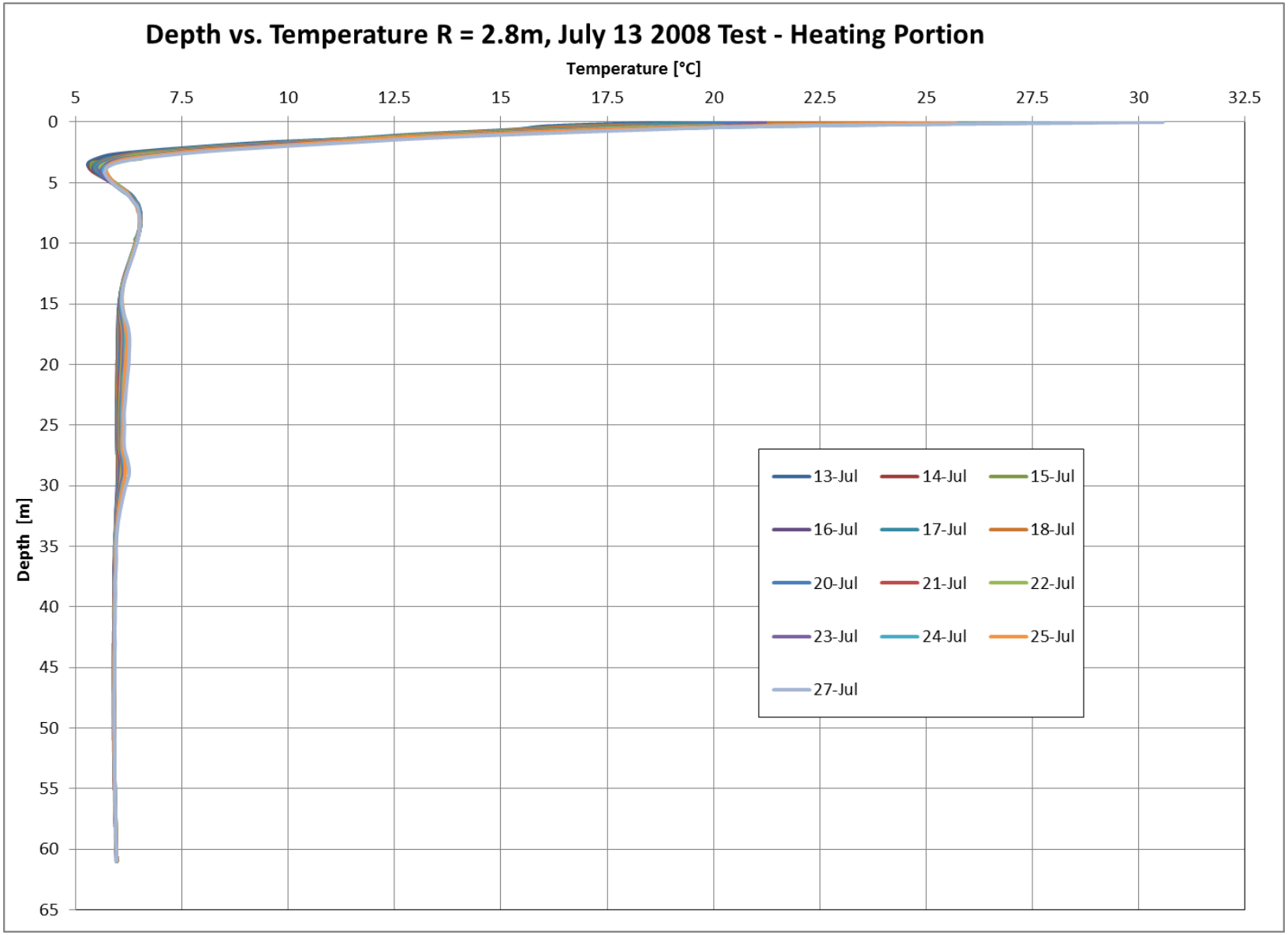

Figure 23 Ground temperature profile over time for the Farther observation well during the heating portion of the test.

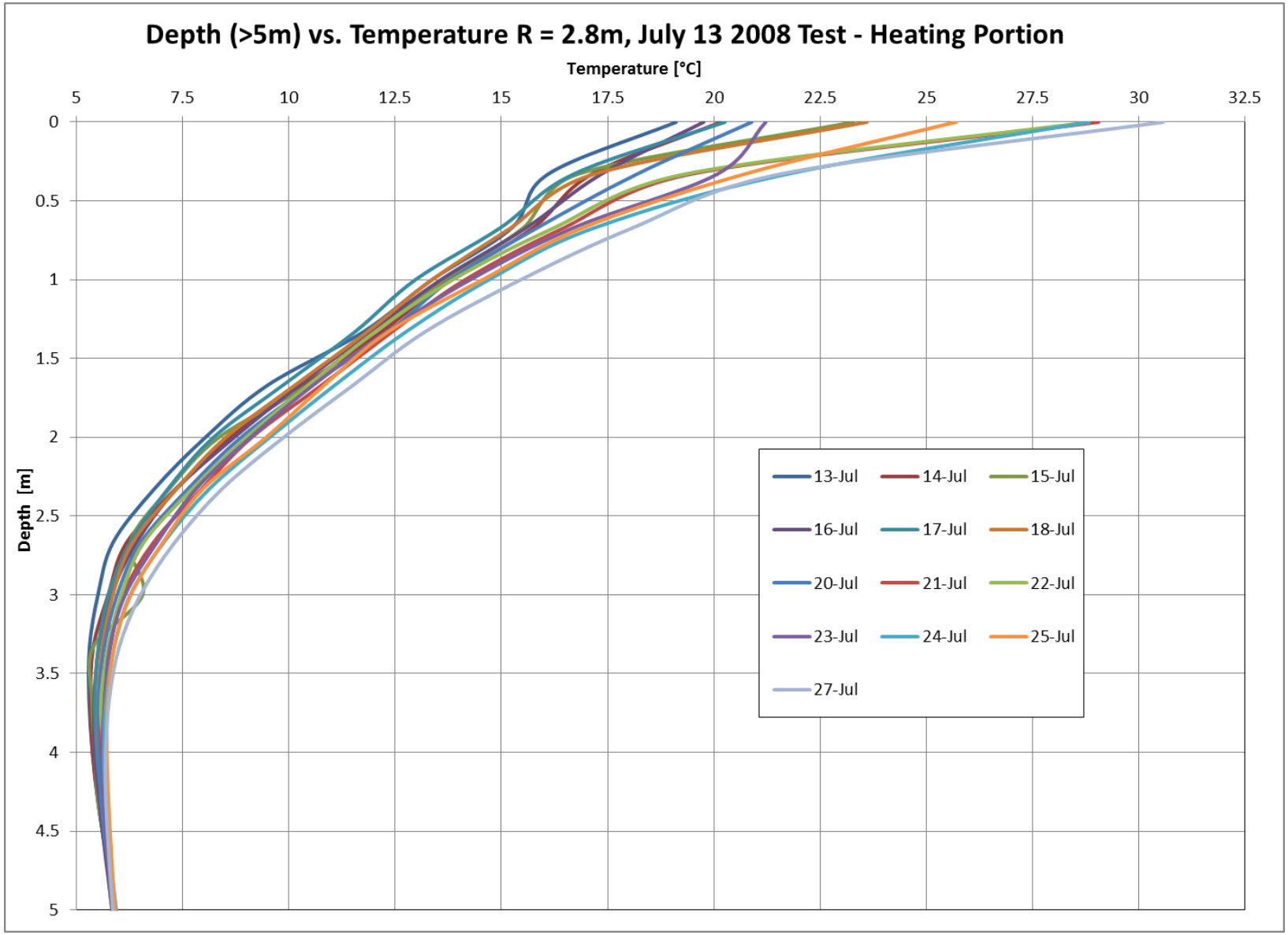

Figure 24 Reduced scale of Figure 23 to show detail.

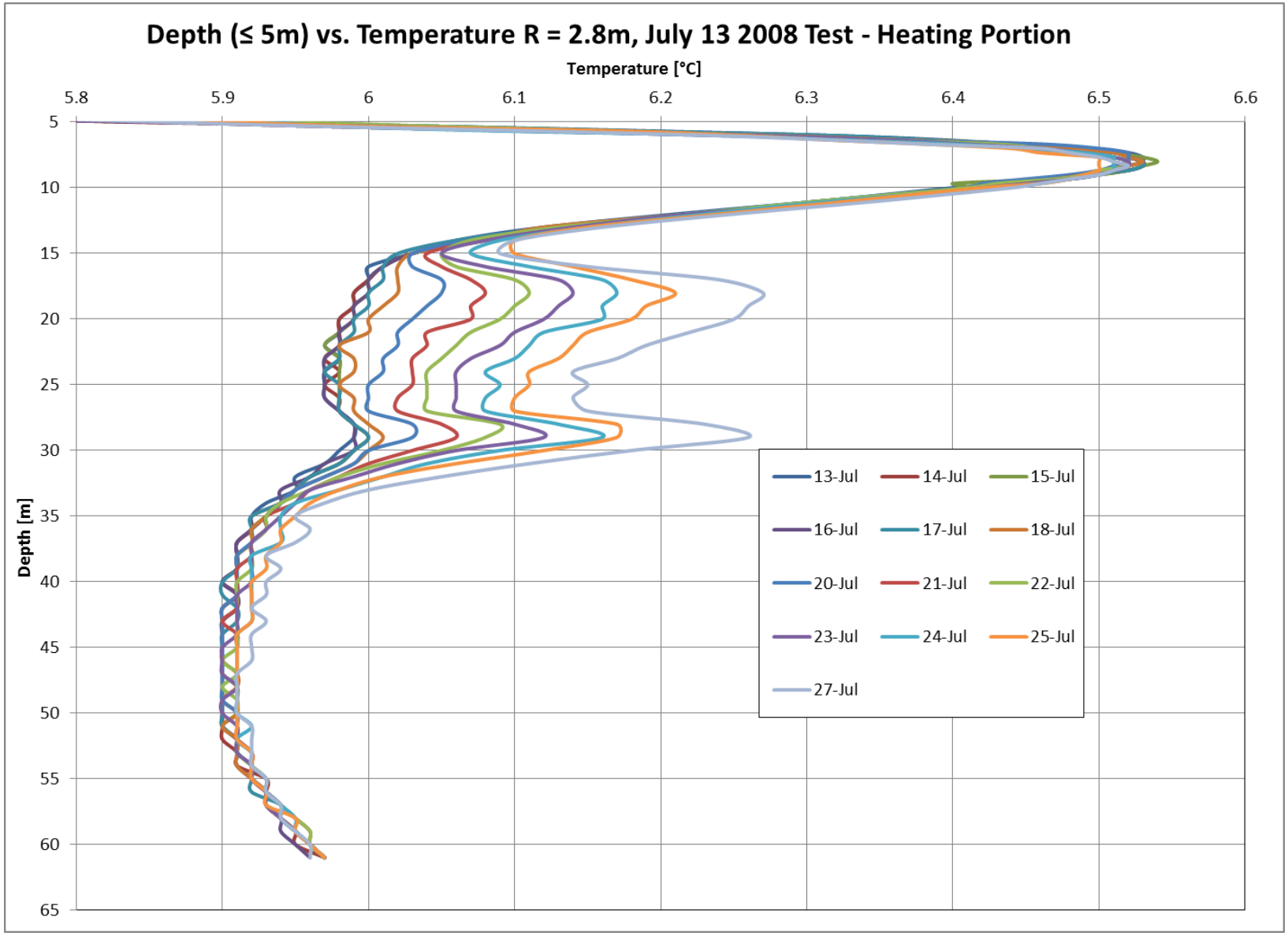

Figure 25 Reduced scale of Figure 23 to show detail. Note that increased temperature corresponds to increased time.

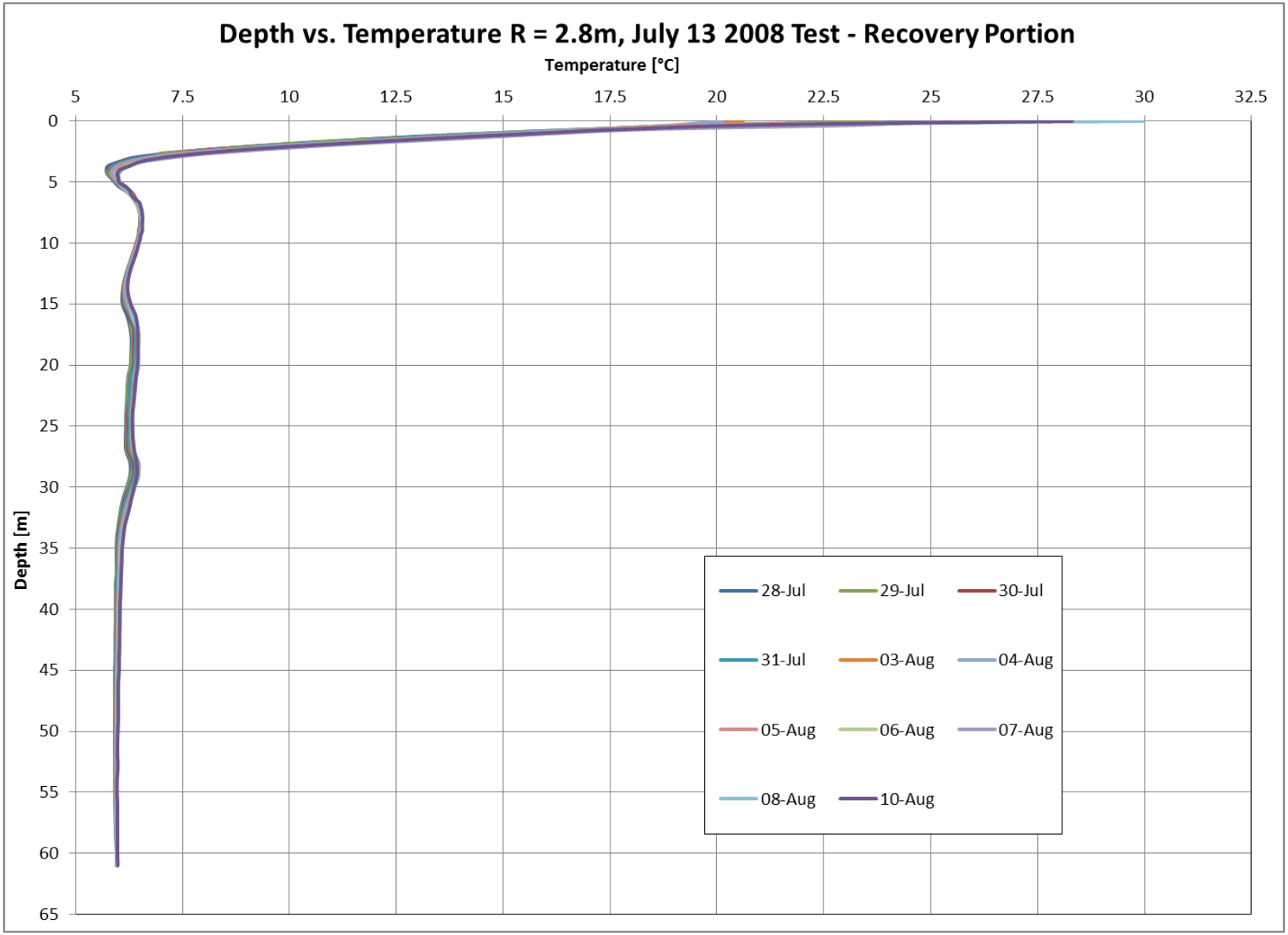

Figure 26 Measurements from the further observation well in the natural ground recovery phase.

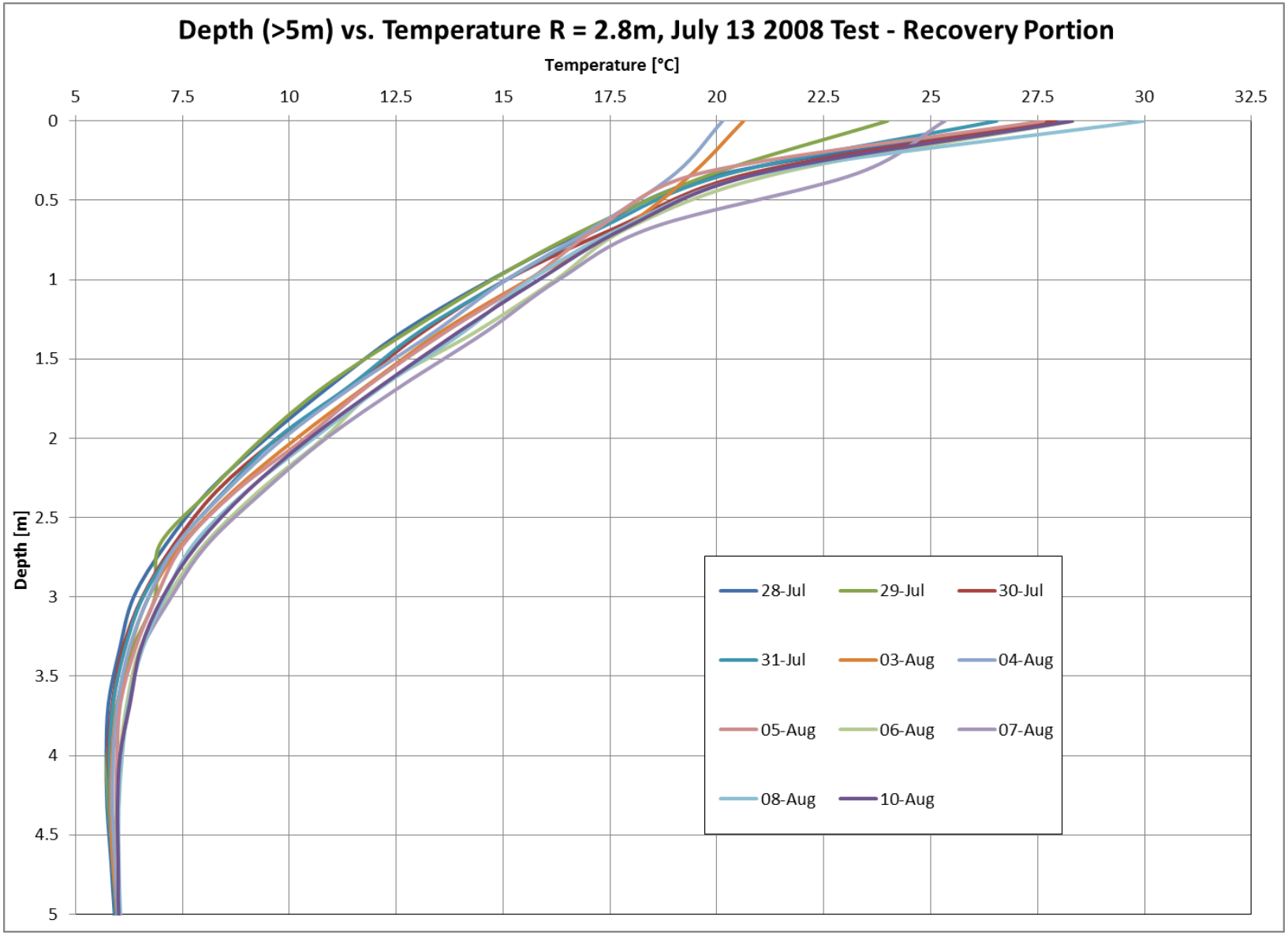

Figure 27 Reduced scale of Figure 26 to show detail.

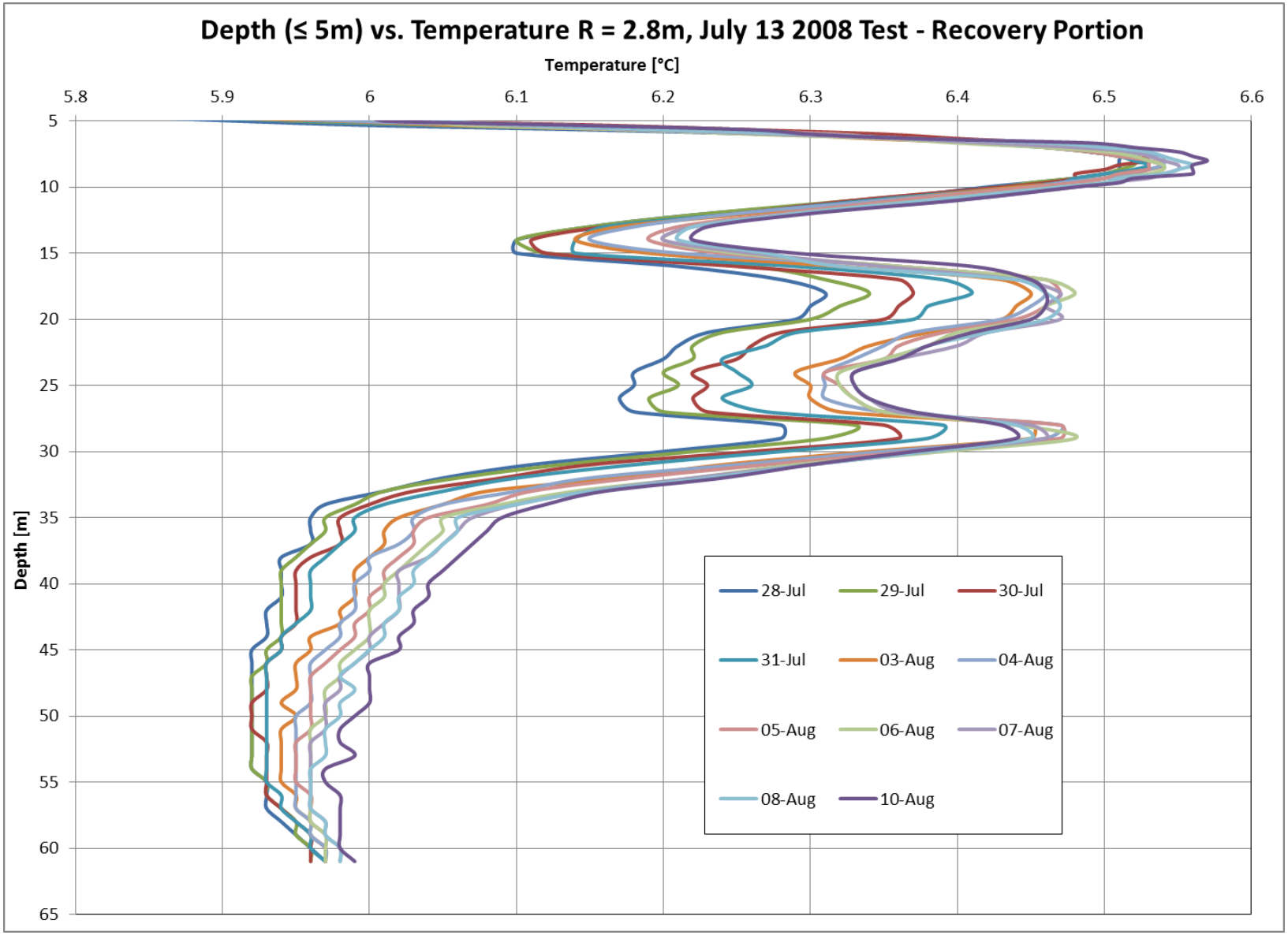

Figure 28 Reduced scale of Figure 26 to show detail.

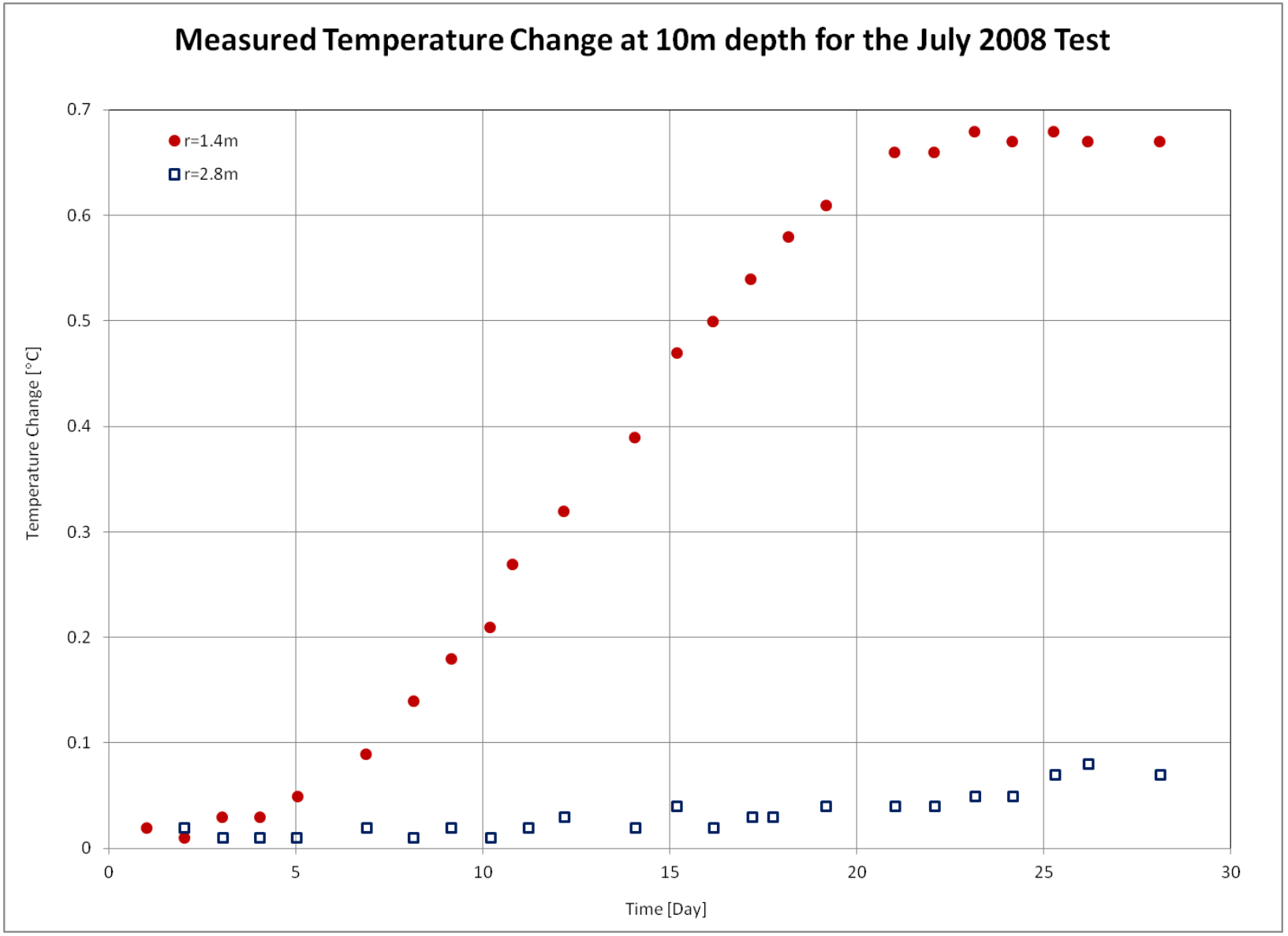

Figure 29 Measured temperature change (present temperature – initial temperature) at both the nearer and further observation wells at 10m depth.

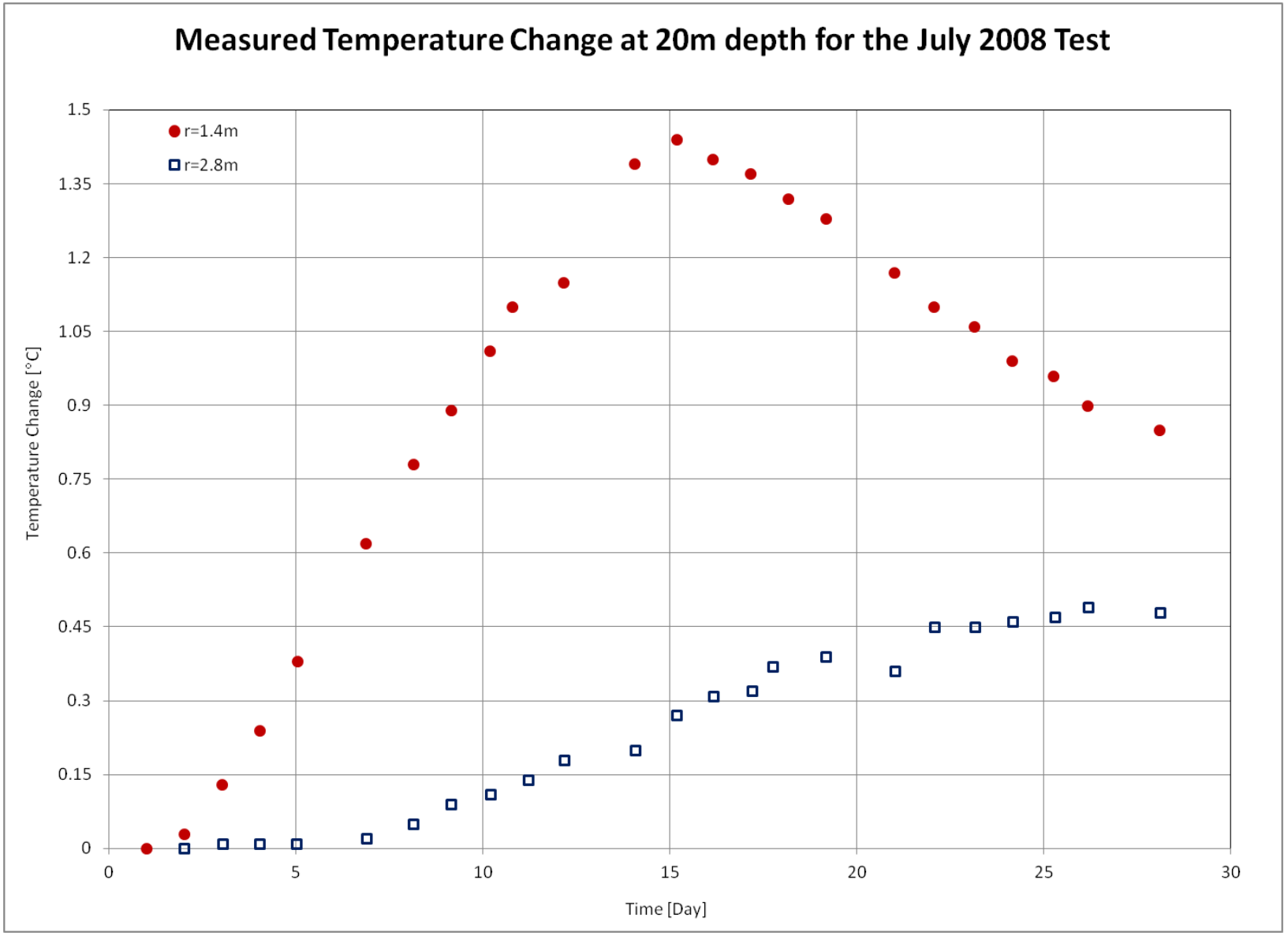

Figure 30 Measured temperature change (present temperature – initial temperature) at both the nearer and further observation wells at 20m depth.

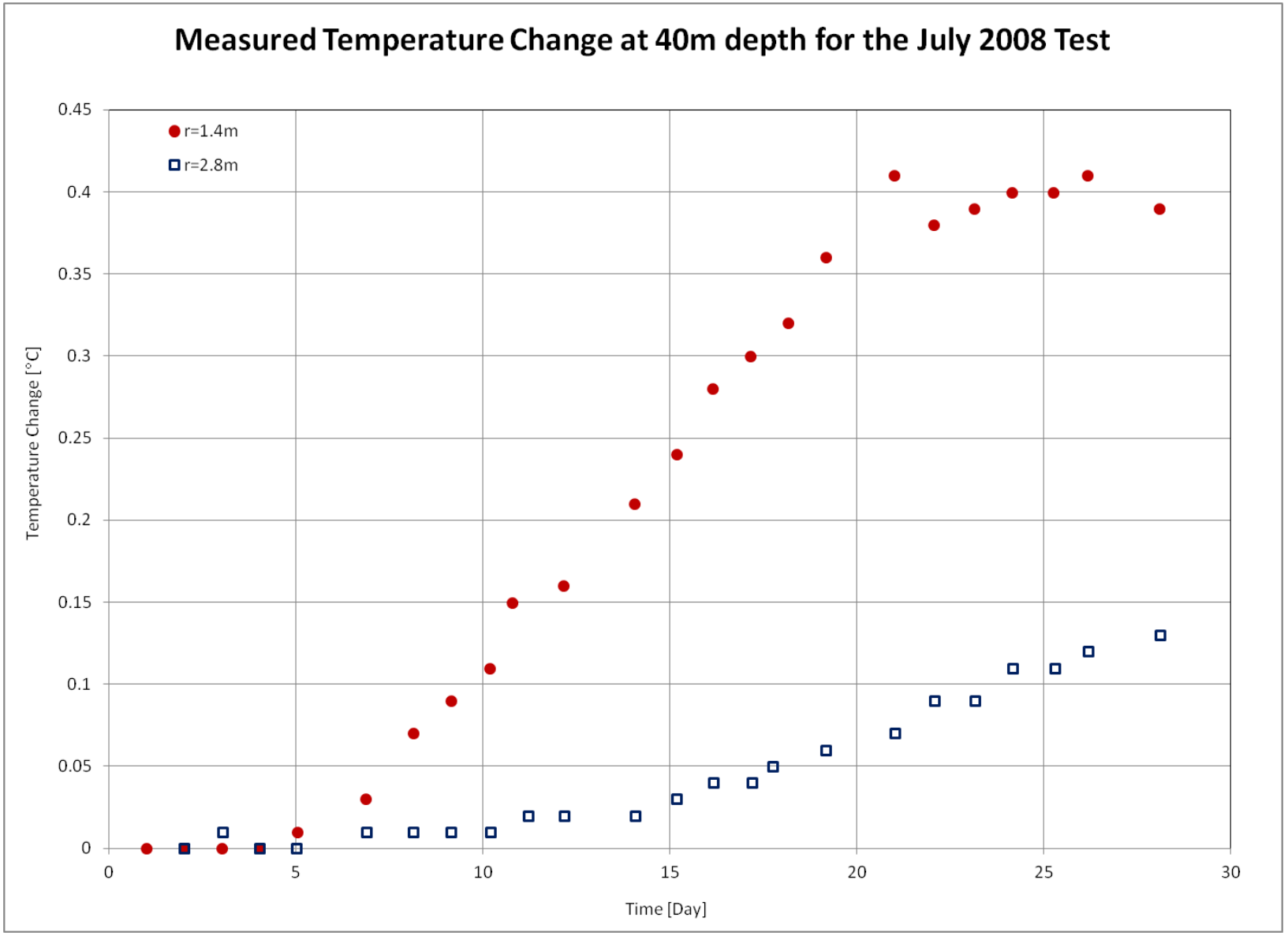

Figure 31 Measured temperature change (present temperature – initial temperature) at both the nearer and further observation wells at 40m depth.

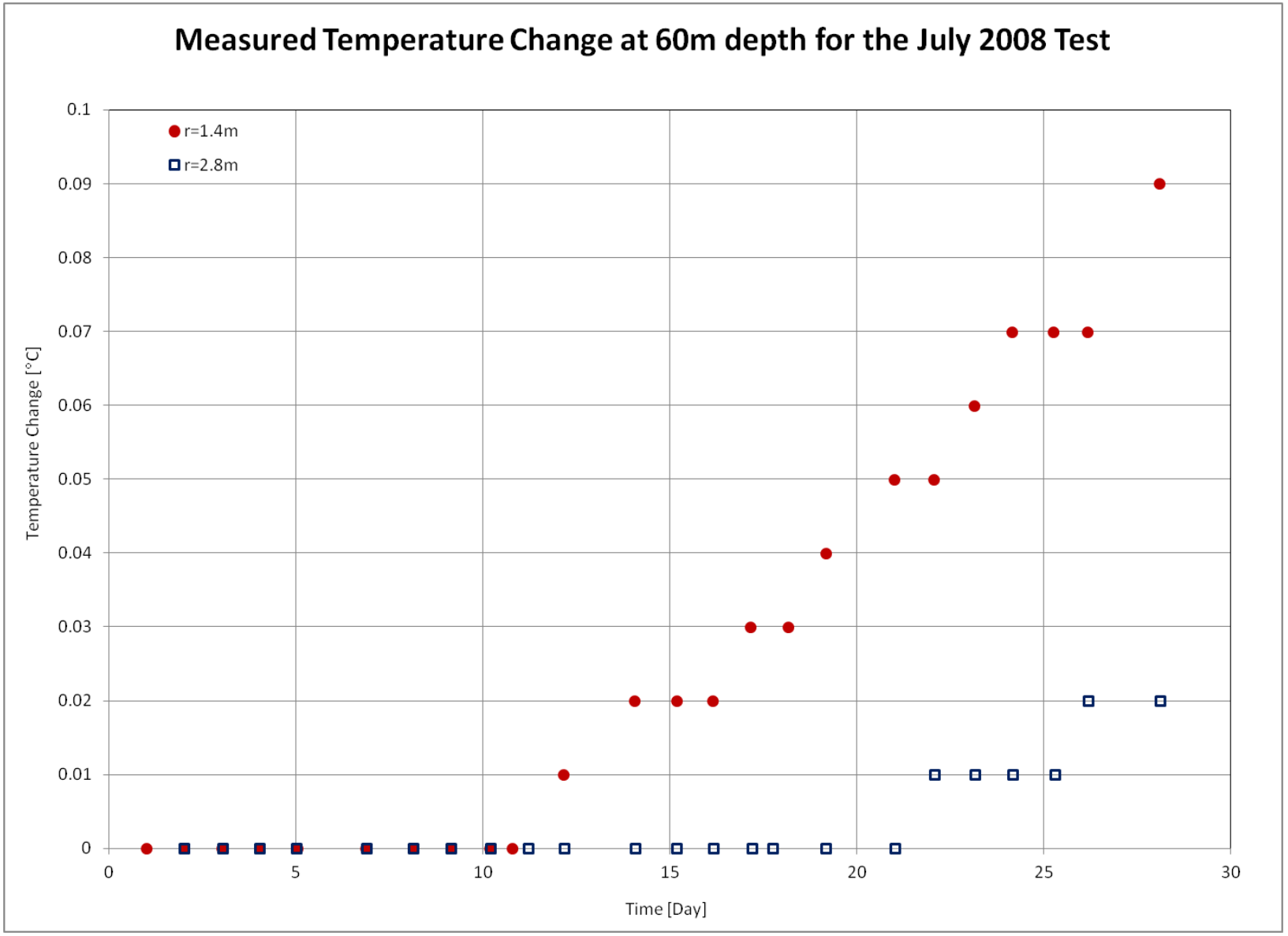

Figure 32 Measured temperature change (present temperature – initial temperature) at both the nearer and further observation wells at 60m depth.

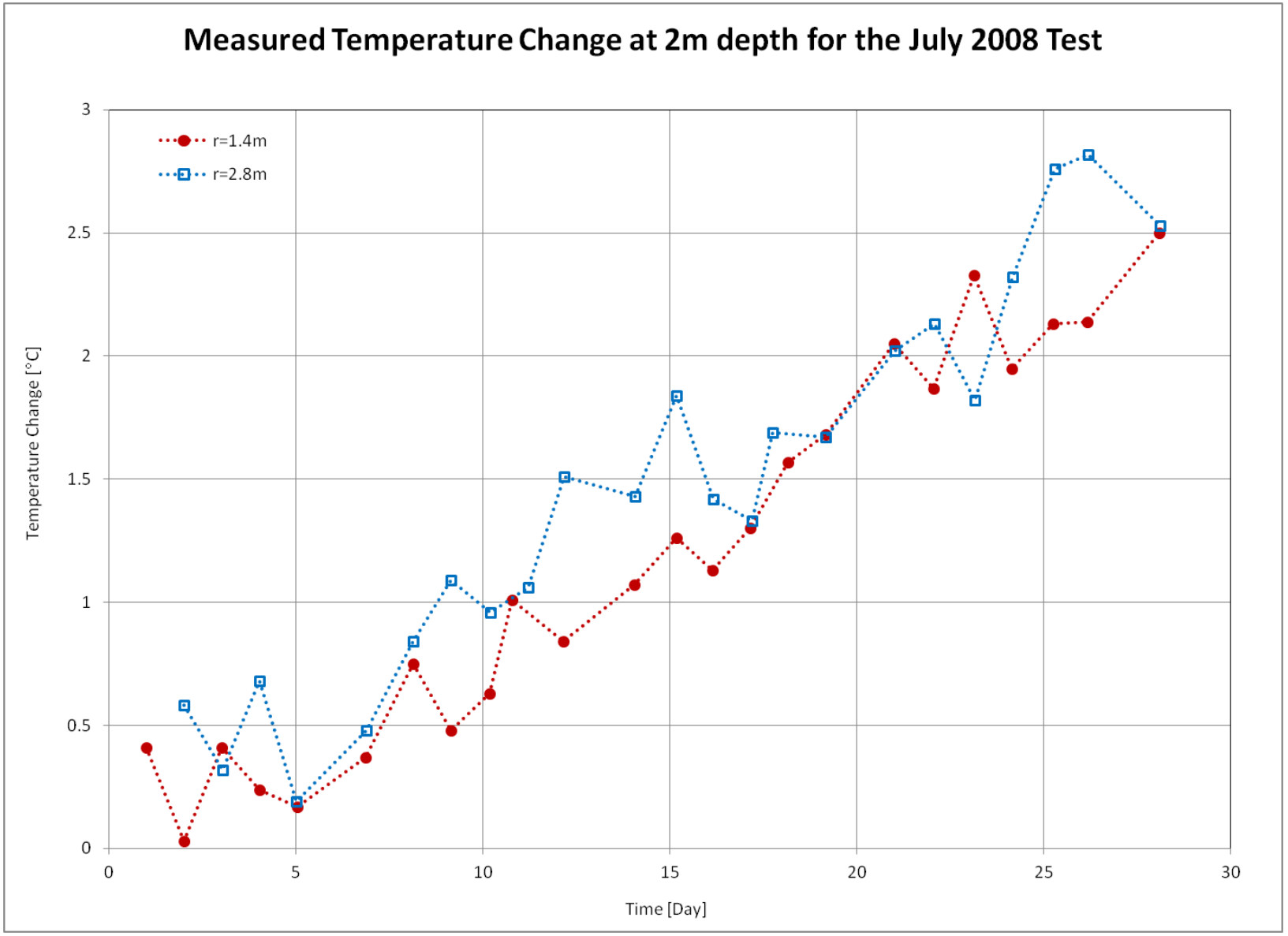

Figure 33 Temperature change at 2m depth that strongly shows both the oscillatory behaviour and continued temperature rise of the near surface region.

4.1.2 Deep Range

The results between 6m and 61m depth seem to divide into three intervals. These three intervals roughly correspond with the material stratification of the underground materials. These regions each have their own peculiarities. However, some of the features of the temperature response are common to more than one range. The measures of comparison are the relative magnitudes of the temperature responses, the times of the first temperature response, the time of the maximum temperature response, the trends in these response times, and the nature of the temperature response before and after the maximum. Please refer to Figure 29, Figure 30, Figure 31, and Figure 32 for examples of the observations that the following discussion describes.

The temperature response magnitude shows stratification that corresponds to the ground material stratification. The greatest temperature response magnitude occurred in the upper carbonate aquifer. The magnitude of the temperature response is the least in the lower carbonate aquifer. This is despite the fact that both of these aquifers consist of carbonate rock in the form of limestone or dolomite. The magnitude of the temperature response in the clay layer is in between the magnitudes associated with the two carbonate rock layers.

The time of the first temperature response, and the time of the temperature maxima also differ by material layer. All three layers have sub-regions where both the time of the initial temperature response and the maximum temperature response do not change rapidly with depth. Typically, the depths that are close to the boundary between material layers experience a transition where the behaviour in one layer transitions continuously to

the behaviour of the other. However, the majority of the lower limestone layer is in transition. The general trend in that layer is that these times increase with depth. Despite this, the time interval between the first temperature response and the maximum temperature response is consistent within each material, even where the other times are in transition.

The nature of the temperature maxima differs by depth. The maxima in the clay layer and the lower limestone layers are very flat. The maxima in the upper limestone layers form distinct temperature peaks. The maxima all occur after the end of heating time. The maxima in the upper limestone layer occur much closer to the end of heating time than in either of the layers physically above or below.

4.1.3 Analysis of the Heat Output of the Heat Pump Unit

The initial analysis showed that the power output of the Heat Pump Unit varied periodically in time after an initial phase. Figure 34 shows the data for the temperature difference (ΔT_f) between the temperature of the heat transfer fluid at the inlet ($T_{f,i}$) and outlet ($T_{f,o}$) of the Heat Pump Unit. The product of this value (ΔT_f), the heat transfer fluid's mass flow rate ($\dot{m}_f$), and the fluid's specific heat capacity ($c_{P,f}$) gives the heat output of the Heat Pump Unit ($\dot{Q}_{HPU}$). The graph also shows a comparison between the raw data and two curve fits. These curve fits attempt to reveal the nature of the bulk behaviour of the heat output.

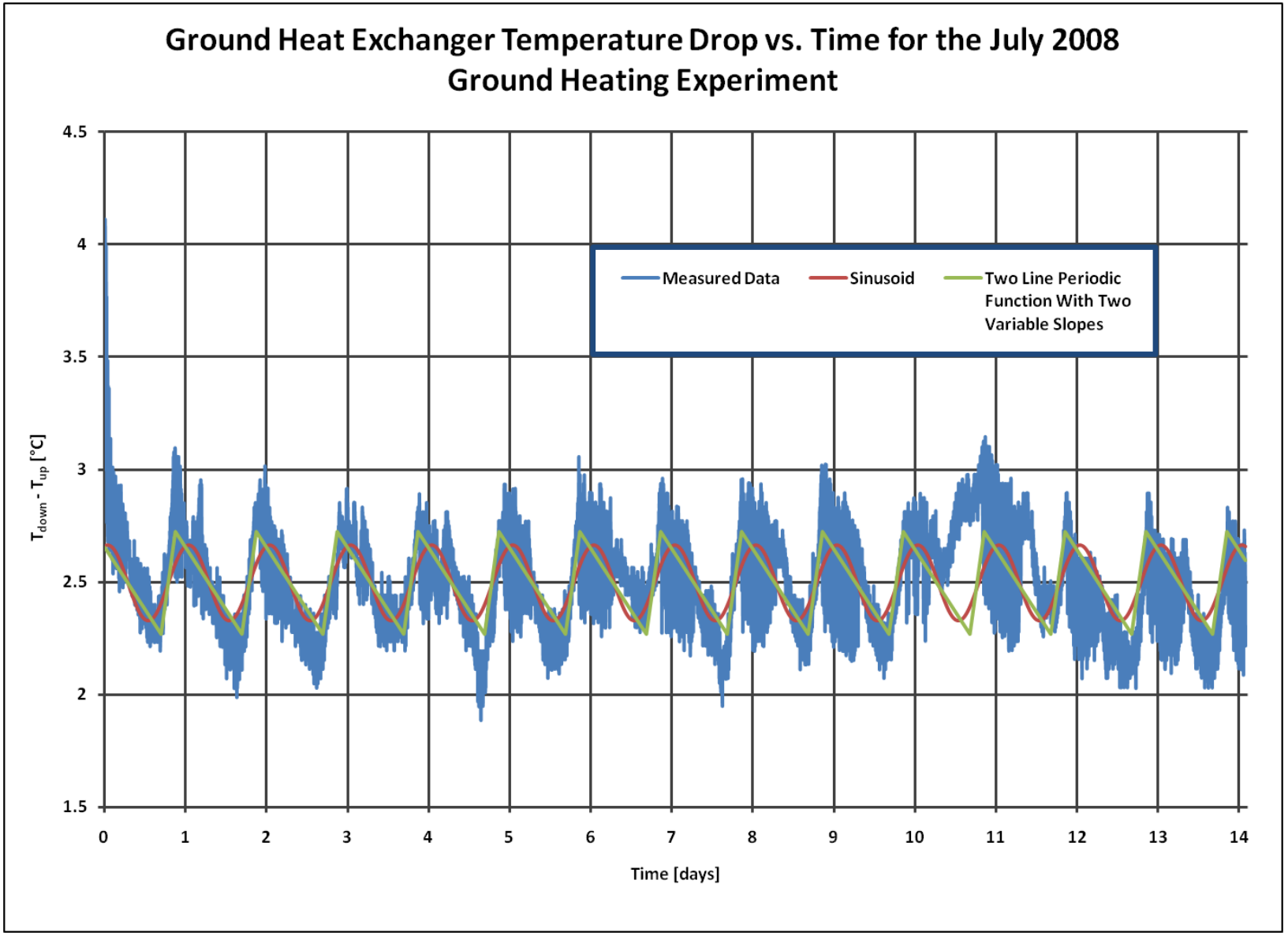

Figure 34 Entering and Exiting Heat Transfer Fluid Temperature difference Measured at the Heat Pump Unit for the July 2008 Test

$$\Delta T_f = T_{f,o} - T_{f,i} \quad \textbf{[1]}$$

$$\dot{Q}_{HPU} = \dot{m}_f c_{P,f} \Delta T_f \quad \textbf{[2]}$$

The periodic nature and appearance of the data show that either a sinusoid or a saw-tooth wave could represent the data. The curve fits used minimum RMS Error as the fitting criterion. The period of the sinusoid is 1440.011 minutes or one day plus 0.661 seconds. The amplitude of the sinusoid is 0.17°C. The saw-tooth has two variable slopes to represent the finite rise and fall that the data seemed to show. The period of this function is 1437.54 minutes, or one day less 2.46 minutes. The amplitude of this function is 0.23°C. Both of the periodic curve fit functions oscillate about the same value of 2.50°C.

Both periodic curve fits have the same average and essentially the same period. The average equals the arithmetic average of the data. The period essentially equals one day. This shows that the oscillations result from daily environmental fluctuations around the Geothermal Research Trailer. Both periodic curve fits have the same average, and each of their amplitudes is less than ten percent of the mean inlet and outlet temperature difference. Furthermore, the periodic functions repeat about fourteen times over the duration of the test. Therefore, the power output of the Heat Pump Unit is approximately a constant value plus or minus a small percentage of error. The amplitudes of the periodic curve fits, 0.17°C and 0.23°C, result in an estimate of the error as between 6.8% and 9.2% of the average. Thus, a conservative estimate of the heat transfer fluid temperature difference is; $\Delta T_f = 2.50°C \pm 0.23°C$.

One can determine the rate of heat exchange from a fluid flowing in a closed loop of pipes based on the difference between the inlet and outlet fluid temperatures (ΔT_f) with the product of the mass flow rate and specific heat capacity of the heat transfer fluid (see [2]). As best determined, the heat transfer fluid is a 20% methanol and 80% water solution. The density and specific heat capacity of water is $\rho_W = 1000\text{kg/m}^3$ and $c_{P,W} = 4200\text{KJ/Kg·K}$, respectively. According to the Chemical Engineering Research Information Center (2011), the density and heat capacity of liquid methanol is $\rho_{CH_3OH} = 791\text{Kg/m}^3$ and $c_{P,CH_3OH} = 2543\text{KJ/Kg·K}$, respectively. The volumetric flow rate of the heat transfer fluid measured by a water meter in the trailer was $Q_f = 16.60\text{L/min}$. Combining these data gives the density, specific heat capacity, and mass flow rate for the heat transfer fluid as $\rho_f = 958\text{Kg/m}^3$, $c_{P,f} = 3867\text{KJ/Kg·K}$, and $\rho_f Q_f = \dot{m}_f = 0.265\text{Kg/s}$, respectively. Therefore, the product of the mass flow rate and the specific heat capacity gives $\dot{m}_f c_{P,f} = 1024.8\text{W/K}$. It is now possible to estimate the power supplied to the ground heat exchanger. Combining all of the above information, we find that the Heat Pump Unit outputs about $\dot{Q}_{HPU} = \dot{m}_f c_{P,f} \Delta T_f = 2562\text{W}\pm233\text{W}$. The error term comes from the larger of the two amplitude estimates of the periodic function, which the saw-tooth wave gave. The power input to the ground heat exchanger ($\dot{Q}_{GHX}$) includes two other terms. These are the power output of the circulation pump (W_P) and the power lost between the HPU and the ground surface ($\dot{Q}_{Loss}$). An electric power meter gave the power output of the circulation pump as $W_P = 230\text{W}$.

There were no measurements of $\dot{Q}_{Loss}$ because there were no measurements of the heat transfer between the circulation fluid and its surroundings as it flowed between the HPU

and the ground surface. An insulated duct forms the path between the trailer and the ground surface. Furthermore, the path between the HPU and the outside of the trailer is much shorter than the total U-Loop path length. Therefore, the research proceeded from the assumption that this portion does not experience appreciable heat transfer. Therefore, the estimated power output to the ground is $\dot{Q}_{GHX} = \dot{Q}_{HPU} + W_P - \dot{Q}_{Loss} \approx$ 2562W±233W+230W-0W = 2792±233W. However, the computer modelling suggests that heat transfer between the heat transfer and its surroundings fluid en route between the HPU and the ground may not be negligible.

4.1.4 Implications of the Preliminary Findings on the Model Definition

The preliminary findings show that the depths to 5m experience effects that are outside of the focus of this investigation. Specifically, they experience temperature change resulting from insolation and other meteorological phenomena. This thesis aims to analyse the effect on the ground from heating by a deep vertical borehole heat exchanger. Furthermore, considering the near-surface region would at least double the complexity of the analysis. Therefore, this thesis does not consider the top 5m.

The complexity of the near surface region results from its many distinguishable features. The near-surface region shows three distinct subdivisions that would each require at least one borehole boundary condition step for the model to reproduce the observed behaviour. In addition, there would be at least two material layers corresponding to topsoil, and the underlying clay. The oscillatory behaviour of the first 3m adds additional complications. The surface temperature readings occurred simultaneously with the rest of the readings, during the afternoon. Thus, there are only data for the afternoon, which corresponds

approximately with the maximum daily surface temperature. Consequently, analysing the top 5m would also require a parametric study to determine appropriate ground surface temperature values for the remainder of the simulation.

The divisions in the data for the deep underground region also influenced the model. The divisions at about 15m and 30m correspond to material boundaries. The model incorporates these as different material layers. The six vertical divisions of the boundary condition that models the ground heat exchanger output also account for the differences in temperature response magnitude. However, the results of the primary modelling (section 4.2) showed that this, time-invariant model of the ground heat exchanger output was not sufficient to reproduce the chronology of the experimentally observed phenomena in the lower portion of the depth. Modelling scenarios that considered time and depth variation in the ground heat exchanger output (section 4.3) were more successful.

4.2 Parametric Study Results

4.2.1 Depth Varying Borehole Wall Temperature Case

This test used a consistent borehole wall-temperature test-matrix for material combinations B to I that evolved from an initial test matrix. The initial test matrix assumed a linear decrease in the borehole wall temperature with depth. Therefore, the basis of the original test matrix was a linear decrease of temperature with borehole depth. The values were those at the centre of each of, L_1 to L_6. These initial temperature values were 18°C, 16°C, 14°C, 12°C, 10°C, and 8°C. As Anderson and Woessner (1992)

suggest, the test matrix results from applying a set of calibration coefficients to the temperature on each of the parameters. Table 6 shows the resulting test matrix and the calibration coefficient set.

Unfortunately, the assumption of linear borehole wall-temperature variation with depth was not satisfactory. The resulting calibrated borehole wall temperatures values were 18.96°C, 18.39°C, 13.83°C, 10.08°C, 7.79°C, and 6.20°C for each respective line segment. This is not a linear progression. Therefore, this calibrated result formed the basis for the test matrix that the remainder of the constant borehole wall temperature used. The basis for this test matrix was the following series of temperatures; 19.00°C, 18.40°C, 13.80°C, 10.10°C, 7.80°C, and 6.60°C.

Table 6 Initial Test Matrix for the Depth Varying Borehole Wall Temperature study

Line Segment Location	Calibration Coefficients:					
	0.85	0.91	0.97	1.03	1.09	1.15
	Temperature By Line segment For Each Calibration Coefficient [°C]					
L_1	15.30	16.38	17.46	18.54	19.62	20.70
L_2	13.60	14.56	15.52	16.48	17.44	18.40
L_3	11.90	12.74	13.58	14.42	15.26	16.10
L_4	10.20	10.92	11.64	12.36	13.08	13.80
L_5	8.50	9.10	9.70	10.30	10.90	11.50
L_6	6.80	7.28	7.76	8.24	8.72	9.20

The calibrated borehole wall temperatures for material type-A formed the basis for the test matrices for the remaining material property combinations. However, the remaining tests for material property combinations B to I used an expanded calibration coefficient

set on the first five line segments to ensure that all of the remaining tests would be within the test matrix. The bottom line segment used a condensed calibration coefficient set to prevent testing impossible temperature values that were below ambient. Table 7 shows the final test matrix. This test matrix proved satisfactory because all of the results for each of the remaining material property combinations, cases B to I, were within the test matrix. Table 8 gives a complete summary of the results for the depth varying borehole wall-temperature study and Figure 35 shows a graphical representation of a calibration.

Table 7 Final Test Matrix for the Depth Varying Borehole wall Temperature Case

Line Segment Location	Calibration Coefficients (L_1 to L_5)					
	0.80	0.89	0.98	1.07	1.16	1.25
	Temperature By Line segment For Each Calibration Coefficient (L_1-L_5) [°C]					
L_1	15.200	16.910	18.620	20.330	22.040	23.750
L_2	14.720	16.376	18.032	19.688	21.344	23.000
L_3	11.040	12.282	13.524	14.766	16.008	17.250
L_4	8.080	8.989	9.898	10.807	11.715	12.625
L_5	6.240	6.942	8.7644	8.346	9.048	9.750

Calibration Coefficients (L_6)					
0.90	0.94	0.98	1.02	1.06	1.10
Temperature By Line segment For Each Calibration Coefficient (L_6) [°C]					
5.940	6.204	6.468	6.732	6.996	7.260

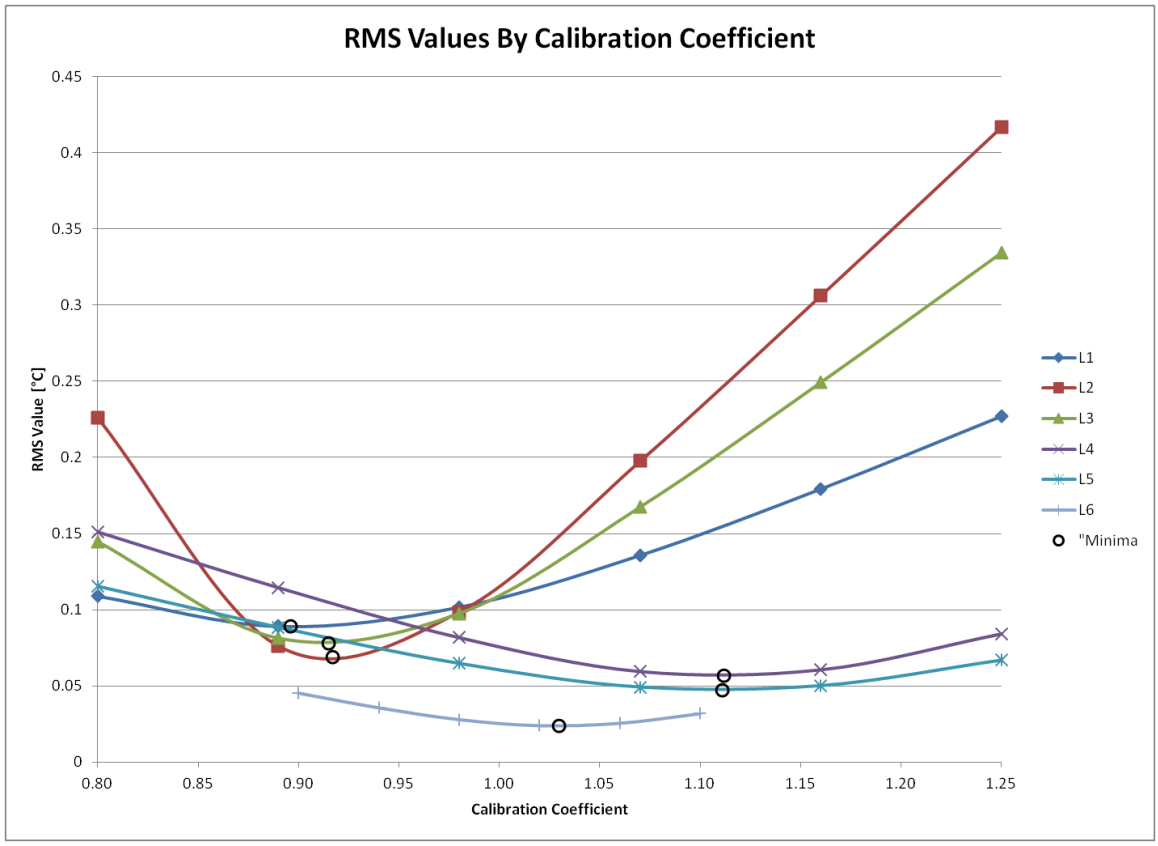

Figure 35 Calibration Graph for material combination H in the constant borehole wall temperature series.

As Table 8 shows, the most likely material property combination is combination H. You may notice that some of the minimum RMS Error values occurred in other material property combinations. However, they only occurred in materials whose property values were the same as those in combination H. Therefore, material combination H is most likely to represent the material composition of the experimental site. The graphs in Figure 37 to Figure 43 (see pages 128 to 134) show the comparison between modelling and experiment for the calibrated model using material combination H.

Table 8 Summary of The Depth Varying Borehole-Wall Temperature Calibration. Minimum RMS Error values are shaded in orange.

Layer	Line Segment	Case	Calibrated Borehole Wall Temperature [°C]	RMS Error [°C/100]	Case	Calibrated Borehole Wall Temperature [°C]	RMS Error [°C/100]	Case	Calibrated Borehole Temperature [°C]	RMS Error [°C/100]
M_1	L_1	A	18.96	9.15	D	20.80	9.55	G	17.44	9.20
M_2	L_2		18.39	9.52		16.91	6.89		21.32	16.74
	L_3		13.84	8.53		12.62	7.40		14.96	12.77
M_3	L_4		10.08	7.13		11.23	6.09		9.18	8.64
	L_5		7.79	5.69		8.66	4.70		7.44	6.54
	L_6		6.20	3.10		6.38	2.81		5.99	3.60
M_1	L_1	B	21.63	9.93	E	20.80	9.55	H	17.02	8.89
M_2	L_2		21.44	16.85		16.91	6.90		16.87	6.51
	L_3		15.44	12.56		12.42	7.29		12.62	7.41
M_3	L_4		11.26	5.78		9.15	8.82		11.23	6.09
	L_5		8.66	4.70		7.44	6.52		8.66	4.70
	L_6		6.38	2.81		5.99	3.60		6.38	2.81
M_1	L_1	C	21.63	9.93	F	17.44	9.20	I	17.02	8.89
M_2	L_2		21.44	16.85		21.32	16.66		16.87	6.53
	L_3		14.96	12.77		15.44	12.60		12.42	7.30
M_3	L_4		9.18	8.64		11.26	5.82		9.15	8.82
	L_5		7.44	6.52		8.66	4.73		7.44	6.53
	L_6		5.99	3.60		6.38	2.37		5.99	3.60

Despite the success of these models, there are certain aspects of the experimental results that no model in this series of simulations was able to reproduce. The computer models were not able to reproduce the value of overall heat transfer rate ($\dot{Q}_{GHX}$), as estimated inside the trailer (see section 4.1.3). This is not entirely surprising, given the nature of the boundary condition. The overall heat transfer rate from the heat pump unit was approximately constant. However, as Figure 36 shows, the value that the model predicted decreased throughout the modelling time. The average computer simulated value of the overall heat transfer was $\dot{Q}_{model} = 1569\text{W}$. This is noticeably lower than the estimate of $\dot{Q}_{GHX} = 2792\text{W} \pm 233\text{W}$ from inside the trailer.

The $\dot{Q}_{model}$ value should be smaller than the estimate from measurements taken inside the trailer. The computer model does not simulate the top 5m of depth. Consequently, the computer model estimate is always missing the contribution to $\dot{Q}_{GHX}$ from the first five metres ($\dot{Q}_{GHX,z>5m}$). The computer model simulates the remaining fraction of the overall heat transfer rate – from 5m and below ($\dot{Q}_{model} = \dot{Q}_{GHX,05m\leq z\leq 61m}$). The sum of these two values would equal the total ($\dot{Q}_{GHX} = \dot{Q}_{GHX,z>5m} + \dot{Q}_{GHX,05m\leq z\leq 61m}$). Therefore, the value that the model simulated should be less than the estimate from inside the trailer ($\dot{Q}_{model} = \dot{Q}_{GHX,z>5m} < \dot{Q}_{GHX}$).

However, the value of the discrepancy is very large. It is unlikely that nearly one third of the heat transfer from the GHX occurs in the first twelfth of the depth (from 0m to 5m). Therefore, the present model may need improvement. In addition, the assumption of zero heat loss while the heat transfer fluid travels too and from the HPU, in the trailer, and the ground surface (i.e. $Q_{Loss} \approx 0$) may not be appropriate. In addition, both of these factors may have contributed.

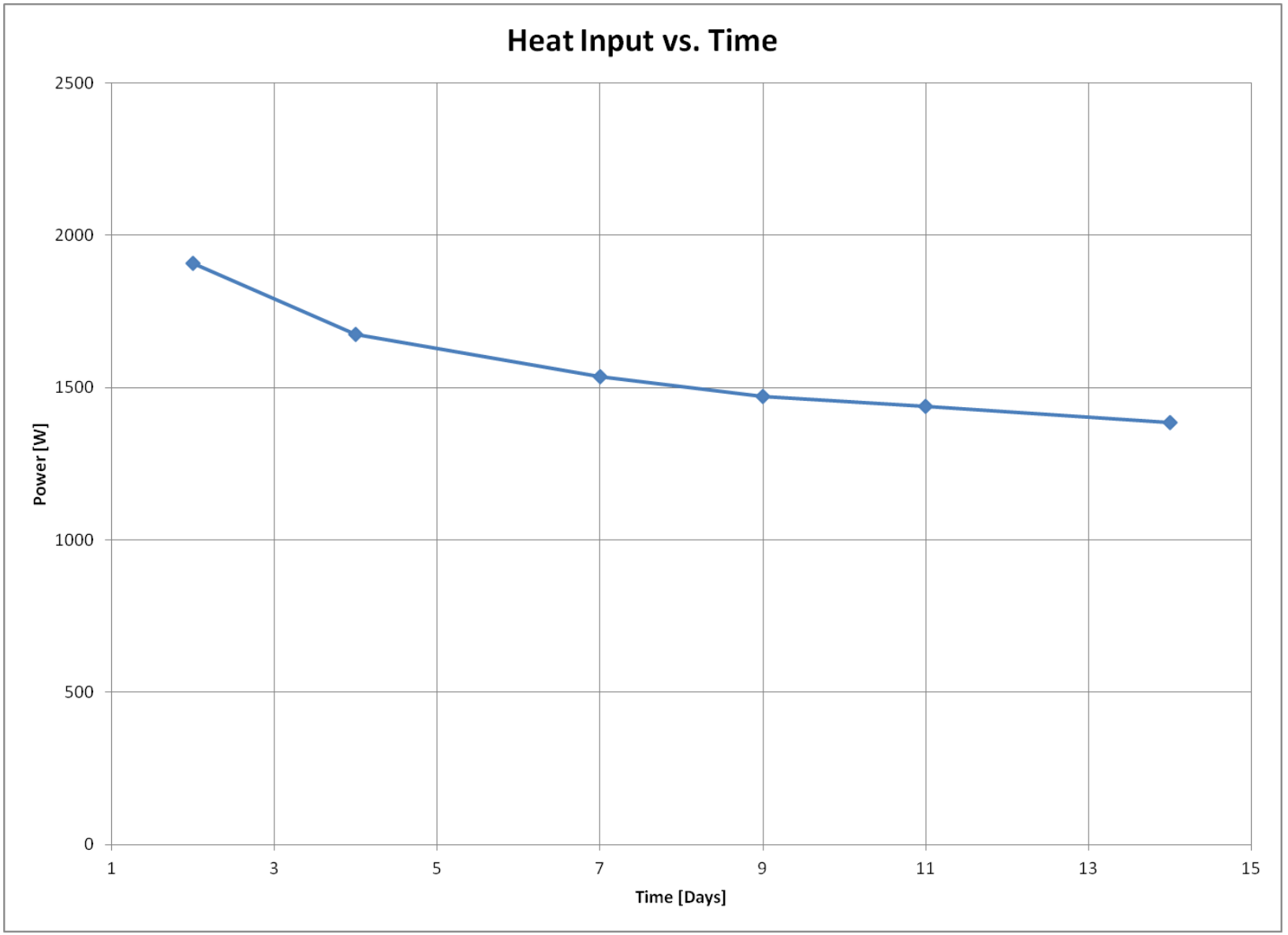

Figure 36 Overall Ground Heat Exchanger Output for the Depth Varying (Time Invariant) Borehole Wall-Temperature Case.

One can find an explanation for the discrepancy between the measured and simulated data in Figure 40. This figure shows the correct trend with depth for the simulated data. However, it also shows that the simulated temperatures rise to a maximum between the eighteenth and twenty-third day, and decreases until the end of the simulation. This is in contrast to the measured data, which generally continues rising throughout the test. This may suggest a flaw in the simulation model. The simulated data had to overshoot the experimental data during the heating phase because the temperatures in the model decrease during the natural recovery phase. Without the overshoot, the predicted values would be much lower than the experimental values during recovery because this simulation predicted the temperature decrease much earlier than the experiment showed. Section 4.3 presents hypotheses that attempt to account for this behaviour.

The most significant difference between the simulation and the experiment occurs in the natural ground temperature recovery phase in the lower portion of the domain. This is most prominent in the results from the nearer observation well, at 1.4 horizontal metres from the ground heat exchanger. The computer simulation predicts a temperature maximum at 21 days, followed by a reduction in temperature, from 35m to 61m depth, except for the later times it predicted from 53m depth to 55m depth. The experimental results show that between 35m and 43m, the temperature changes very little from 21 days until the end of measurement time, though some depths near the top of this range may show a slight temperature reduction in the last few days of measurements. The experiment also shows that the ground temperature continues to rise throughout the simulation from 44m depth to the maximum measurement depth of 61m. This is in contrast to the simulation, which predicts a temperature reduction after 21 days.

The difference in the simulated and measured chronology is apparent in Figure 40. The day 28 line in the simulation is clearly behind, and at a lower temperature, than the two lines for the earlier days. In contrast, the day 28 data from the experiment separates from the earlier data more with increasing depth. This shows that there is a prominent, transient effect that the simulation does not predict. Consequently, there may be an additional process that this simulation does not model which is the cause of this effect. Section 4.3 explores more advances modelling scenarios. This section finds that it is possible to reproduce these additional transient effects with a more advanced model.

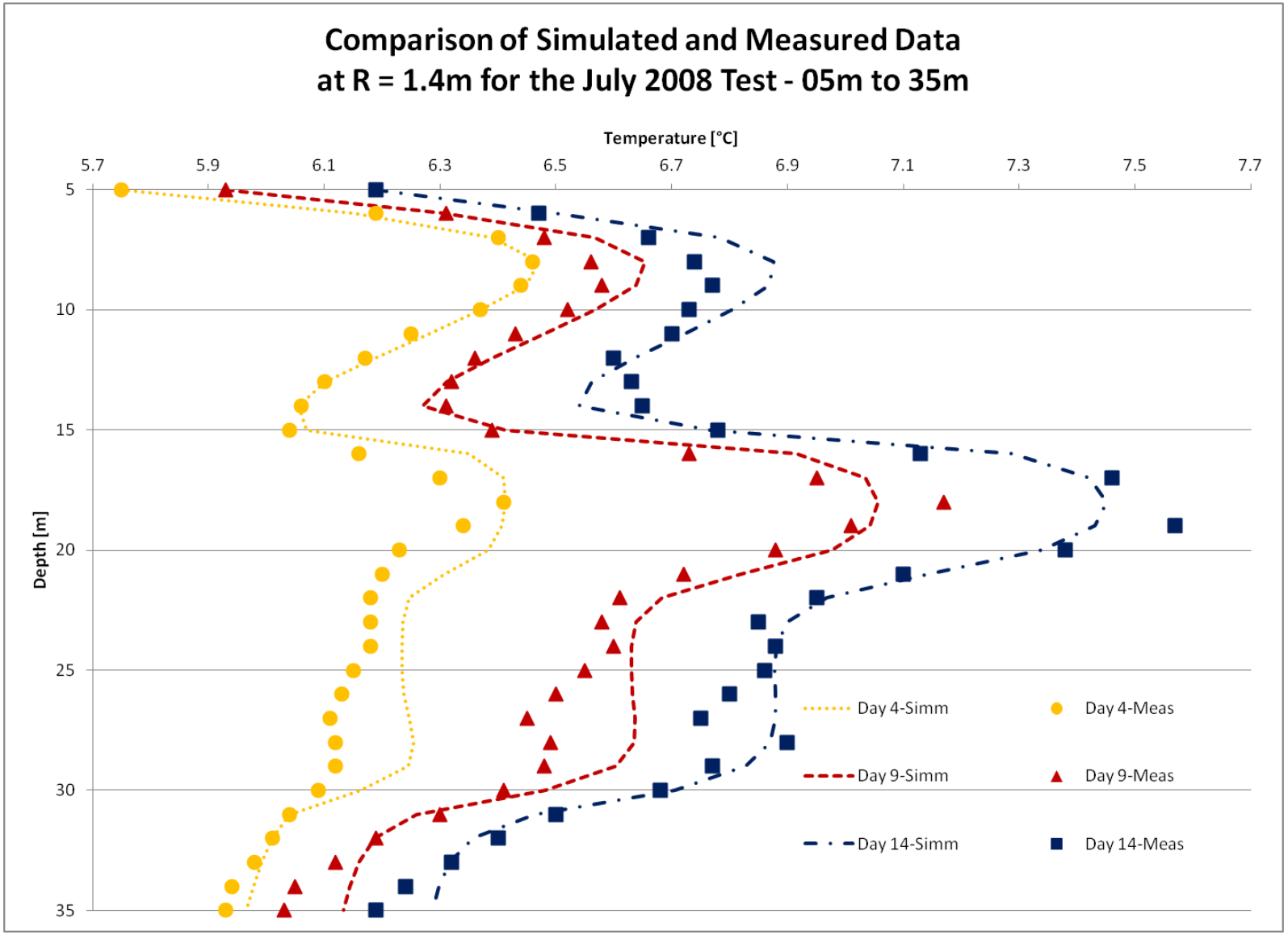

Figure 37 Results for Material Combination H. Best Calibration Results for the Depth Varying Borehole Wall Temperature Case in the Upper Portion of the Domain During the Ground-Heating Phase for the Nearer Observation Well.

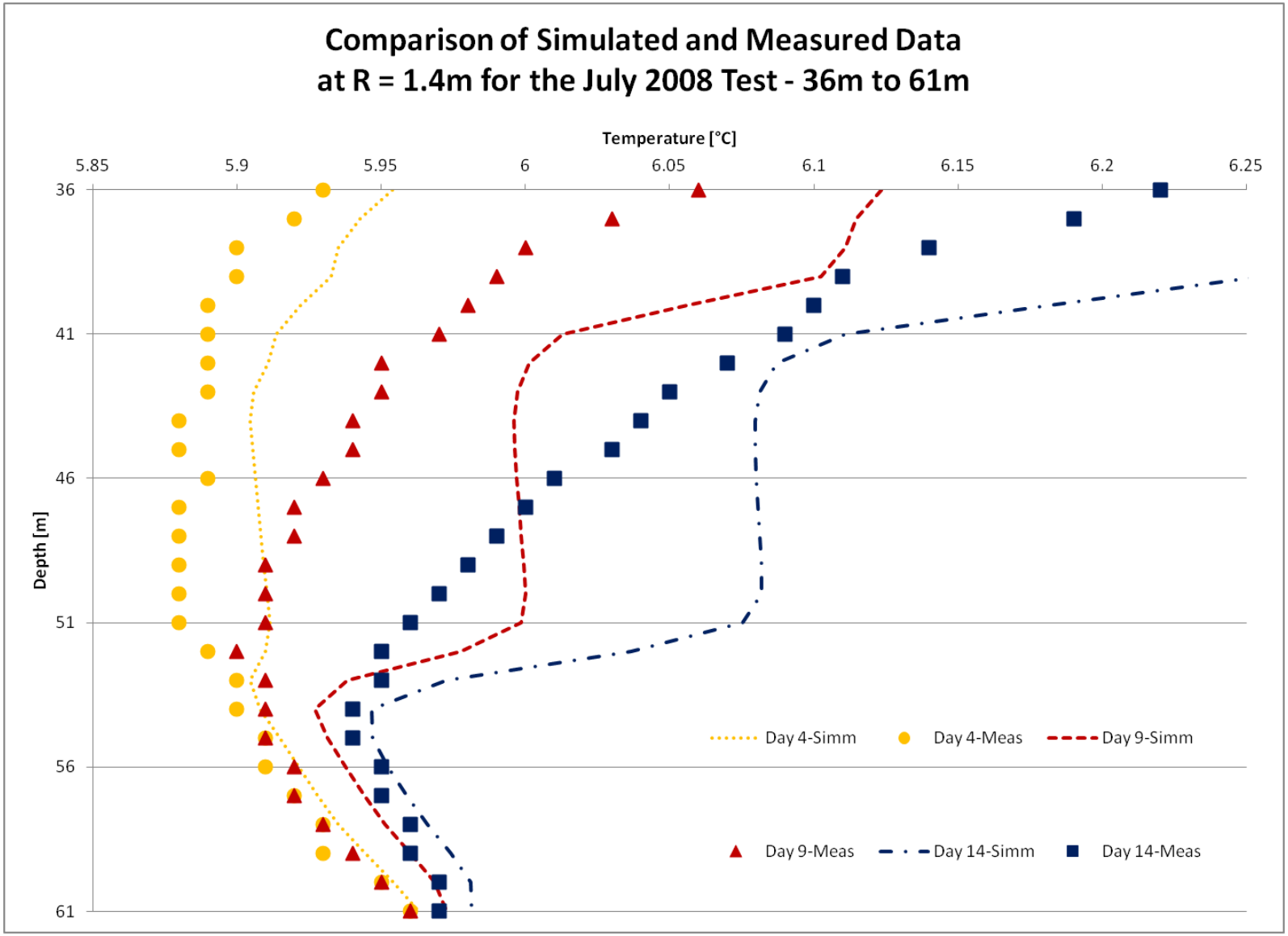

Figure 38 Results for Material Combination H. Best Calibration Results for the Depth Varying Borehole Wall Temperature Case in the Lower Portion of the Domain During the Ground-Heating Phase for the Nearer Observation Well.

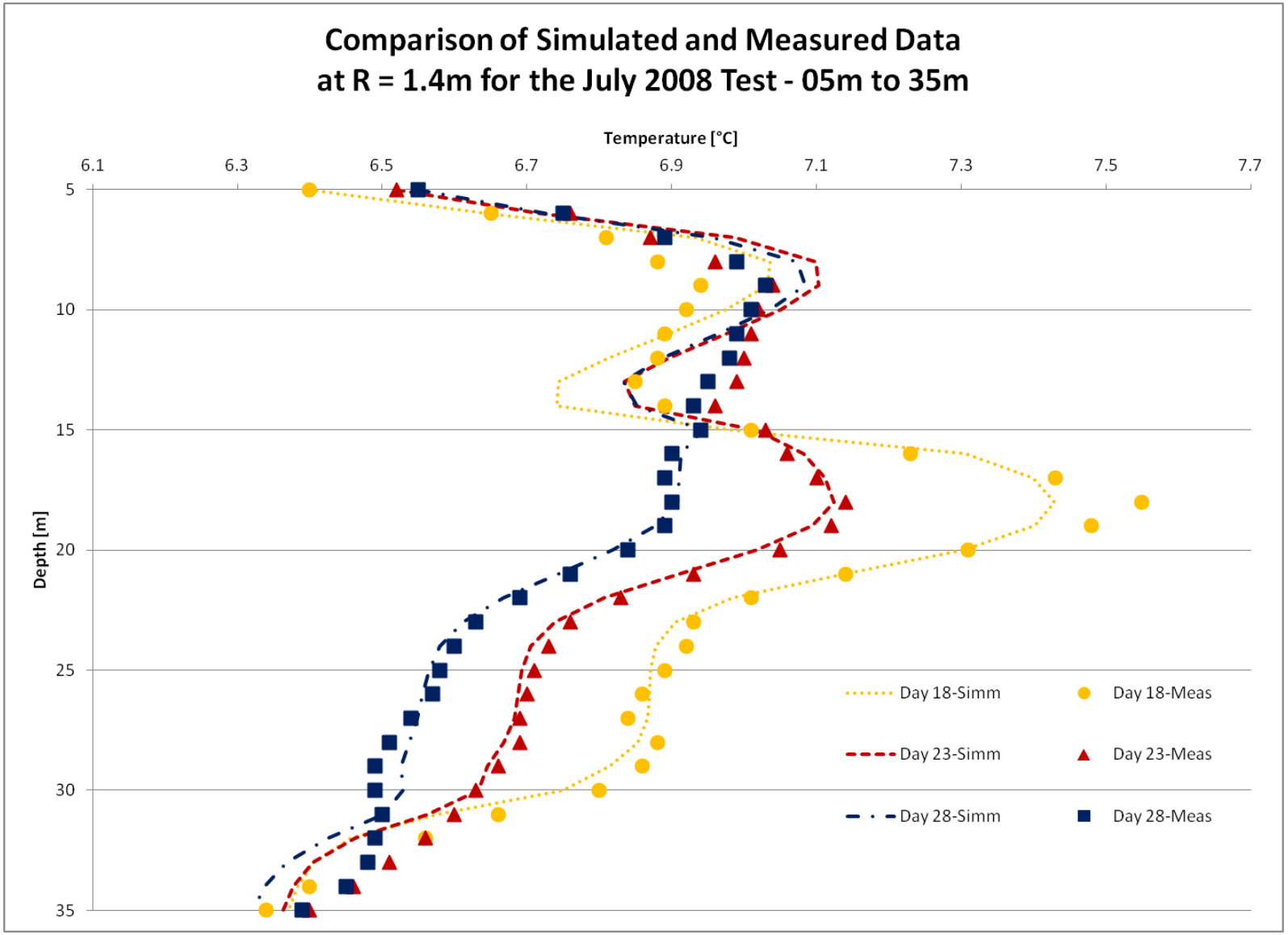

Figure 39 Results for Material Combination H. Best Calibration Results for the Depth Varying Borehole Wall Temperature Case in the Upper Portion of the Domain During the Natural Ground-Temperature Recovery Phase for the Nearer Observation Well.

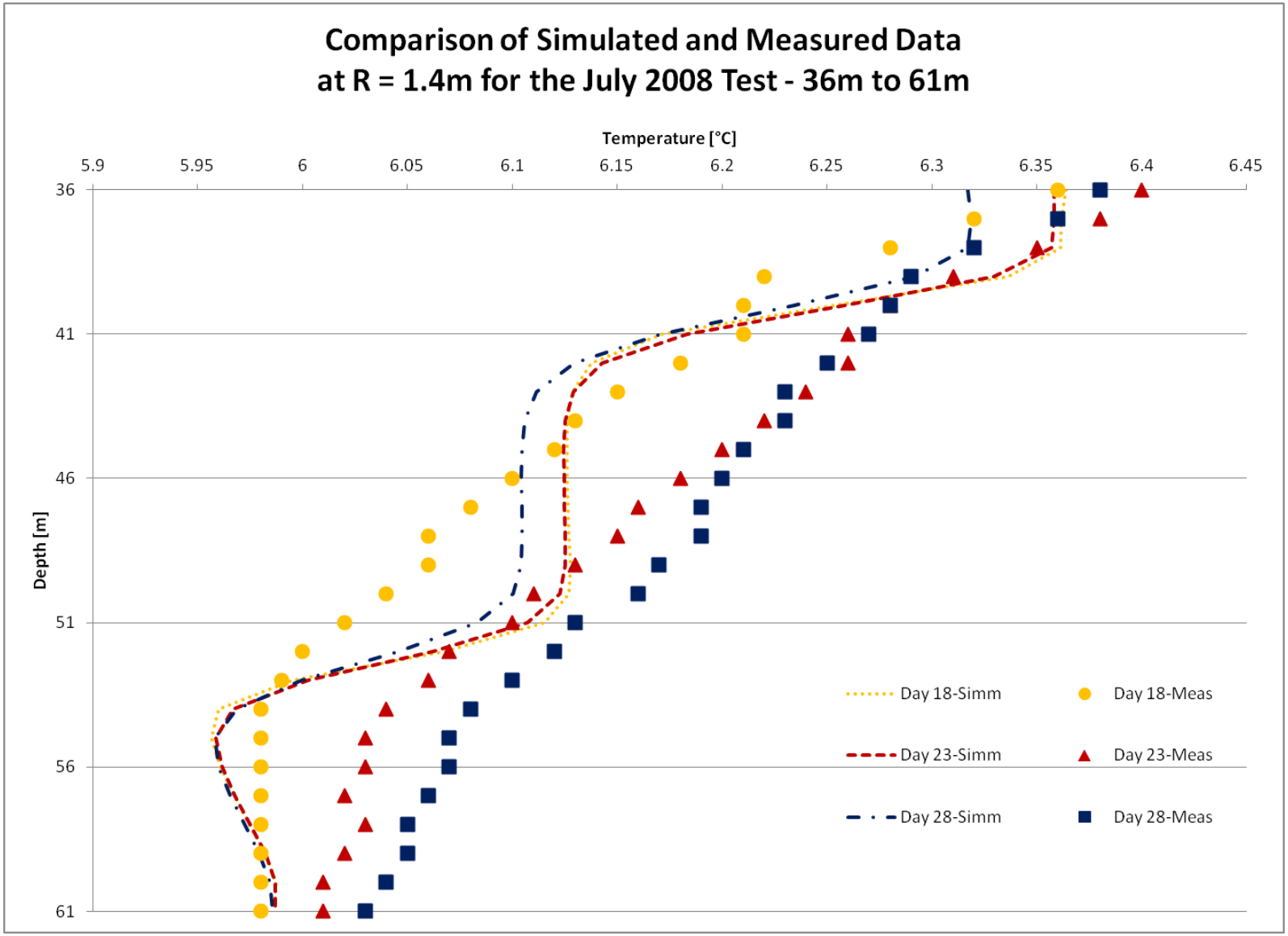

Figure 40 Results for Material Combination H. Best Calibration Results for the Depth Varying Borehole Wall Temperature Case in the Lower Portion of the Domain During the Natural Ground-Temperature Recovery Phase for the Nearer Observation Well.

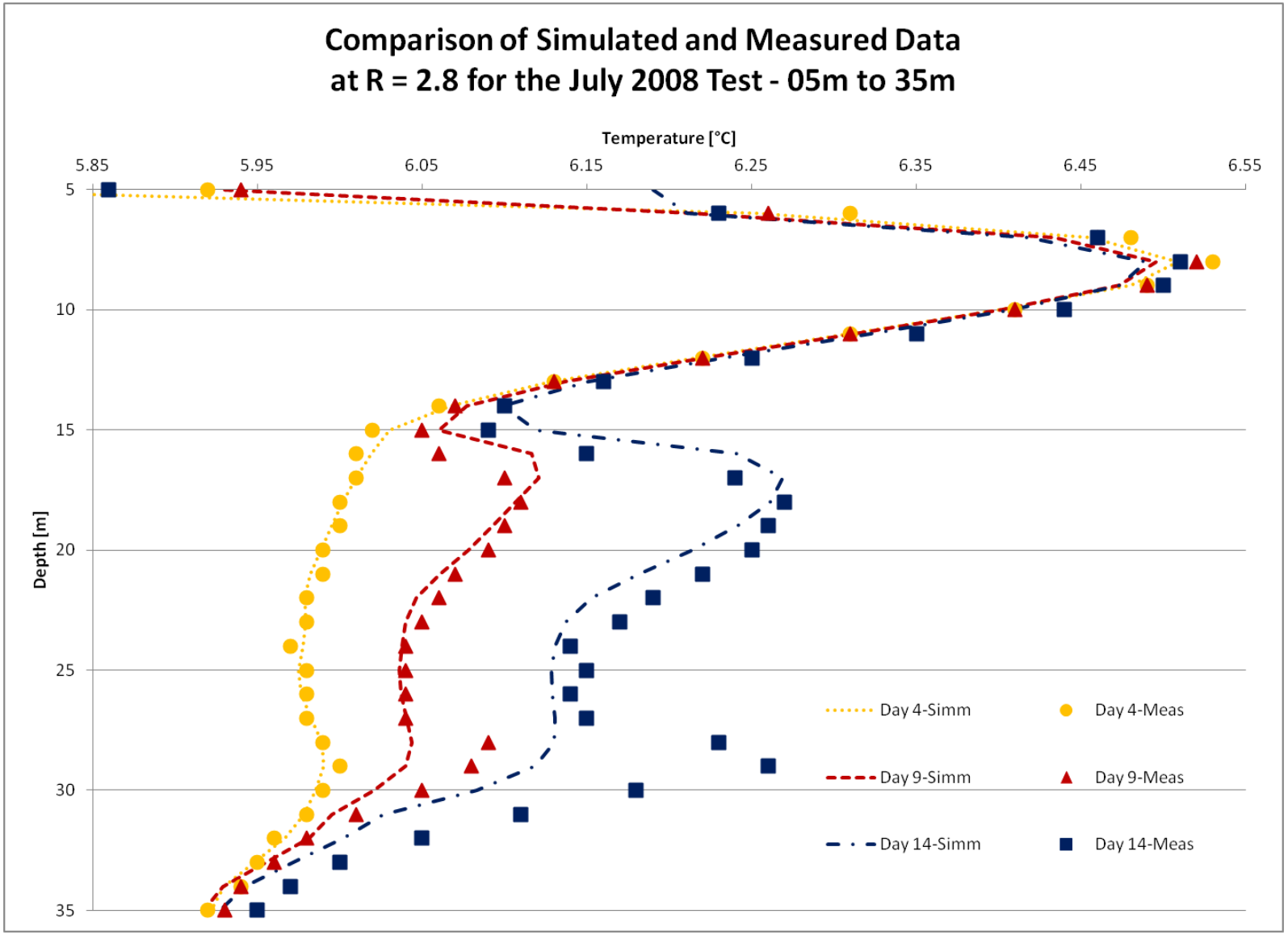

Figure 41 Results for Material Combination H. Best Calibration Results for the Depth Varying Borehole Wall Temperature Case in the Upper Portion of the Domain During the Ground-Heating Phase for the Further Observation Well.

Figure 42 Results for Material Combination H. Best Calibration Results for the Depth Varying Borehole Wall Temperature Case in the Lower Portion of the Domain During the Ground-Heating Phase for the Further Observation Well.

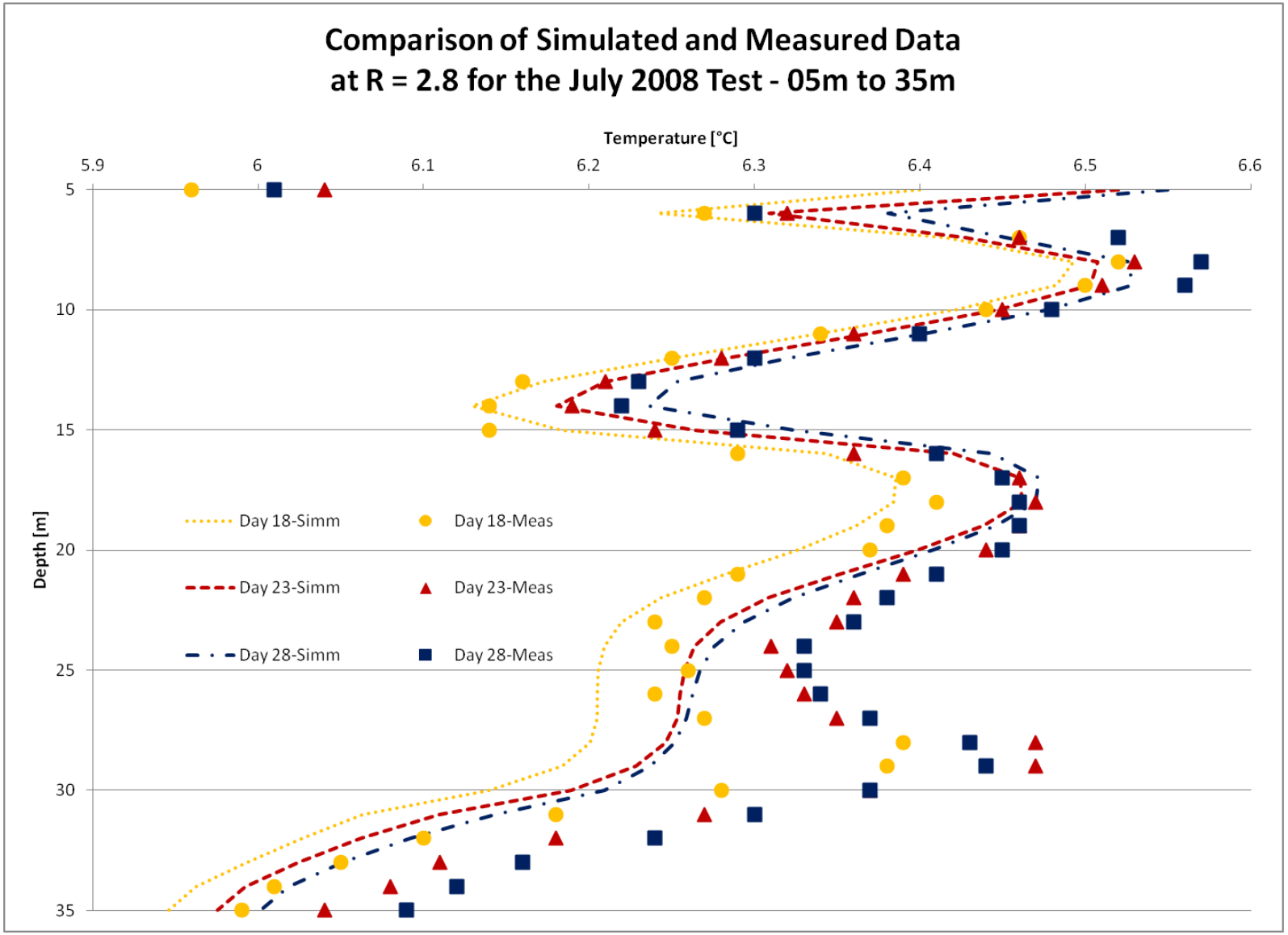

Figure 43 Results for Material Combination H. Best Calibration Results for the Depth Varying Borehole Wall Temperature Case in the Upper Portion of the Domain During the Natural Ground-Temperature Recovery Phase for the Further Observation Well.

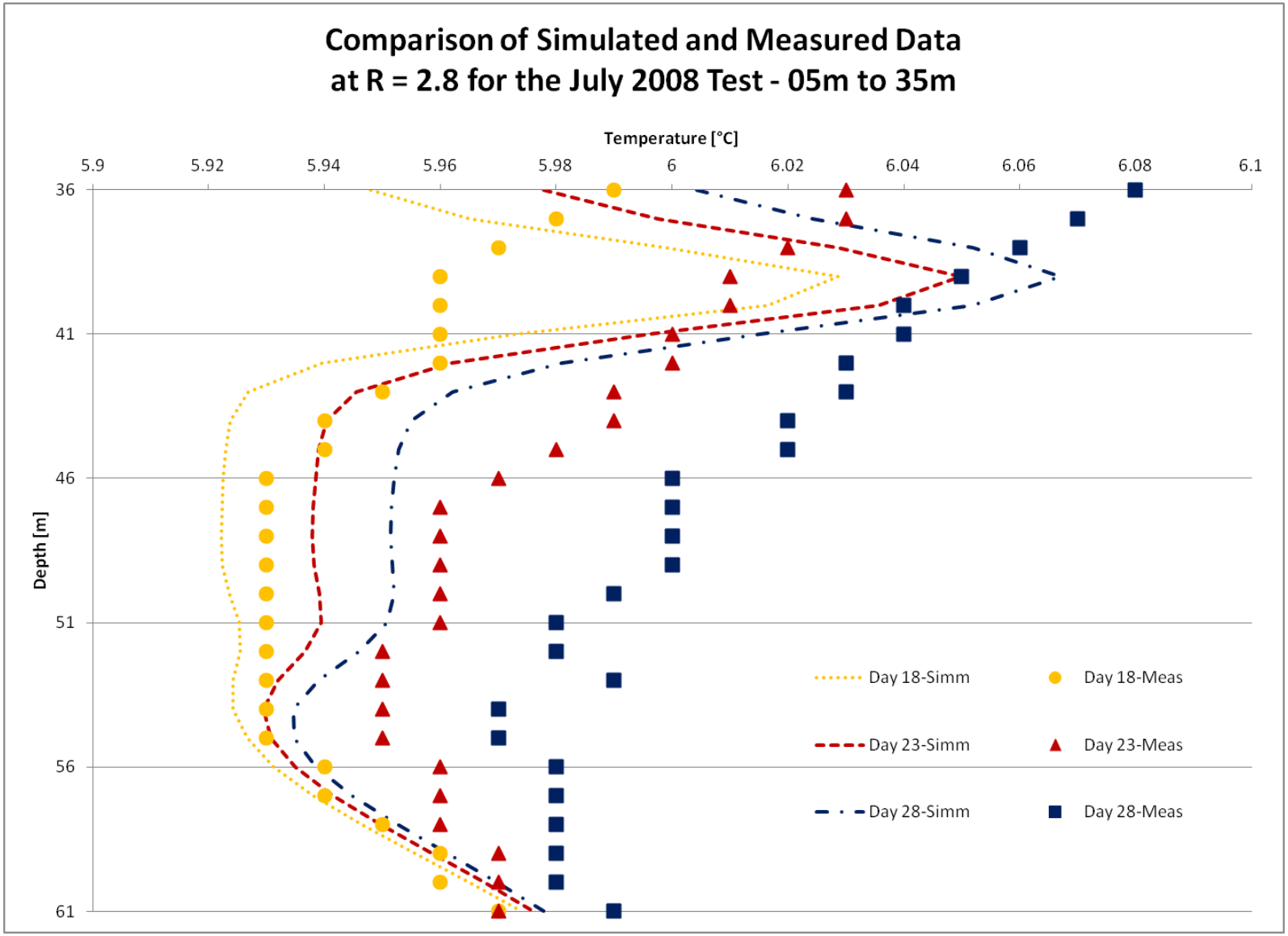

Figure 44 Results for Material Combination H. Best Calibration Results for the Depth Varying Borehole Wall Temperature Case in the Lower Portion of the Domain During the Natural Ground-Temperature Recovery Phase for the Further Observation Well.

4.2.2 Depth Varying Borehole Wall Heat Flux Case

This test used a consistent borehole flux test-matrix for material combinations B to I that evolved from an initial test matrix. The test also used a consistent set of calibration coefficients throughout. The basis for the initial test matrix was a series of trial and error simulations designed to locate a starting point for the mathematically based calibration. The outcome of this preliminary investigation resulted in the initial test matrix, as in Table 9. The basis of the test matrix for material combinations B to I came from the initial calibration with material combination A. The resultant test matrix is in Table 9.

Table 9 Test Matrices for the Depth Varying Borehole Flux study

Line Segment Location	Initial Calibration Coefficients (Combination A only)					
	0.50	0.75	1.00	1.33	1.67	2.00
	Heat Flux By Line segment For Each Calibration Coefficient [W]					
L_1	55.00	82.50	110.00	146.30	183.70	220.00
L_2	135.00	202.50	270.00	359.10	450.90	540.00
L_3	80.00	120.00	160.00	212.80	267.20	320.00
L_4	20.00	30.00	40.00	53.20	66.80	80.00
L_5	7.50	11.25	15.00	19.95	25.05	30.00
L_6	4.00	6.00	8.00	10.64	13.36	16.00
Line Segment Location	Main Calibration Coefficients (Combinations B to I)					
	0.50	0.75	1.00	1.33	1.67	2.00
	Heat Flux By Line segment For Each Calibration Coefficient [W]					
L_1	59.13	88.69	118.25	157.28	197.48	236.50
L_2	132.27	198.41	264.54	351.48	441.78	529.08
L_3	77.04	115.57	154.09	204.98	257.33	308.17
L_4	31.85	47.78	63.70	84.72	106.38	127.40
L_5	17.00	25.50	34.00	45.22	56.78	68.00
L_6	4.00	6.00	8.00	10.64	13.36	16.00

The procedure and qualitative results of this computer study were identical to the constant borehole wall-temperature study. The only qualitative result that was not identical between the two studies was that the total heating power was constant. Of course, this is because the heat-flux values do not vary with time in this test. The same material property combination, H, proved to be best, the model performed well in the upper region and less well in the lower region, and the predicted overall heat transfer rate of 1720W was lower than the expected value of $\dot{Q}_{GHX} = 2792\text{W}\pm233\text{W}$. In addition, the lower region exhibited the same overshoot during the ground-heating phase and premature temperature-reduction in the second phase of the simulation as in the depth varying borehole-wall temperature case.

The consistency between the two models implies a number of factors. The material combination H (see Table 10, 139Figure 45) is likely a good representation of the physical domain. The heating power dissipated by the ground heat exchanger is most likely much less then $\dot{Q}_{GHX} = 2792\text{W}\pm233\text{W}$ measured adjacent to the HPU. This throws into question the assumption of negligible heat transfer from the heat transfer fluid in transit between the ground and the heat pump unit (e.g. $\dot{Q}_{Loss} \neq 0$). Either a depth varying borehole wall heat-flux or a depth varying borehole wall-temperature will reproduce the ground temperature response well in the upper portion of the domain. However, only the constant heat-flux case will result in a constant total heat transfer rate. It is not possible to reproduce the temporal effects in the bottom region of the modelling domain with a temporally constant, depth varying boundary condition value on the

borehole wall. This resulted in re-evaluating the data and modelling assumptions to find a better model.

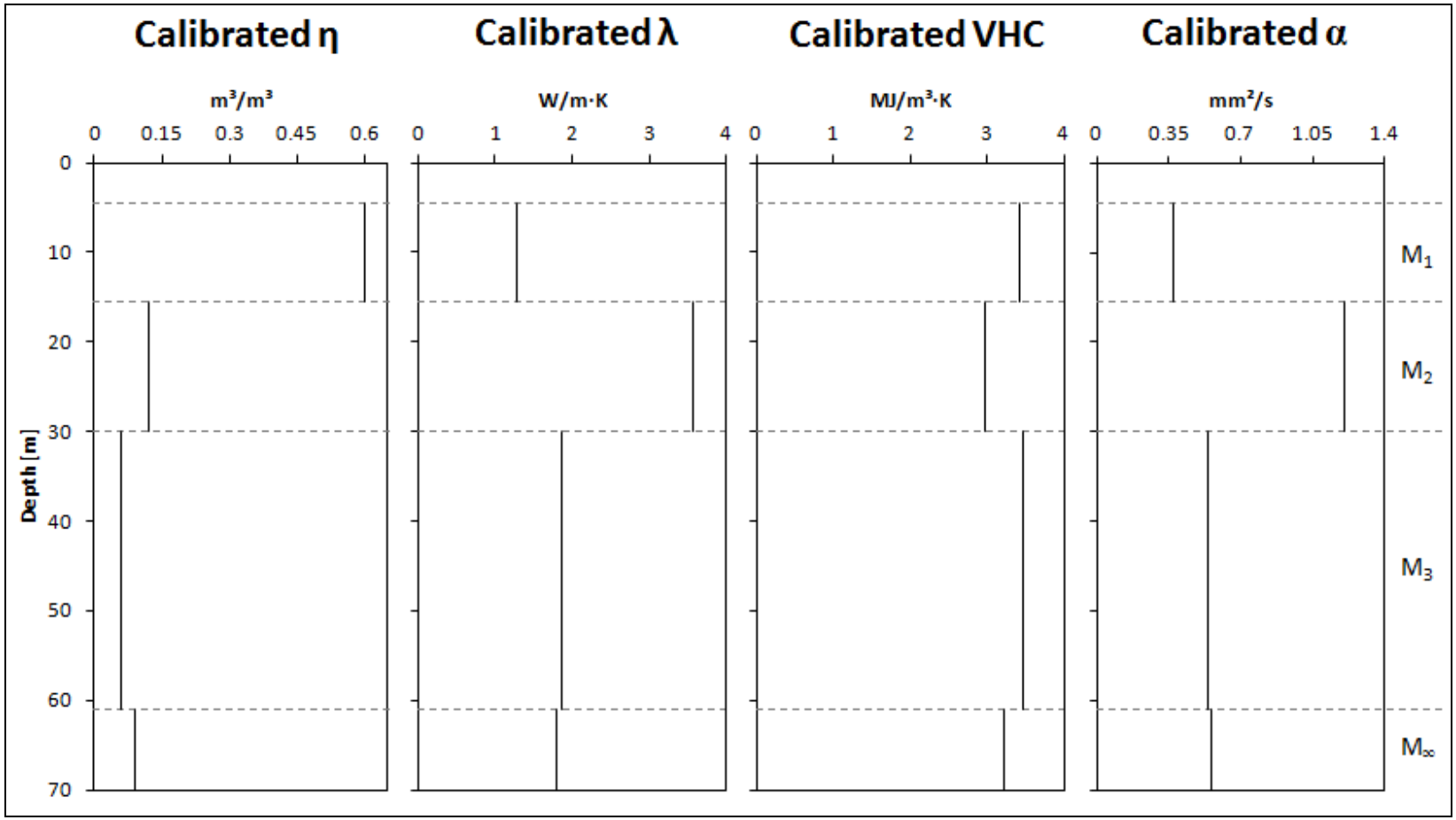

Figure 45 Calibrated Material Model

Table 10 Summary of the Depth Varying Borehole Wall Heat-Flux Calibration. Minimum RMS Error values are shaded in orange .

Layer	Line Segment	Case	Calibrated Borehole Wall Flux [W/m^2]	RMS Error [°C/100]	Case	Calibrated Borehole Wall Flux [W/m^2]	RMS Error [°C/100]	Case	Calibrated Borehole Wall Flux [W/m^2]	RMS Error [°C/100]
M_1	L_1	A	118.25	9.59	D	129.23	10.30	G	115.47	9.33
M_2	L_2		264.54	11.18		264.52	5.64		260.90	19.64
	L_3		154.09	9.25		152.44	6.86		151.73	13.60
M_3	L_4		63.70	6.40		75.12	5.05		65.75	7.78
	L_5		34.00	5.28		40.73	4.29		33.59	6.09
	L_6		11.95	2.54		13.05	2.23		10.08	2.76
M_1	L_1	B	130.45	10.75	E	129.23	10.30	H	116.22	9.04
M_2	L_2		260.68	19.80		264.52	5.64		264.95	5.31
	L_3		151.47	14.09		152.46	6.58		152.44	6.86
M_3	L_4		75.18	5.09		65.66	7.76		75.12	5.05
	L_5		40.73	4.29		33.59	6.09		40.73	4.29
	L_6		13.05	2.23		10.08	2.76		13.05	2.23
M_1	L_1	C	130.45	10.75	F	115.47	9.33	I	116.22	9.04
M_2	L_2		260.68	19.80		260.90	19.64		264.95	5.32
	L_3		151.73	13.60		151.47	14.09		152.46	6.59
M_3	L_4		65.75	7.78		75.18	5.09		65.66	7.76
	L_5		33.59	6.09		40.73	4.29		33.59	6.09
	L_6		10.08	2.76		13.05	2.23		10.08	2.76

The estimate of the overall heat transfer rate from the best model in this section has merit despite the discrepancy between this estimate and the estimate from measurements inside the trailer. Firstly, the computer model was very successful in two of the three material layers and mostly successful in the third. Secondly, the model estimates only part of the total heat transfer rate ($\dot{Q}_{GHX}$) because it neglects the first five metres of the ground. Finally, the assumption of zero loss in the pipes that carry the heat transfer fluid between the HPU and the ground surface may be unrealistic. Consequently, a value of $\dot{Q}_{model} = \dot{Q}_{GHX,05m\leq z\leq 61m}$ that is noticeably lower than $\dot{Q}_{GHX}$ from measurements inside the trailer is realistic.

The figures that follow show the success of the model. They show that the simulation was indeed able to model the experimental data in the two material layers in the upper portion of the domain. As section 4.2.1 discussed, there are some issues with the trends in the remaining layer in the lower part of the simulated data. However, the numerical values of the simulation are similar to the measured data, even in the less successful part of the model. Another merit to the simulation in the lower portion of the domain is that it predicts a much lesser heat input that corresponds to the much lower temperature response that the experiment measured in the lower portion of the domain. This is reasonable because of the much lower temperature response in the lower limestone as compared to the upper limestone. Furthermore, the value of $\dot{Q}_{model}$ from the present section is similar with the result from the past section. These facts leads to the speculation that the reality is that $\dot{Q}_{Loss}$ is significant, which this section proposes as the explanation for the large discrepancy between the computer model estimate of $\dot{Q}_{GHX,05m\leq z\leq 61m}$ and the estimate for $\dot{Q}_{GHX}$ based on measurements from inside the trailer.

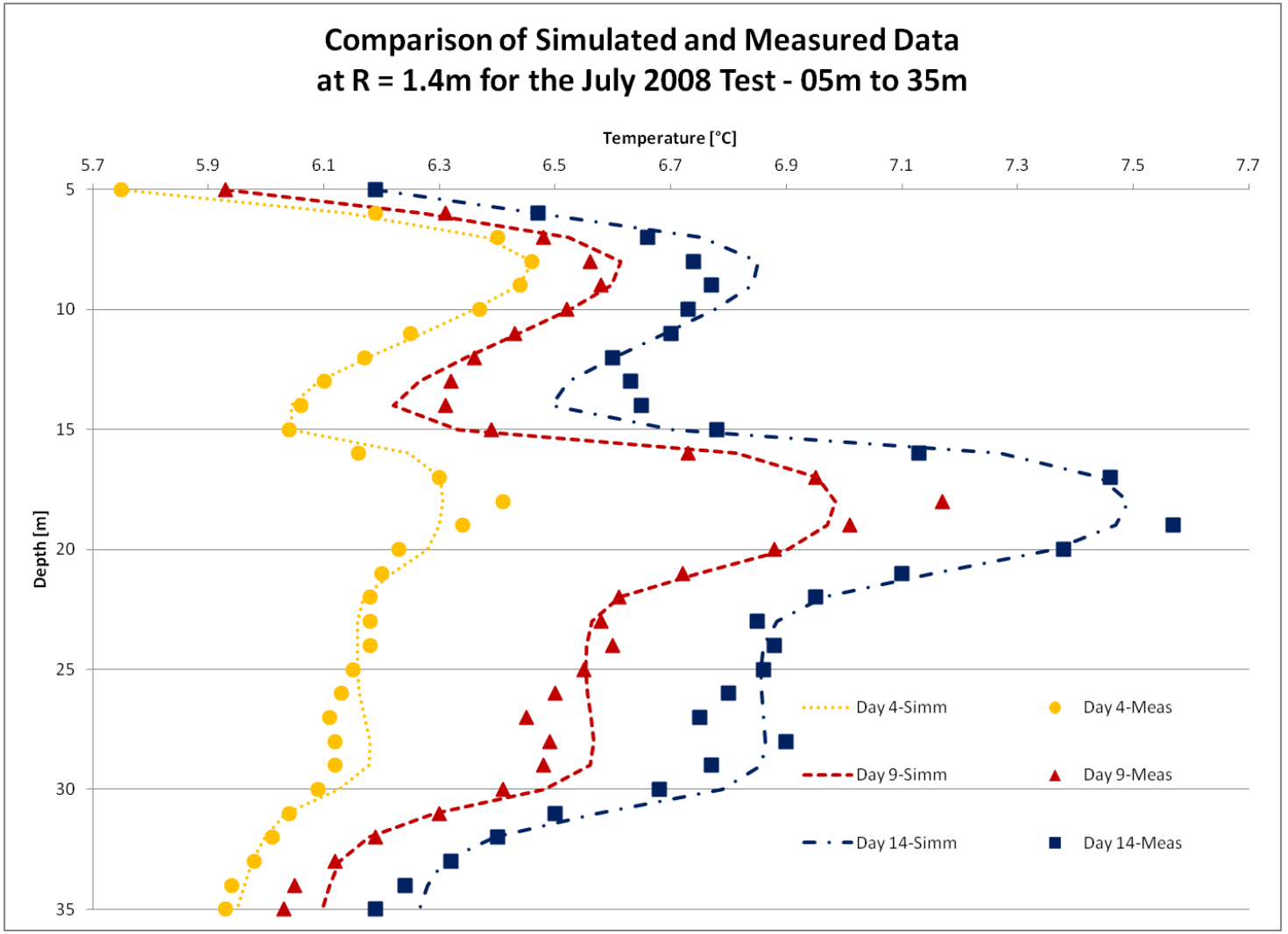

Figure 46 Results for Material Combination H. Best Calibration Results for the Depth Varying Borehole Wall Heat-Flux Case in the Upper Portion of the Domain During the Ground-Heating Phase for the Nearer Observation Well.

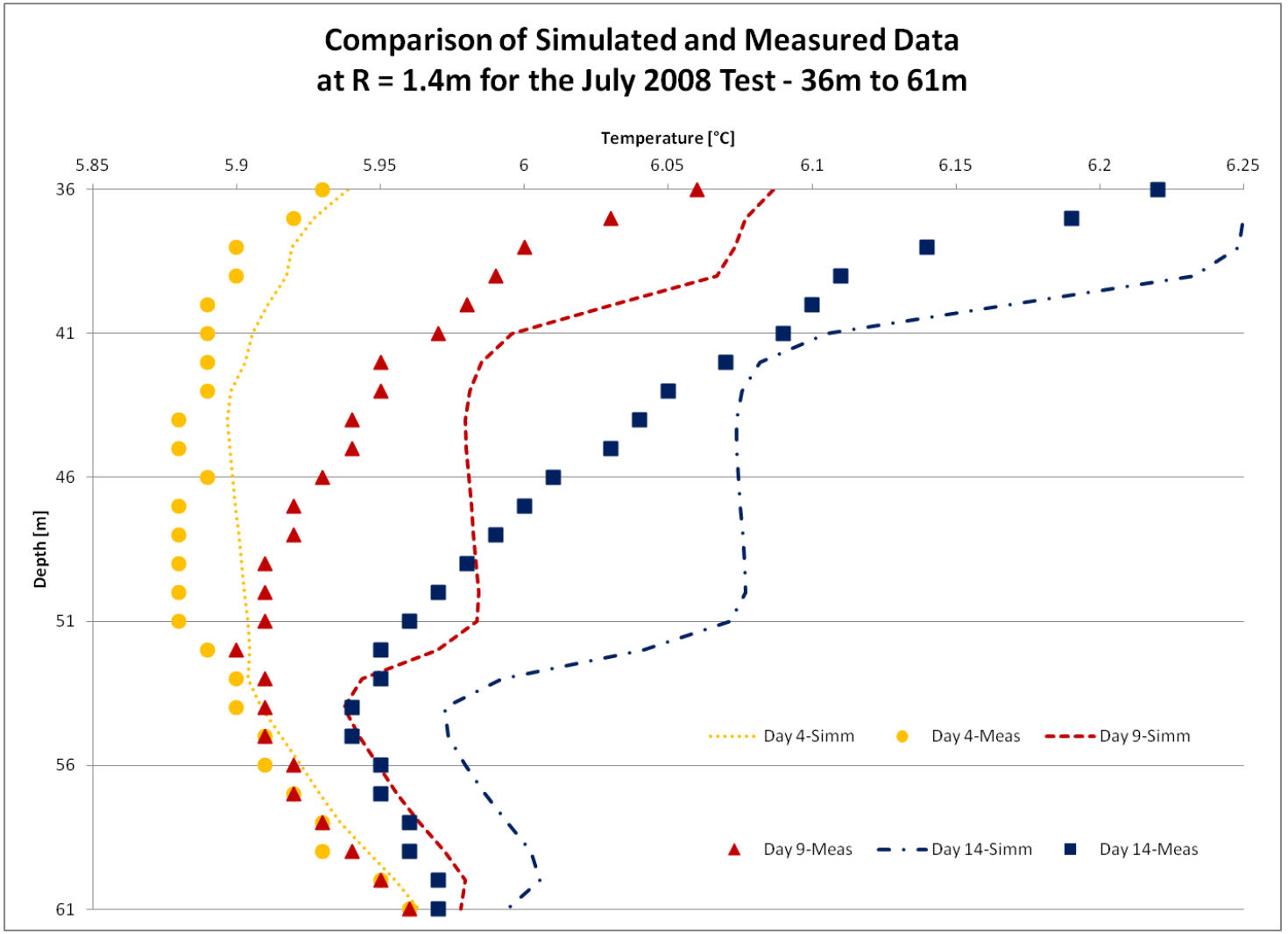

Figure 47 Results for Material Combination H. Best Calibration Results for the Depth Varying Borehole Wall Heat-Flux Case in the Lower Portion of the Domain During the Ground-Heating Phase for the Nearer Observation Well.

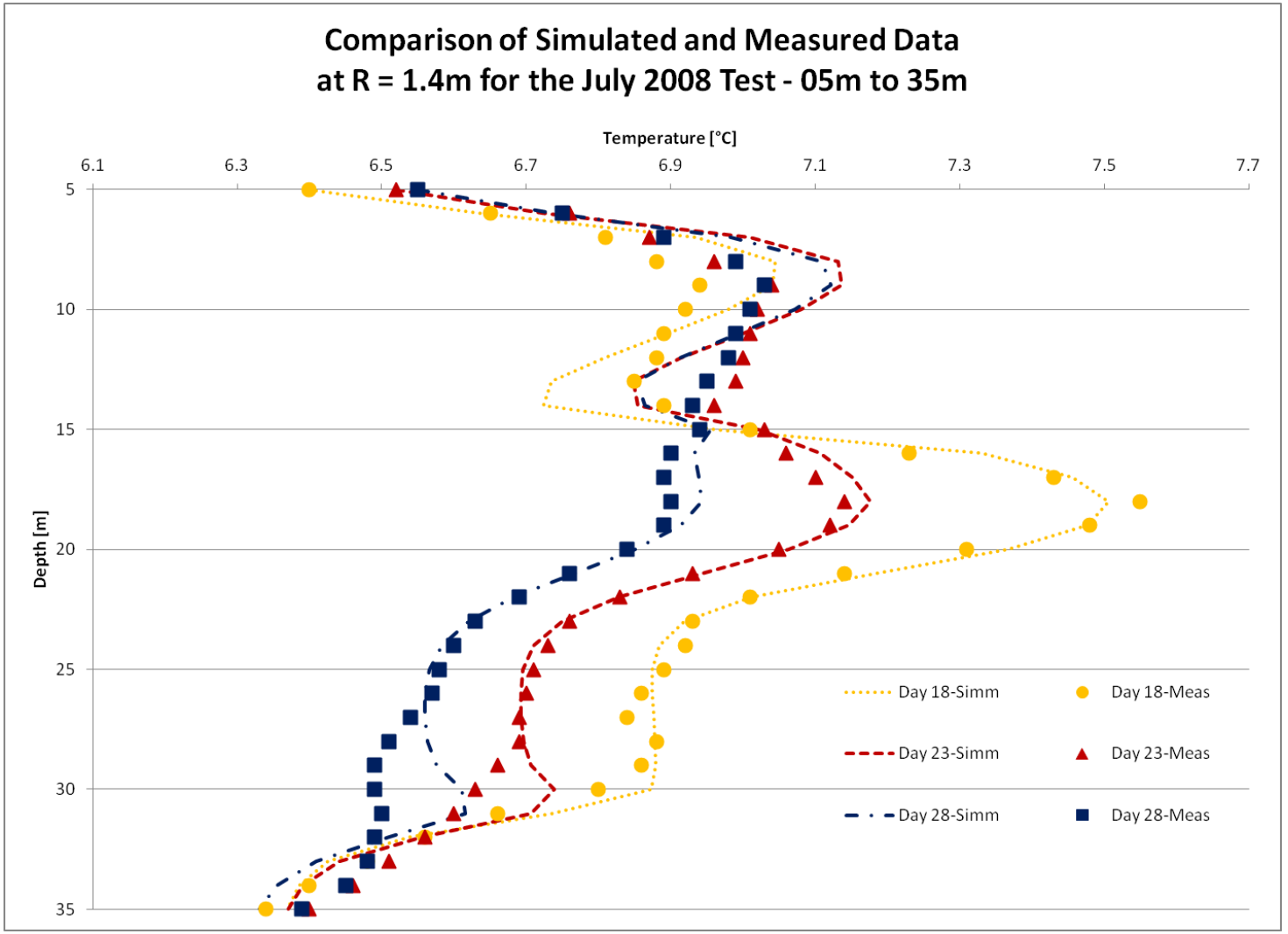

Figure 48 Results for Material Combination H. Best Calibration Results for the Depth Varying Borehole Wall Heat-Flux Case in the Upper Portion of the Domain During the Natural Ground-Temperature Recovery Phase for the Further Observation Well.

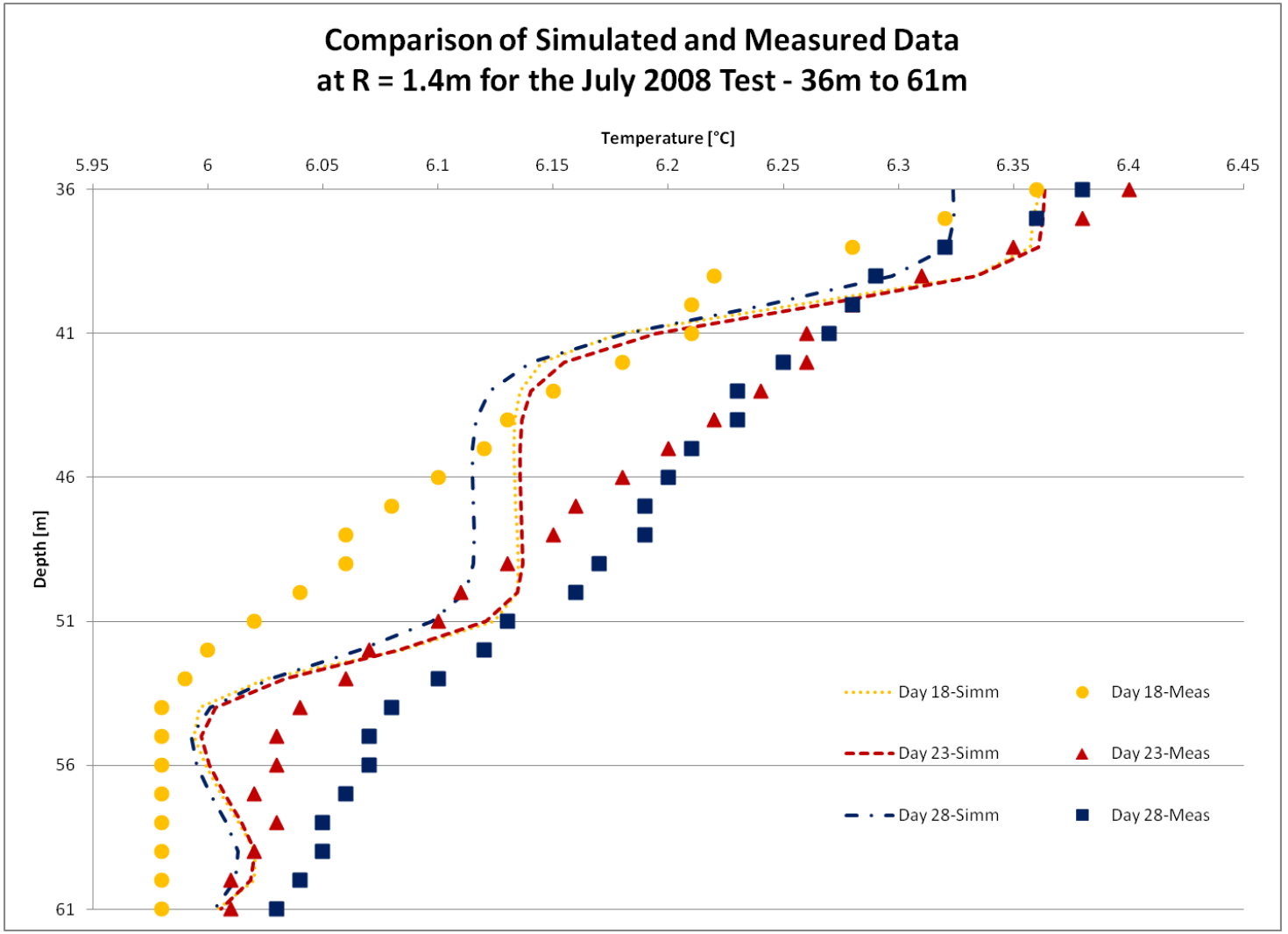

Figure 49 Results for Material Combination H. Best Calibration Results for the Depth Varying Borehole Wall Heat-Flux Case in the Lower Portion of the Domain During the Natural Ground-Temperature Recovery Phase for the Nearer Observation Well

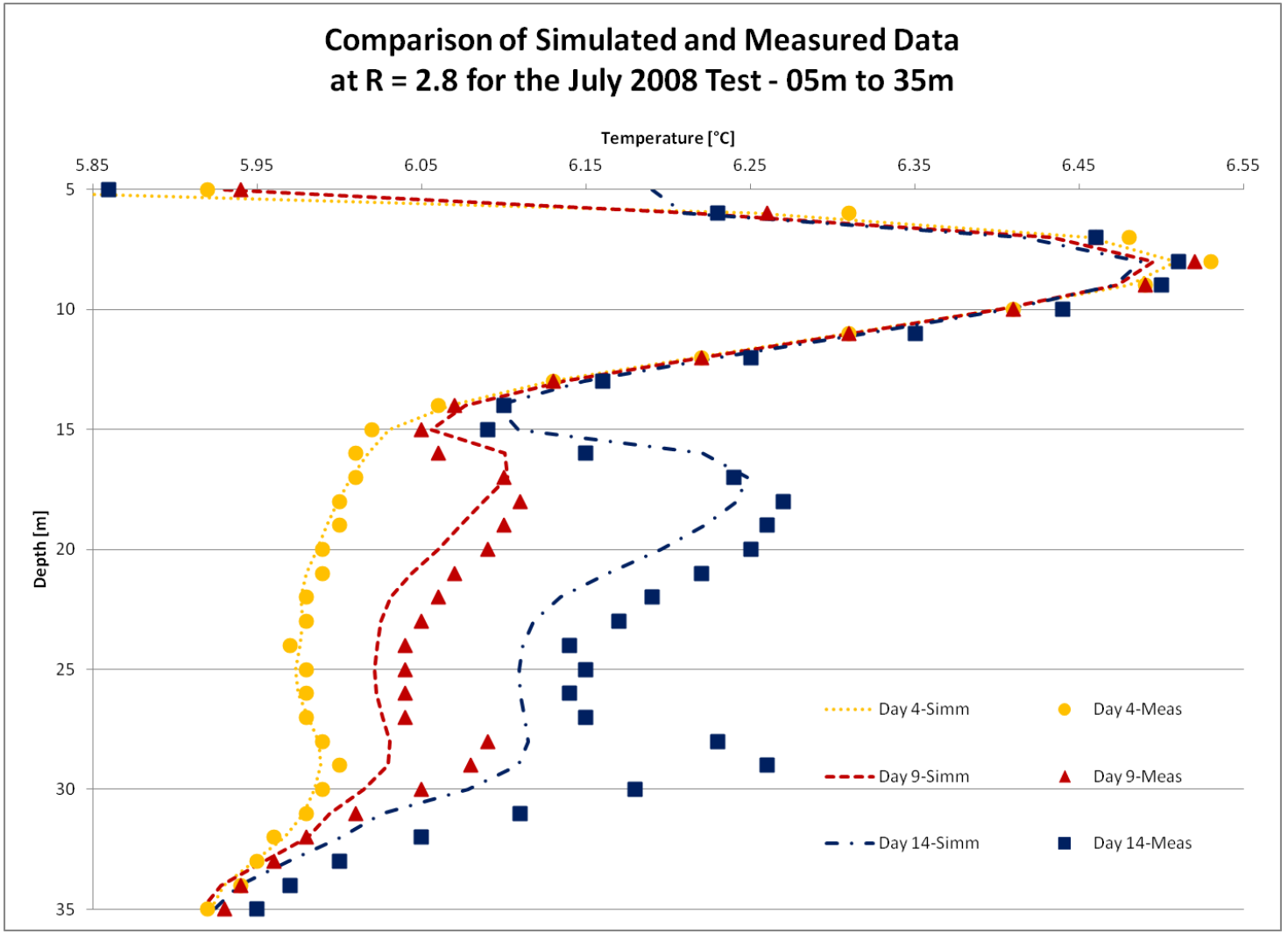

Figure 50 Results for Material Combination H. Best Calibration Results for the Depth Varying Borehole Wall Heat-Flux Case in the Upper Portion of the Domain During the Ground-Heating Phase for the Further Observation Well.

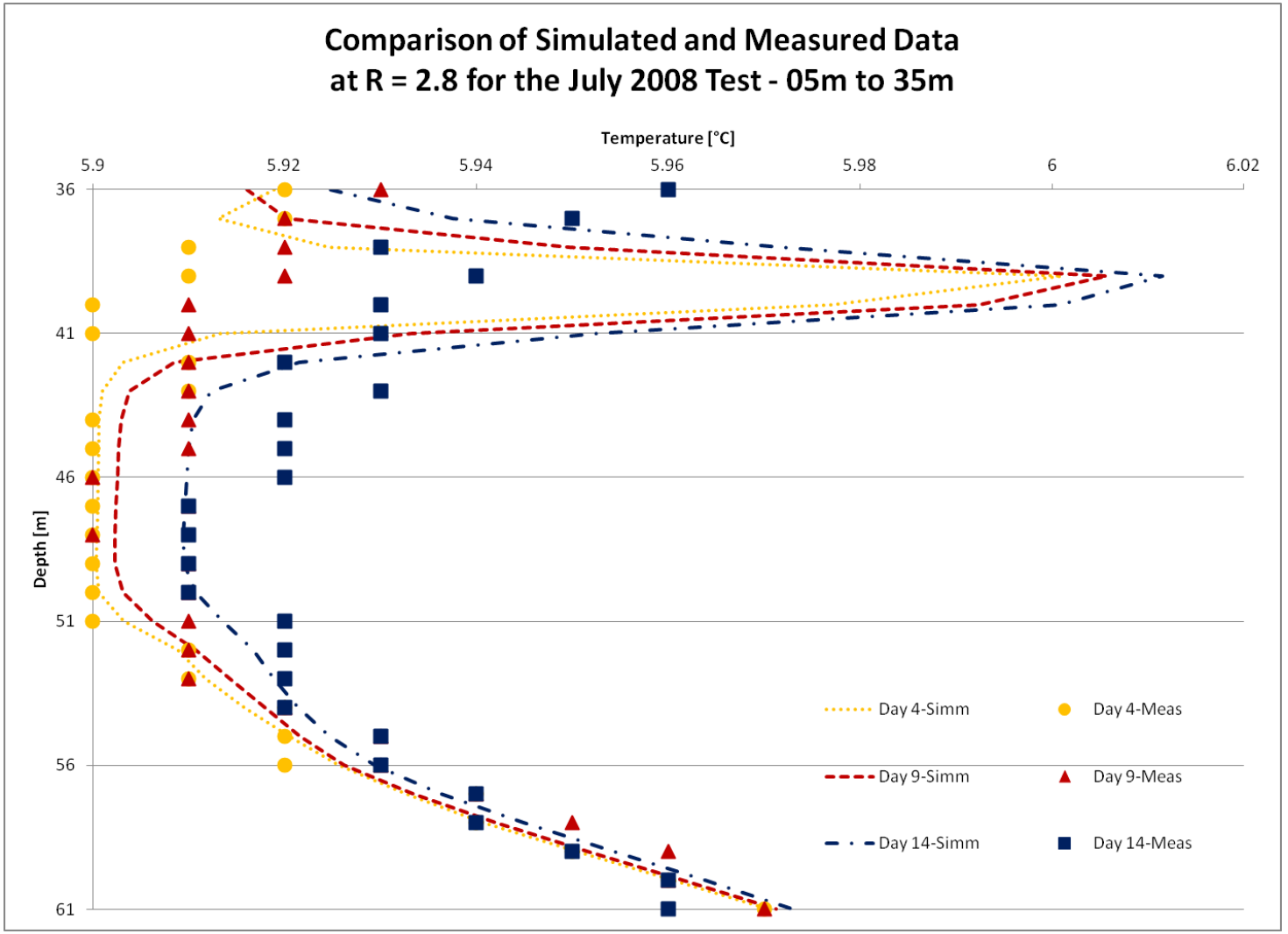

Figure 51 Results for Material Combination H. Best Calibration Results for the Depth Varying Borehole Wall Heat-Flux Case in the Lower Portion of the Domain During the Ground-Heating Phase for the Further Observation Well.

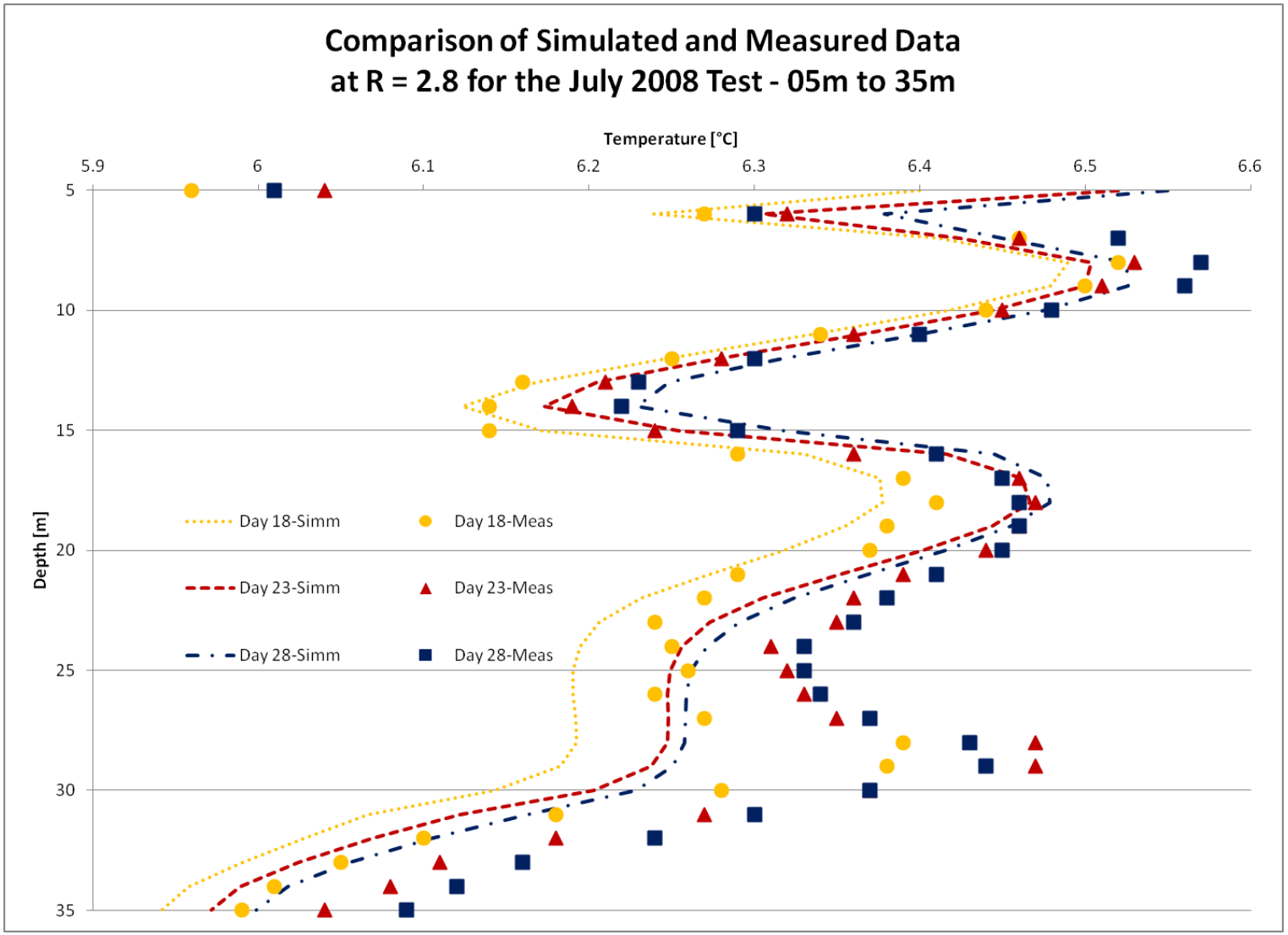

Figure 52 Results for Material Combination H. Best Calibration Results for the Depth Varying Borehole Wall Heat-Flux Case in the Upper Portion of the Domain During the Natural Ground-Temperature Recovery Phase for the Further Observation Well.

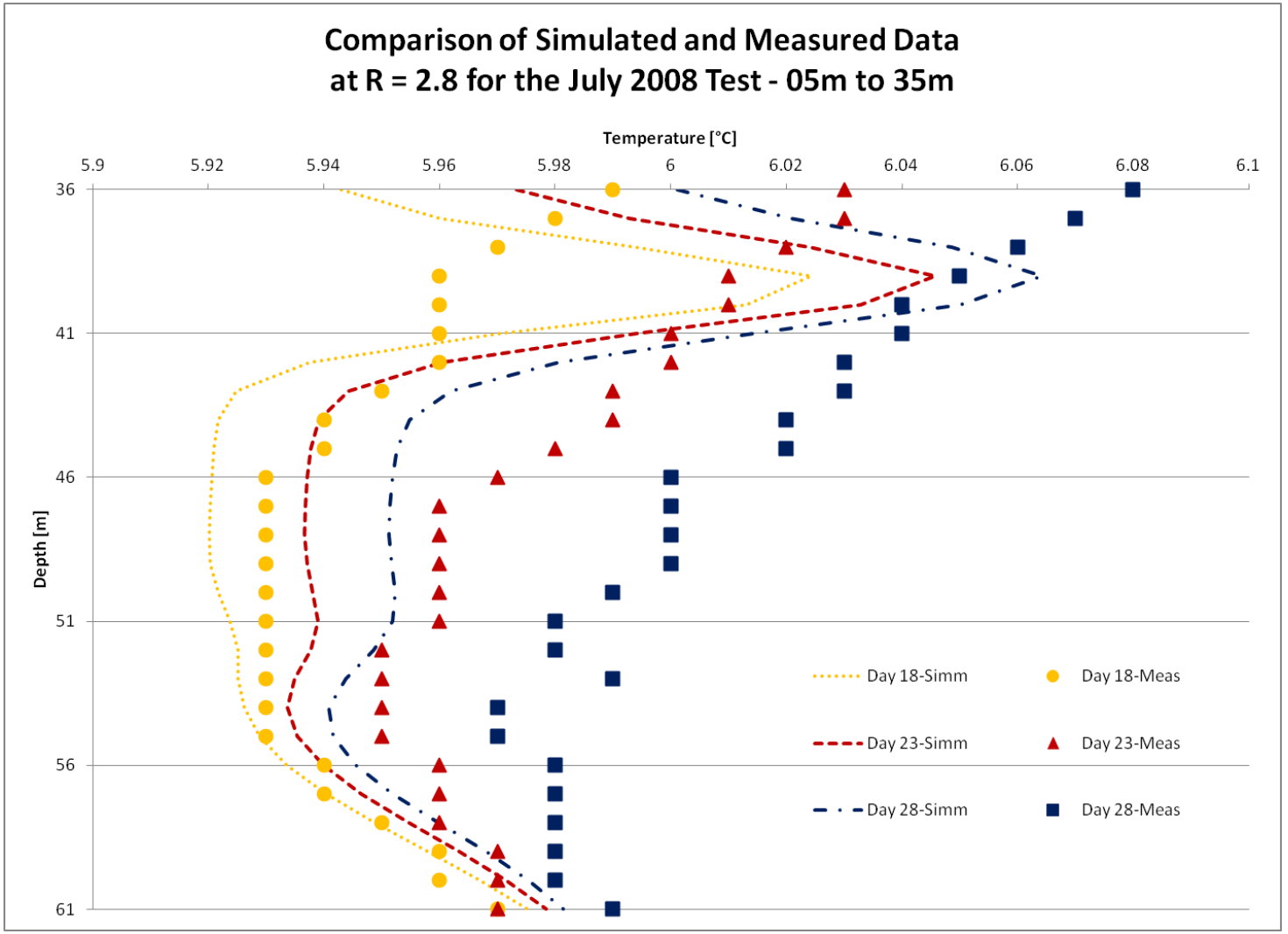

Figure 53 Results for Material Combination H. Best Calibration Results for the Depth Varying Borehole Wall Heat-Flux Case in the Lower Portion of the Domain During the Natural Ground-Temperature Recovery Phase for the Further Observation Well.

4.2.3 The Effect of Vertical Heat Conduction

One of the most intriguing observations from the experimental results was that the hottest portion of the depth range cooled while the surrounding regions warmed, after the deactivation of the heat pump unit. The simplest conclusion would have been that the heat travelled vertically from the hottest part of the underground domain to the cooler regions via vertical conduction through the underground materials. In addition, the vertical distances are over an order of magnitude larger than the horizontal distances. The experimental observations show that the heat from the ground heat exchanger dissipated significantly after only 2.75m of horizontal travel from the borehole wall to the measurement point at 2.8m radial distance from the centre of the borehole in the two weeks of ground-heating. This makes it unlikely that a significant portion of the heat from the elevated temperature region, between about 15m and 32m, could have travelled 10m vertically to the shallowest examined depths, or 29m vertically downward to the lowest measured point in the two additional weeks that this experiment recorded. This is reinforced by the fact that the Temp/W model does not exhibit the same trends in thermal behaviour in the lower regions. However, some vertical heat transfer is bound to occur.

The Temp/W model can give insight into the effect of vertical heat transfer. The Temp/W model is axisymmetric in three dimensions. It solves the transient heat conduction equation in cylindrical coordinates, neglecting angular variations. This means that it models both horizontal and vertical heat flow. Thus it can give us additional information regarding the significance of vertical heat transfer to the phenomenon under study in this thesis. This comes from a comparison of the best of the above models with an approximation of the best of those models which neglects vertical heat conduction.

With additional constraints, the Temp/W model can approximate the simulations of this section such that they exclude vertical heat transfer. This approximation involves slicing the domain into vertical depth intervals that correspond to L_1 through L_6 (see Figure 11). However, L_3 straddles M_2 and M_3. Therefore, there is an additional division that creates a layer that includes the portion of L_3 on M_2, and another layer that includes the portion of L_3 on M_3. Placing no heat flux boundaries on the top and bottom of each of these slices is one of two approximations that guarantees zero vertical heat conduction. The other approximation is to average the initial condition over each of the seven depth intervals. The heat flux and the material properties do not vary on any of these seven depth intervals. Therefore, no vertical heat conduction occurs on each of the seven subsections.

Comparing between the results of the experiment, the calibrated depth varying borehole-wall heat flux computer model with material combination H, and the simplification of that computer model which excludes vertical heat conduction reveals the effect of vertical heat conduction. The models that excluded vertical heat conduction show no variation with depth within each of the seven depth intervals. In addition, the predicted temperature response is not continuous from one depth interval to the next, in the no-vertical-heat-conduction models. In contrast, the temperature response is varied and continuous throughout the entire depth in the computer model that considers vertical conduction. This shows the effect of vertical heat conduction in the computer model.

The comparison between the model that included vertical heat conduction and the model that excluded it also showed much of the same temperature results. This is most prominent near the middle of any of the seven depth intervals. This shows that the effect

of vertical heat conduction has a limited range. If vertical heat conduction was highly significant, one would expect that the model predictions would differ significantly between the model that included it and those that excluded it. Consequently, vertical heat conduction is only significant over a limited distance on the length and time scales of this test. However, vertical heat conduction is quite apparent in the results.

This comparison between the no-vertical-heat-conduction model and the one that allows it shows marked differences at the depth interval boundaries. Vertical heat transfer resulted in the steep slopes of the models that included it. The no-vertical-heat-conduction models showed sharp jumps at the boundaries. Without this effect, a model with the accuracy that the parametric study achieved would have undoubtedly required additional boundary condition steps. This would have increased the complexity of the parametric study and the modelling effort. Therefore, although the range of influence for vertical heat conduction may have been limited, it was not inconsequential. The graphs showing the comparison follow.

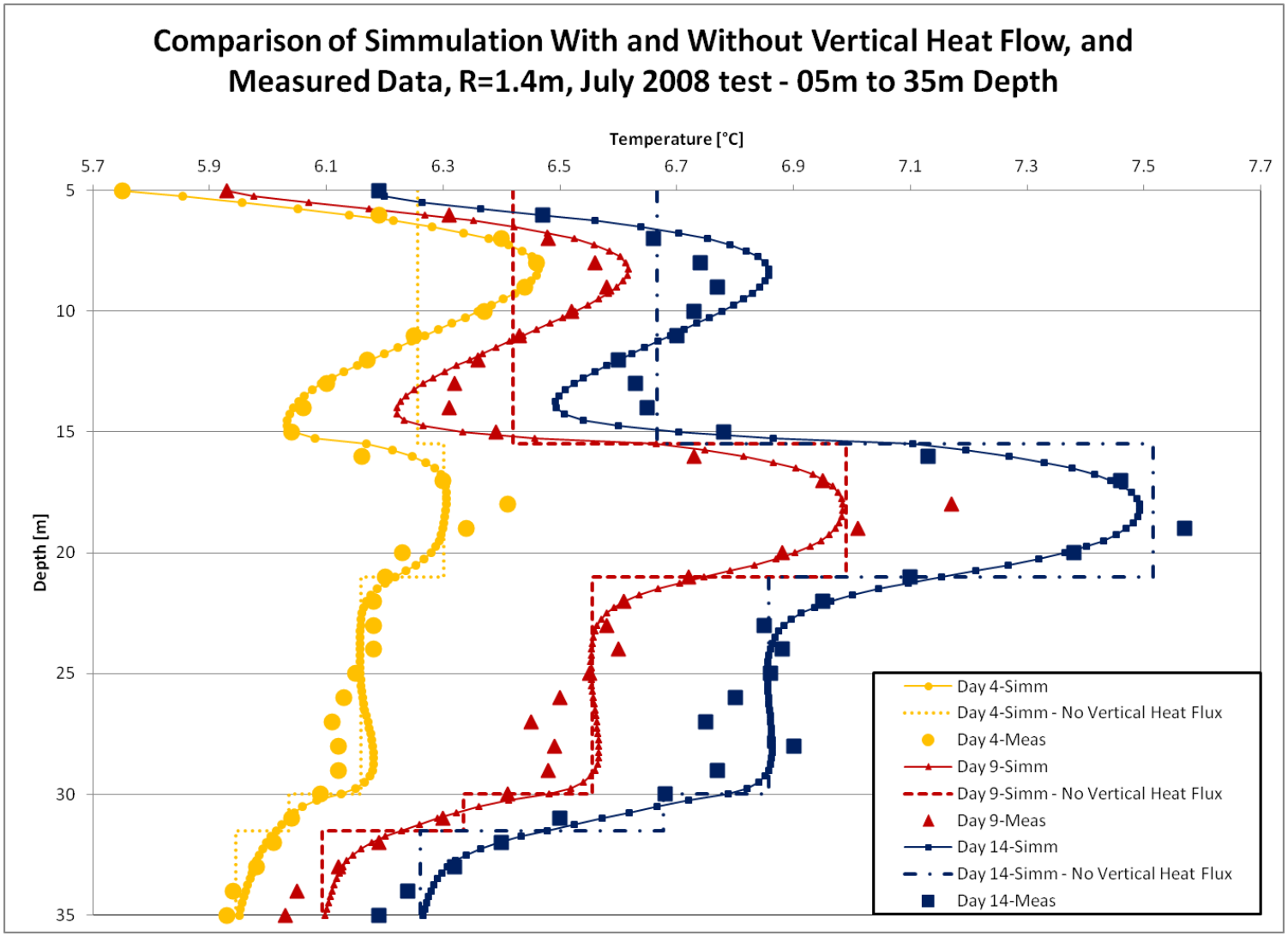

Figure 54 Effect of Vertical Heat Conduction on Computer Modelling for R=1.4m, July 2008 Test 05-35m - Heating Phase.

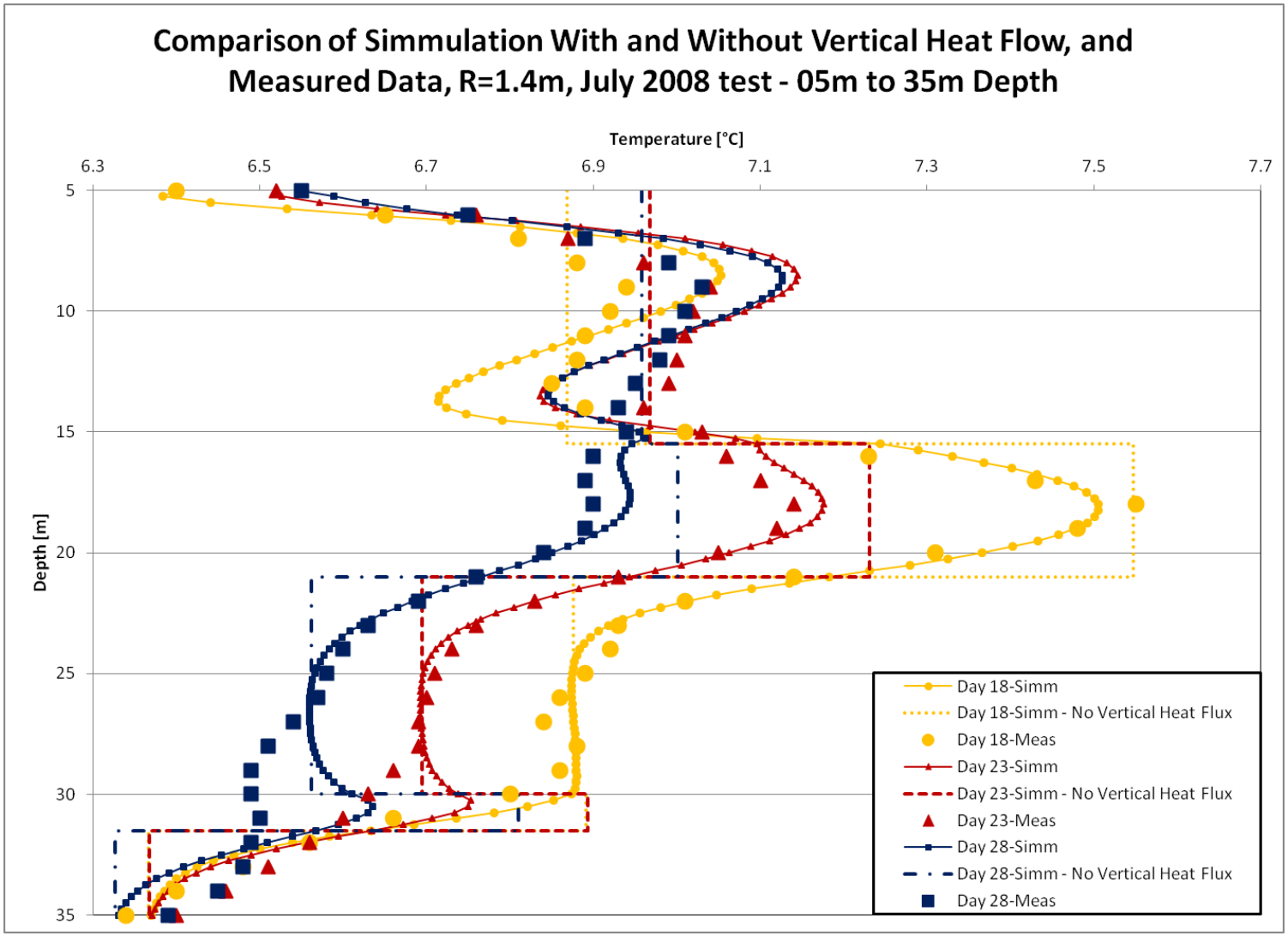

Figure 55 Effect of Vertical Heat Conduction on Computer Modelling for R=1.4m, July 2008 Test 05-35m - Recovery Phase.

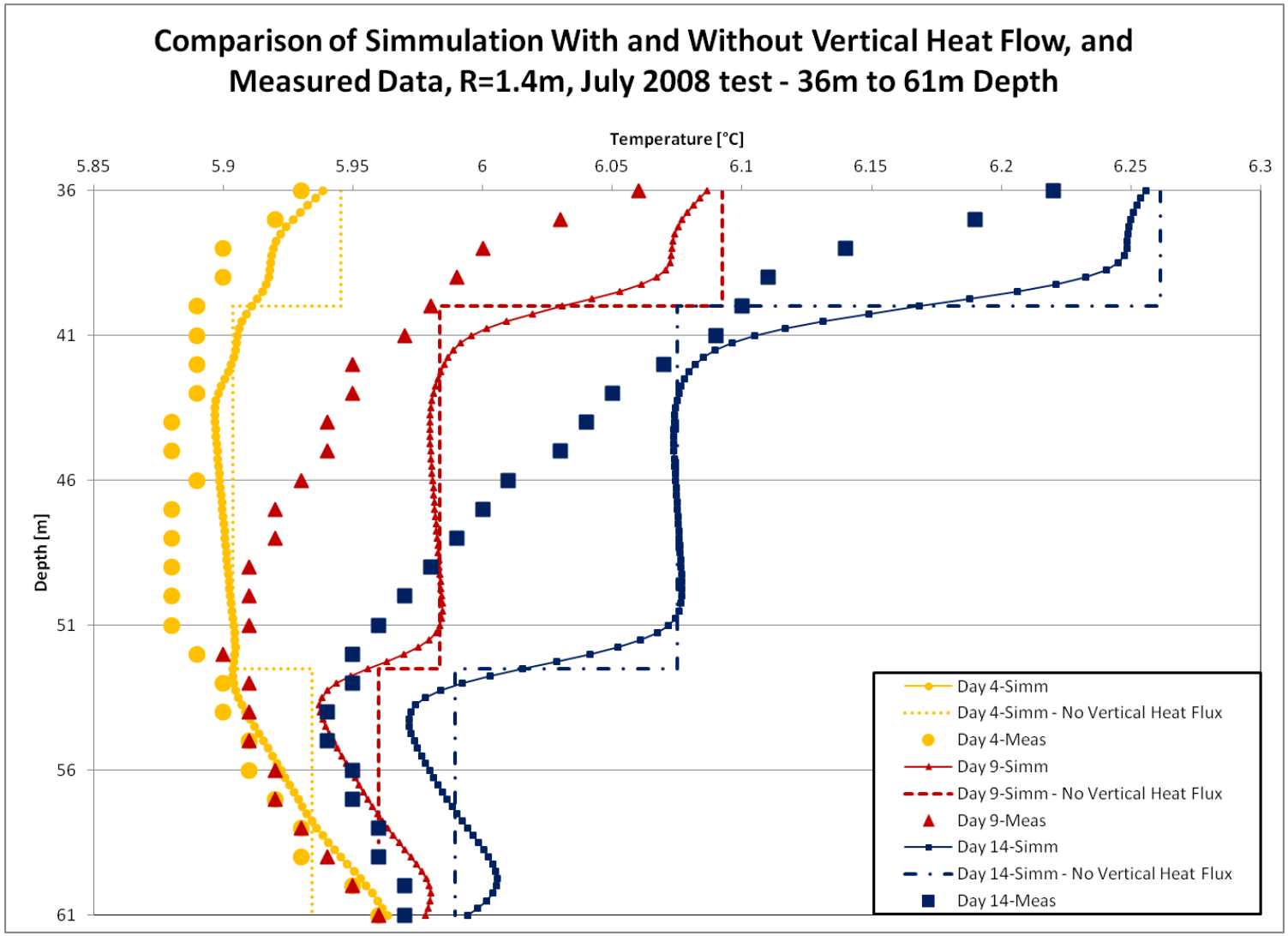

Figure 56 Effect of Vertical Heat Conduction on Computer Modelling for R=1.4m, July 2008 Test 36-61m - Heating Phase.

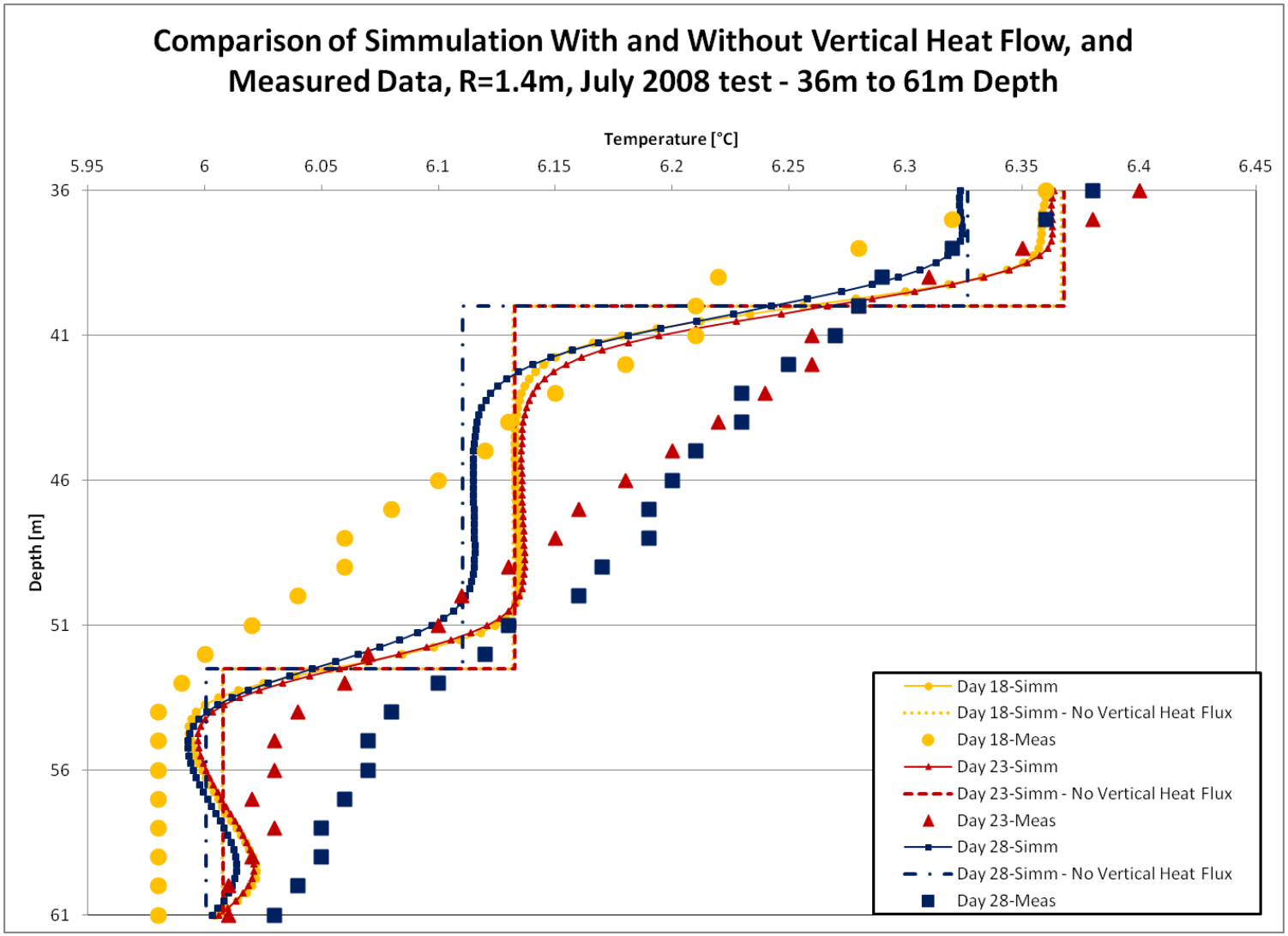

Figure 57 Effect of Vertical Heat Conduction on Computer Modelling for R=1.4m, July 2008 Test 36-61m - Recovery Phase.

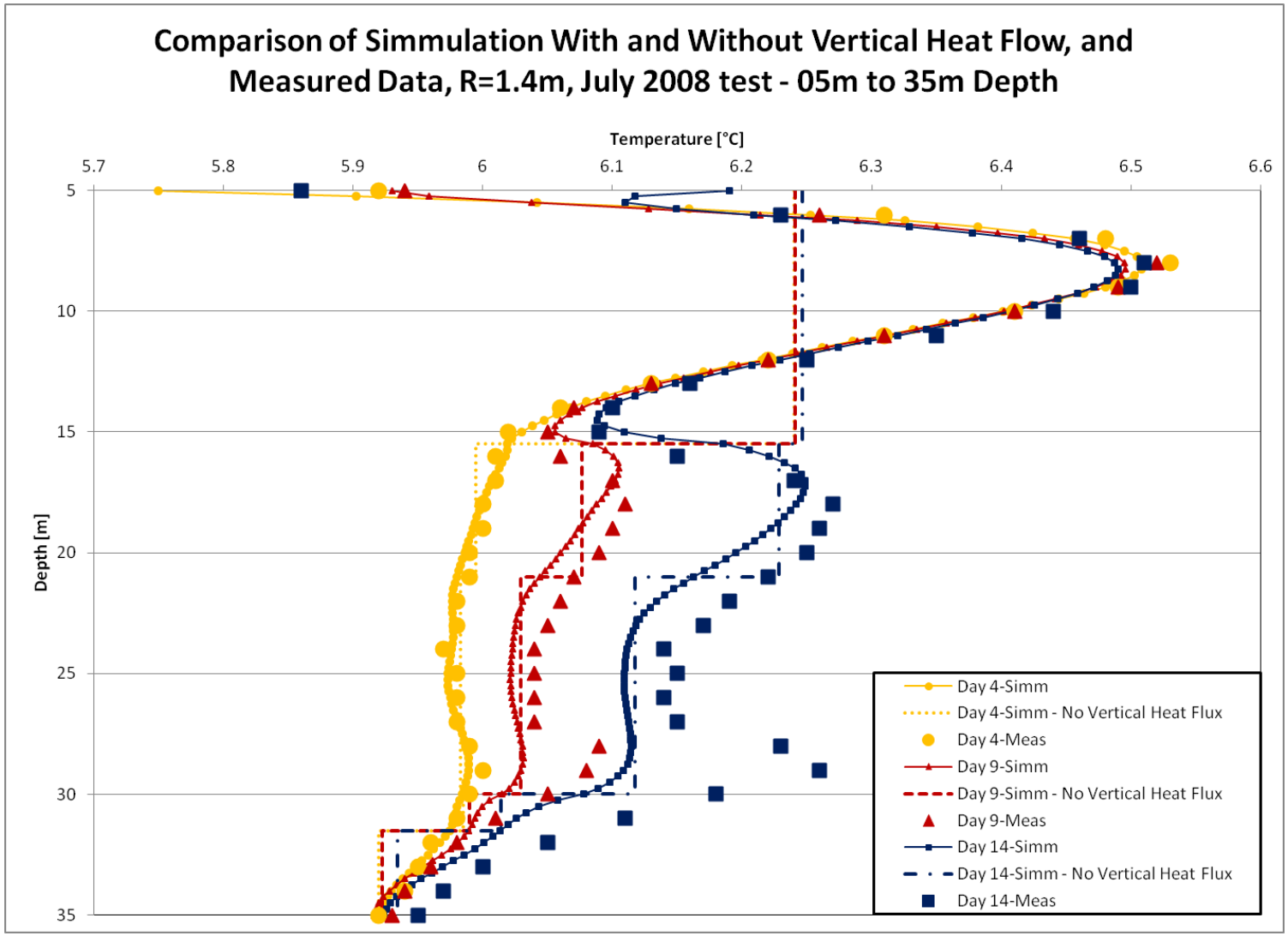

Figure 58 Effect of Vertical Heat Conduction on Computer Modelling for R=2.8m, July 2008 Test 05-35m - Heating Phase.

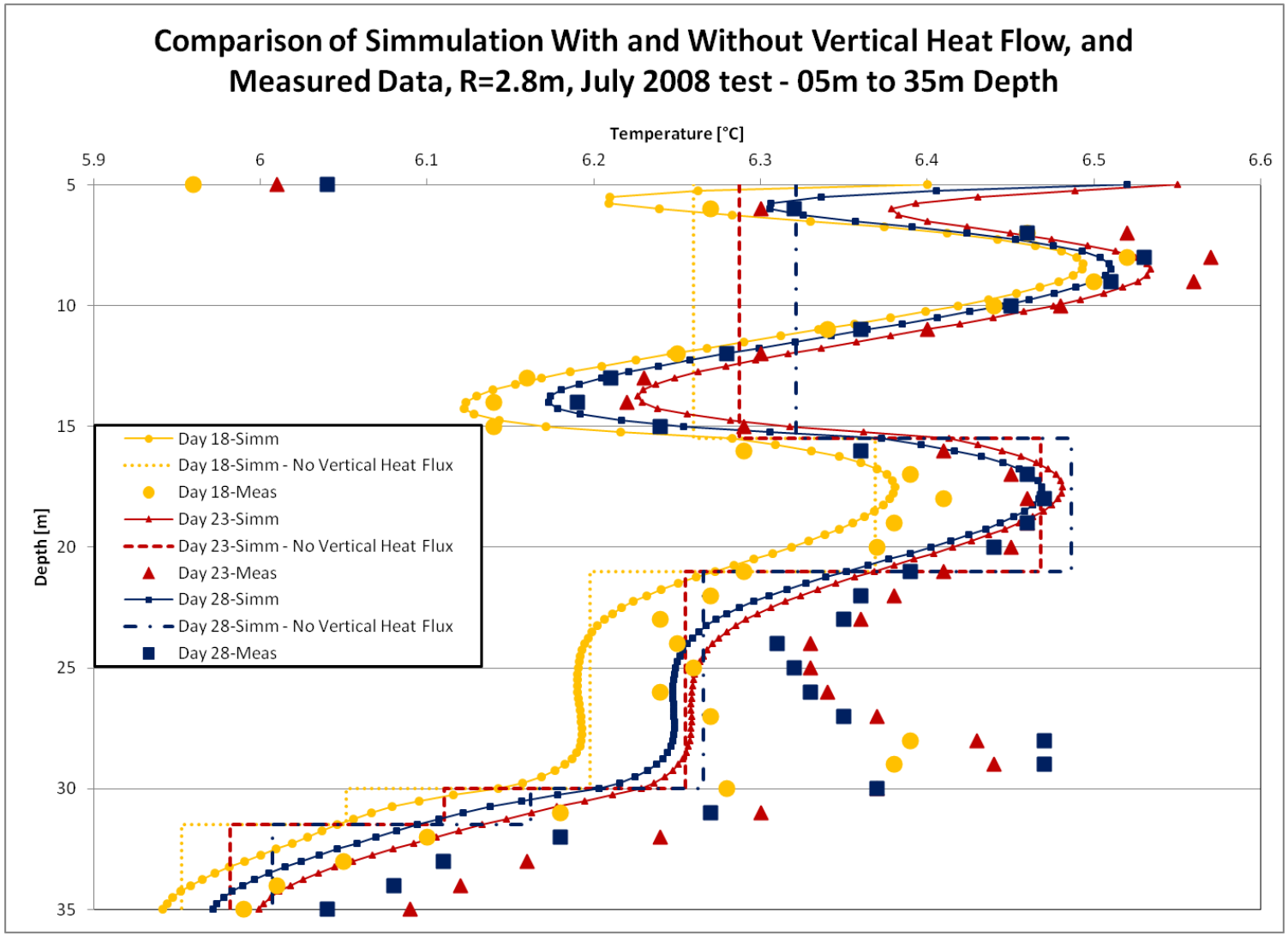

Figure 59 Effect of Vertical Heat Conduction on Computer Modelling for R=2.8m, July 2008 Test 05-35m - Recovery Phase.

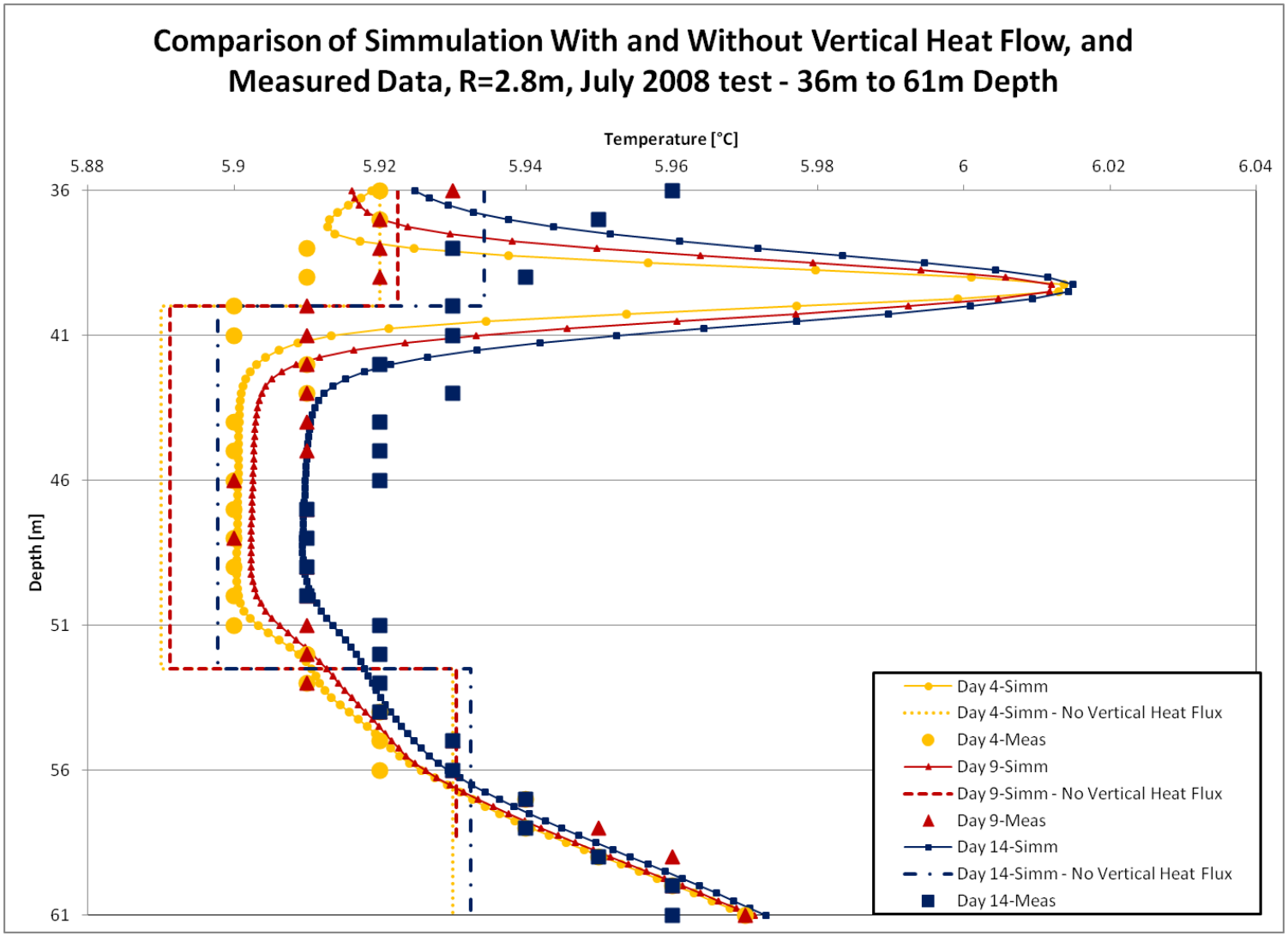

Figure 60 Effect of Vertical Heat Conduction on Computer Modelling for R=2.8m, July 2008 Test 36-61m - Heating Phase.

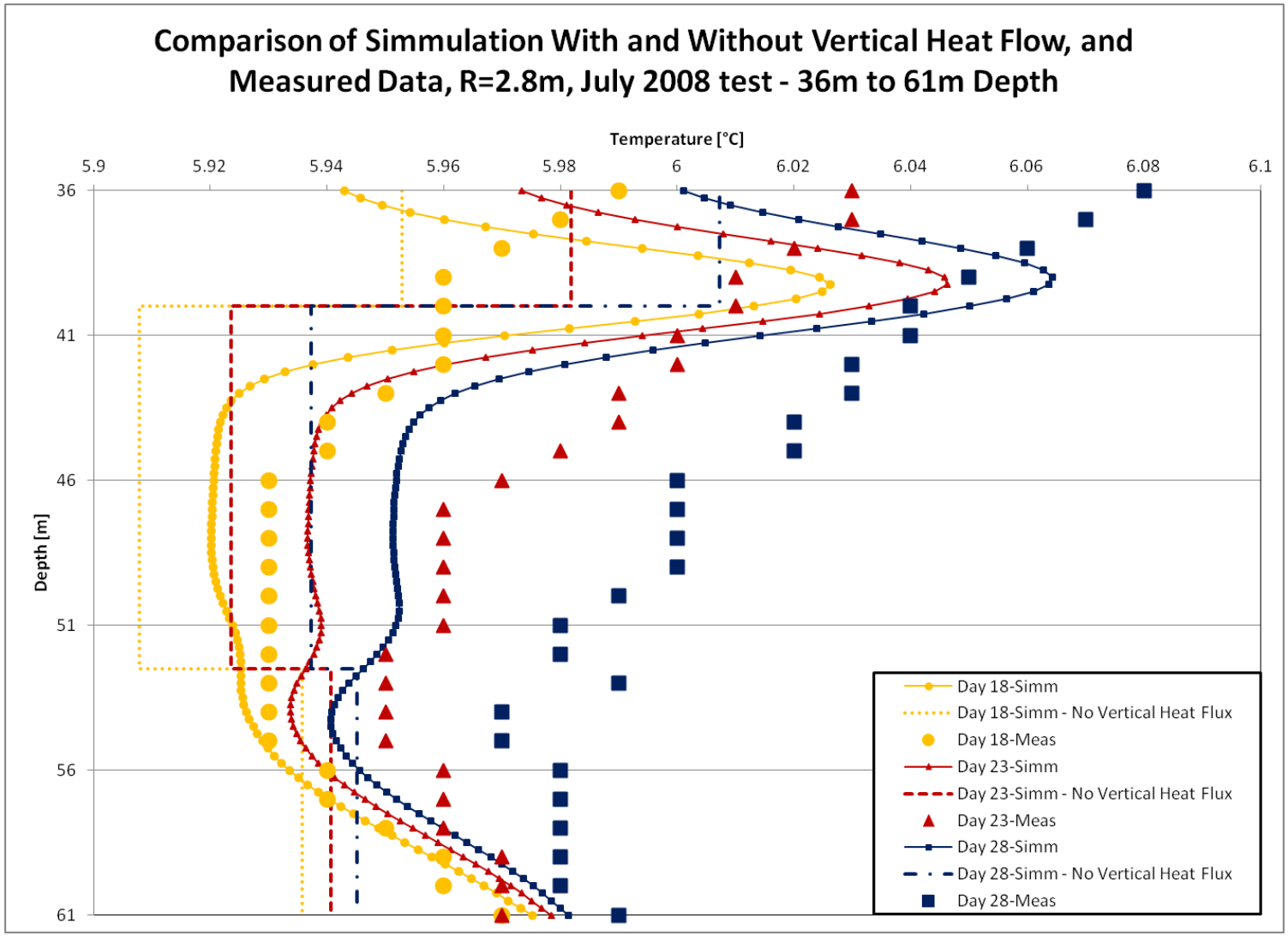

Figure 61 Effect of Vertical Heat Conduction on Computer Modelling for R=2.8m, July 2008 Test 36-61m - Recovery Phase.

4.3 Alternate Modelling Scenarios

This section covers the alternate modelling scenarios that this investigation evaluated after the depth varying and time invariant borehole wall temperature and heat flux boundary condition models of the ground heat exchanger output did not reproduce some of the features of the experimental results. The alternatives include different models of the ground heat exchanger, and convective effects within the porous underground media. This section evaluates the two additional boundary condition models that the Temp/W software provides, called the convective surface and thermosyphon boundary conditions, for their utility in modelling the ground heat exchanger. In addition to those possibilities, this study also considered various options for time-varying temperature and flux models. Finally, this section discusses the possibility that free convection within the porous underground media caused the effects that the previous conceptual model did not predict.

4.3.1 Alternate Models of the Ground Heat Exchanger

One alternative model for the ground heat exchanger is forced-convective heat transfer. Temp/W has a limited convective heat transfer model. The convection option in Temp/W allows the user to simulate convection on the surface of a modelling domain. The only inputs for the convection model are the convective-heat transfer-coefficient and the far-field fluid temperature, which may vary in time. However, the software does not accept any information regarding the fluid's velocity field, temperature distribution, or specific heat capacity. This means that Temp/W's convection model can only accommodate modelling scenarios where the heat transfer characteristic, such as the fluid temperature, convective heat transfer coefficient, and the resultant heat transfer rate are approximately spatially constant throughout the area where convection occurs.

The purpose of modelling the ground heat exchanger using a convection model would be to capture transient or spatial effects resulting from convection in the borehole that the previous modelling efforts did not reproduce. However, Temp/W would not be able to predict the fluid temperature throughout the U-Loop because of its limitations. Instead, the user would have to supply an estimate of the fluid temperature distribution with depth, as well as an estimate of the appropriate heat transfer coefficient. Consequently, this would be like using the temperature boundary condition except that it would have the added uncertainty of the convective-heat-transfer-coefficient. Further confounding the utility of the convection boundary condition type in this analysis is that an intercomparison between this boundary condition type and the temperature boundary condition type showed that they give the same results for cases relevant to this study.

This study also considered the thermosyphon boundary condition type to see if it could model the convection occurring in the ground heat exchanger of this experiment. The purpose of the thermosyphon model is to simulate the effect of a specific type of thermosyphon. This is a gas-filled system that uses natural convection in an air-to-gas heat exchanger installed above the ground surface to transfer heat between the atmosphere and the underground. The thermosyphon model calculates a time-varying flux from the aboveground heat exchanger based on climactic data, such as air temperature and wind speed. The model applies the heat flux from the surface heat exchanger evenly over a line in the model of the ground.

The thermosyphon model is actually a special case of the flux boundary condition type. Both of these boundary condition types apply heat flux evenly over a line. In addition, the

flux boundary condition type will model time varying flux. The advantage to using the thermosyphon boundary condition type is that it does all of the work of converting climactic data into heat flux automatically. However, there is no advantage to using the thermosyphon model in the analysis for this thesis.

Time varying boundary conditions that simulate the ground heat exchanger output became attractive after the parametric study showed that time invariant boundary conditions were unsatisfactory in reproducing the more intricate temporal behaviour observed experimentally in the bottom half of the domain. The simplest variable function is a straight-line variation in time. However, a straight-line time dependency model is unsatisfactory for a number of reasons. The model would only be valid for a short time period because a straight line tends to either positive or negative infinity as time increases. Therefore, a linearly varying transient model of either borehole-wall heat flux or temperature would always eventually predict unrealistic values for these quantities. Furthermore, computer modelling in Temp/W showed the ramp temperature case is almost identical to the temperature response at the borehole wall for the depth varying (and time invariant) heat flux case, on the timescale of this study. Finally, additional computer modelling in Temp/W showed that the ramp flux case did not significantly affect the temporal behaviour of the model during the recovery phase. Therefore, this thesis considered more complicated boundary condition models, as in section 4.3.

4.3.2 Regarding the Possibility of Underground Convection

One possible explanation for why the experiment observed effects that the pure-conduction based models did not predict is that there was groundwater convection in the

porous underground media. If this occurred, it would result in a different model of the energy transport in the underground domain. Therefore, this thesis investigated the likelihood of underground convection before considering a new conceptual model that includes convective mixing of groundwater. Domenico and Schwartz (1998, p. 207) give a criterion for the onset of underground convection. The criterion that Domenico and Schwartz (1998, p. 207) quote states that free convection will begin when the Rayleigh Number ($\mathrm{N_{RA}}$) is greater than or equal to $4\pi^2$ (≈ 40), based on the following formula.

$$N_{RA} = \frac{g\rho_0\left(c_{P,W}\rho_W\right)H\kappa\alpha_f\Delta T}{\mu k_e} \qquad \textbf{[3]}$$

The above formula comes from a mathematical model of a porous medium with a vertical temperature gradient. This model assumes a horizontal porous layer with an initially still fluid, where the upper and lower boundaries are isothermal layers that are impermeable to groundwater flow. The temperature difference across the aquifer (ΔT) is supposed to be uniform. This is not exactly the case for in the present study. However, the Rayleigh Number criterion should still be helpful for commenting on the likelihood that underground convection is possible in the present case.

The model for the onset of free convection based on the Rayleigh Number assumes three things that are not like the present study. Firstly, the model assumes that the vertical temperature gradient is uniform with depth. Secondly, it assumes a confined aquifer. Thirdly, the model assumes that the vertical temperature gradient does not vary with horizontal position. Thus, any predictions based on the above formulation are approximate, here. Consequently, this study selected values representative of the present experiment where there was uncertainty in a quantity for the Rayleigh number.

Table 11 Table of definitions for the Rayleigh Number and their associated values, in this study.

Symbol	Name	Value	Units	Comment
N_{RA}	Rayleigh Number	2.02	Dimensionless	Representative value (See below)
g	Acceleration due to Gravity	9.81	m/s^2	
ρ_0	Reference Density	1000	Kg/m^3	Interpreted as in Domenico and Schwartz (1998, p. 208)
$c_{P,W}$	Specific Heat Capacity of water	4200	J/kg·K	
ρ_W	Density of Water	1000	Kg/m^3	Approximate
H	Aquifer Thickness	15	m	Representative value (See below)
κ	Permeability	6.2e-11	m^2	Adapted from (Render, 1983, p. 76)
α_f	Coefficient of Thermal Expansion of Water	8.89e-5	K^{-1}	Incropera and DeWitt (2002, p. 924) @ 10°C
ΔT	Temperature Change Across the Layer	2.75	K	Representative value (See below)
μ	Dynamic Viscosity	1.298e-3	Kg/s·m	Incropera and DeWitt (2002, p. 924) @ 10°C
k_e	Equivalent Thermal Conductivity of the Porous Medium	0.096 to 3.58	W/m·K	From the Parametric Study (see Table 5)

Some of the quantities for the Rayleigh Number are easier to estimate then others. This is because some of them are simply material property values or constants, like the acceleration due to gravity. However, other values are less easy to define. The temperature change across the aquifer layer, the aquifer thickness, the equivalent thermal conductivity, and the representative permeability of the aquifer are difficult to define. The primary reasons for this are that the temperature both increases and decreases with depth at any fixed radial distance from the borehole, and there are multiple underground materials at the experimental site. Consequently, this section used quantities for the unknown values of the formula that were representative of the present experiment.

The best computer model in the parametric study (see 4.2.2) gives vertical temperature profiles at the borehole wall and further radial distances from the centre of the borehole, at 0.05m, 0.125m, 0.25m, 0.50m, 1.4m, and 2.8m. The slope of a linear fit through each of these temperature profiles gives the average vertical temperature gradients at those positions and at the time corresponding to the temperature profile. The temperature profiles from the end of heating time gives the depth-averaged value for the maximum temperature gradients near the borehole and nearly the maximum value at positions further away from the borehole. The respective values of these vertical temperature gradients are; –0.25K/m, –0.183K/m, –0.129K/m, –0.079K/m, and –0.021K/m. The negative sign indicates that the temperature decreased with depth, on average.

There are many choices for the possible representative temperature gradient and depth interval values. However, the smaller temperature gradients are the least likely to result in free convection. Consequently, this section prefers the larger vertical temperature gradients for selecting the representative value. The reasonable choice for the representative value of the vertical temperature gradient is –0.183K/m. There are also a number of possible depths to consider for the depth interval. The ground heat exchanger and its associated ground temperature response penetrate a number of underground layers. However, the present discussion considers the 15m thick upper carbonate aquifer as representative of the system. For consistency, this section will take the equivalent thermal conductivity of the upper carbonate aquifer from the parametric study as the representative value.

The resultant Rayleigh number of 2.02 is much smaller than the minimum requirement ($4\pi^2$). This value makes the likelihood of convection small. However, this number resulted from many estimates. In addition, the model and the physical system differ. Therefore, the Rayleigh Number result for the current system is not completely conclusive. Consequently, this investigation will elaborate on the likelihood of significant natural groundwater convection by discussing its possible role in the transport of energy.

For the sake of argument, let us say that there is free convection in the porous media near the ground heat exchanger. This would only be significant in this study if the groundwater were able to flow fast enough to contribute to the transportation of energy. Domenico and Schwartz (1998, p. 194) give an equation for the groundwater flow velocity that results from convection in a hydrothermal system. This equation uses the same terms that this section has already defined, in addition to the difference between the local and ambient ground temperatures ($T - T_0$) and a gradient ($\partial z/\partial x$). The value of this gradient is one for vertical flow, as in the present discussion.

$$v = \frac{\kappa g \rho_0 (T - T_0)}{\eta \mu} \frac{\partial z}{\partial x} \qquad \textbf{[4]}$$

Table 11 gives the relevant material values for [4] and the parametric study gave the porosity value as 0.12, for the upper carbonate aquifer. The computer model predicts that the ground temperature in the warmest part of the upper carbonate aquifer at the end of heating time would be about 8.6°C, on average throughout the natural ground temperature recovery phase. The location for this data was at a radial distance of 0.125m, which is the location of the representative temperature gradient for the Rayleigh Number

calculation. The ambient ground temperature is about 6°C. This gives the difference between the local and ambient ground temperatures as 2.6°C. Under these circumstances, the average vertical groundwater velocity resulting from convection during the part of the natural ground temperature recovery phase that this experiment recorded would be a mere 9.06e-7m/s, or 7.83cm/day. Of course, the local ground temperature would be less at greater depths or radial distances from the borehole centre. Consequently, this is nearly the maximum average groundwater velocity.

The potential groundwater velocity of 7.83cm/day indicates that if there had been any groundwater flow due to free convection, that groundwater could have only travelled a total of 1.10m in the 14 days that this study investigated the ground temperature after the end of the ground temperature heating phase. Thus, it is highly unlikely that the warmer, upper regions could have affected the cooler lower regions by free groundwater convection. This is because the groundwater could not have travelled far enough to convey heat from the warmer regions to the colder ones. The groundwater simply could not have moved fast enough, if it were in fact flowing. In addition, the graphs of section 4.2.3 show that the effects of vertical heat conduction in a purely conductive scenario are several vertical metres, every day. Clearly, this is a much smaller distance than the 7.83cm/day that the groundwater could have travelled. Thus, these are two additional reasons to discount free convective groundwater flow as an effective method of energy transport in this study.

The potential groundwater travelling distance of 1.10m is also very significant because it indicates that it would not have been possible for a convective loop to make a single

mixing cycle in the representative 15m thick underground layer. Consequently, if there had been any convective mixing in the underground, the warmer groundwater would have been rising for the entire measurement time, except for within one metre of the top of the unit. If the groundwater near the ground heat exchanger rose, slightly, during the natural ground temperature recovery phase, the surrounding groundwater would have had to take its place. This means that the rising, warmer water would have been replaced by cooler water from its surroundings. This is because the ground temperature decreased with greater depth, and with greater radial distance from the borehole.

The result of the warmer groundwater rising would have been to draw up the cooler surrounding groundwater. This would have resulted in an unexplained reduction in the local ground temperature throughout the area where convection may have occurred – except, perhaps for the shallowest of depths. However, the experiment showed an unexplained resilience in the ground temperature value where the experimental results differed significantly from the purely-convection model. In addition, the experimental results in those regions also showed a significant depth range where the ground temperature rose consistently. Thus, the experiment showed the opposite affect from what natural groundwater convection would have likely caused. This supports the conclusion of unlikely groundwater convection based on the low Rayleigh Number and the initial discussion of the implications of the short potential groundwater travel distance. Therefore, this section concludes that natural groundwater convection was likely not present or significant in the experiment for this study.

4.4 More Advanced Modelling Scenarios

The experimental results show that the ground temperature does not increase by a measureable amount at the nearer observation point until at least a few days after the ground heat exchanger began heating the ground. This time in reasonably consistent within the clay layer and in the upper carbonate layer, although the value in the clay layer is larger than the value in the upper carbonate layer. However, the time to the initial measurable temperature change increases with depth in the lower carbonate aquifer. Similarly, the day on which the maximum temperature occurred was reasonably consistent within each of the two shallower ground layers. In this case, the time was greater in the clay layer. However, the number of days until the occurrence of the maximum measured temperature increased with depth in the lower carbonate aquifer. However, the computer simulations based on the time invariant models of the ground heat exchanger output predicted that these events occurred at roughly the same time in the lower carbonate layer, as in the upper carbonate layer and the clay layer. In addition, unlike the computer simulations, the form of the measured temperature maximum in the lower carbonate aquifer changed from a rounded peak at higher elevations, to a temperature plateau at mid elevations, finally becoming a continual temperature increase from about 44m to 61m depth (see Figure 62 to Figure 65).

The more advanced modelling puts forth two hypotheses to explain the discrepancies between the experimental results and the computer simulations based on the depth varying (time invariant) borehole-wall heat flux and temperature models of the ground heat exchanger in the lower carbonate aquifer. The two hypotheses are the ‘staggered start hypothesis’, and the ‘U-Loop natural convection hypothesis’. Together, these

hypotheses seek to explain the aspects of the temperature response in the bottom half of the experimental domain that the previous models could not explain. The staggered start hypothesis seeks to explain the fact that the ground temperature begins to change by a measurable amount increasingly later with increasing depth below about 32m. In addition, this hypothesis seeks to partially explain why the maximum ground temperature also occurs progressively later with depth. The U-Loop natural convection hypothesis seeks to complete this explanation as well as to explain the plateau-like temperature maxima that occur in the lower carbonate aquifer.

4.4.1 Staggered Start Hypothesis

The staggered start hypothesis holds that the ground heat exchanger is initially ineffective below a certain depth, and that this depth actually becomes deeper with time. The experimental observation that leads to this hypothesis is that the time to the initial temperature response increases with depth in the lower limestone layer. There is further evidence of this in that the duration between the initial temperature response and the maximum temperature is consistent for almost all of the lower depth range. All of the material ranges between 5m and 61m depth showed this consistency. However, the clay and upper limestone began warming and peaked at roughly the same time in each layer. A consistent start time for the heating explained these phenomena very well. Therefore, a heating start-time that effectively increases with depth should explain why all of the features occur increasingly later with depth in the lowest range.

There are other supporting factors for the staggered start hypothesis. The computer modelling indicates that the bottom half of the domain probably experiences a small

fraction of the total heat transfer. The extremely low temperature response in the lower limestone layer that also decreases with depth seems to support this point, experimentally. This supports the staggered start hypothesis because of the overall constant heat transfer from the heat pump unit. The constant HPU output implies that the total heat transfer rate within the ground is also essentially constant. Therefore, the clay and upper limestone layers would experience greater heating at the beginning of the test due to the lower region experiencing little or no heat transfer. This could only work if the extra heat is not very significant because the constant heat transfer model worked so well in the clay and upper limestone layers. The graphs that follow show the improvement associated with the Staggered Start Hypothesis over the time invariant model, as well as a comparison with the subsequent model that includes the second transient assumption.

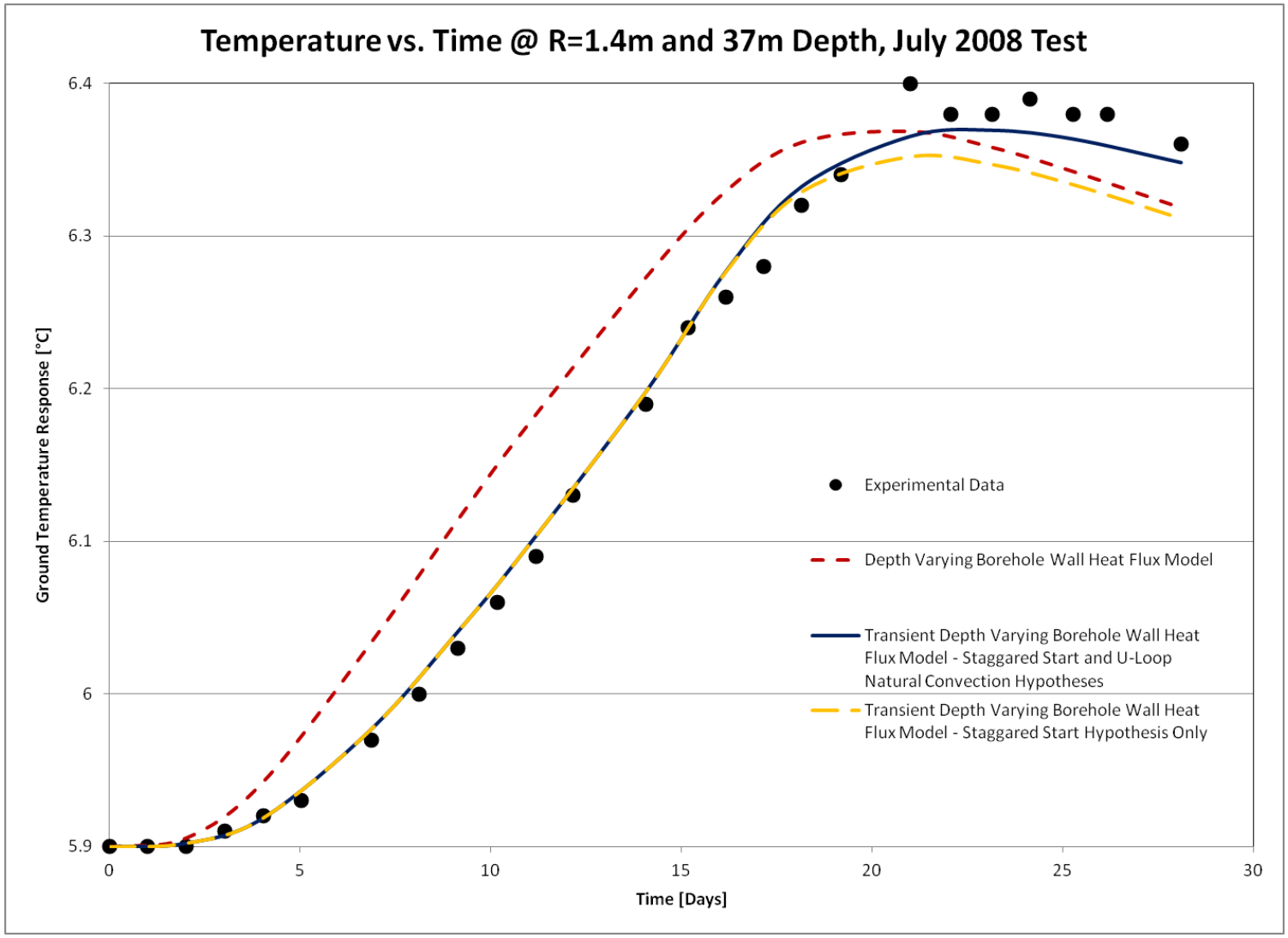

Figure 62 Comparisons Between The Three Depth Dependant Borehole Wall Heat Flux Models and The Experimental Results at R=1.4m and 37m Depth.

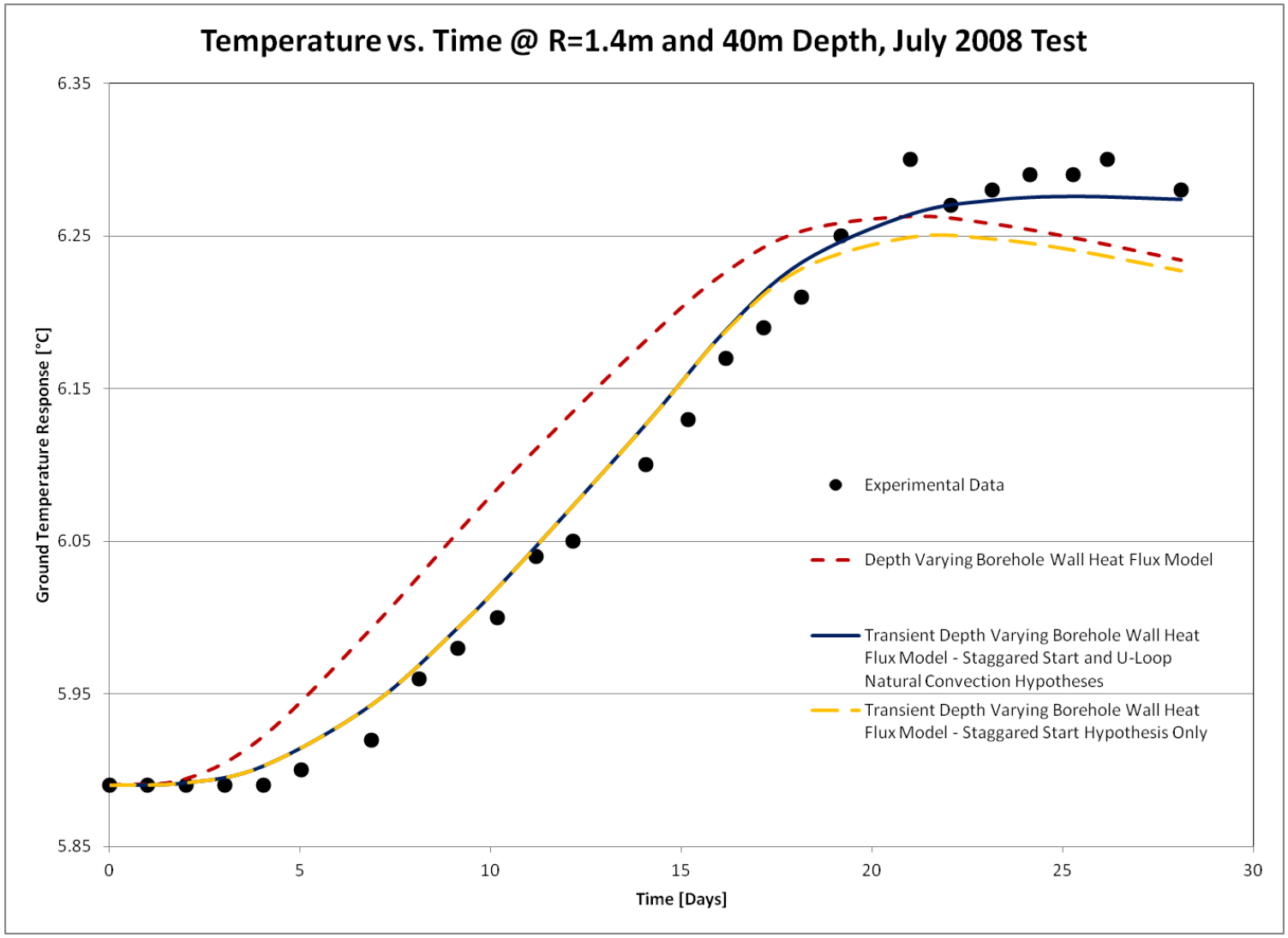

Figure 63 Comparisons Between The Three Depth Dependant Borehole Wall Heat Flux Models and The Experimental Results at R=1.4m and 40m Depth.

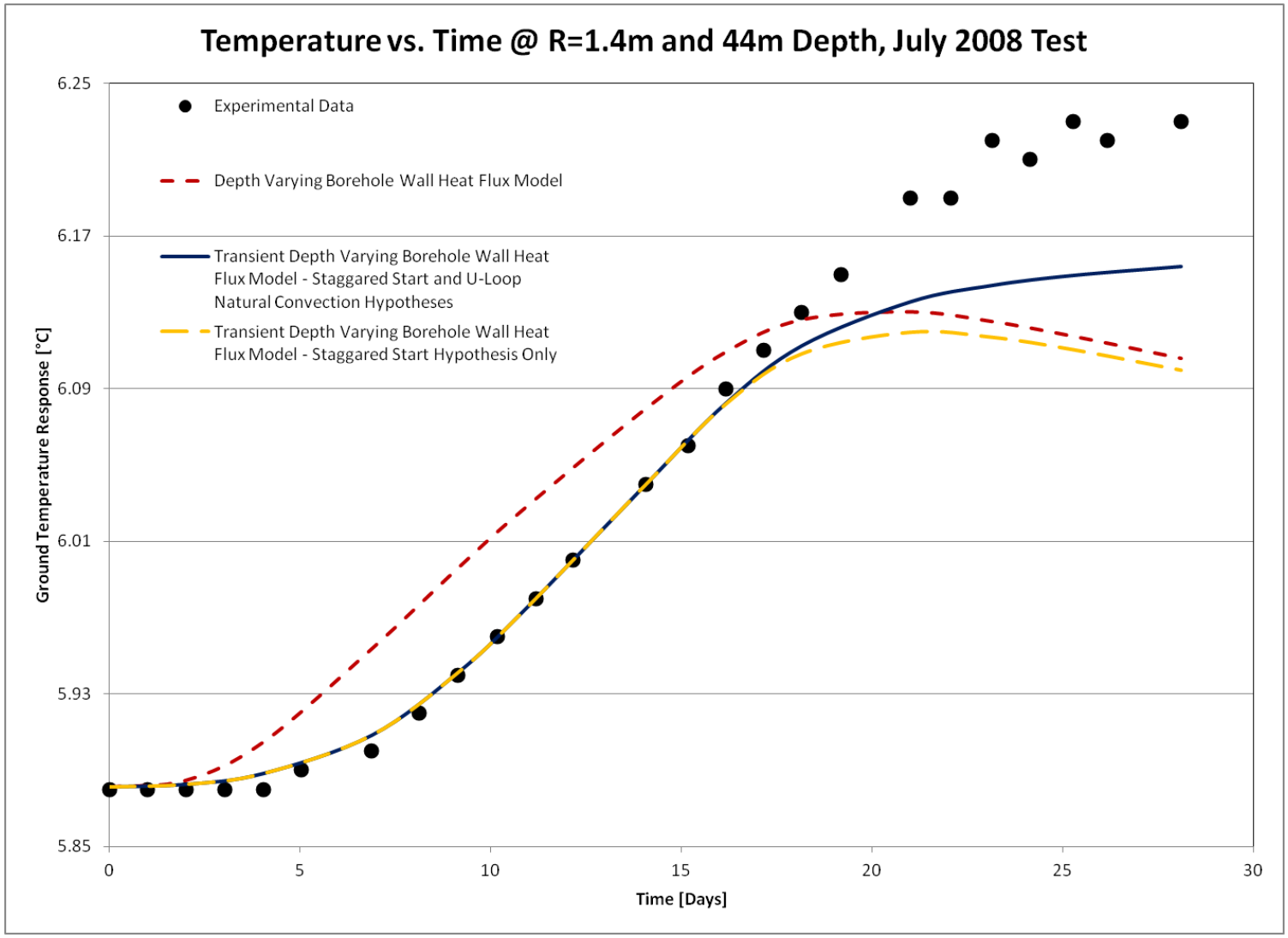

Figure 64 Comparisons Between The Three Depth Dependant Borehole Wall Heat Flux Models and The Experimental Results at R=1.4m and 44m Depth.

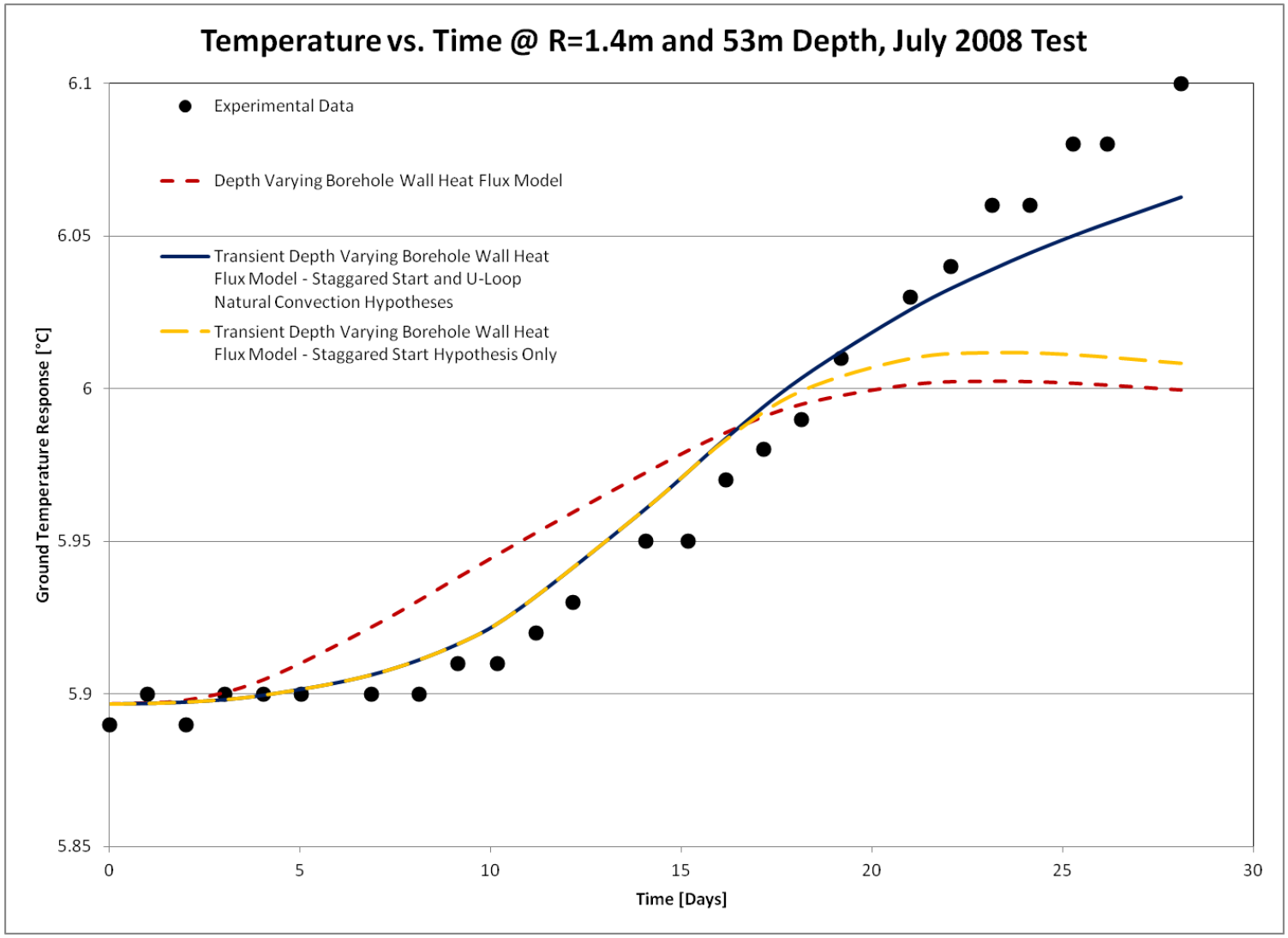

Figure 65 Comparisons Between The Three Depth Dependant Borehole Wall Heat Flux Models and The Experimental Results at R=1.4m and 53m Depth.

4.4.2 U-Loop Natural Convection Hypothesis

The above figures show that the staggered start hypothesis improves model performance during the ground heating phase. These figures also show that this hypothesis alone does not improve upon the time-invariant model during the recovery phase. These models both predicted a more rapid temperature decline than the experiment measured despite the fact that optimum ground thermal property and heating values were used (see 4.2.2). Typically, these models also predicted the same temperature values during the recovery phase. This shows that the lower region in unlike the clay layer, which showed a similarly slow temperature recovery. The computer modelling showed that the lower recovery rate in the clay layer was because of the material properties of the clay layer.

Incorporating only the staggered start hypothesis into the computer model resulted in distinct temperature peaks throughout bottom half of the domain. This is in contrast to the plateau-like temperature response (see Figure 63) and continued temperature increase during the natural recovery phase in the lower region of the domain (see Figure 64 and Figure 65). This suggests that something is causing the ground temperature to remain elevated. This is particularly peculiar because it seems to require an active heat source, after the deactivation of the ground heat exchanger. This conjecture results from the fact that no combination of reasonable material property values and heating during the heating phase could reproduce the slow temperature decrease observed in experiment. One possible explanation for this behaviour is that natural convection occurring in the U-Loops of the ground heat exchanger after shutdown provides the extra heat.

One important note about both of these hypotheses is that they imply a small deviation from the time invariant depth varying borehole wall heat flux case in the upper portion of the domain. This is crucial because the time invariant depth varying borehole wall heat flux explains the temperature response in both of the two upper layers very well. Clearly, one criterion for any valid explanation for the behaviour in the lower half of the domain is that does not worsen the comparison between modelling and experiment in the upper half of the modelling domain. The simplest way of accomplishing this is to make no more than very slight changes to the model of the upper portion of the domain. Fortunately, the two hypotheses presented do not degrade the results in the upper portion of the domain, as the graphs that follow demonstrate.

The computer model to demonstrate the feasibility of the staggered start and natural conversion hypotheses used the best results from section 4.2. These results were the depth varying borehole wall heat-flux model that used material combination H. Representing the two new hypotheses for the advanced modelling required changing the time invariant flux values to time varying functions. These changes included altering the flux in the top half of the domain so that it would experience slightly more heat transfer for the beginning portion of the heating phase. This accounts for the lower portion of heat exchanger being ineffective at the beginning of the experiment. The lower regions experienced little or no heat transfer for the beginning of the heating phase to simulate the staggered start hypothesis. To simulate the convection hypothesis, the zero-heat transfer assumption at the borehole wall during the natural temperature recovery phase changed. The top half of the domain experienced slight heat extraction while the bottom half of the domain experienced slight heat addition during this phase.

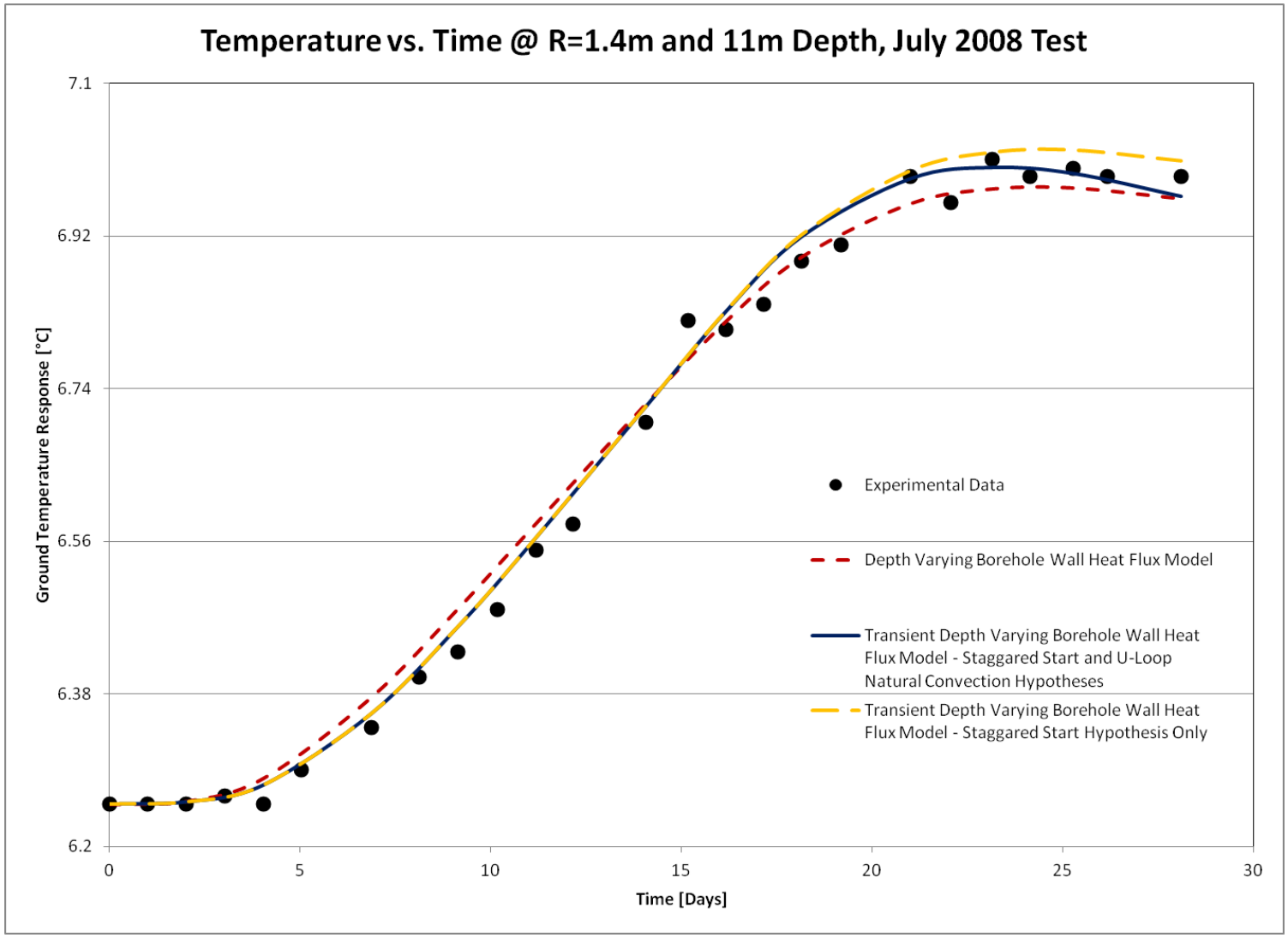

Figure 66 Comparisons Between The Three Depth Dependant Borehole Wall Heat Flux Models and The Experimental Results at R=1.4m and 11m Depth.

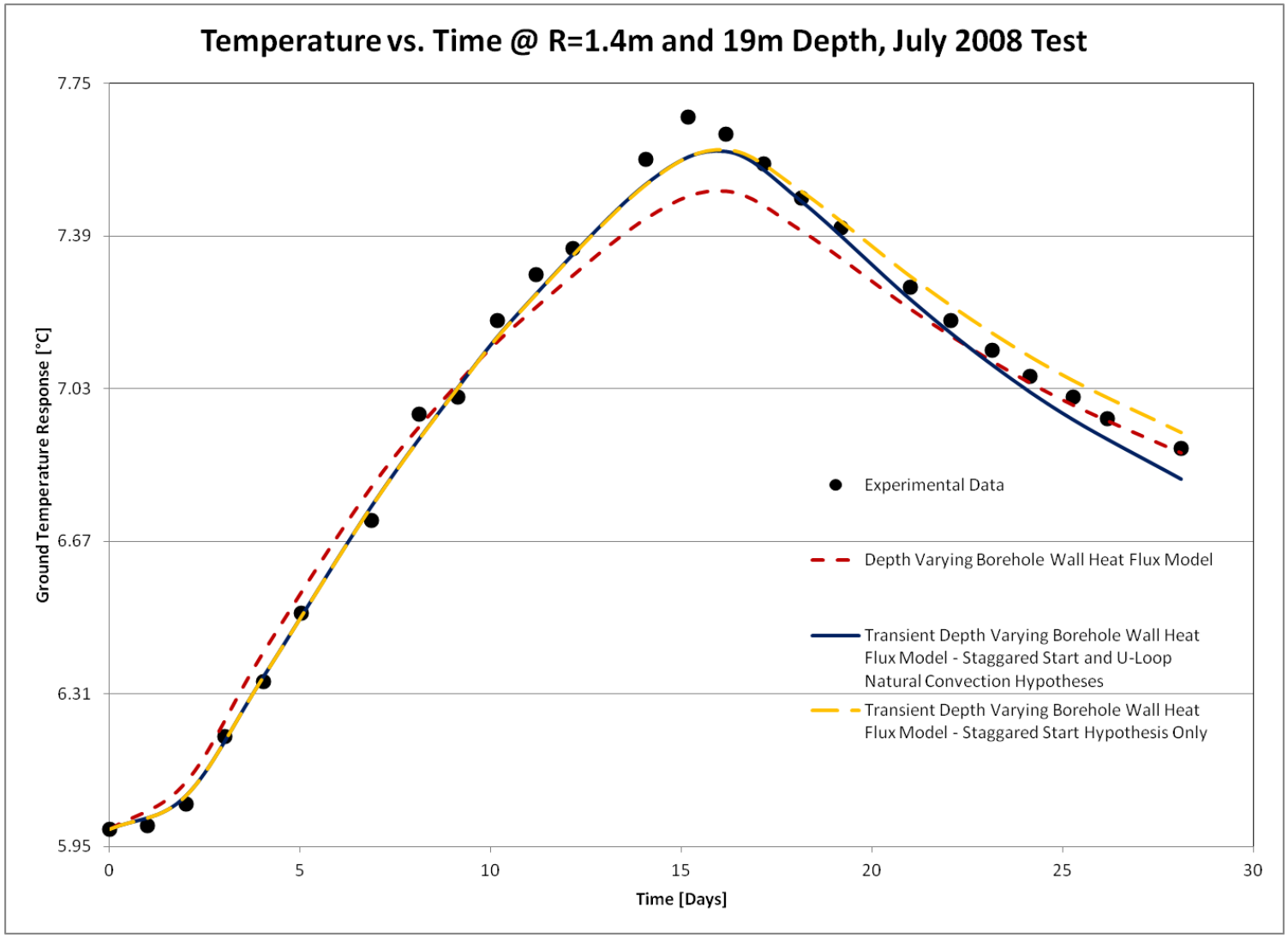

Figure 67 Comparisons Between The Three Depth Dependant Borehole Wall Heat Flux Models and The Experimental Results at R=1.4m and 19m Depth.

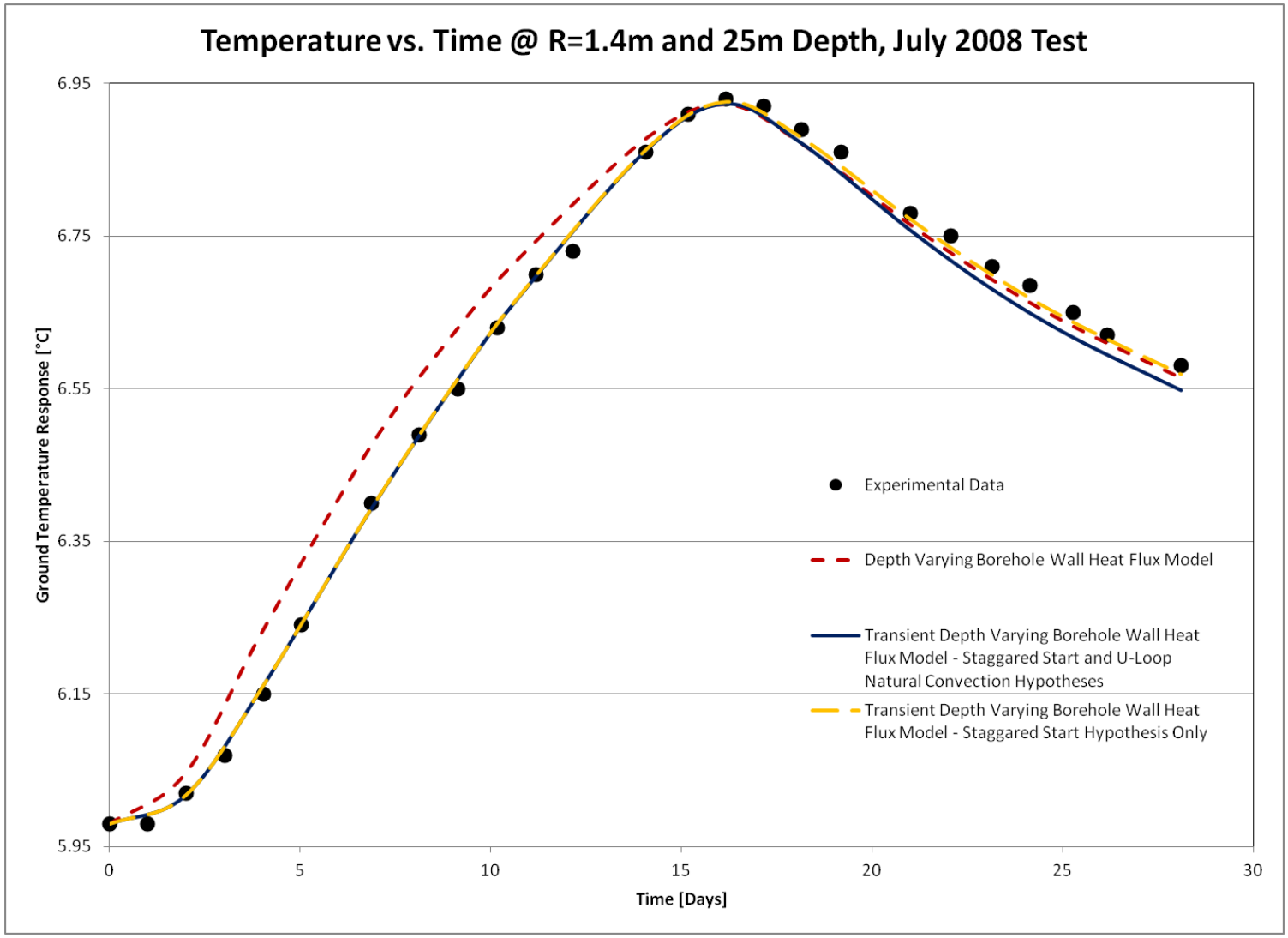

Figure 68 Comparisons Between The Three Depth Dependant Borehole Wall Heat Flux Models and The Experimental Results at R=1.4m and 25m Depth.

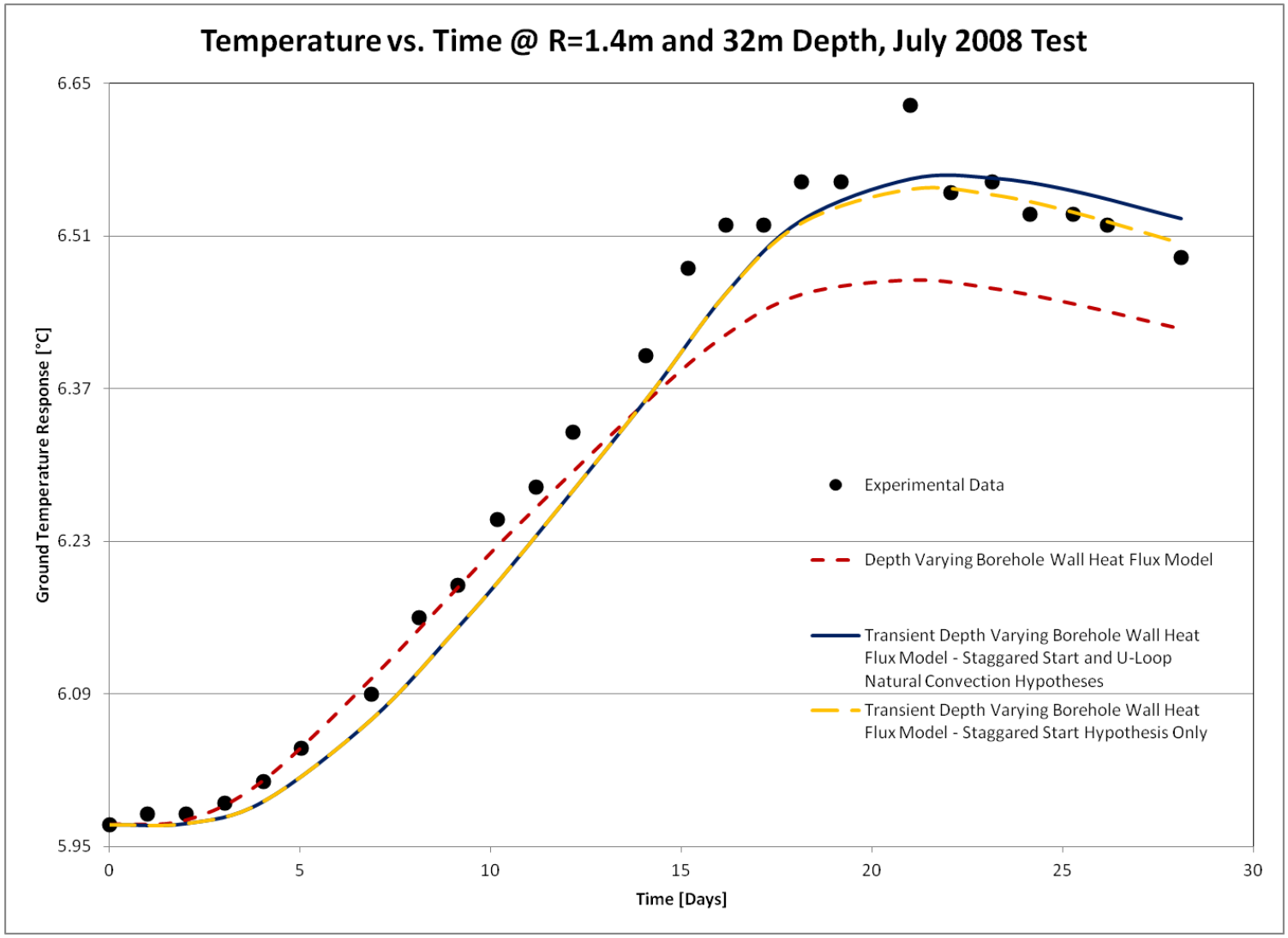

Figure 69 Comparisons Between The Three Depth Dependant Borehole Wall Heat Flux Models and The Experimental Results at R=1.4m and 32m Depth.

This later conceptual model proved quite effective. This model was able to improve the match in the lower region of the model significantly without adversely affecting the match in the upper portion of the domain. The model did so while maintaining a nearly constant overall heat transfer rate during the heating phase of $\dot{Q}_{model} = 1732\text{W}\pm31\text{W}$. The overall heat transfer rate was negligibly small during the recovery phase, ranging between 12.28W and 18.00W. However, there should not be any overall heat transfer rate after deactivating the heat pump and associated systems.

According to the natural convection hypothesis, all of the power that the bottom portion of the domain transfers should comes from the top portion. According to the computer simulation model, the lower part of the domain receives 105.5W from day 14 to day 21, 90.5W from day 21 to day 25, and 89.9W from day 25 to the end of the experiment on day 28. The computer simulation model predicted that the upper portion of the domain gives 87.8W, 77.8W, and 74.2W over the same respective time intervals. Thus, the heating deficit from the upper portion is less than ten percent for all modelling time. The excess heating power that the model predicted may be an estimate of the contribution of the uppermost 5m that the computer simulation does not consider. It may also give an indication of the accuracy of the model. Most likely, it is a combination of these two.

The detailed model results follow. The flux values that produced the improved model are in Table 13. Figure 70 shows the overall heat transfer rate versus time of the entire model for both experimental stages. Figure 72and Figure 73 show the improved match between the simulation and the experiment. These graphs show that the more advanced model is able to reproduce the experimentally observed temporal trends. All of the temperature

lines now occur in the same chronological order in both the model and the experiment. This represents a major improvement over the simpler modelling that was not able to accomplish this.

The comparison between the best model using depth varying borehole boundary conditions and the current, transient, depth varying model are in Table 12. This table qualitatively shows the significant improvement in the level of agreement between simulation and experiment in the bottom portion of the domain that this more advanced modelling sought. Additionally, the table shows that incorporating the staggered start and continued convective heating hypotheses did not adversely affect the upper portion of the domain. Two out of the three effects were positive, with the improvements in L_1 and L_2 outweighing the decline in L_3. This is significant because it shows that in addition to greatly improving the model performance in the lower half of the model, the application of the more advanced assumptions is not a detriment to the upper layers and may even improve the performance of the model there.

Table 12 Comparison Between the Time Invariant and Transient Borehole Wall Heat Flux Models of the Ground Heat Exchanger Output

Depth Interval Line	Best RMSE From the Best Simple Model [°C/100]	RMSE From the Advanced Modelling [°C/100]	Relative Improvement [°C/°C]
L_1	9.04029	9.02121	0.21%
L_2	5.31496	5.18658	2.42%
L_3	6.73109	6.89314	-2.41%
L_4	5.45800	4.69590	13.96%
L_5	4.28691	3.35151	21.82%
L_6	2.23234	1.31953	40.89%

Table 13 Transient Boundary Conditions Used in the More Advanced Modelling.

Time Varying Borehole Wall Heat-Flux Values

L_1

Day	t [Sec]	q [W/m^2]
0	0	130
4^+	347821	112.5
14^+	1214401	-11

L_3

Day	t [Sec]	q [W/m^2]
0	0	155
9+	789211	150
14^+	1214401	-5
21	1813860	-2

L_5

Day	t [Sec]	q [W/m^2]
0	0	15
4^+	347820	45
14^+	1214401	12

L_2

Day	t [Sec]	q [W/m^2]
0	0	318
2+	172381	270
11	931652	250
14^+	1214401	-21
23^+	1999231	-19

L_4

Day	t [Sec]	q [W/m^2]
0	0	50
2	172380	65
11	931652	100
14^+	1214401	10
21	1813860	4

L_6

Day	t [Sec]	q [W/m^2]
0	0	2.5
7	593610	15
14^+	1214401	12

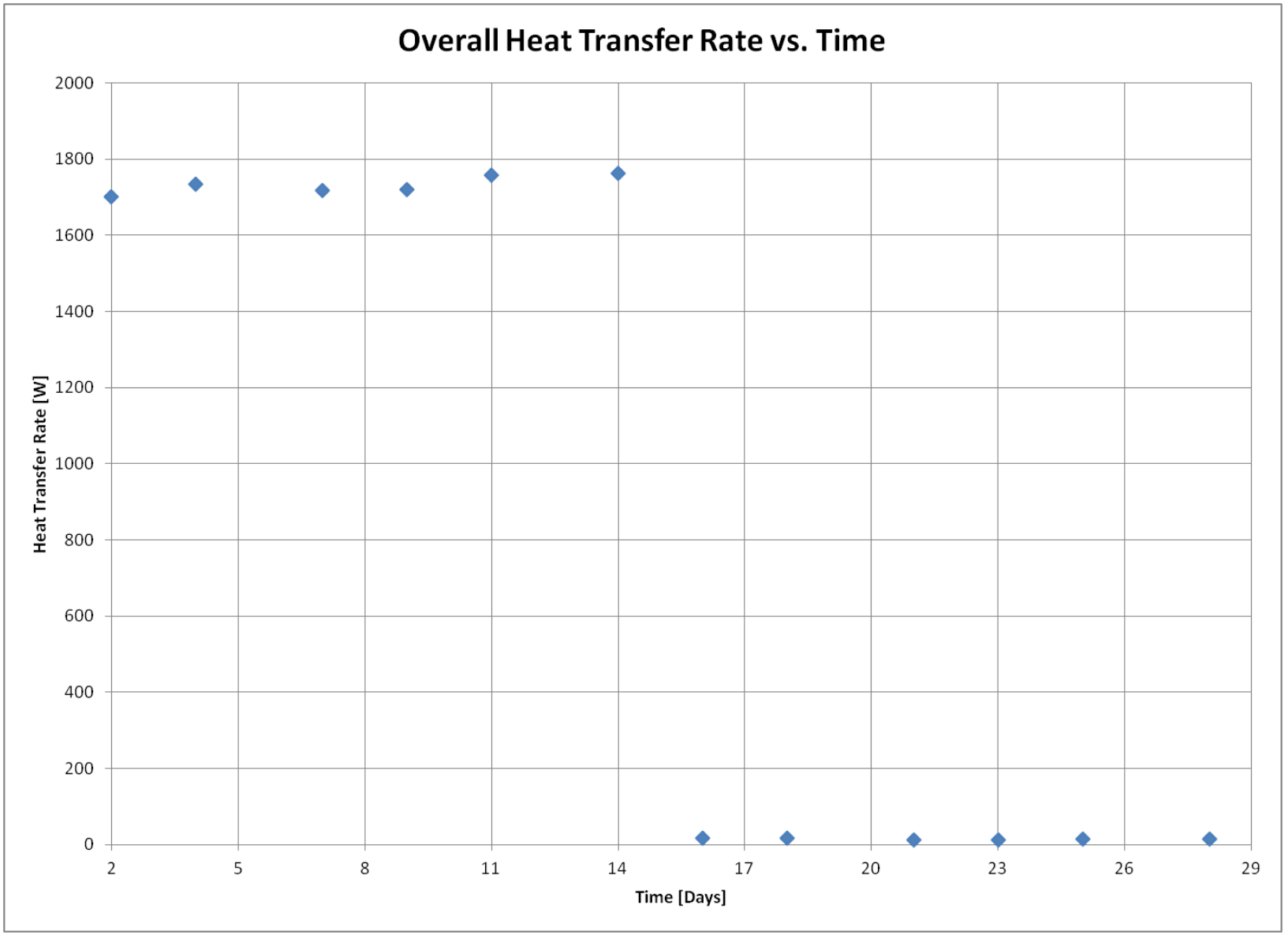

Figure 70 Overall Heat Transfer Rate versus Time Throughout the More Advanced Model

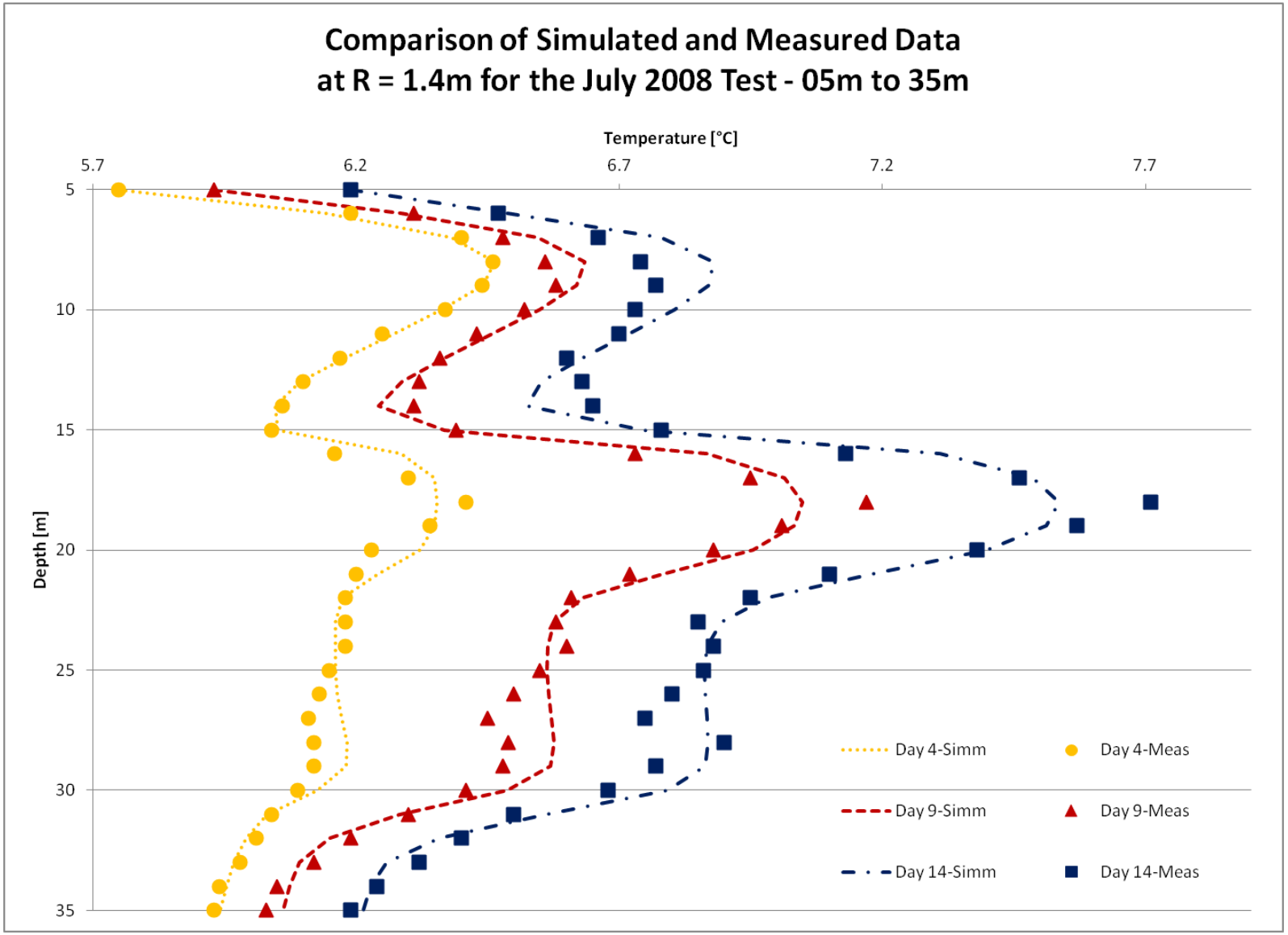

Figure 71 Results for Material Combination H Using Depth and Time Varying Borehole Wall Heat-Flux in the Upper Portion of the Domain During the Ground-Heating Phase for the Nearer Observation Well.

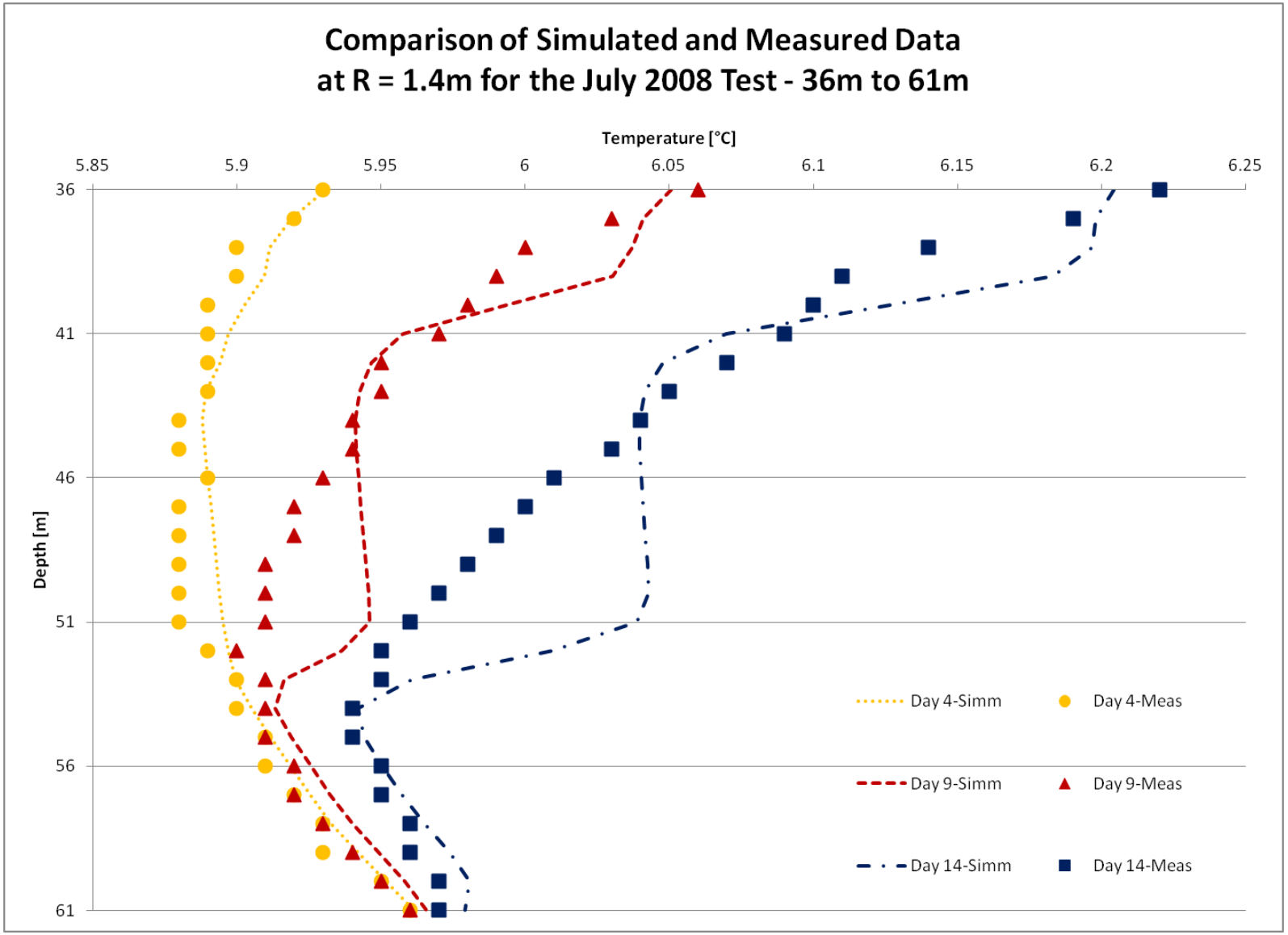

Figure 72 Results for Material Combination H Using Depth and Time Varying Borehole Wall Heat-Flux in the Lower Portion of the Domain During the Ground-Heating Phase for the Nearer Observation Well.

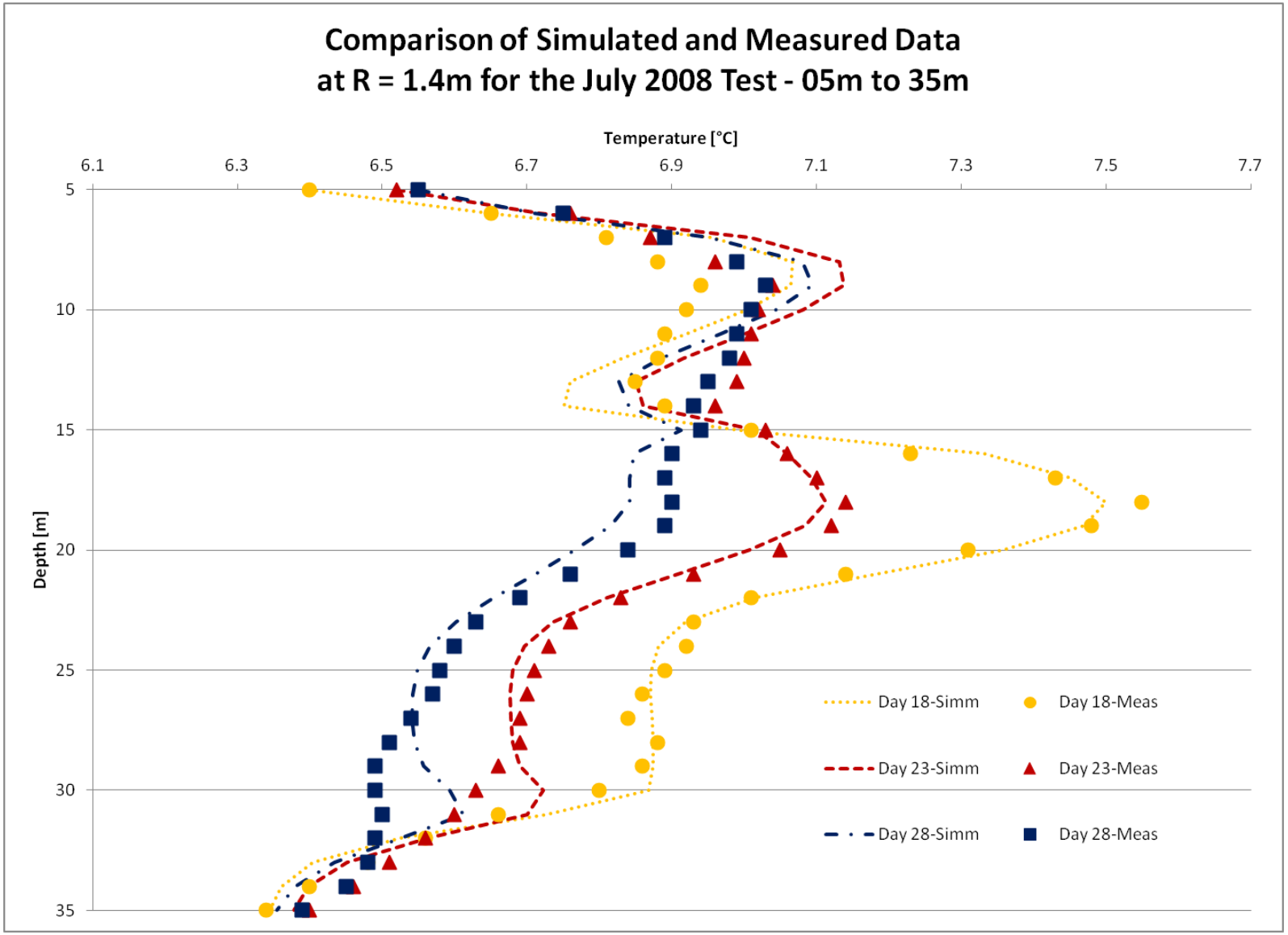

Figure 73 Results for Material Combination H Using Depth and Time Varying Borehole Wall Heat-Flux in the Upper Portion of the Domain During the Natural Ground-Temperature Recovery Phase for the Nearer Observation Well.

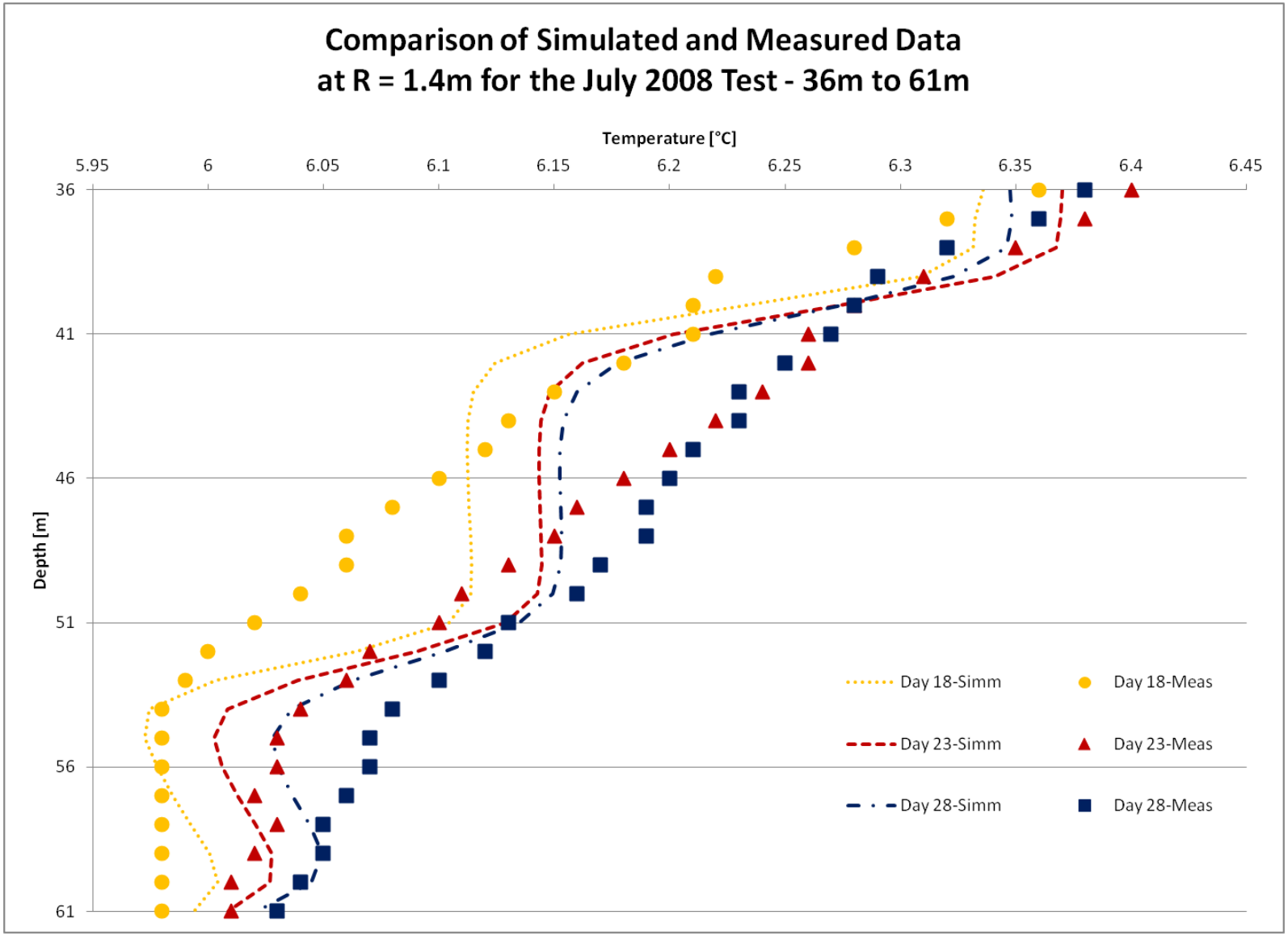

Figure 74 Results for Material Combination H Using Depth and Time Varying Borehole Wall Heat-Flux in the Lower Portion of the Domain During the Natural Ground-Temperature Recovery Phase for the Nearer Observation Well.

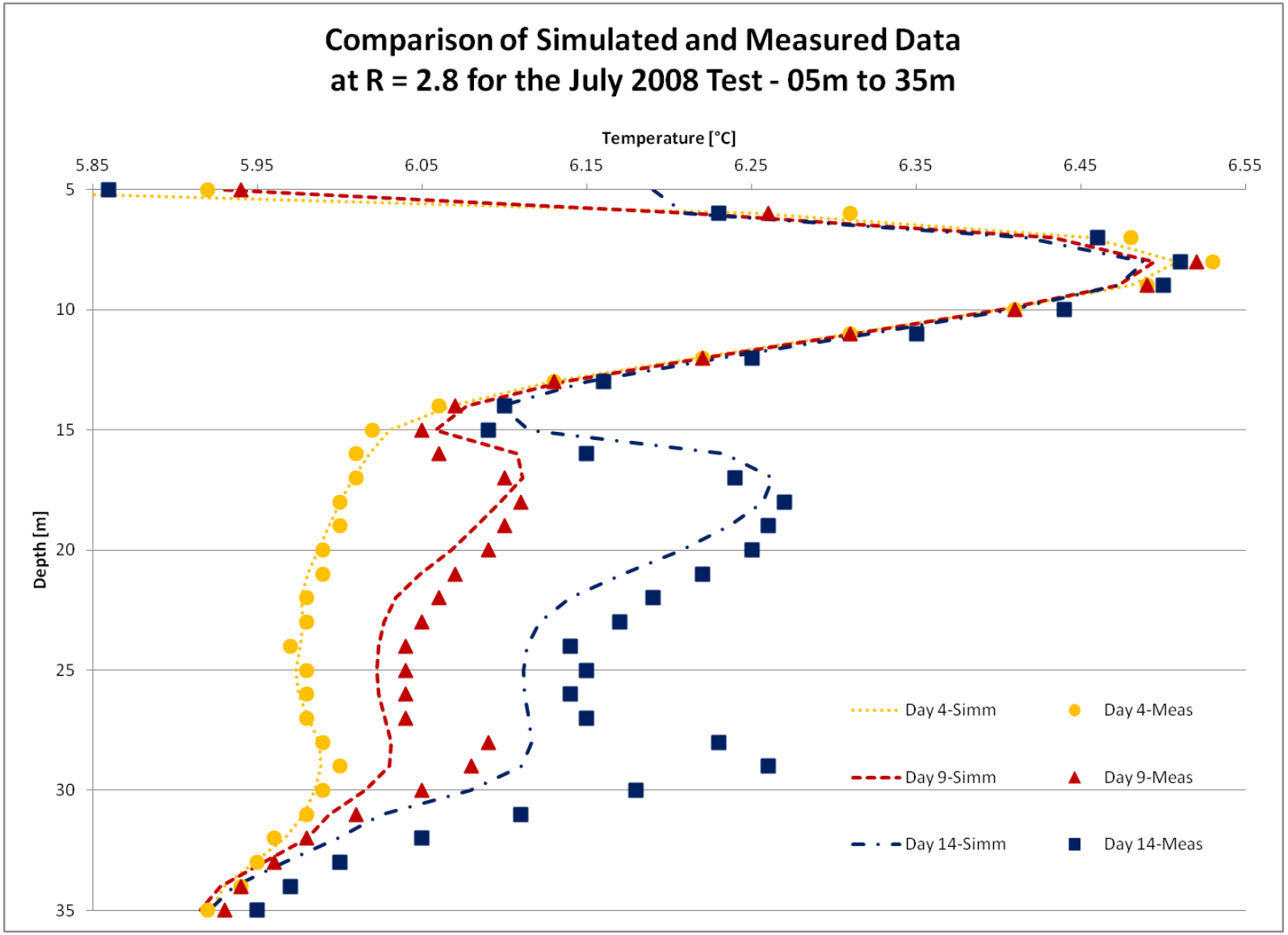

Figure 75 Results for Material Combination H Using Depth and Time Varying Borehole Wall Heat-Flux in the Upper Portion of the Domain During the Ground-Heating Phase for the Further Observation Well.

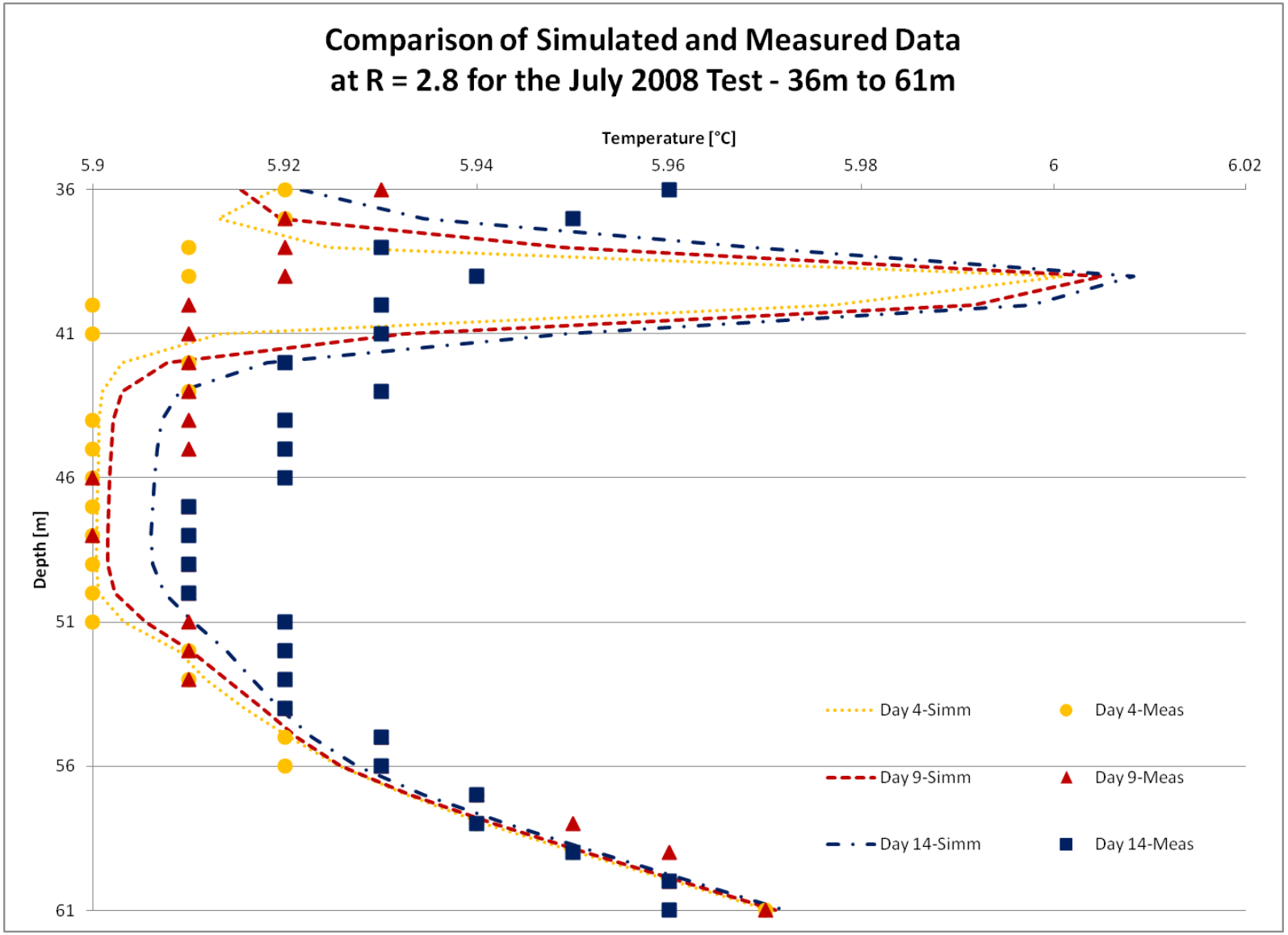

Figure 76 Results for Material Combination H. Best Calibration Results Using Depth and Time Varying Borehole Wall Heat-Flux in the Lower Portion of the Domain During the Ground-Heating Phase for the Further Observation Well.

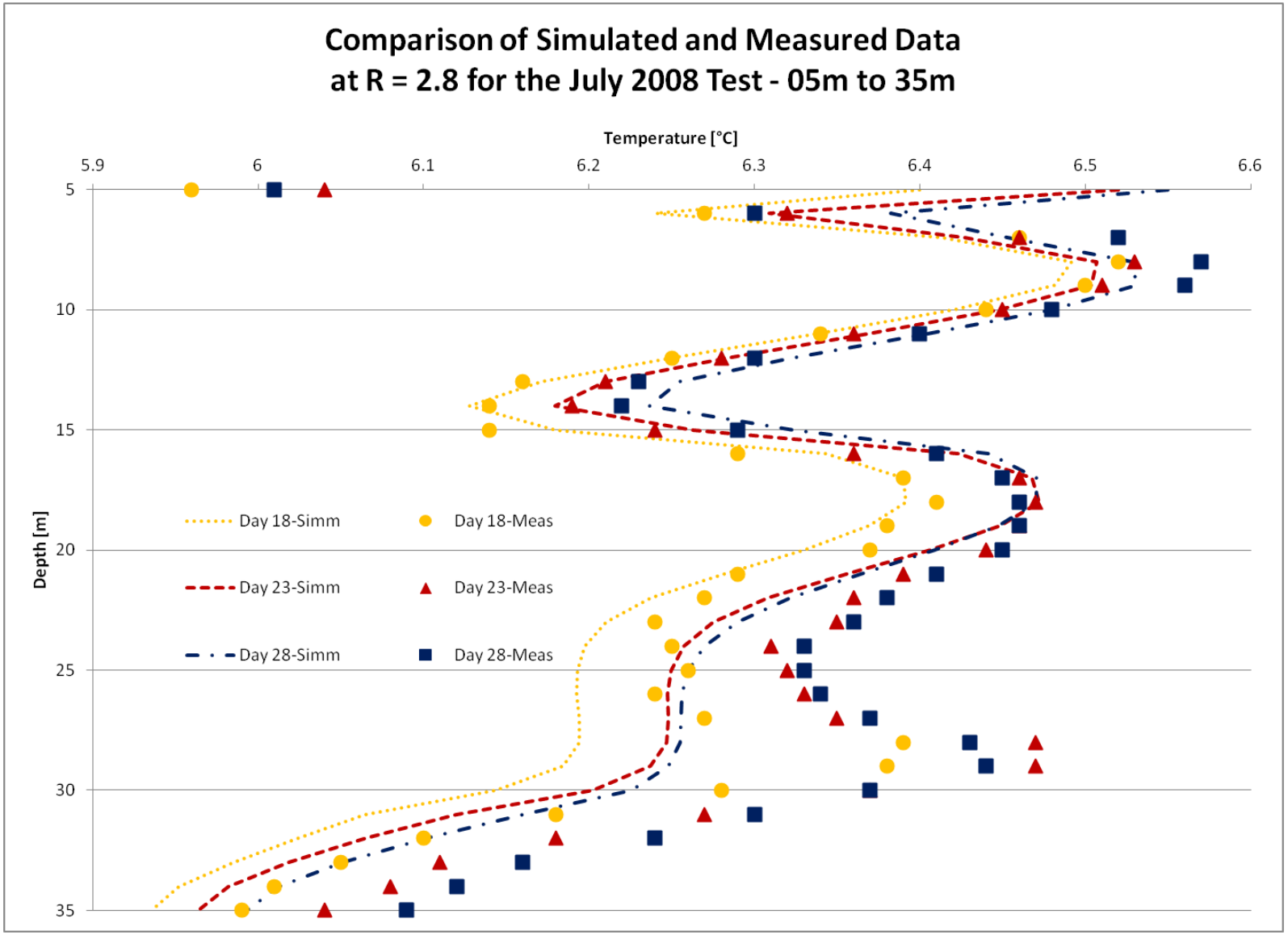

Figure 77 Results for Material Combination H Using Depth and Time Varying Borehole Wall Heat-Flux in the Upper Portion of the Domain During the Natural Ground-Temperature Recovery Phase for the Further Observation Well.

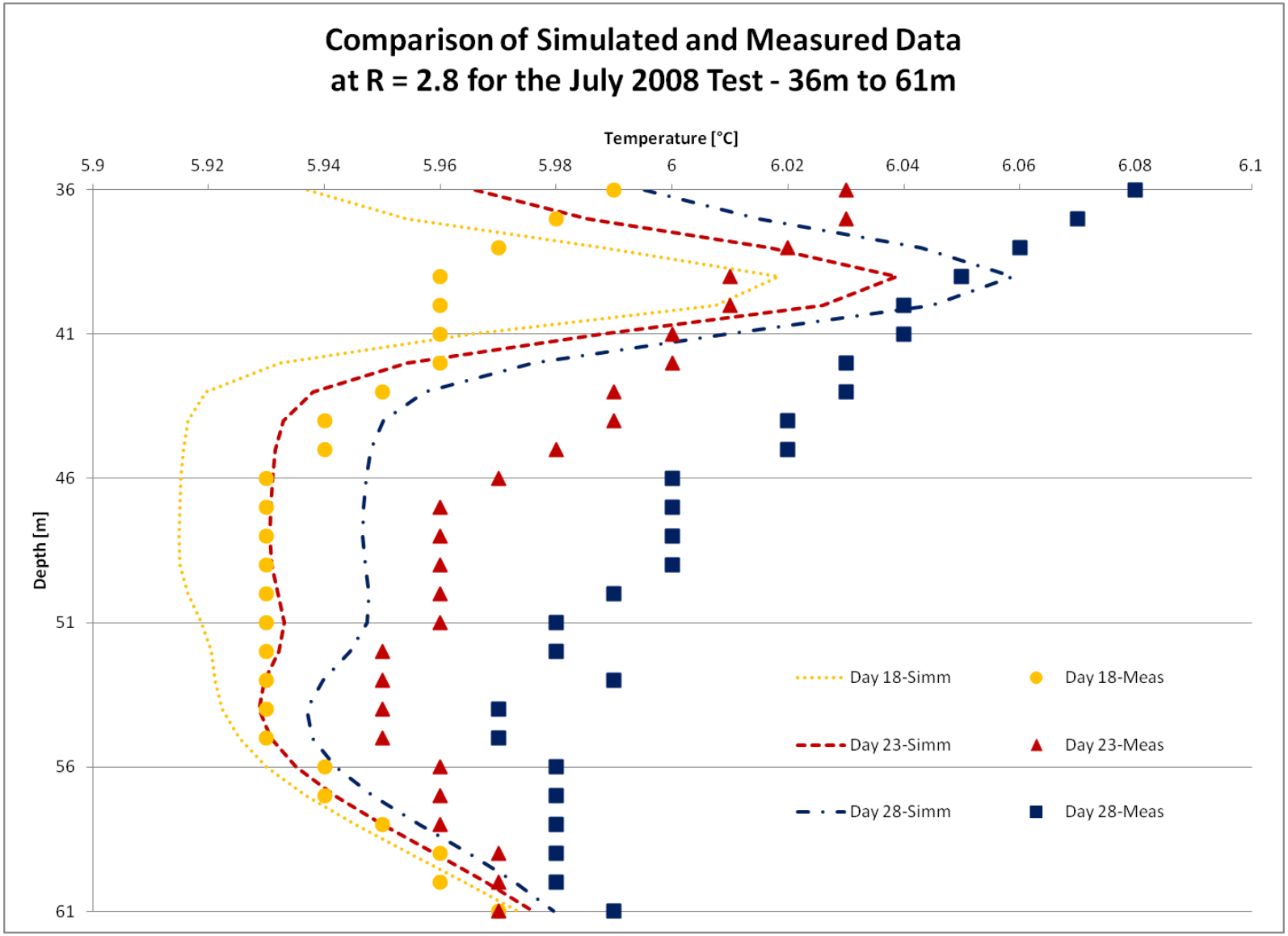

Figure 78 Results for Material Combination H. Best Calibration Results Using Depth and Time Varying Borehole Wall Heat-Flux in the Lower Portion of the Domain During the Natural Ground-Temperature Recovery Phase for the Further Observation Well.

4.5 Chapter 4 Nomenclature

c_{P,CH_3OH}	Specific Heat Capacity of liquid Methanol
$c_{P,f}$	Specific Heat Capacity of the heat transfer fluid
$c_{P,W}$	Specific Heat Capacity of Water
g	Acceleration due to Gravity
H	Aquifer Thickness
k_e	Equivalent Thermal Conductivity of the Porous Medium
N_{RA}	Rayleigh Number
Q_f	Volumetric Flow Rate of the heat transfer fluid
$\dot{Q}_{GHX}$	Rate of heat transferred by the GHX
$\dot{Q}_{GHX,z>5m}$	Rate of heat transferred by the portion of the GHX that is between 0m and 5m depth
$\dot{Q}_{GHX,05m\leq z\leq 61m}$	Rate of heat transferred by the portion of the GHX that is between 05m and 61m depth
$\dot{Q}_{HPU}$	Rate of heat transferred by the HPU
$\dot{Q}_{Loss}$	Rate of heat lost by the heat transfer fluid in transit between the HPU and the ground surface
$\dot{Q}_{model}$	Rate of heat that a computer model predicts the GHX transferred within the modelling domain (from 05m to 61m depth)
$\dot{m}_f$	Mass flow rate of the heat transfer fluid
$T_{f,i}$	Temperature of the heat transfer fluid entering the HPU
$T_{f,o}$	Temperature of the heat transfer fluid exiting the HPU
W_P	Power Output of the Circulation Pump that pumps the heat transfer fluid
α_f	Coefficient of Thermal Expansion of Water
ΔT	Temperature Change Across the Layer (for Rayleigh number)

ΔT_f	Temperature difference between the exiting and entering fluid temperatures of the HPU
κ	Permeability
μ	Dynamic Viscosity
ρ_0	Reference Density (for Rayleigh number)
ρ_{CH_3OH}	Density of liquid Methanol
ρ_f	Density of the heat transfer fluid
ρ_W	Density of Water

Chapter 5 Discussion and Conclusions

5.1 Summary

This thesis presents the results of an experiment to verify common assumptions in ground heat transfer modelling for deep vertical borehole heat exchangers. These are the assumptions of homogenous ground media, and spatially uniform heat flux from the ground heat exchanger. The experiment showed that both the magnitude and the chronology of the ground temperature response vary with material and with depth. This may be significant for both design and modelling. In this particular experiment, it would appear that a significant portion of the depth of the ground heat exchanger was ineffective. In addition, the greater speed with which certain depth ranges warm compared to others shows that models that do not consider ground stratification and depth variations in heat flux would not predict the ground temperature correctly. This suggests a limit on the accuracies for a long-term model that assumes homogenous ground media, and spatially uniform heat flux from the ground heat exchanger.

This thesis presents evidence that ground heat exchangers may contain effectively inactive regions near the bottom of their depth. The experiment in this thesis also showed that the extent of the inactive portion may change with time. The low temperature response in the experiment from about 35m depth to 61m depth and the results of the computer modelling of the experiment indicate that most of the heat exchange occurred in the upper portion of the ground heat exchanger. The fact that the temperature response decreased with depth and the fact that the time to the initial temperature response increased with depth in the lower region suggested that the effective length of the ground

heat exchanger may have increased with time, in the experiment for this thesis. This is significantly different from the vast majority of the current models which assume that the ground heat exchanger is equally effective throughout the duration of the simulation and throughout its physical length. This may be significant to design and simulation as future designs may be able to take advantage of the transient and vertical phenomena occurring in the ground heat exchanger.

This thesis also presents evidence that suggest that the assumption of zero ground heat exchanger output during inactivity may not be realistic. The combination of the computer modelling and experimental results suggest that the lower region of the ground receives a small amount of heat input during system activity. This seems to be the only explanation for the low rate of temperature reduction, and continued temperature increase observed at various depths experimentally. Vertical heat transfer within the solid domain did not account for this in any of the models that used the zero ground heat exchanger output condition for the period after the system shut down. This is significant because the modelling software used a 3D, axisymmetric model of the ground. The natural U-Loop convection hypothesis suggests that natural convection within the paths of the U-Loop tends to redistribute heat throughout the depths via the ground heat exchanger. Inclusion of this effect and a transient effective ground heat exchanger length could be significant for long-term computer modelling or extensive ground heat exchanger installations.

Additional computer modelling shows the feasibility of the two hypotheses that this thesis presented. The computer model incorporating both of these hypotheses showed great improvement in the comparison between the simulation and the experiment over the

earlier models. This computer model marginally improved the performance in the upper portions of the domain. The significance of this finding is that the implementation of the assumptions that corrected the errors in the lower portion of the model did not reduce the model effectiveness in the upper portion. This is important because these assumptions implied altering the model of the upper region, where simpler boundary conditions had already simulated the experimental results.

5.2 Speculations Regarding Ground Heat Exchanger Design and Modelling

One of the most prominent features of the temperature response is the sharp decline in its response from the middle of the depth and below. This thesis proposes two forms of transient vertical behaviour within the ground heat exchanger to explain the observations in the lower portion of the domain. One of these hypotheses attempts to explain the low temperature response and associated low heat exchanger output at those depths that this thesis proposes. The other hypothesis attempts to explain the tendency of the lower depth range to resist cooling despite the deactivation of the entire heat pump system. These observations and hypotheses bring about numerous questions about deep vertical borehole ground heat exchangers.

Naturally, one would want to know if the discrepancy between the upper and lower parts of the depth is a common feature of all deep vertical borehole ground heat exchangers. Based on the literature review (Chapter 1, section4), the present status of ground heat exchanger research is such that the answer for this question does not exist. This thesis cannot offer results for other sites. However, it stands to reason that a ground heat exchanger would be less effective at locations further and further away from the heat

pump because the heat exchange fluid would have had more opportunity to equilibrate with its subsurface surroundings. Furthermore, given that the thermal properties of ground materials do vary and that this thesis shows that this variation can be significant, it also stands to reason that ground heat exchange in stratified geology should have some depth dependence.

This thesis also provided evidence to suggest that there is a transient component to the vertical variation in ground heat exchanger output. This brings about the question of quantifying the time-scale of the vertical transient behaviour in the ground heat exchanger. The experimental evidence suggested that the ground heat exchanger is ineffective below a certain depth and that this depth increases with time. The mechanism that this thesis suggests for the vertical transient behaviour is the equilibration that the heat transfer fluid experiences with the ground as it progresses down the ground heat exchanger's supply-line. This implies that the lower portion of the ground heat exchanger spent a significant part of the investigation literally warming-up. Thus, after sufficient time, the lower portion of the ground heat exchanger may have become more active. Consequently, this thesis reasons that if steady state conditions are ever attained, they would include a variation in heat output along the length of the ground heat exchanger. The analysis of the experiment for this thesis indicated that parts of the lower portion of the ground heat exchanger continued to increase in activity throughout the two-week heating portion of the experiment.

The duration of the transient period would depend on a number of factors. Firstly, the duration of operation and off cycles would affect the transient period. If the deactivation

periods were sufficiently long, then the natural convection that this thesis proposed may begin to redistribute energy along the length of the borehole. This would result in an evening of the borehole temperature that would contribute to returning the system to its initial state of nearly uniform ground temperature. This could lengthen the transient period. The total heat extraction rate would also affect the duration of the transient period. In addition, the ground and ground heat exchanger materials would affect the duration of the transient period. Finally, the transient period may not end in practical heat pump applications.

The next obvious question is if it is possible to devise a method to optimize a ground heat exchanger's depth that improves on current sizing schemes by considering that the heat exchanger's output depends on depth and that this distribution depends on time. The temperature response results imply an avenue of optimization. The bottom half of the domain did not respond significantly and computer modelling showed that this was in-part due to low heat exchanger output at those depths. This implies that a significant part of the bottom portion of the ground heat exchanger may have been unnecessary. Therefore, one may speculate that it could be possible to use shallower boreholes, perhaps in greater numbers, to achieve the same effect as the deeper borehole.

The above discussion implies that considering transient and depth varying effects within the ground heat exchanger may result in using the ground more efficiently than modelling based on the uniformity assumptions would predict. This would result in reducing the total amount of drilling, heat transfer fluid volume, piping length, and pumping costs. A greater number of boreholes in the same area may increase the likelihood of interference

among the heat exchangers. However, this system may also require less heat transfer from each individual borehole and mitigate this problem naturally. Clearly, this could not work if the heat transfer characteristics of the ground heat exchange system were uniform with depth. Therefore, considering the transient and depth dependent effects might result in some unexpected ground heat exchanger design improvements.

Depth dependent interference is another factor to consider in an optimization. The disparity in the ground thermal response suggests two speculations. Firstly, the more active depth ranges in neighbouring wells in the same geologic unit may begin to interfere sooner and at greater separation distances than in the less active region due to their greater activity. Secondly, the disparity in the temperature response at various depths may mean it is not practical to locate ground heat exchangers sufficiently far from one another that they do not interfere at any depth. Interference results when the temperature effects of two or more ground heat exchangers coincide in space.

The superposition principal guarantees that the total temperature response at any location is the sum of the temperature response to the individual heat exchangers at that location. The practical implication of uneven interference is that the temperature in the borehole will change faster in depth ranges that experience interference than in depths that do not. This might reduce the ability of the more active regions to transfer heat with the heat exchange fluid due to the increased temperature change in the more active parts of the ground heat exchanger. A consequence of this occurrence may be that the maximum effective depth of the ground heat exchanger would increase. Thus, the inactive depth range might compensate for the interference-related reduced activity of the more active

region. Another possible implication is that the ground heat exchanger system would become ineffective earlier than a model that assumes uniform heat exchanger output and ground temperature response would have predicted. Therefore, depth dependent modelling could be quite significant for long-term predictions.

The transient vertical effects that this thesis discovered may be useful in at least two ways. Firstly, the results of this thesis show the potential for more accurate ground thermal property investigations to find ways of improving ground heat exchanger design. This thesis shows that these investigations may not be possible without the additional assumptions that this thesis presented. Secondly, whenever a phenomenon is more completely understood, researchers and designers have the confidence and ability to look further into the future with more accurate simulations. However, additional experimentation would answer some of the questions where this section can only speculate.

5.3 Future Work

This thesis uncovered some interesting effects. However, the time-scale of the thesis was very short by comparison to the decades that a heat pump system would service a home or business. Therefore, a more long-term study would be prudent. However, any study should include monitoring within the ground heat exchanger. This could verify the transient and depth dependent ground heat exchanger behaviour that this thesis discovered. A longer term study could also validate the feasibility of improving ground heat exchanger design and simulation. One aspect of operating a ground heat exchanger that a future study could explore is the effect of the on and off cycles. Specifically, this

study could determine if excluding continued convective heating from a model of daily operation during relatively short off-cycles affects its long-term accuracy.

A future study that investigates the effect of transient and depth dependent interference is also important. If the interrelation between the transient and depth dependent behaviour of the borehole and interference exists, then this research would be necessary for improved borehole spacing design. The experiment in this thesis showed that the average temperature response is very different from the local value. Therefore, it is safe to speculate that interference occurs over some depth ranges in systems where modern design methods would not predict otherwise. Furthermore, if there are depth ranges that transmit the ground heat exchanger's influence many times farther than the depth averaged distance, it may not be practical to design for zero interference. Therefore, a study of partially interfering boreholes may improve the long-term performance of ground heat exchange systems.

The analysis in the present thesis concluded that both depth and material composition are significant in the ground heat exchanger's performance. However, it was not possible to consider the relative significance of the one effect versus the other with the present apparatus because the ground heat exchanger had a fixed length. In this thesis, the upper carbonate aquifer was the most active region. However, it was also closer to the heat pump and provided less thermal resistance due to its greater thermal conductivity. One question that a future researcher might want to consider is how differently the ground thermal response might have been if the ground heat exchanger only penetrated the upper layer. The speculative section reasoned that in regions that exhibit a highly depth

dependent ground heat transfer rate, removing the less active portions of the heat exchanger might reduce the performance of the ground heat exchanger much less, proportionately, than the reduction in installation effort and materials. A future investigation may wish to verify this by testing various ground heat exchangers of various lengths using the same thermal load.

An additional point of interest for a future study is the effect of groundwater freezing. The study in this thesis conducted two limited experiments in ground-cooling mode. These experiments showed sub-zero heat transfer fluid in the Geothermal Research Trailer after 12 hours of continuous operation. Insulation of the lines of the ground heat exchanger might have had an effect on these results, as in the energy calculation (see chapter 4). However, there is an indication that after a relatively brief period of winter-time operation, the ground loop may begin to expose the underground environment to freezing conditions. This could freeze the groundwater in the underground materials adjacent to the ground heat exchanger. Therefore, the effect of groundwater freezing may be important in normal operation.

5.4 Conclusion

In conclusion, this thesis presents an experiment and a parametric study that tests long-standing assumptions regarding the nature of heat exchange from a deep vertical borehole ground heat exchanger. The result was to suggest that these assumptions may not permit a simulation to contain as many major details as the physical system. This thesis showed that ground heterogeneity can be significant. This thesis also showed that the ground heat exchanger does not output uniformly with depth and that there may be a transient

component to this. In addition, this thesis showed that the ground heat exchanger may redistribute the heat within the ground while inactive by natural convection.

This thesis provides data from an experiment that measured the transient, depth dependent temperature response to heating by a deep vertical ground heat exchanger at two radial positions. This thesis also provided a detailed computer simulation of the data. This simulation formed a parametric study that allowed the thesis to characterize the ground thermal response to heating by a deep vertical borehole heat exchanger. The experiment and modelling showed that the ground thermal response depends on depth and material type. The depth dependence comes from vertical dependence of the ground heat exchanger's output as well as the disparity in ground thermal properties. In addition, this thesis provided speculation as to the impact that these findings may have on design and simulation. This thesis also indicated areas of additional research.

Appendix A Introduction

A.1 Introduction

The computer optimization procedure detailed in the body of this thesis involved three time-consuming steps. These were the property-range estimation, computer model construction, and the optimization itself. The primary reason for the complexity of the analysis was the surprising result that the temperature response depended strongly on depth and ground material properties. The literature review section (Chapter 1.4) clearly shows that most ground heat exchange research related to deep vertical borehole ground heat exchangers had not considered this, or neglected it. In addition, the lack of information regarding the ground materials' properties further complicated matters. Clearly, a reduction in the effort required for any one of the optimization steps would greatly assist future investigations. This appendix presents preliminary and unexamined work on reducing the effort to characterize the ground thermal response to heating by a deep vertical borehole heat exchanger beyond the procedure of the body of the thesis.

An exact analytical solution to the problem of modelling the ground temperature response to heating by a deep vertical borehole heat exchanger installed in a stratified geological regime would be most instructive. However, the complexity of the mathematics of such a solution is likely the reason that researchers have yet to discover this solution. There have been numerous attempts to obtain analytical solutions to a mathematical model that seeks to approximate the physical system, most notably Ingersoll (1954), Carslaw and Jaeger (1959), and Eskilson (1987) and Zeng, Diao, and Fang (2002). This thesis provides evidence that some of the assumptions of solutions such as these may oversimplify the

problem for depth dependant analysis. However, this appendix presents a conceptual model that accounts for vertical property and temperature response variations while remaining mathematically tractable by incorporating one of the infinite-length source theories.

A.2 Conceptual Model

One way of accounting for the vertical heterogeneity of the ground thermal properties and the heat transfer rate from the ground heat exchanger would be to divide the ground into a vertical stack of unique material layers that are each homogenous. This is the conceptual model in the parametric study (see Chapter 3 and Chapter 4). However, the physical scale of the problem also suggests that vertical heat transfer may be less significant than horizontal heat flow because the ground heat exchanger is 61m deep and primarily affects a region only between 3m and 4m around it, in this experiment. Neglecting vertical variations over a small number of finite depth intervals would be a great simplification. It would be a great simplification because it would reduce the number of variables by allowing investigators to neglect depth within each of the layers in the vertical stack. Work for this thesis had included a development of this concept before the literature review uncovered a paper in which Sutton, Couvillion, Nutter, and Davis (2002) proposed this simplification.

The work for this thesis and of Sutton et al. (2002) suggests representing vertical heterogeneity in a stratified geologic regime as a stack of material layers. They also suggest neglecting the effect of vertical heat transfer both within and between these layers. This conceptual model is very much like the conceptual model for the computer

simulations in this thesis. The main difference between the conceptual model of the appendix and the model of the body is that the model in the appendix neglects vertical heat transfer within material layers and at their interface. Sutton et al. (2002) also ensure that vertical heat-flux steps were always consistent with material layer boundaries. Neglecting vertical heat transfer makes it possible to use either the infinite-length line or cylindrical source theory to model the temperature response on each of the individual layers. This is true because the infinite-length theories implicitly assume zero vertical heat transfer due to the infinite length of the heat source.

The main theoretical reason that Sutton et al. (2002) gave for neglecting vertical heat transfer is that the length of the vertical heat exchanger is so much larger than its diameter. Therefore, they contended that the heat exchanger is approximately infinitely long. One might further extend this argument to include other relevant dimensions in the approximation that the heat exchanger is infinitely long. These relevant dimensions include a significant region surrounding the ground heat exchanger, where the most prominent ground temperature response occurs. In the experiment for this thesis, the length ratios ranged from 61:0.05 [m/m] (1220:1) for the length to radius ratio of the borehole to 61:2.8 [m/m] (nearly 22:1) for the borehole length to radial distance of the further near-field measurement point.

This thesis provided additional evidence that suggests that vertical heat transfer is less significant than horizontal heat transfer. Experimental evidence showed that the bottom half of domain responded to heating by the ground heat exchanger differently than the top half of the domain. However, the computer modelling showed that vertical heat transfer

through underground materials was not sufficient to reproduce the temperature response the bottom of the domain. Mechanisms in the ground heat exchanger itself proved more reasonable explanations. Other evidence that vertical heat transfer is not significant to the ground temperature response comes from the fact that the finite-length line source theory did not match the experimental results of this study even though it considered vertical heat transfer (see Chapter 3). Therefore, vertical heat transfer may not be very significant form of energy transport from a deep vertical borehole heat exchanger.

A.3 The Infinite-length Line and Cylindrical Source Solutions

The infinite-length line source theory from Carslaw and Jaeger (1959, p. 261) gives the solution for the temperature field in a homogenous medium initially at zero temperature that experiences heating from an infinitely thin heat source. This can also give the temperature increase in a material initially at uniform temperature (T_0 in °C). Clearly, this formula can also approximate the temperature response in a region that is initially at approximately constant temperature. This solution relates the temperature of the medium ($T(r,t)$ in °C) with the heat transfer rate (Q in Watts), heat exchanger length (L in metres), the ground's thermal conductivity (λ in Watts per metre per Kelvin), the radial position (r in metres) of the temperature change, time (t in seconds) of the temperature change, and the ground's thermal diffusivity (α in square metres per second). This solution is:

$$\Delta T(r,t) = \frac{-Q}{4\pi L\lambda}\,\mathrm{Ei}\left(-\frac{r^2}{4\alpha t}\right) \qquad \textbf{[1]}$$

$$\Delta \mathrm{T}(r,t) = \mathrm{T}(r,t) - \mathrm{T}_0 \quad \textbf{[2]}$$

$$-\mathrm{Ei}(-x) = -\int_x^{\infty} \frac{e^{-u}}{u}\, du \quad \textbf{[3]}$$

The definition of the mathematical function ($-\mathrm{Ei}(-x)$) appears on the page following the infinite-length line source solution in Carslaw and Jaeger (1959, p. 262).

Most sources cite Ingersoll (1954, p. 147) as the source for the infinite-length line source solution. However, most sources also cite Carslaw and Jaeger (1959) as the source for the infinite-length cylindrical source solution. This might create the impression that these authors derived different solutions for the infinite-length line source solution and that the earlier solution (Ingersoll, 1954) is superior to the later solution (Carslaw & Jaeger, Conduction of Heat in Solids, 1959). The two solutions appear different upon first examination. However, the two authors' solutions are actually the same.

The reference (Ingersoll, 1954) gives the infinite-length line source solution as:

$$\Delta \mathrm{T}(r,t) = \frac{Q}{2\pi L \lambda} \int_{r\eta}^{\infty} \frac{e^{-\zeta^2}}{\zeta}\, d\zeta \quad \textbf{[4]}$$

$$\eta = \frac{1}{2\sqrt{\alpha t}} \quad \textbf{[5]}$$

$$\int_y^{\infty} \frac{e^{-\zeta^2}}{\zeta}\, d\zeta = -\frac{1}{2}\mathrm{Ei}(-y^2) \quad \textbf{[6]}$$

The first page of the reference (Ingersoll, 1954, p. 1) defines η and Appendix F (Ingersoll, 1954, p. 297) defines the integral. Substituting equations [4] and [5] into [6]

yields [1]. Thus, the solution in Ingersoll (1954) is identical to the solution from Carslaw and Jaeger (1959).

The infinite-length cylindrical source theory from Carslaw and Jaeger (1959, p. 338) gives the solution to the temperature field in the ground from a cylinder of radius (a in metres) as:

$$\Delta \mathrm{T}(r,t) = \frac{-Q}{\pi^2 r_b \mathrm{L}\lambda} \int_0^\infty \left(1 - e^{-\alpha t u^2}\right) \frac{\mathrm{J}_0(ru)\mathrm{Y}_1(r_b u) - \mathrm{Y}_1(ru)\mathrm{J}_0(r_b u)}{u^2\left(\mathrm{J}_1^2(r_b u) + \mathrm{Y}_1^2(r_b u)\right)} du \qquad \textbf{[7]}$$

The dimensionless form of the integral results in:

$$\Delta \mathrm{T}(\mathrm{R},t) = \frac{-Q}{\pi^2 \mathrm{L}\lambda \mathrm{R}} \int_0^\infty \left(1 - e^{-\frac{\alpha t}{r^2}u^2}\right) \frac{\mathrm{J}_0(u)\mathrm{Y}_1(\mathrm{R}u) - \mathrm{Y}_1(u)\mathrm{J}_0(\mathrm{R}u)}{u^2\left(\mathrm{J}_1^2(\mathrm{R}u) + \mathrm{Y}_1^2(\mathrm{R}u)\right)} du \qquad \textbf{[8]}$$

$$\mathrm{R} = \frac{r_b}{r} \qquad \textbf{[9]}$$

One can also scale the integrand so that the cylindrical source solution is easier to compare with the line source solution as follows:

$$\Delta \mathrm{T}(\mathrm{R},\mathrm{U}) = \frac{-Q}{2\pi^2 \mathrm{RL}\lambda} \int_0^\infty \Big(1 - e^{-u^2/\mathrm{U}}\Big) \frac{\mathrm{J}_0(2u)\mathrm{Y}_1(2\mathrm{R}u) - \mathrm{Y}_1(2u)\mathrm{J}_0(2\mathrm{R}u)}{u^2\left(\mathrm{J}_1^2(2\mathrm{R}u) + \mathrm{Y}_1^2(2\mathrm{R}u)\right)} du \qquad \textbf{[10]}$$

$$\mathrm{U} = \frac{r^2}{4\alpha t} \qquad \textbf{[11]}$$

Note that the argument of the exponential function in the integrand now contains the argument of the infinite-length line source solution.

A.3.1 Comparing the Infinite-Length Line Source and Cylindrical Source Theories:

It is difficult to say if the infinite-length line or cylinder model of the ground heat exchanger is more appropriate for modelling the physical system. Neither of these solutions models the true geometry or heat transfer processes of the physical system. The real ground heat exchanger has a loop of pipes with a flowing fluid that exchanges heat with the inner surface of the U-Loop pipes by forced convection. These pipes communicate the heat with the ground by either a grouting material that surrounds the U-Loop (Kavanaugh, 2010) or the groundwater that fills the borehole when there is no grout (Gehlin, 1998). The line and cylinder models do not include convection, and they do not include the internal structure of the mechanism within the borehole. Therefore, neither one of the models is obviously superior to the other.

The difficulty with determining a correct model of the ground heat exchanger is evident in the literature review (see chapter 1.4). The literature contains many different models of a ground heat exchanger. Some comparisons between the infinite-length line and cylindrical models have shown that the infinite-length line source model is inferior to the infinite-length cylindrical source model (Austin (1998), Gahlin and Hellström (2003), etc.). In addition, many authors neglect the line and cylinder ground heat exchanger models entirely in favour of more complex geometries (Yavuzturk (1999), Xu and Spitler (2006), Lamarche and Beauchamp (2007a), Nam, Ooka, and Hwang (2008), etc.). Yet there is ongoing research in models that represent the ground heat exchanger as a line source of finite length (Eskilson (1987), Zeng, Diao, and Fang (2002), Lamarche and Beauchamp (2007b)), and at least one model that uses a combination of the infinite-length line and cylindrical source theories (Kavanaugh, 2010). Therefore, neither the line

or cylinder source models are obviously better approximations of real ground heat exchangers.

Speaking computationally, the line source theory is clearly superior. The unsolved integral in the cylindrical source theory [10] results from the fact that there is no known antiderivative for that integrand. However, as Carslaw and Jaeger (1959) mention, the integral in the line source solution is a mathematical function called the exponential integral. The mathematical handbook Abramowitz and Stegunx (1972, p. 229) gives series expansion for the exponential integral in their equation 5.1.10 as:

$$\mathrm{Ei}(x) = \gamma + \ln(x) + \sum_{h=1}^{\infty} \frac{x^h}{(h)(h!)} \quad \textbf{[12]}$$

$$\gamma = 0.5772156649 \ldots \quad \textbf{[13]}$$

The series expansion uses the Euler–Mascheroni constant, γ. Thus, the series expansion for the form of the exponential integral in the infinite-length line source solution is:

$$-\mathrm{Ei}(-x) = -\gamma - \ln(x) - \sum_{h=1}^{\infty} \frac{(-x)^h}{(h)(h!)} \quad \textbf{[14]}$$

Therefore, the line source solution can be implemented in simple computational software, such as EXCEL, while the cylindrical source solution requires advanced mathematics software, such as MatLab.

A.4 Theory for the Property Estimation Method

Both the line and cylinder conceptual models of the ground heat exchanger result in a mathematical model that depends on the product of a constant and an integral. In the extension to the stacked model, as in Sutton, Couvillion, Nutter, and Davis (2002), each material (m) has a unique value of heat rate (Q_m) and thermal conductivity (λ_m). It is possible to use either the infinite-length line source or the cylindrical source theories to model the heat transfer within a material layer. In either case, the constant coefficient contains the ratio of heat rate to thermal conductivity of the material (Q_m/λ_m). Both integrals contain the thermal diffusivity of the material layer (α_m). The subscript ($m = 1,2, \dots, \mathrm{M}$) distinguishes between the various materials in the vertical stack. The remaining terms in both mathematical models contain mathematical functions and operations, the physical dimensions of the borehole, and the time and the radial position of each temperature change datum.

In the present case, the goal is to determine unknown information about the experimental domain. One can form a system of equations to solve for unknown parameters by equating experimentally derived data to a mathematical function that models the phenomenon that the experiment measured. In the case of the present experiment, there are numerous temperature change readings ($\Delta \mathrm{T}_i$), each at a specific radial distance (r_i), and time (t_i), where i is an index. Measurements for the experiment occurred at numerous depths (z_n), and traversed a certain number of underground material layers (M). Within a given material layer (m), there is a value for heat rate (Q_m), thermal conductivity (λ_m), thermal diffusivity (α_m), and layer thickness (L_m). All of these relate

to a mathematical function that simulates the temperature change ($\Delta T(r_i, t_i, L_m, Q_m, \alpha_m, \lambda_m)$). In this study, the position, time, and layer thickness are known values of the system and the other quantities (Q_m, α_m, λ_m) are unknown. A system of equations formed by equating the measured data (ΔT_i) to the mathematical function that attempts to describe this data ($\Delta T(r_i, t_i, L_m, Q_m, \alpha_m, \lambda_m)$) will permit a solution for unknown parameters.

Where there are a total of I useable measurements, the general form of the system of equations is as follows:

$$\Delta T_i = \Delta T(r_i, t_i, L_m, Q_m, \alpha_m, \lambda_m), \qquad i = 1,2,3, \dots, I, \qquad m = 1,2,3, \dots, M \qquad \textbf{[15]}$$

The most general form of the system of equations [1] would involve simultaneously considering all of the experimental data. As a simplification, the parameter estimation method in this appendix limits the system to a subset of the total readings ($a \leq i \leq b$) at a single depth. The method obtains the remaining quantities at the other depths by repeating the procedure for all measurement depths.

$$\begin{gathered} \Delta T_i = \Delta T(r_i, t_i, L_m, Q_m, \alpha_m, \lambda_m), \qquad a \leq i \leq b \\ b \leq I, \qquad m = \text{Const}, \qquad z = \text{Const} \end{gathered} \qquad \textbf{[16]}$$

In the case of the line source model, the function is:

$$\Delta T(r_i, t_i, L_m, Q_m, \alpha_m, \lambda_m) = \frac{-Q_m/\lambda_m}{4\pi L_m} \text{Ei}\left(-\frac{r_i^2}{4\alpha_m t_i}\right) \qquad \textbf{[17]}$$

Similarly, the cylindrical source model results in:

$$\Delta \mathrm{T}(r_i, t_i, \mathrm{L}_m, Q_m, \alpha_m, \lambda_m)$$

$$= \frac{-Q_m/\lambda_m}{\pi^2 \mathrm{L}_m \mathrm{R_i}} \int_0^\infty \Big(1 - e^{-u^2/4\mathrm{U}_i}\Big) \frac{\mathrm{J}_0(\mathrm{u})\mathrm{Y}_1(\mathrm{R_i u}) - \mathrm{Y}_1(\mathrm{u})\mathrm{J}_0(\mathrm{R_i u})}{\mathrm{u}^2\big(\mathrm{J}_1^2(\mathrm{R_i u}) + \mathrm{Y}_1^2(\mathrm{R_i u})\big)} \mathrm{du} \quad \textbf{[18]}$$

$$\mathrm{R}_i = \frac{r_b}{r_i} \quad \textbf{[19]}$$

$$\mathrm{U}_i = \frac{r_i^2}{4\alpha_m t_i} \quad \textbf{[20]}$$

In both systems, it is only possible to solve for the ratio of heat rate and thermal conductivity (Q_m/λ_m) and not Q_m or λ_m individually. Any attempt to separate the numerator and denominator results in a homogeneous system because the conceptual model explicitly assumes that both Q_m and λ_m are constant within a material layer. The designers of the ground heat exchanger in this experiment could not have foreseen the significance of measuring Q_m because research has typically ignored variations with depth (see chapter 1.4). However, future investigators may wish to measures the total heat rate acting within a material layer. A record of the temperature of each of the fluid streams in the U-Loop near material boundaries would provide this information. Without this information, an investigator must use other means to obtain the missing data such as conducting a significantly simplified version of the parametric study in the body of this thesis.

The mathematical model in this appendix uses the usual method of superposition for simulating the natural ground temperature recovery phase of the experiment. This method appears as a general theoretical discussion in references such as Carslaw and Jaeger

(1959) and in research papers by authors such as Sutton, Couvillion, Nutter, and Davis (2002). In general, the superposition principal states that if there are two or more separate heat transfer phenomena occurring simultaneously in a domain, then the temperature response in the domain is the sum of each the temperature responses to the individual stimuli. Therefore, if we have a series of heat rates ($Q_{m,1}, Q_{m,2}, Q_{m,3}$, ...) valid on a series of time intervals ($0 \leq t < t_1, t_1 \leq t < t_2, t_2 \leq t < t_3$, ...), the temperature response function becomes a summation.

Assuming the line source model, the temperature response from zero time until the end of the latest interval (t_J) becomes:

$$\Delta \mathrm{T}(r_i, t_i, Q_m(t), \mathrm{L}_m, \alpha_m, \lambda_m) = \frac{-1}{4\pi \mathrm{L}_m \lambda_m} \sum_{j=1}^{\mathrm{J}} \left(Q_{m,j} - Q_{m,j-1}\right) \mathrm{Ei}\left(-\mathrm{U}_{i,j-1}\right) \qquad \textbf{[21]}$$

$$0 \leq t < t_\mathrm{J}, \qquad j = 1,2,3, \ldots, \mathrm{J}$$

$$\mathrm{U}_{i,j-1} = \frac{r_i^2}{4\alpha_m \left(t_i - \mathrm{t}_{\mathrm{j}-1}\right)}, \qquad t_0 = 0 \qquad \textbf{[22]}$$

$$Q_m(t) = \begin{cases} Q_{m,0}, & t < 0 \\ Q_{m,1}, & 0 \leq t < t_1 \\ Q_{m,2}, & t_1 \leq t < t_2 \\ Q_{m,3}, & t_2 \leq t < t_3 \\ \vdots & \vdots \\ Q_{m,\mathrm{J}}, & t_{\mathrm{J}-1} \leq t < t_\mathrm{J} \end{cases}, \qquad Q_{m,0} = 0 \qquad \textbf{[23]}$$

Assuming the cylinder source model, the temperature response is, similarly:

$$\Delta \mathrm{T}(r_i, t_i, Q_m(t), \mathrm{L}_m, \alpha_m, \lambda_m) = \frac{-1}{\pi^2 \mathrm{L}_m \lambda_\mathrm{m}} \sum_{j=1}^{\mathrm{J}} \left(Q_{m,j} - Q_{m,j-1}\right) \mathrm{g}\left(\mathrm{R_i}, \mathrm{U}_{i,j-1}\right) \qquad \textbf{[24]}$$

$$\mathrm{g}\left(\mathrm{R_i}, \mathrm{U}_{i,j-1}\right) = -\frac{1}{\mathrm{R_i}} \int_0^{\infty} \left(1 - e^{-u^2/4\mathrm{U}_{i,j-1}}\right) \frac{\mathrm{J_0(u)Y_1(R_i u) - Y(u)J_0(R_i u)}}{\mathrm{u^2}\left(\mathrm{J_1^2(R_i u) + Y_1^2(R_i u)}\right)} \mathrm{du}$$

In the simple model of the natural ground temperature recovery phase, the heat transfer rate is zero during recovery. If we let the recovery time start at $t = t_{rec}$ and use the line source model, then the temperature response becomes:

$$\Delta \mathrm{T}(r_i, t_i, \mathrm{L}_m, Q_m, \alpha_m, \lambda_m) = \frac{-Q_m/\lambda_m}{4\pi \mathrm{L}_m} \begin{cases} \mathrm{Ei}\left(-\mathrm{U}_{i,1}\right), & 0 < t < t_{rec} \\ \mathrm{Ei}\left(-\mathrm{U}_{i,1}\right) - \mathrm{Ei}\left(-\mathrm{U}_{i,rec}\right), & t \geq t_{rec} \end{cases} \quad \textbf{[25]}$$

$$\mathrm{U}_{i,1} = \frac{r_i^2}{4\alpha_m t_i}, \qquad \mathrm{U}_{i,rec} = \frac{r_i^2}{4\alpha_m (t_i - \mathrm{t_{rec}})}$$

Under the same conditions, the cylindrical source model yields:

$$\Delta \mathrm{T}(r_i, t_i, \mathrm{L}_m, Q_m, \alpha_m, \lambda_m) = \frac{-Q_m/\lambda_m}{\pi^2 \mathrm{L}_m \mathrm{R_i}} \begin{cases} \mathrm{g}\left(\mathrm{R_i}, \mathrm{U}_{i,1}\right), & 0 < t < t_{rec} \\ \mathrm{g}\left(\mathrm{R_i}, \mathrm{U}_{i,1}\right) - \mathrm{g}\left(\mathrm{R_i}, \mathrm{U}_{i,rec}\right), & t \geq t_{rec} \end{cases} \quad \textbf{[26]}$$

The mathematical model in Sutton, Couvillion, Nutter, and Davis (2002) includes a term that would permit a complete solution of the system without logging any data in the ground heat exchanger during the experiment. Their mathematical model incorporates a borehole resistance term ($\mathrm{R_B}$) that results in an additional additive term ($Q_m \mathrm{R_B}$) that is constant within any material layer. The addition of this term would result in an inhomogeneous system of equations that one could solve for all of the necessary property and heat rate information. However, there are numerous difficulties associated with using

this method. Primary among these difficulties is that there is no accepted method of reliably determining the borehole resistance.

Authors such as Hellström (1991), Paul (1996), and Kavanaugh (2010) each have different methods for calculating borehole thermal resistance. Each of these methods results in different values for borehole resistance. In addition, the borehole resistance comprises only a small portion of the total borehole resistance (Kavanaugh, 2010). Attempts in this thesis to solve for $Q_m \mathrm{R_B}$ by inverting the data resulted in a variety of values within a single material layer, both positive and negative. Thus the borehole resistance value was probably composed of mostly experimental and modelling errors because negative values of either thermal resistance or conductivity are impossible. Therefore, using the borehole thermal resistance to complete the solution is ineffective at this time.

The property estimation method seeks to solve the system of equations given above as [18], and using the definition in [25]. The property estimation method seeks to estimate the value of the ratio between the total heat rate and the thermal conductivity of the material layer (Q_m/λ_m), and the thermal diffusivity of the layer (α_m) as two independent variables. The method proceeds with an initialization value of the diffusivity (α_m^0), and an initialization value of the ratio (β_m^0), where the subscripted Greek letter β_m represents the ratio (Q_m/λ_m) to simplify the notation. The method takes an iterative approach to solve for the value of the diffusivity and the ratio by successive approximations of these values. Once the successive approximations of diffusivity and the ratio are sufficiently accurate, the method encounters a stopping criterion and quits.

The property estimation method evaluates the accuracy of the results at each iteration step based on how well the results simulate experimental data. The quality of the simulation depends on how closely it matches the data. Therefore, the method calculates the error (E_i^k) or residual at each iteration step (k) as well as the sum of the squares of those errors (S^k):

$$\mathrm{E}_i^k = \Delta\mathrm{T}_i - \Delta\mathrm{T}(r_i, t_i, \mathrm{L}_m, Q_m^k, \alpha_m^k, \lambda_m^k) \quad \textbf{[27]}$$

$$S^k = \sum_{i=a}^{\mathrm{b}} \left(\mathrm{E}_i^k\right)^2, \qquad a \le i \le b, \qquad b \le \mathrm{I}, \qquad m = \mathrm{Const} \quad \textbf{[28]}$$

$$z = \mathrm{Const}, \qquad k = 0,1,2,\ldots,\mathrm{K}$$

$$\beta_m^k = Q_m^k / \lambda_m^k \quad \textbf{[29]}$$

The above equation uses the form of the mathematical model from [25].The stopping criterion for the parameter estimation method occurs when it reaches iteration level K such that the parameter estimates α_m^{K} and β_m^{K} minimize of the sum of the square of the error terms. The Solver Add-In that Microsoft includes in EXCEL performs the parameter estimation minimization procedure in the EXCEL spreadsheet that implements the present mathematical model.

The data available from the measurements from the experiment in the present study and the parameter estimation method result in an incomplete description of the underground heat transfer. This is because the experiment only measured the total heat rate to the ground heat exchanger and did not measure the value of the heat rate on individual horizontal layers in the stack (Q_m). However, the designers of the ground heat exchanger

could not have anticipated the significance of this omission because researchers typically neglect vertical heat transfer variations entirely (see chapter1 section 4). Without the heat rate on the individual layers, it is impossible to solve for the heat transfer rate (Q_m) or the thermal conductivity of the individual layers (λ_m). The experimental data and the derived data available to this study give the thermal diffusivity of each layer (α_m) and the quotient of the heat rate on each layer and the thermal conductivity of that layer ($\beta_m = Q_m/\lambda_m$). However, only values of all three quantities; layer thermal conductivity (α_m), layer heat rate (Q_m), layer thermal conductivity (λ_m), form a complete description of the heat transfer process.

A.4.1. Parametric Study Complement of the Simplified Investigation of the Appendix

A parametric study in one variable could estimate one of the missing quantities and complete the solution. Clearly, it is not necessary to estimate both of the missing quantities because the parameter estimation method of this appendix obtains their ratio (Q_m/λ_m). If successful, the technique of the appendix that includes a one-variable parametric study is an improvement over the parametric study that the body of this thesis details because that study considered three variables. However, the parametric study for the method in the appendix still requires a separate model of the ground heat exchange system. An example of such a model is the computer model in Temp/W that the body of the thesis discusses. Therefore, measuring the heat rate to each layer would be the simplest because it should avoid all parametric studies.

There are three options for the parameter to study in the one variable parametric study to complete the investigation for cases such as this thesis where there is not sufficient information to solve these quantities directly. Obviously, one could estimate either the heat rate on the layer (Q_m) or the thermal conductivity on the layer (λ_m). However, there is a third quantity that is also useful. The definition of the thermal diffusivity of one of the material layers (α_m) is thermal conductivity of the layer (λ_m) divided by the volumetric heat capacity of the layer (VHC_m), as in [30]. Therefore, a parametric study that varies the volumetric heat capacity of the layer would also yield the thermal conductivity of the layer, as in [31], and the heat flux into the layer, as in [32].

$$\alpha_m = \frac{\lambda_m}{\mathrm{VHC}_m} \quad \textbf{[30]}$$

$$\lambda_m = \alpha_m \mathrm{VHC}_m \quad \textbf{[31]}$$

$$Q_m = \alpha_m \beta_m \mathrm{VHC}_m \quad \textbf{[32]}$$

The advantage that varying the volumetric heat capacity of a layer has over varying the thermal conductivity or heat rate of the layer is that volumetric heat capacity may only take on a limited range of values as compared to these other parameters. The maximum physically possible range for the heat rate on a layer (Q_m) is from zero to the total heat rate of the system ($\sum Q_m$). The range of possible thermal conductivity and volumetric heat capacity values depends on the ground material type, the ground material's porosity, and the material properties of the contents of the voids in the porous material. In the present study, the percent difference between reasonable estimates of the maximum and minimum thermal conductivity values are 33.5%, 60.5%, and 60.1% for M_1, M_2, and M_3, respectively (see Table 5 in Chapter 3). However, the percent difference between the

maximum and minimum reasonable estimates of volumetric heat capacity are 4.39% for M_1 and 17.23% for both M_2 and M_3 (see Table 5 in Chapter 3). Consequently, errors in estimating the volumetric heat capacity of the layer (VHC_m) may be less significant than errors in estimating the other properties because volumetric heat capacity varies less than those other quantities. Therefore, analysis in this appendix will use the parametric study from the body of this thesis and the best value for volumetric heat capacity that it found.

A.5 Property Estimation Methodology

There were multiple temperature readings in each underground material layer. There were temperature readings for every metre of depth. Consequently, there are ten measurements from 5m to 15m depth, sixteen measurements from 16m to 31m depth, and thirty readings from 32m to 61m depth. These ranges roughly correspond to the underground material boundaries and, likewise, the boundaries in the computer model. Each reading within a material layer at depth (z_n) can provide an estimate for α_m and β_m within the layer. Thus, there the data produces 10, 16, and 30 respective estimates of the thermal diffusivity on layers 1 to 3 ($\alpha_1, \alpha_2, \alpha_3$), as well as for the quotient of heat rate and thermal conductivity ($\beta_1, \beta_2, \beta_3$). The notation for a sample estimate of α_m is $(\alpha_m)_n$, and for β_m, the notation is $(\beta_m)_n$

The approach in this appendix is to use each of the measurements within a layer to obtain an estimate of the various quantities within that material layer. This method took the average of those estimates as the value of the quantity on the layer. Therefore, the values that the results section reports for thermal diffusivity in layer M_1 is the average of the ten estimates in that layer from 10m to 15m depth, the value in M2 is the average of the 16

values in that layer from 16m to 31m depth, and the value in M3 is the average of the 30 estimates from 32m to 61m depth. The value of thermal conductivity is the product of the thermal diffusivity and the volumetric heat capacity that the parametric study in the body of the thesis obtained, as in [31]. This method obtains estimates of the heat rate once per measurement depth as the product of the volumetric heat capacity, thermal diffusivity, and heat rate to thermal conductivity ratio as in [32]. For comparison to the computer model, the table in the results section averages these estimates on the depth intervals consistent with the boundary condition line segments (p) (see Chapter 3), rather than over the entire material layer. The following equations summarize the process:

$$\alpha_m = \frac{1}{d-c}\sum_{n=d}^{c}(\alpha_m)_n \qquad \textbf{[33]}$$

$$\beta_m = \frac{1}{d-c}\sum_{n=d}^{c}(\beta_m)_n \qquad \textbf{[34]}$$

In the above equation, the material layer (m) ranges from measurement depth z_c to z_d.

$$q_{\mathrm{Line}_p} = \frac{1}{2\pi r_0 \mathrm{L}_m}\frac{\mathrm{C}_m}{f-e}\sum_{n=e}^{f}\{(\alpha_m)_n(\beta_m)_n\} \qquad \textbf{[35]}$$

This equation expresses the average heat flux rate in [W/m^2] for a depth range between z_e and z_f. This measurement depth range defines one of the boundary six condition lines (Line_p) that are on the left hand side of Figure 4 in chapter 3.

A.6 Results

The simulation data that the mathematical model [25] generated agreed with the experimental data in the upper portion of the domain. The graphs in Figure 79 and Figure 80 show the agreement between the experimental data and the mathematical model typical for the 5m to 25m depth range. The graph in Figure 81 shows the intermediate level of agreement between the mathematical model and the experiment typical of the 26m to 31m depth range. The lower depth range, from 32m to 61m shows lesser agreement between the mathematical model and the experiment, as Figure 82 and Figure 83 show. The level of agreement between the mathematical model and the experiment decreases with depth from 32m to 61m. A comparison between the results of the property and flux estimation methods of the thesis body and the appendix are in Table 14 and Table 15. The agreement between the mathematical model of the appendix and the experiment in the top half of the domain echoes the results of the Temp/W modelling, as does the lesser agreement in the lower region.

Table 14 Comparison of material property estimates from the thesis body (Combination H) and the Appendix

Material Layers	α [mm^2/s]		C [MJ/m^3·K]	λ [W/m·K]	
	Combination H	Appendix	Combination H	Combination H	Appendix
M1	0.375	0.392	3.42	1.282	1.341
M2	1.207	1.292	2.96	3.58	3.79
M3	0.541	0.320	3.47	1.874	1.110

Table 15 Comparison of thermal flux estimations from the thesis body (Combination H) and the Appendix

Line Segment	q_{Line_p} [W/m^2]	
	Estimation From The Thesis Body	Estimation From The Appendix
L1	116.2	116.3
L2	264.9	243.3
L3	152.4	151.4
L4	75.1	78.0
L5	40.7	46.5
L6	13.04	24.0

A possible reason for the poorer performance in the lower range is that the model in the appendix neglects the processes that the body of this thesis identified as possible explanations for the unusual behaviour at those depths. It is possible to implement the staggered start and continued natural convective heating hypotheses in as in the above analysis by using [22] instead of [25]. This introduces multiple new variables because the experiment did not record the variation in heat rate with depth along the ground heat exchanger. As previously noted, this omission is consistent with the typical assumption of depth invariance prevalent in the literature (see Chapter 1.4). The purpose of neglecting the additional assumptions that the body of the thesis suggested was to begin the analysis with the simplest possible model.

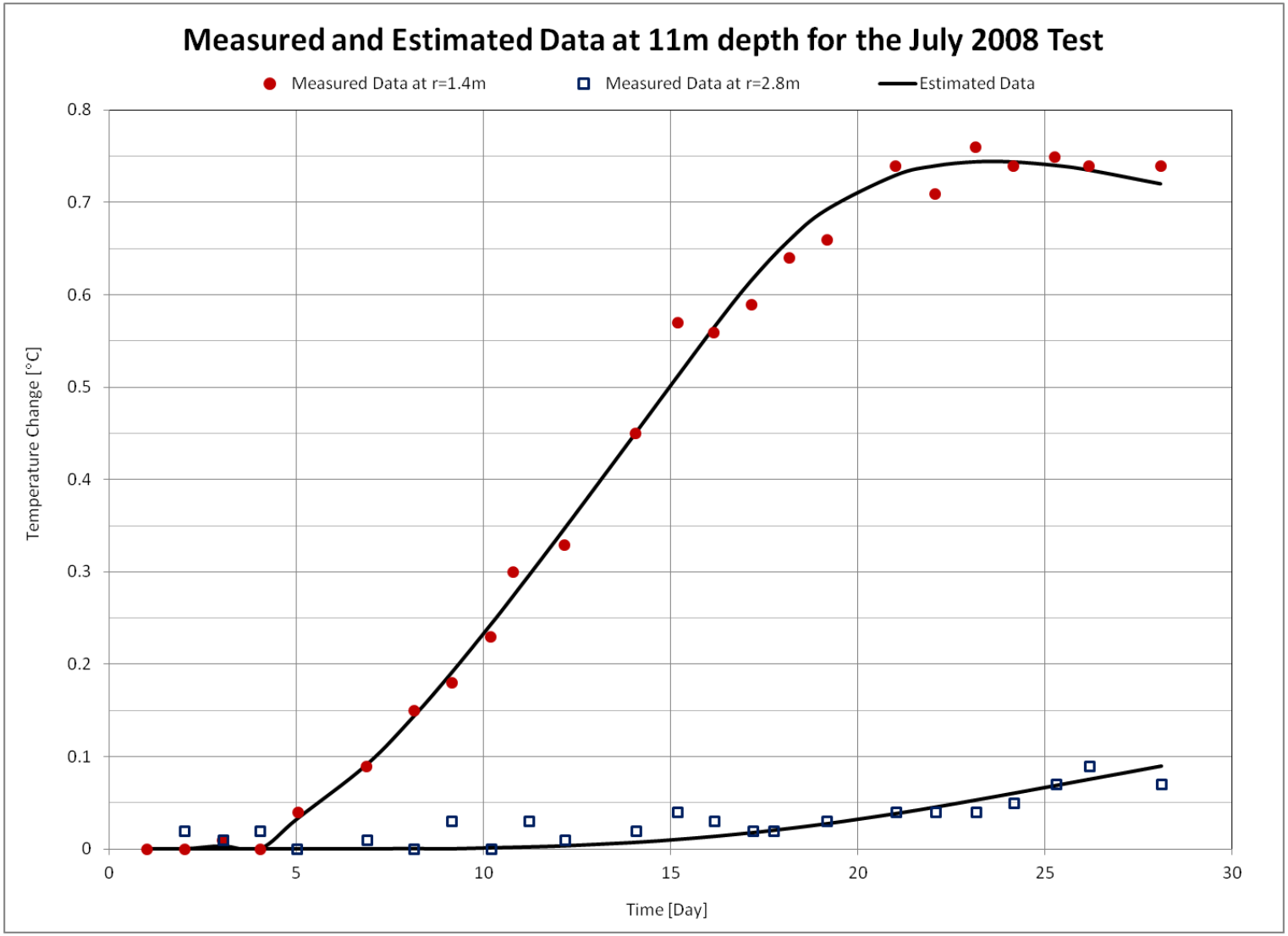

Figure 79 Example of a match between measured and simulated data after completing the parameter estimation method of this appendix for 11m depth.

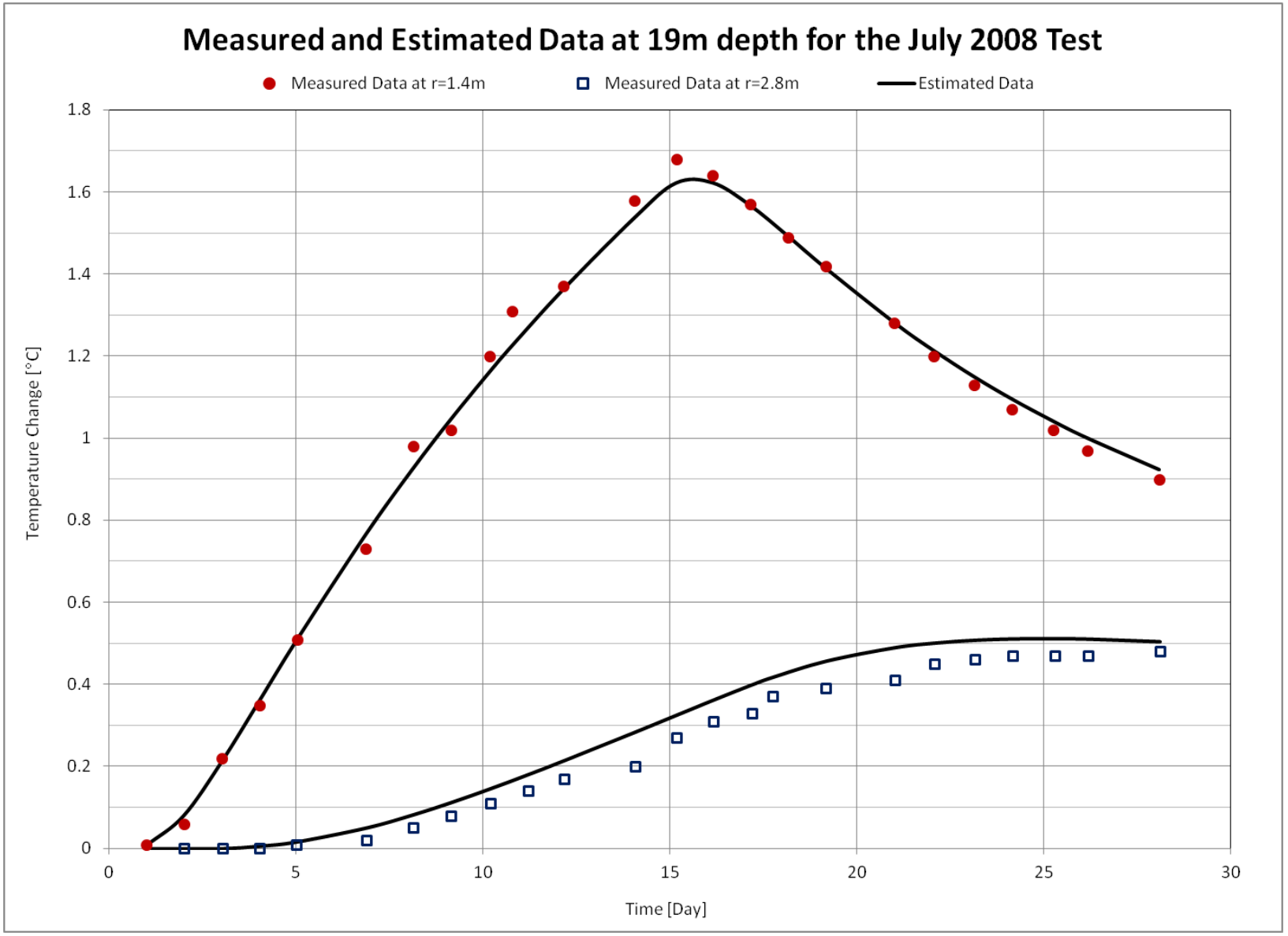

Figure 80 Example of a match between measured and simulated data after completing the parameter estimation method of this appendix for 19m depth.

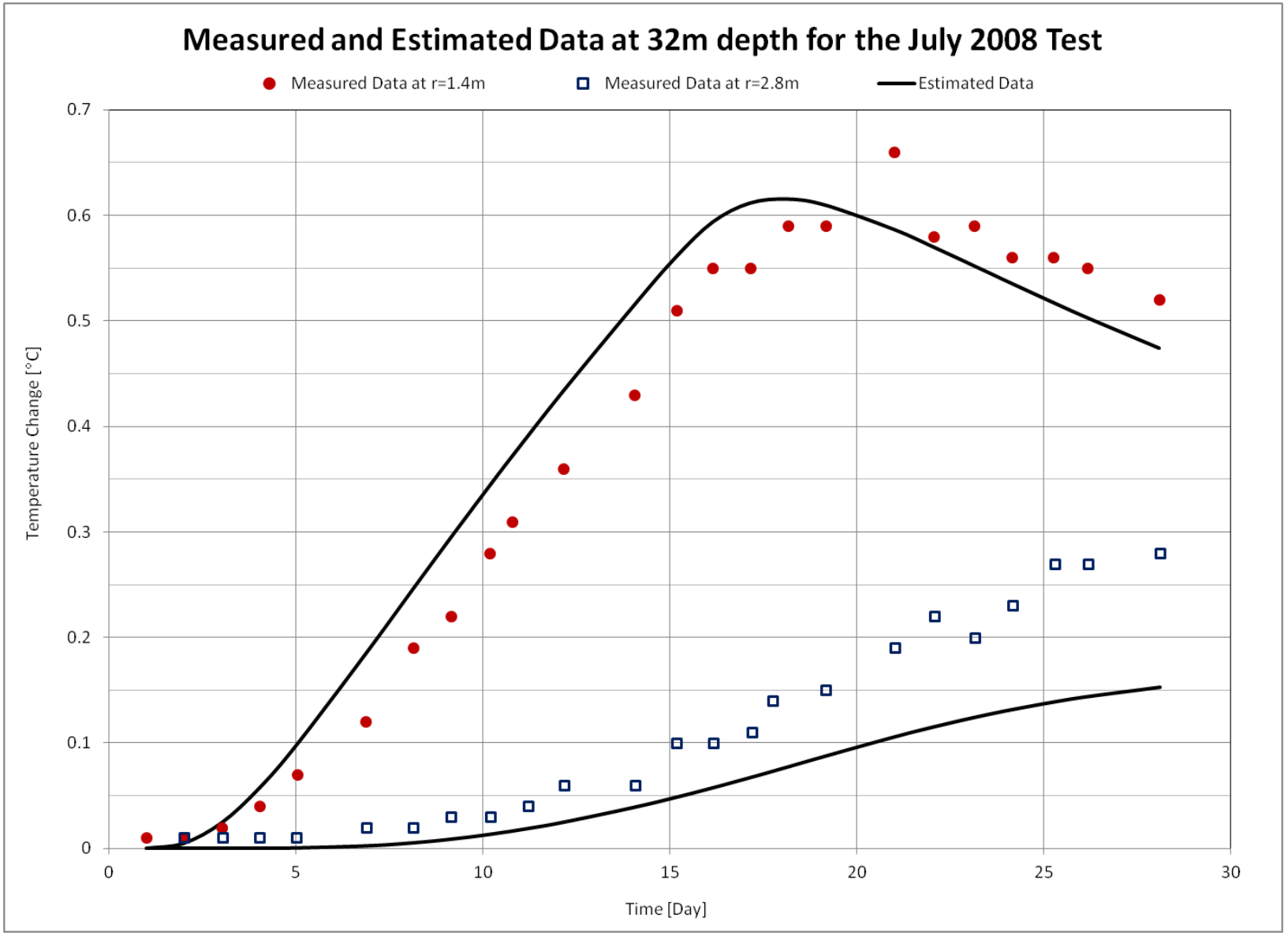

Figure 81 Example of a match between measured and simulated data after completing the parameter estimation method of this appendix for 32m depth.

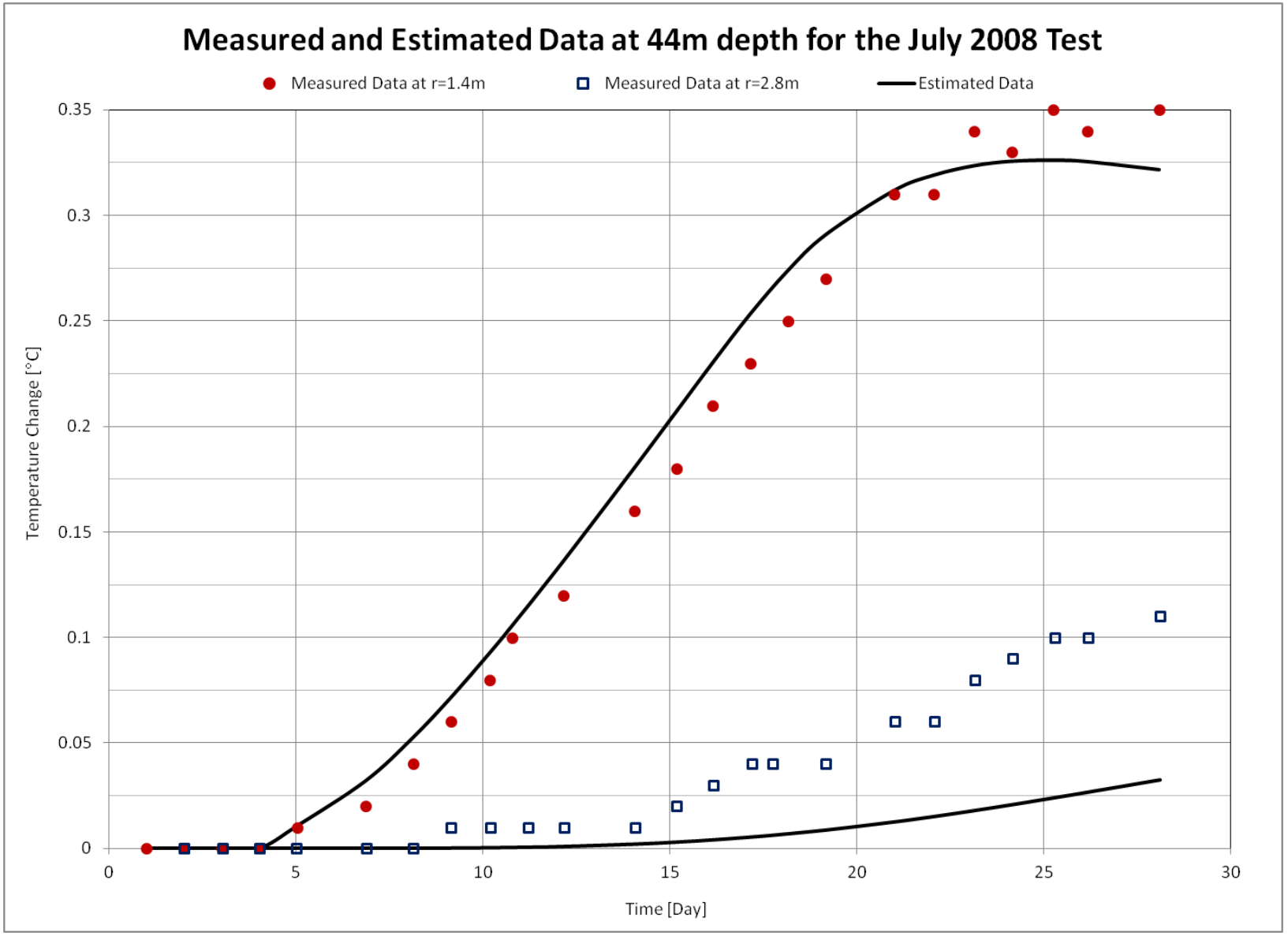

Figure 82 Example of a match between measured and simulated data after completing the parameter estimation method of this appendix for 44m depth.

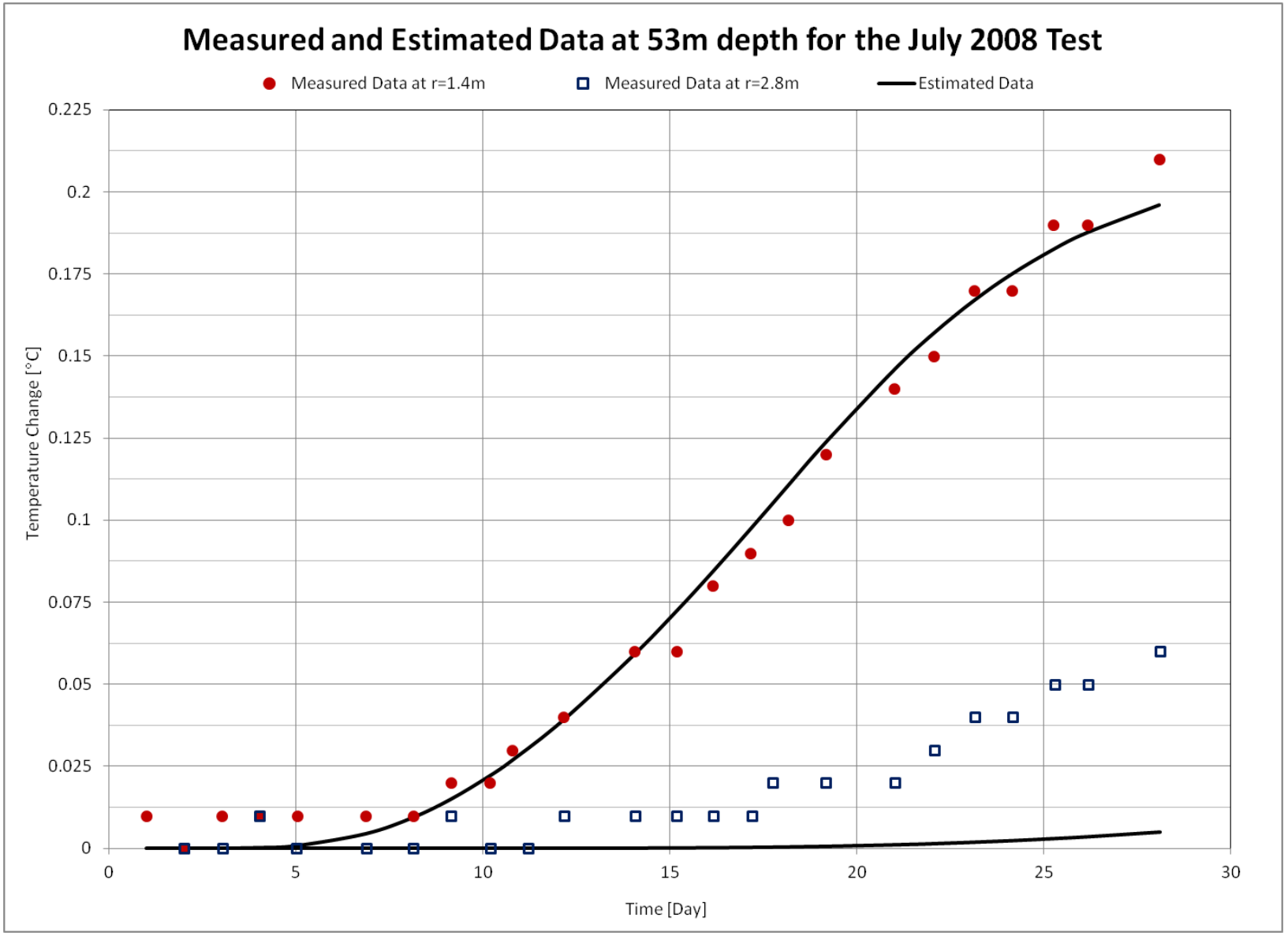

Figure 83 Example of a match between measured and simulated data after completing the parameter estimation method of this appendix for 53m depth.

Incorporating the assumptions that the body of the thesis suggested will result in additional variables that the parameter estimation needs to solve. Thermal diffusivity of a material layer is one unknown parameter. In addition, each time interval has a unique value of heat rate that requires the parameter estimation to vary a separate value of the ratio of heat rate to the layer divided to thermal conductivity of the layer (β_m) per time interval. Each time interval (j) begins at $t = t_{j-1}$ and ends on $t = t_j$. Therefore, any time intervals that end between zero time and the beginning of the natural ground recovery phase (t_{rec}) add another variable. The end times of those time intervals would not be known in advance. Similarly, any time intervals that end during the natural ground temperature recovery phase also add another variable.

It is important to note that measuring the heat rate at various depth intervals within the borehole would have greatly simplified the analysis. Including the staggered start and continued convective heating hypotheses would not add any variables to the parameter estimation in this case. This is because the experiment would have logged the time interval end-points as well as the heat rate for each of the time intervals. The remaining variables of thermal conductivity and diffusivity are constant in time for a ground heating experiment. Therefore, measuring the heat rate within the ground heat exchanger on various depth intervals over time would have made this more complex analysis possible without adding any new unknowns.

Including the staggered start and continued natural convection hypotheses greatly improved the agreement between the experiment and the mathematical model. The results of the parameter estimations showed the characteristics of the hypotheses that the body of

this thesis suggested. The beginning of the significant heat transfer stages occurred after the start of heating time. In addition, the model predicted that the heating continued after the end of heating time. However, where the previous, simpler approach under-predicted the thermal diffusivity (see Table 14), this more complex method tended to over-predict it.

The fact that the more advanced method over-predicted the thermal diffusivity value in the lower region is unfortunate. However, holding the thermal diffusivity value constant and varying all other parameters provided simulation results that agreed with the experimental data. The graph in Figure 84 shows the comparison between measured and simulated data using the maximum reasonable thermal diffusivity estimate from Chapter 3 and four time intervals at 44m depth. The significance of this finding is the improved match with these additional hypotheses. The level of agreement shows the merit of the mathematical model that this appendix presents.

One possible reason why the more advanced method over-predicted thermal diffusivity in the lower depth range is that vertical heat transfer is small however not negligible. This may be limited to a specific depth rang or range of radial distances. The lesser agreement that progresses with depth indicates this possible depth dependency. The significance of radial distance comes from the rationale for suspecting negligible vertical heat transfer. This was that the radial distance to the measurement point was much smaller than the length of the ground heat exchanger. Therefore, difficulties with the match may be due to the radial distance of the further measurement point. The results in the lower depth range show that the match is more difficult for the data in the further measurement point.

However, another explanation for why the more advanced method prefers high thermal diffusivity values may be that there should be restrictions on how the method varies the parameters. Clearly, the graph in Figure 84 shows that this theory predicts the ground temperature response with reasonable thermal diffusivity values. Therefore, the parameter estimation method might have simply found a false minimum. These questions are difficult to answer without knowing the true values of the heat transfer rate or other parameters. Therefore, future investigations may be more appropriate forums for solving these mysteries.

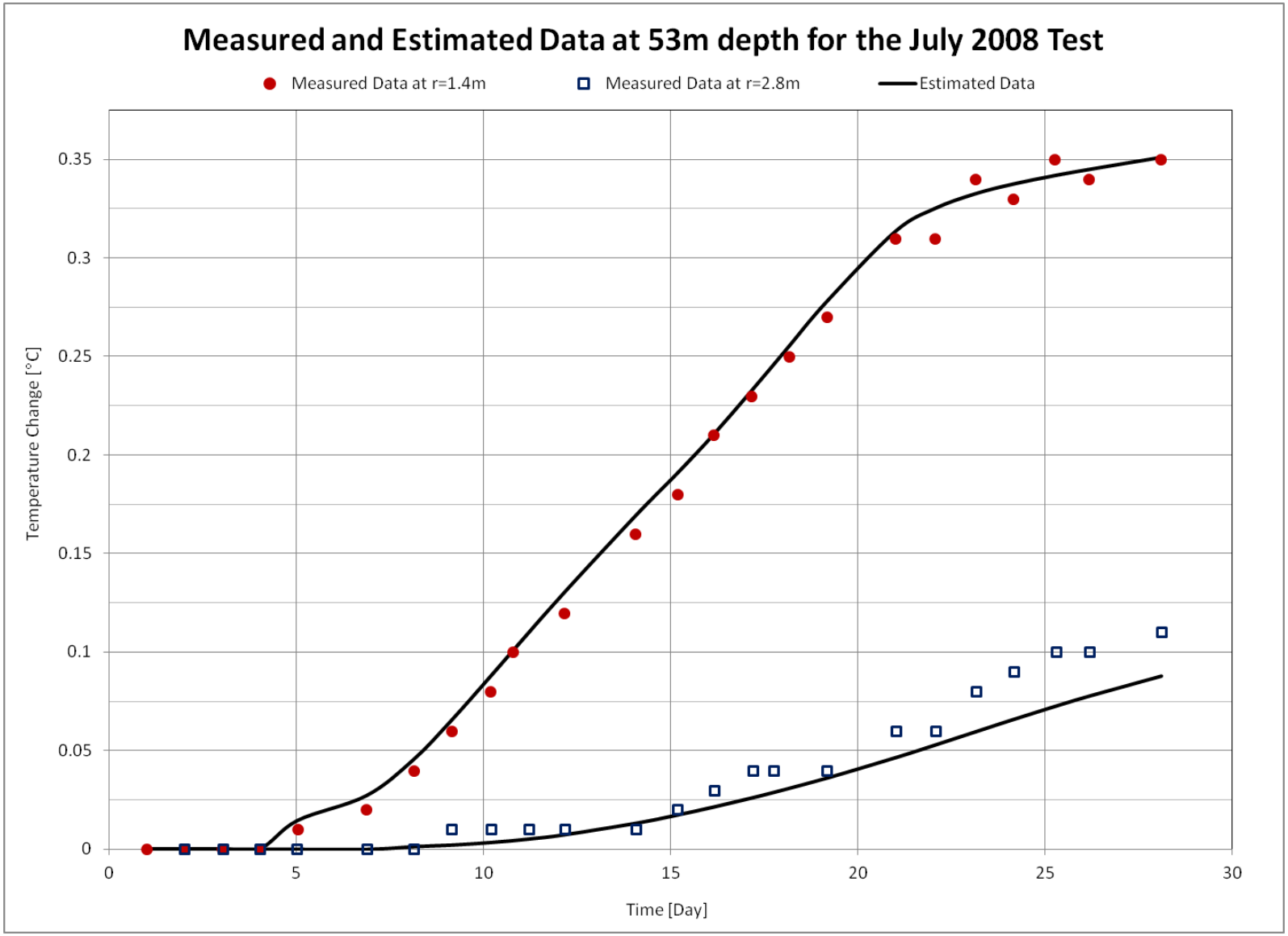

Figure 84 Example of a match between measurement and experiment using the staggered start and continued natural convective heating hypothesis with fixed diffusivity.

Use of the finite-length line source solution instead of the cylindrical source solution is not a cause for the difficulty in the lower layer. Mathematics software such as MatLab can evaluate the relative difference between the two models by evaluating the quotient of the cylindrical source solution [10] and the line source solution [1], as in [36]. The integrand in [36] is infinite at the lower integration limit and the upper limit of integration is infinity. The MatLab documentation recommends the adaptive Gauss-Kronrod quadrature function, quadgk(), for such integrals. It is possible to evaluate this function at the times and locations of experimental measurements. The relative difference values were typically less than 0.05 for the early times and the majority of the values were less than 0.01. The result is that the discrepancy between temperature change predictions would be either in the thousandths of a degree or the ten-thousandths of a degree. Therefore, there is no advantage to using the cylindrical source theory for the present analysis.

$$\mathrm{F(R,U)} = \left| 1 - \frac{2\int_0^{\infty}\left(1 - e^{-u^2/\mathrm{U}}\right)\dfrac{\mathrm{J_0}(2u)\mathrm{Y_1}(2\mathrm{R}u) - \mathrm{Y_1}(2u)\mathrm{J_0}(2\mathrm{R}u)}{u^2\left(\mathrm{J_1^2}(2\mathrm{R}u) + \mathrm{Y_1^2}(2\mathrm{R}u)\right)}du}{\pi\mathrm{REi}(-\mathrm{U})} \right| \qquad \textbf{[36]}$$

A.7 Conclusion

This appendix presents a way of reducing the effort to characterize the heat transfer from a deep vertical borehole ground heat exchanger. The method proposes a conceptual model that incorporates the vertical variations in ground thermal properties and ground heat exchanger output that the body of this thesis suggests. This conceptual model incorporates pre-existing mathematical models for tractability. The comparison between this mathematical model and the experimental results, as well as the comparison between

this mathematical model and the computer modelling results from this thesis are favourable. These show that the mathematical model that this thesis is a useful approximation of the physical phenomenon it sought to model. This is because the mathematical model of this appendix was able to predict the ground temperature response at numerous depths. However, greater time or radial length scales may be problematic because the results show that vertical heat transfer may be small however not negligible in these cases.

The model that this appendix presented was able to predict the ground temperature response while simultaneously estimating the thermal diffusivity of the ground layers that comprised about half of the experimental domain. This success showed that the model is also useful in predicting one of the two remaining unknowns of the system at those depths. These are the heat transfer rate and the thermal conductivity. The model showed this because it estimated their quotient and because the estimate of this quotient compared well with the same value that the study in the body of the thesis predicted. Therefore, this method would reduce the number of variables that the parametric study from the body of the thesis would have had to consider from three to one. Thus, it was successful in its goal of reducing the complexity of the analysis, there. The modelling was also useful in the lower region as its heat flux estimates were similar to the estimates from the Temp/W modelling of the thesis body. In future work, the investigators may wish to measure the heat output of the ground heat exchanger over various depth intervals to eliminate the need for any parametric study by instead providing an additional variable from experimental observations.

The method of this appendix also showed promise in the lower portion of the depth. This model will predict the ground temperature response well with additional assumptions. These assumptions are the validity of the hypotheses that the body of this thesis suggests are necessary to model the behaviour of the bottom half of the domain, and a given value of thermal diffusivity. This suggests that the model from this appendix could be very useful in simulating the ground temperature response in the bottom half of the domain with some additional refinement. It also suggests the validity of the staggered start and continued natural convective eating hypotheses because of the improvement that their use made to the predictive ability of the mathematical model of this appendix. This appendix could not uncover the specific areas of refinement because this answer requires the time and depth dependent borehole heat transfer data that experiment did not record. The experiment did not record these data because the need for these data would not have been apparent until the novel results of the present study uncovered this need.

The specific areas of refinement for the mathematical model in the lower half of the domain could include a vertical heat transfer term or a more restrictive method of parameter estimation. However, it is also possible that the number of variables was too great for the chosen multivariable equation solver. Recall that including the staggered start and continued natural convective heating hypotheses required adding many additional interrelated variables. If future investigators choose to measure the heat transfer rate from various depth intervals over time, then they could more thoroughly investigate the mathematical model from this appendix. In this case, there would not need to be a parametric study, as in the case of the upper half of the domain, due to the reduction in the unknowns of the system.

This conclusion emphasizes the need to measure the heat transfer rate over various depth intervals of the ground heat exchanger over time. However, it should also emphasize that this need is an unexpected result of the research for this thesis. The literature review (chapter 1.4) shows that models of ground heat transfer from a deep borehole ground heat exchanger do not normally consider depth variations. Therefore, the realization of the significance of vertical depth variations is an interesting and useful result in itself. Furthermore, the designers of the ground heat exchanger would not have expected that they needed to do this.

A.8 Appendix A Nomenclature

Lower Case
Latin Scripts

a Lower bound on a subset of all readings ($a \leq i \leq b$)

b Upper bound on a subset of all readings ($a \leq i \leq b$)

c Number indicating the upper bound of material layer, m

d Number indicating the lower bound of material layer, m

e Number indicating the upper bound of line, p (see Figure 11, page 70 and below)

f Number indicating the lower bound of line, p (see Figure 11, page 70) and below)

$\mathrm{g}(\mathrm{R_i}, \mathrm{U}_{i,j-1})$ A dimensionless function that represents an integral:

$$-\frac{1}{\mathrm{R_i}}\int_0^\infty \left(1-e^{-u^2/4\mathrm{U}_{i,j-1}}\right)\frac{\mathrm{J_0(u)Y_1(R_i u)-Y(u)J_0(R_i u)}}{\mathrm{u^2\left(J_1^2(R_i u)+Y_1^2(R_i u)\right)}}\mathrm{du}$$

h Integer index used in a summation

i An integer index that numbers the experimental readings

j Integer index that counts the number of steps in $Q_m(t)$

k An Integer index that counts the iterations in the iteration procedure

m Integer index that differentiates between material layers in the stacked material model of the ground

n An integer index that numbers the depths of the experimental readings

p Integer index that numbers the depth intervals that line number p indicates (See Figure 11, page 70)

q_{Line_p} Heat flux (energy per unit time per unit area) acting on the depth interval that line number p indicates (See Figure 11, page 70)

r Radial position

r_b The radius of the borehole

r_i	The radial position of measurement, i
t	Time
t_i	The time of measurement, i
t_j	The end time of one of the steps in $Q_m(t)$
t_{rec}	The beginning time of the natural ground temperature recovery phase
u	A dummy variable used in an integration
x	An argument of a function
y	An argument of a function
z	Depth position
z_n	One of the measurement depths in the experiment

Upper Case Latin Scripts

E_i^k	Error (Residual): The difference between a measured value and the mathematical simulation of that value $\Delta\mathrm{T}_i - \Delta\mathrm{T}(r_i, t_i, \mathrm{L}_m, Q_m^k, \alpha_m^k, \lambda_m^k)$
Ei	A mathematical function called the Exponential Integral (various definitions are in the appendix)
I	Total number of usable experimental readings
J	The total number of steps that j counts
J_0	Bessel Function of the first kind, order zero
J_1	Bessel Function of the first kind, order one
K	The total number of iterations, k, in the iteration procedure
L	The depth of the subsurface part of the ground heat exchanger
L_m	The thickness of material layer, m
M	The total number of material layers under consideration

Q	Total heat transfer rate (energy per unit time) from the ground heat exchanger to the ground
Q_m	The total heat transfer rate (energy per unit time) to material layer, m
$Q_m(t)$	The time dependant step-wise heat transfer rate (energy per unit time) function on material layer, m
$Q_{m,j}$	The value of one of the steps in $Q_m(t)$
R	Radial position ratio r_b/r
R_B	Borehole thermal resistance
R_i	Value of the radial position ratio that corresponds to measurement, i
S^k	sum of the squares of the Error (Residual), $\sum_{i=a}^{b}\left(E_i^k\right)^2$
$T(r,t)$	Temperature of the ground at a specific point and time
T_0	The initial temperature of the ground (assumed uniform or approximately so)
U	Dimensionless number , $r^2/4\alpha t$
U_i	Value of the dimensionless number (U) that corresponds to measurement, i
$U_{i,j-1}$	The value of the dimensionless number (U) corresponding to measurement i appropriate for superposition an analysis $r_i^2/4\alpha_m\left(t_i - t_{j-1}\right)$
VHC_m	The volumetric heat capacity of material layer, m
Y_0	Bessel Function of the second kind, order zero
Y_1	Bessel Function of the second kind, order one

Lower Case Greek Scripts

α	The thermal diffusivity of the ground
α_m	The thermal diffusivity of material layer, m
α_m^k	An estimate of α_m in the iteration procedure at iteration level k
$(\alpha_m)_n$	An estimate of α_m at depth z_n in material layer m

β_m	Represents the ratio Q_m/λ_m
β_m^k	An estimate of β_m in the iteration procedure at iteration level k, Q_m^k/λ_m^k
$(b_m)_n$	An estimate of b_m at depth z_n in material layer m
γ	Euler–Mascheroni constant, 0.5772156649…
$\Delta T(r,t)$	The Temperature Change of the ground at a specific point and time since initial time, $T(r,t) - T_0$
ΔT_i	An experimental temperature change reading, number i
$\Delta T(r_i, t_i, L_m, Q_m, \alpha_m, \lambda_m)$	Any mathematical function that may simulate the experimental data, which depends on the radial position and time of the datum, as well as the thickness, heat transfer rate (energy per time), thermal diffusivity, and thermal conductivity of the present material layer
ζ	A dummy variable used in an integration
η	A quantity in an integration, $\left(2\sqrt{\alpha t}\right)^{-1}$
λ	Thermal conductivity of the ground
λ_m	The thermal conductivity of material layer, m

Appendix B Experimental Data

Table 16 Nearer Well Temperature Data, Experiment 1 246

Table 17 Further Well Temperature Data, Experiment 1 259

Table 18 Nearer Well Temperature Data, Experiment 2 273

Table 19 Farther Well Temperature Data, Experiment 2 281

Table 16 Nearer Well Temperature Data, Experiment 1

Well 1, R = 1.4m Expt 1 2008

Date:	13-Jul	14-Jul	15-Jul	16-Jul	17-Jul	18-Jul	20-Jul	21-Jul	22-Jul	23-Jul	24-Jul
Beginning Time	13:48	13:59	13:44	14:22	14:30	14:37	10:48	16:57	17:07	17:40	18:08
End Time	14:46	14:36	14:36	15:16	15:18	15:33	11:33	17:36	17:54	19:15	19:18
Effective Time	14:17	14:17	14:10	14:49	14:54	15:05	11:10	17:16	17:30	18:27	9:04
Depth [m]	T [°C]	T [°C]	T [°C]	T [°C]	T [°C]	T [°C]	T [°C]	T [°C]	T [°C]	T [°C]	T [°C]
0.00	22.88	22.35	24.43	21.16	24.47	25.29	20.06	33.72	30.87	24.01	31.82
0.33	16.04	17.94	17.00	17.61	17.75	17.25	18.57	21.38	19.57	19.66	22.06
0.67	15.64	16.10	15.77	16.21	15.96	15.79	16.37	17.28	16.57	17.06	17.86
1.00	14.60	14.98	14.49	14.61	14.55	14.14	14.45	14.98	14.73	14.90	15.58
1.33	12.75	13.12	12.58	12.97	12.83	12.42	12.68	13.12	12.63	12.77	13.44
1.67	10.69	11.12	10.79	11.05	10.90	10.48	10.76	11.21	10.88	10.98	11.64
2.00	8.75	9.16	8.78	9.16	8.99	8.92	9.12	9.50	9.23	9.38	9.76
2.33	7.64	8.02	7.80	7.94	7.75	7.62	7.89	8.29	8.04	8.22	8.62
2.67	6.45	6.50	6.46	6.68	6.62	6.53	6.77	7.19	7.03	7.19	7.54
3.00	5.74	5.92	5.85	5.96	5.98	5.93	6.15	6.40	6.34	6.47	6.78
3.33	5.37	5.52	5.50	5.55	5.60	5.60	5.77	5.98	5.93	6.03	6.16
3.67	5.28	5.35	5.38	5.43	5.44	5.50	5.59	5.75	5.77	5.82	5.94
4.00	5.29	5.36	5.41	5.41	5.43	5.52	5.55	5.68	5.73	5.77	5.87
4.33	5.40	5.45	5.53	5.53	5.54	5.60	5.62	5.68	5.79	5.80	5.87
4.67	5.58	5.57	5.71	5.66	5.65	5.70	5.72	5.77	5.85	5.87	5.92
5.00	5.74	5.70	5.78	5.75	5.75	5.80	5.84	5.87	5.93	5.98	5.94
5.33	5.89	5.84	5.94	5.86	5.92	5.93	5.98	6.09	6.04	6.08	6.03
5.67	6.03	5.95	6.06	5.99	6.06	6.06	6.09	6.14	6.23	6.25	6.13

Well 1, R = 1.4m Expt 1 2008

Date:	13-Jul	14-Jul	15-Jul	16-Jul	17-Jul	18-Jul	20-Jul	21-Jul	22-Jul	23-Jul	24-Jul
Beginning Time	13:48	13:59	13:44	14:22	14:30	14:37	10:48	16:57	17:07	17:40	18:08
End Time	14:46	14:36	14:36	15:16	15:18	15:33	11:33	17:36	17:54	19:15	19:18
Effective Time	14:17	14:17	14:10	14:49	14:54	15:05	11:10	17:16	17:30	18:27	9:04
Depth [m]	T [°C]	T [°C]	T [°C]	T [°C]	T [°C]	T [°C]	T [°C]	T [°C]	T [°C]	T [°C]	T [°C]
6.00	6.15	6.08	6.16	6.14	6.19	6.16	6.21	6.24	6.31	6.33	6.28
6.33	6.26	6.20	6.24	6.23	6.27	6.30	6.32	6.33	6.37	6.41	6.37
6.67	6.34	6.31	6.33	6.32	6.33	6.35	6.38	6.38	6.43	6.48	6.44
7.00	6.39	6.38	6.38	6.39	6.40	6.40	6.43	6.42	6.48	6.52	6.51
7.33	6.42	6.42	6.41	6.42	6.43	6.44	6.47	6.47	6.51	6.55	6.54
7.67	6.45	6.45	6.45	6.44	6.45	6.46	6.49	6.51	6.54	6.57	6.57
8.00	6.46	6.45	6.46	6.46	6.46	6.48	6.50	6.53	6.56	6.59	6.60
8.33	6.46	6.45	6.45	6.45	6.46	6.47	6.51	6.54	6.58	6.60	6.63
8.67	6.45	6.44	6.44	6.45	6.46	6.47	6.51	6.54	6.58	6.61	6.65
9.00	6.43	6.43	6.43	6.43	6.44	6.45	6.49	6.54	6.58	6.61	6.65
9.33	6.40	6.41	6.41	6.42	6.42	6.43	6.48	6.52	6.56	6.60	6.65
9.67	6.38	6.39	6.38	6.39	6.40	6.41	6.45	6.50	6.54	6.58	6.65
10.00	6.34	6.36	6.35	6.37	6.37	6.39	6.43	6.48	6.52	6.55	6.61
11.00	6.25	6.25	6.25	6.26	6.25	6.29	6.34	6.40	6.43	6.48	6.55
12.00	6.14	6.15	6.16	6.16	6.17	6.18	6.26	6.32	6.36	6.42	6.46
13.00	6.06	6.08	6.08	6.09	6.10	6.12	6.19	6.27	6.32	6.37	6.44
14.00	6.02	6.05	6.02	6.04	6.06	6.09	6.18	6.24	6.31	6.36	6.44
15.00	6.00	6.00	6.01	6.01	6.04	6.10	6.17	6.26	6.39	6.48	6.55
16.00	6.00	6.00	6.03	6.08	6.16	6.27	6.45	6.50	6.73	6.80	7.03

Well 1, R = 1.4m Expt 1 2008

Date:	13-Jul	14-Jul	15-Jul	16-Jul	17-Jul	18-Jul	20-Jul	21-Jul	22-Jul	23-Jul	24-Jul
Beginning Time	13:48	13:59	13:44	14:22	14:30	14:37	10:48	16:57	17:07	17:40	18:08
End Time	14:46	14:36	14:36	15:16	15:18	15:33	11:33	17:36	17:54	19:15	19:18
Effective Time	14:17	14:17	14:10	14:49	14:54	15:05	11:10	17:16	17:30	18:27	9:04
17.00	6.00	6.00	6.06	6.17	6.30	6.43	6.67	6.83	6.95	7.06	7.20
18.00	6.00	6.00	6.09	6.23	6.41	6.57	6.86	7.03	7.17	7.30	7.41
19.00	5.99	6.00	6.05	6.21	6.34	6.50	6.72	6.97	7.01	7.19	7.30
20.00	5.99	5.99	6.02	6.12	6.23	6.37	6.61	6.77	6.88	7.00	7.09
21.00	5.98	5.98	6.02	6.10	6.20	6.31	6.48	6.64	6.72	6.82	6.93
22.00	5.98	5.98	6.02	6.09	6.18	6.28	6.42	6.53	6.61	6.68	6.77
23.00	5.98	5.98	6.02	6.08	6.18	6.26	6.41	6.52	6.58	6.63	6.72
24.00	5.98	5.98	6.02	6.09	6.18	6.26	6.42	6.53	6.60	6.67	6.74
25.00	5.98	5.98	6.02	6.07	6.15	6.24	6.40	6.49	6.55	6.63	6.70
26.00	5.98	5.99	6.01	6.06	6.13	6.19	6.33	6.42	6.50	6.56	6.63
27.00	5.99	5.99	6.01	6.05	6.11	6.16	6.29	6.38	6.45	6.48	6.56
28.00	6.01	6.00	6.02	6.05	6.12	6.20	6.33	6.41	6.49	6.54	6.59
29.00	6.01	6.01	6.02	6.06	6.12	6.19	6.31	6.41	6.48	6.55	6.63
30.00	6.01	6.01	6.02	6.04	6.09	6.15	6.26	6.36	6.41	6.48	6.54
31.00	5.99	6.00	6.00	6.01	6.04	6.07	6.16	6.24	6.30	6.32	6.37
32.00	5.97	5.98	5.98	5.99	6.01	6.04	6.09	6.16	6.19	6.25	6.28
33.00	5.95	5.95	5.96	5.96	5.98	5.99	6.04	6.09	6.12	6.17	6.22
34.00	5.93	5.94	5.94	5.95	5.94	5.96	6.00	6.04	6.05	6.11	6.15
35.00	5.92	5.92	5.92	5.92	5.93	5.94	5.97	6.00	6.03	6.06	6.09
36.00	5.91	5.91	5.91	5.91	5.93	5.94	5.98	6.02	6.06	6.08	6.12

Well 1, R = 1.4m Expt 1

Date:	13-Jul	14-Jul	15-Jul	16-Jul	17-Jul	18-Jul	20-Jul	21-Jul	22-Jul	23-Jul	24-Jul
Beginning Time	13:48	13:59	13:44	14:22	14:30	14:37	10:48	16:57	17:07	17:40	18:08
End Time	14:46	14:36	14:36	15:16	15:18	15:33	11:33	17:36	17:54	19:15	19:18
Effective Time	14:17	14:17	14:10	14:49	14:54	15:05	11:10	17:16	17:30	18:27	9:04
37.00	5.90	5.90	5.90	5.91	5.92	5.93	5.97	6.00	6.03	6.06	6.09
38.00	5.89	5.89	5.90	5.90	5.90	5.91	5.94	5.97	6.00	6.02	6.06
39.00	5.89	5.89	5.90	5.89	5.90	5.90	5.93	5.95	5.99	6.01	6.04
40.00	5.89	5.89	5.89	5.89	5.89	5.90	5.92	5.96	5.98	6.00	6.04
41.00	5.89	5.88	5.89	5.89	5.89	5.90	5.92	5.95	5.97	5.99	6.02
42.00	5.89	5.88	5.89	5.89	5.89	5.90	5.91	5.94	5.95	5.98	6.00
43.00	5.88	5.88	5.88	5.88	5.89	5.89	5.90	5.93	5.95	5.96	5.99
44.00	5.88	5.88	5.88	5.88	5.88	5.89	5.90	5.92	5.94	5.96	5.98
45.00	5.88	5.88	5.89	5.88	5.88	5.89	5.90	5.92	5.94	5.95	5.97
46.00	5.88	5.88	5.88	5.88	5.89	5.89	5.90	5.91	5.93	5.94	5.95
47.00	5.88	5.88	5.88	5.88	5.88	5.89	5.89	5.91	5.92	5.93	5.95
48.00	5.88	5.88	5.88	5.88	5.88	5.89	5.89	5.91	5.92	5.93	5.95
49.00	5.88	5.88	5.88	5.88	5.88	5.89	5.89	5.90	5.91	5.92	5.94
50.00	5.88	5.88	5.88	5.88	5.88	5.89	5.89	5.90	5.91	5.92	5.94
51.00	5.88	5.89	5.88	5.89	5.88	5.89	5.89	5.90	5.91	5.91	5.94
52.00	5.89	5.89	5.89	5.89	5.89	5.89	5.90	5.90	5.90	5.91	5.92
53.00	5.89	5.90	5.89	5.90	5.90	5.90	5.90	5.90	5.91	5.91	5.92
54.00	5.90	5.89	5.90	5.90	5.90	5.90	5.90	5.90	5.91	5.91	5.92
55.00	5.90	5.91	5.90	5.91	5.91	5.91	5.91	5.91	5.91	5.91	5.92
56.00	5.91	5.91	5.91	5.92	5.91	5.91	5.92	5.91	5.92	5.92	5.93

Well 1, R = 1.4m Expt 1

Date:	13-Jul	14-Jul	15-Jul	16-Jul	17-Jul	18-Jul	20-Jul	21-Jul	22-Jul	23-Jul	24-Jul
Beginning Time	13:48	13:59	13:44	14:22	14:30	14:37	10:48	16:57	17:07	17:40	18:08
End Time	14:46	14:36	14:36	15:16	15:18	15:33	11:33	17:36	17:54	19:15	19:18
Effective Time	14:17	14:17	14:10	14:49	14:54	15:05	11:10	17:16	17:30	18:27	9:04
57.00	5.92	5.92	5.92	5.92	5.92	5.92	5.92	5.93	5.92	5.93	5.93
58.00	5.93	5.92	5.93	5.93	5.93	5.93	5.93	5.93	5.93	5.93	5.94
59.00	5.94	5.94	5.94	5.94	5.93	5.94	5.94	5.94	5.94	5.94	5.95
60.00	5.95	5.94	5.95	5.95	5.95	5.95	5.95	5.95	5.95	5.95	5.95
61.00	5.96	5.96	5.96	5.96	5.96	5.96	5.96	5.96	5.96	5.96	5.96

Well 1, R = 1.4m Expt 1 2008

Date:	25-Jul	27-Jul	28-Jul	29-Jul	30-Jul	31-Jul	01-Aug	03-Aug	04-Aug	05-Aug	06-Aug
Beginning Time	17:35	15:16	17:48	17:20	16:24	17:20	18:01	13:38	15:15	17:05	17:00
End Time	18:19	15:58	18:52	18:20	18:46	18:16	18:44	14:38	16:10	18:10	18:09
Effective Time	17:57	15:37	18:20	17:50	17:35	17:48	18:22	14:08	15:42	17:37	17:34
Depth [m]	T [°C]	T [°C]	T [°C]	T [°C]	T [°C]	T [°C]	T [°C]	T [°C]	T [°C]	T [°C]	T [°C]
0.00	27.60	29.04	30.96	23.88	29.24	30.34	32.58	21.16	21.61	29.29	28.39
0.33	20.17	19.96	20.66	19.70	20.22	18.82	21.23	19.23	18.88	20.41	19.98
0.67	17.10	17.67	17.82	17.55	17.69	17.90	18.07	18.35	17.56	18.72	17.67
1.00	15.05	15.54	15.84	15.65	15.96	16.11	16.24	16.70	16.28	16.50	16.26
1.33	12.95	13.27	13.43	13.34	13.57	13.87	14.11	14.41	14.25	15.18	14.60
1.67	10.86	11.38	11.68	11.46	11.70	11.83	12.24	12.66	12.26	13.06	12.38
2.00	9.59	9.82	10.01	9.88	10.05	10.32	10.43	10.80	10.62	11.08	10.70
2.33	8.37	8.52	8.61	8.71	8.86	9.08	9.13	9.43	9.37	9.85	9.35
2.67	7.28	7.53	7.76	7.59	7.84	8.02	8.13	8.29	8.24	8.65	8.32
3.00	6.65	6.86	7.01	7.06	7.15	7.20	7.33	7.51	7.49	7.79	7.58
3.33	6.21	6.43	6.57	6.53	6.61	6.73	6.81	7.02	6.94	7.22	7.11
3.67	6.03	6.15	6.25	6.30	6.37	6.48	6.52	6.66	6.65	6.90	6.76
4.00	5.98	6.06	6.12	6.20	6.26	6.37	6.39	6.51	6.47	6.61	6.61
4.33	5.96	6.05	6.18	6.19	6.23	6.32	6.34	6.44	6.43	6.53	6.57
4.67	6.00	6.10	6.23	6.24	6.26	6.33	6.35	6.43	6.44	6.50	6.52
5.00	6.07	6.19	6.18	6.30	6.33	6.40	6.42	6.47	6.49	6.52	6.54
5.33	6.21	6.30	6.23	6.38	6.41	6.47	6.48	6.53	6.54	6.57	6.60
5.67	6.30	6.39	6.31	6.52	6.51	6.56	6.55	6.63	6.64	6.65	6.66
6.00	6.37	6.47	6.44	6.59	6.58	6.65	6.65	6.71	6.72	6.76	6.74

Well 1, R = 1.4m Expt 1 2008

Date:	25-Jul	27-Jul	28-Jul	29-Jul	30-Jul	31-Jul	01-Aug	03-Aug	04-Aug	05-Aug	06-Aug
Beginning Time	17:35	15:16	17:48	17:20	16:24	17:20	18:01	13:38	15:15	17:05	17:00
End Time	18:19	15:58	18:52	18:20	18:46	18:16	18:44	14:38	16:10	18:10	18:09
Effective Time	17:57	15:37	18:20	17:50	17:35	17:48	18:22	14:08	15:42	17:37	17:34
Depth [m]	T [°C]	T [°C]	T [°C]	T [°C]	T [°C]	T [°C]	T [°C]	T [°C]	T [°C]	T [°C]	T [°C]
6.33	6.45	6.57	6.54	6.65	6.64	6.71	6.72	6.78	6.77	6.80	6.80
6.67	6.50	6.62	6.61	6.68	6.71	6.77	6.78	6.82	6.83	6.84	6.87
7.00	6.56	6.66	6.66	6.72	6.75	6.81	6.82	6.85	6.89	6.87	6.91
7.33	6.60	6.70	6.70	6.76	6.82	6.85	6.87	6.91	6.93	6.91	6.95
7.67	6.63	6.71	6.73	6.78	6.85	6.87	6.91	6.93	6.96	6.94	6.97
8.00	6.67	6.74	6.75	6.82	6.88	6.88	6.94	6.95	6.99	6.96	6.99
8.33	6.69	6.75	6.76	6.84	6.91	6.91	6.98	6.98	7.01	7.00	7.01
8.67	6.69	6.77	6.79	6.86	6.91	6.93	6.98	6.99	7.02	7.01	7.03
9.00	6.70	6.77	6.80	6.87	6.91	6.94	6.98	7.02	7.03	7.04	7.03
9.33	6.70	6.77	6.82	6.86	6.91	6.94	6.98	7.02	7.03	7.04	7.03
9.67	6.68	6.75	6.82	6.85	6.90	6.93	6.97	7.01	7.01	7.03	7.03
10.00	6.66	6.73	6.81	6.84	6.88	6.92	6.95	7.00	7.00	7.02	7.01
11.00	6.58	6.70	6.82	6.81	6.84	6.89	6.91	6.99	6.96	7.01	6.99
12.00	6.53	6.60	6.78	6.76	6.84	6.88	6.90	6.95	6.97	7.00	6.99
13.00	6.51	6.63	6.76	6.74	6.81	6.85	6.89	6.95	6.95	6.99	6.96
14.00	6.53	6.65	6.72	6.77	6.83	6.89	6.90	6.94	6.95	6.96	6.96
15.00	6.66	6.78	6.88	7.14	7.03	7.01	7.04	6.99	7.05	7.03	7.00
16.00	7.15	7.13	7.22	7.30	7.30	7.23	7.24	7.15	7.14	7.06	7.03
17.00	7.28	7.46	7.52	7.56	7.49	7.43	7.35	7.23	7.15	7.10	7.04

Well 1, R = 1.4m Expt 1 2008

Date:	25-Jul	27-Jul	28-Jul	29-Jul	30-Jul	31-Jul	01-Aug	03-Aug	04-Aug	05-Aug	06-Aug
Beginning Time	17:35	15:16	17:48	17:20	16:24	17:20	18:01	13:38	15:15	17:05	17:00
End Time	18:19	15:58	18:52	18:20	18:46	18:16	18:44	14:38	16:10	18:10	18:09
Effective Time	17:57	15:37	18:20	17:50	17:35	17:48	18:22	14:08	15:42	17:37	17:34
18.00	7.49	7.71	7.74	7.74	7.67	7.55	7.45	7.30	7.22	7.14	7.09
19.00	7.36	7.57	7.67	7.63	7.56	7.48	7.41	7.27	7.19	7.12	7.06
20.00	7.14	7.38	7.43	7.39	7.36	7.31	7.27	7.16	7.09	7.05	6.98
21.00	6.94	7.10	7.19	7.18	7.17	7.14	7.11	7.03	6.98	6.93	6.90
22.00	6.80	6.95	7.02	7.03	7.03	7.01	6.98	6.91	6.87	6.83	6.80
23.00	6.78	6.85	6.93	6.97	6.97	6.93	6.92	6.83	6.80	6.76	6.73
24.00	6.80	6.88	6.95	6.98	6.97	6.92	6.89	6.81	6.78	6.73	6.70
25.00	6.73	6.86	6.91	6.93	6.92	6.89	6.86	6.78	6.75	6.71	6.69
26.00	6.68	6.80	6.85	6.88	6.87	6.86	6.82	6.77	6.73	6.70	6.67
27.00	6.62	6.75	6.80	6.84	6.83	6.84	6.81	6.77	6.72	6.69	6.65
28.00	6.70	6.90	6.84	6.88	6.91	6.88	6.84	6.78	6.73	6.69	6.65
29.00	6.66	6.77	6.83	6.86	6.88	6.86	6.84	6.76	6.71	6.66	6.62
30.00	6.58	6.68	6.74	6.76	6.78	6.80	6.78	6.76	6.68	6.63	6.60
31.00	6.46	6.50	6.56	6.62	6.65	6.66	6.65	6.71	6.61	6.60	6.57
32.00	6.33	6.40	6.48	6.52	6.52	6.56	6.56	6.63	6.55	6.56	6.53
33.00	6.24	6.32	6.37	6.41	6.44	6.48	6.46	6.57	6.49	6.51	6.50
34.00	6.17	6.24	6.29	6.32	6.34	6.40	6.39	6.51	6.42	6.46	6.44
35.00	6.13	6.19	6.23	6.27	6.29	6.34	6.35	6.44	6.39	6.40	6.41
36.00	6.17	6.22	6.25	6.28	6.32	6.36	6.36	6.38	6.40	6.40	6.41
37.00	6.13	6.19	6.24	6.26	6.28	6.32	6.34	6.40	6.38	6.38	6.39

Well 1, R = 1.4m

Date:	25-Jul	27-Jul	28-Jul	29-Jul	30-Jul	31-Jul	01-Aug	03-Aug	04-Aug	05-Aug	06-Aug
Beginning Time	17:35	15:16	17:48	17:20	16:24	17:20	18:01	13:38	15:15	17:05	17:00
End Time	18:19	15:58	18:52	18:20	18:46	18:16	18:44	14:38	16:10	18:10	18:09
Effective Time	17:57	15:37	18:20	17:50	17:35	17:48	18:22	14:08	15:42	17:37	17:34
38.00	6.10	6.14	6.18	6.20	6.25	6.28	6.30	6.37	6.34	6.35	6.35
39.00	6.06	6.11	6.14	6.18	6.21	6.22	6.26	6.33	6.30	6.31	6.31
40.00	6.05	6.10	6.13	6.17	6.19	6.21	6.25	6.30	6.27	6.28	6.29
41.00	6.03	6.09	6.12	6.14	6.17	6.21	6.22	6.27	6.26	6.26	6.27
42.00	6.03	6.07	6.10	6.13	6.15	6.18	6.19	6.24	6.24	6.26	6.25
43.00	6.00	6.05	6.09	6.11	6.13	6.15	6.18	6.20	6.21	6.24	6.23
44.00	6.00	6.04	6.06	6.09	6.11	6.13	6.15	6.19	6.19	6.22	6.21
45.00	5.99	6.03	6.05	6.07	6.10	6.12	6.14	6.17	6.19	6.20	6.21
46.00	5.98	6.01	6.03	6.06	6.07	6.10	6.13	6.15	6.16	6.18	6.19
47.00	5.97	6.00	6.02	6.04	6.06	6.08	6.11	6.14	6.14	6.16	6.16
48.00	5.96	5.99	6.01	6.03	6.05	6.06	6.10	6.12	6.14	6.15	6.16
49.00	5.95	5.98	6.00	6.02	6.04	6.06	6.09	6.10	6.12	6.13	6.14
50.00	5.94	5.97	5.99	6.00	6.02	6.04	6.05	6.08	6.10	6.11	6.13
51.00	5.94	5.96	5.98	5.99	6.01	6.02	6.03	6.07	6.08	6.10	6.10
52.00	5.93	5.95	5.97	5.97	5.99	6.00	6.02	6.04	6.05	6.07	6.08
53.00	5.93	5.95	5.95	5.97	5.98	5.99	6.01	6.03	6.04	6.06	6.06
54.00	5.93	5.94	5.95	5.96	5.97	5.98	6.00	6.02	6.03	6.04	6.05
55.00	5.94	5.94	5.95	5.95	5.97	5.98	5.99	6.01	6.02	6.03	6.04
56.00	5.93	5.95	5.95	5.96	5.97	5.98	5.99	6.01	6.01	6.03	6.04
57.00	5.94	5.95	5.95	5.96	5.97	5.98	5.99	6.01	6.01	6.02	6.04

Well 1, R = 1.4m

Date:	25-Jul	27-Jul	28-Jul	29-Jul	30-Jul	31-Jul	01-Aug	03-Aug	04-Aug	05-Aug	06-Aug
Beginning Time	17:35	15:16	17:48	17:20	16:24	17:20	18:01	13:38	15:15	17:05	17:00
End Time	18:19	15:58	18:52	18:20	18:46	18:16	18:44	14:38	16:10	18:10	18:09
Effective Time	17:57	15:37	18:20	17:50	17:35	17:48	18:22	14:08	15:42	17:37	17:34
58.00	5.95	5.96	5.95	5.96	5.97	5.98	5.99	6.00	6.01	6.03	6.02
59.00	5.95	5.96	5.96	5.97	5.97	5.98	5.98	6.00	6.01	6.02	6.02
60.00	5.96	5.97	5.97	5.97	5.98	5.98	5.99	6.00	6.00	6.01	6.02
61.00	5.96	5.97	5.97	5.97	5.98	5.98	5.99	5.99	6.00	6.01	6.01

Well 1, R = 1.4m	Expt 1	2008	
Date:	07-Aug	08-Aug	10-Aug
Beginning Time	19:47	17:40	16:03
End Time	20:47	18:30	16:50
Effective Time	20:17	18:05	16:26
Depth [m]	T [°C]	T [°C]	T [°C]
0.00	31.91	31.90	32.00
0.33	21.46	21.37	21.69
0.67	18.10	17.92	18.98
1.00	16.36	16.35	17.08
1.33	14.45	14.42	14.87
1.67	12.64	12.61	13.04
2.00	10.88	10.89	11.25
2.33	9.60	9.69	10.03
2.67	8.52	8.84	8.76
3.00	7.71	7.66	7.86
3.33	7.16	7.20	7.27
3.67	6.82	6.85	6.95
4.00	6.65	6.64	6.67
4.33	6.54	6.58	6.59
4.67	6.53	6.55	6.55
5.00	6.55	6.57	6.55
5.33	6.56	6.62	6.61
5.67	6.67	6.68	6.68
6.00	6.77	6.76	6.75

Well 1, R = 1.4m	Expt 1	2008	
Date:	07-Aug	08-Aug	10-Aug
Beginning Time	19:47	17:40	16:03
End Time	20:47	18:30	16:50
Effective Time	20:17	18:05	16:26
Depth [m]	T [°C]	T [°C]	T [°C]
6.33	6.84	6.80	6.80
6.67	6.87	6.88	6.85
7.00	6.89	6.91	6.89
7.33	6.92	6.95	6.95
7.67	6.96	6.97	6.97
8.00	6.98	6.99	6.99
8.33	7.02	7.00	7.01
8.67	7.04	7.02	7.02
9.00	7.04	7.03	7.03
9.33	7.04	7.03	7.03
9.67	7.03	7.02	7.03
10.00	7.02	7.01	7.01
11.00	7.00	6.99	6.99
12.00	7.00	6.98	6.98
13.00	6.99	6.96	6.95
14.00	6.97	6.95	6.93
15.00	6.98	6.97	6.94
16.00	6.98	6.95	6.90
17.00	7.00	6.95	6.89

Well 1, R = 1.4m	Expt 1	2008		Well 1, R = 1.4m			
Date:	07-Aug	08-Aug	10-Aug	Date:	07-Aug	08-Aug	10-Aug
Beginning Time	19:47	17:40	16:03	Beginning Time	19:47	17:40	16:03
End Time	20:47	18:30	16:50	End Time	20:47	18:30	16:50
Effective Time	20:17	18:05	16:26	Effective Time	20:17	18:05	16:26
18.00	7.02	6.98	6.90	38.00	6.36	6.35	6.32
19.00	7.01	6.96	6.89	39.00	6.33	6.31	6.29
20.00	6.95	6.89	6.84	40.00	6.29	6.30	6.28
21.00	6.85	6.81	6.76	41.00	6.27	6.27	6.27
22.00	6.77	6.74	6.69	42.00	6.27	6.25	6.25
23.00	6.70	6.67	6.63	43.00	6.24	6.23	6.23
24.00	6.67	6.64	6.60	44.00	6.23	6.22	6.23
25.00	6.65	6.62	6.58	45.00	6.21	6.22	6.21
26.00	6.64	6.61	6.57	46.00	6.21	6.20	6.20
27.00	6.63	6.59	6.54	47.00	6.18	6.18	6.19
28.00	6.60	6.57	6.51	48.00	6.17	6.17	6.19
29.00	6.58	6.55	6.49	49.00	6.15	6.16	6.17
30.00	6.57	6.54	6.49	50.00	6.14	6.13	6.16
31.00	6.56	6.53	6.50	51.00	6.12	6.11	6.13
32.00	6.53	6.52	6.49	52.00	6.10	6.10	6.12
33.00	6.51	6.48	6.48	53.00	6.08	6.08	6.10
34.00	6.45	6.44	6.45	54.00	6.06	6.06	6.08
35.00	6.40	6.40	6.39	55.00	6.05	6.05	6.07
36.00	6.40	6.39	6.38	56.00	6.04	6.05	6.07
37.00	6.38	6.38	6.36	57.00	6.04	6.04	6.06

Well 1, R = 1.4m

Date:	07-Aug	08-Aug	10-Aug
Beginning Time	19:47	17:40	16:03
End Time	20:47	18:30	16:50
Effective Time	20:17	18:05	16:26
58.00	6.03	6.04	6.05
59.00	6.03	6.03	6.05
60.00	6.02	6.02	6.04
61.00	6.02	6.02	6.03

Table 17 Further Well Temperature Data, Experiment 1

Well 2, R = 2.8m Expt 1 2008

Date:	13-Jul	14-Jul	15-Jul	16-Jul	17-Jul	18-Jul	20-Jul	21-Jul	22-Jul	23-Jul	24-Jul
Beginning Time	14:37	14:44	14:45	15:25	15:23	15:39	11:52	17:41	17:59	19:21	19:25
End Time	15:18	15:36	15:32	16:16	16:04	14:32	12:52	18:20	18:43	20:10	20:07
Effective Time	14:57	15:10	15:08	15:50	15:43	15:05	12:22	18:00	18:21	19:45	19:46
Depth [m]	T [°C]	T [°C]	T [°C]	T [°C]	T [°C]	T [°C]	T [°C]	T [°C]	T [°C]	T [°C]	T [°C]
0.00	19.11	20.16	23.28	19.76	20.26	23.60	20.89	29.05	28.83	21.22	28.82
0.33	16.10	17.13	16.80	17.35	16.70	17.18	18.19	19.45	19.32	20.08	21.72
0.67	15.25	15.75	15.52	15.59	14.98	15.23	15.85	16.48	16.25	16.70	17.20
1.00	13.37	13.77	13.66	13.58	12.98	13.37	13.81	14.15	13.86	14.27	14.71
1.33	11.76	12.18	11.94	11.91	11.56	11.85	12.35	12.43	12.03	12.30	12.76
1.67	9.50	10.35	10.43	10.24	9.86	10.14	10.52	10.77	10.46	10.57	11.08
2.00	8.04	8.62	8.36	8.72	8.23	8.52	8.88	9.13	9.00	9.10	9.55
2.33	6.83	7.33	7.18	7.35	7.15	7.35	7.62	7.94	7.72	7.81	8.12
2.67	5.86	6.18	6.27	6.41	6.26	6.32	6.51	6.81	6.58	6.89	7.05
3.00	5.51	5.75	6.56	5.82	5.76	5.86	5.96	6.10	6.06	6.15	6.27
3.33	5.31	5.40	5.40	5.53	5.52	5.61	5.66	5.80	5.75	5.79	5.89
3.67	5.30	5.33	5.37	5.42	5.44	5.51	5.52	5.61	5.58	5.67	5.70
4.00	5.38	5.38	5.43	5.43	5.48	5.52	5.53	5.59	5.64	5.60	5.65
4.33	5.52	5.52	5.52	5.55	5.61	5.67	5.59	5.68	5.75	5.65	5.70
4.67	5.71	5.71	5.72	5.69	5.75	5.82	5.73	5.74	5.76	5.74	5.80
5.00	5.87	5.84	5.89	5.85	5.92	5.87	5.86	5.86	5.94	5.86	5.93
5.33	6.05	6.01	6.05	6.00	6.05	6.03	5.97	5.97	6.05	6.01	5.98
5.67	6.19	6.16	6.17	6.10	6.18	6.14	6.11	6.11	6.16	6.14	6.09

Well 2, R = 2.8m Expt 1 2008

Date:	13-Jul	14-Jul	15-Jul	16-Jul	17-Jul	18-Jul	20-Jul	21-Jul	22-Jul	23-Jul	24-Jul
Beginning Time	14:37	14:44	14:45	15:25	15:23	15:39	11:52	17:41	17:59	19:21	19:25
End Time	15:18	15:36	15:32	16:16	16:04	14:32	12:52	18:20	18:43	20:10	20:07
Effective Time	14:57	15:10	15:08	15:50	15:43	15:05	12:22	18:00	18:21	19:45	19:46
Depth [m]	T [°C]	T [°C]	T [°C]	T [°C]	T [°C]	T [°C]	T [°C]	T [°C]	T [°C]	T [°C]	T [°C]
6.00	6.31	6.26	6.29	6.27	6.31	6.27	6.23	6.24	6.26	6.26	6.24
6.33	6.39	6.33	6.38	6.36	6.38	6.36	6.35	6.33	6.34	6.35	6.32
6.67	6.44	6.43	6.44	6.42	6.42	6.45	6.46	6.41	6.43	6.41	6.40
7.00	6.48	6.48	6.49	6.48	6.48	6.48	6.50	6.45	6.46	6.46	6.45
7.33	6.52	6.52	6.51	6.51	6.51	6.51	6.52	6.49	6.49	6.49	6.49
7.67	6.53	6.52	6.53	6.52	6.52	6.52	6.52	6.51	6.51	6.51	6.51
8.00	6.53	6.53	6.54	6.53	6.53	6.53	6.52	6.51	6.52	6.52	6.51
8.33	6.53	6.53	6.53	6.52	6.53	6.52	6.51	6.52	6.52	6.52	6.51
8.67	6.52	6.52	6.52	6.51	6.52	6.51	6.50	6.51	6.50	6.51	6.51
9.00	6.49	6.50	6.50	6.50	6.49	6.49	6.48	6.49	6.49	6.50	6.50
9.33	6.47	6.48	6.47	6.48	6.48	6.47	6.45	6.47	6.47	6.48	6.48
9.67	6.44	6.45	6.40	6.43	6.44	6.44	6.42	6.45	6.43	6.45	6.46
10.00	6.40	6.42	6.41	6.41	6.41	6.42	6.41	6.42	6.41	6.42	6.43
11.00	6.31	6.33	6.32	6.33	6.31	6.32	6.31	6.34	6.31	6.34	6.32
12.00	6.21	6.23	6.22	6.23	6.22	6.22	6.22	6.24	6.22	6.22	6.23
13.00	6.12	6.14	6.13	6.14	6.13	6.12	6.14	6.15	6.13	6.14	6.15
14.00	6.06	6.07	6.07	6.07	6.06	6.08	6.07	6.08	6.07	6.08	6.09
15.00	6.03	6.03	6.03	6.03	6.02	6.03	6.03	6.04	6.05	6.05	6.07
16.00	6.00	6.01	6.01	6.01	6.01	6.02	6.03	6.05	6.06	6.08	6.11

Well 2, R = 2.8m Expt 1 2008

Date:	13-Jul	14-Jul	15-Jul	16-Jul	17-Jul	18-Jul	20-Jul	21-Jul	22-Jul	23-Jul	24-Jul
Beginning Time	14:37	14:44	14:45	15:25	15:23	15:39	11:52	17:41	17:59	19:21	19:25
End Time	15:18	15:36	15:32	16:16	16:04	14:32	12:52	18:20	18:43	20:10	20:07
Effective Time	14:57	15:10	15:08	15:50	15:43	15:05	12:22	18:00	18:21	19:45	19:46
17.00	6.00	6.00	6.00	6.00	6.01	6.02	6.05	6.07	6.10	6.13	6.16
18.00	5.99	5.99	6.00	6.00	6.00	6.02	6.05	6.08	6.11	6.14	6.17
19.00	5.99	5.99	5.99	5.99	6.00	6.01	6.04	6.07	6.10	6.13	6.16
20.00	5.98	5.98	5.99	5.99	5.99	6.00	6.03	6.07	6.09	6.12	6.16
21.00	5.98	5.98	5.98	5.98	5.99	6.00	6.02	6.04	6.07	6.10	6.12
22.00	5.97	5.98	5.97	5.98	5.98	5.98	6.02	6.04	6.06	6.09	6.11
23.00	5.98	5.97	5.98	5.97	5.98	5.99	6.01	6.03	6.05	6.07	6.10
24.00	5.97	5.98	5.98	5.97	5.97	5.99	6.01	6.03	6.04	6.06	6.08
25.00	5.97	5.97	5.98	5.97	5.98	5.98	6.00	6.03	6.04	6.06	6.09
26.00	5.97	5.98	5.98	5.97	5.98	5.99	6.00	6.02	6.04	6.06	6.08
27.00	5.98	5.98	5.98	5.98	5.98	5.99	6.00	6.02	6.04	6.06	6.08
28.00	5.99	5.99	5.99	5.99	5.99	6.00	6.03	6.05	6.09	6.10	6.13
29.00	5.99	6.00	6.00	5.99	6.00	6.01	6.03	6.06	6.08	6.12	6.16
30.00	5.98	5.99	5.99	5.99	5.99	6.00	6.00	6.03	6.05	6.06	6.09
31.00	5.97	5.98	5.98	5.97	5.98	5.99	5.99	6.00	6.01	6.02	6.04
32.00	5.95	5.96	5.96	5.96	5.96	5.97	5.97	5.98	5.98	5.99	6.01
33.00	5.95	5.95	5.95	5.94	5.95	5.95	5.95	5.96	5.96	5.96	5.98
34.00	5.93	5.94	5.94	5.94	5.94	5.94	5.94	5.95	5.94	5.95	5.95
35.00	5.92	5.92	5.93	5.93	5.92	5.93	5.93	5.93	5.93	5.94	5.94
36.00	5.92	5.92	5.92	5.92	5.92	5.92	5.93	5.93	5.93	5.93	5.94

Well 2, R = 2.8m Expt 1 2008

Date:	13-Jul	14-Jul	15-Jul	16-Jul	17-Jul	18-Jul	20-Jul	21-Jul	22-Jul	23-Jul	24-Jul
Beginning Time	14:37	14:44	14:45	15:25	15:23	15:39	11:52	17:41	17:59	19:21	19:25
End Time	15:18	15:36	15:32	16:16	16:04	14:32	12:52	18:20	18:43	20:10	20:07
Effective Time	14:57	15:10	15:08	15:50	15:43	15:05	12:22	18:00	18:21	19:45	19:46
37.00	5.91	5.91	5.92	5.91	5.92	5.92	5.92	5.92	5.92	5.92	5.94
38.00	5.91	5.91	5.91	5.91	5.91	5.91	5.91	5.92	5.92	5.92	5.92
39.00	5.91	5.91	5.91	5.91	5.91	5.91	5.91	5.91	5.92	5.92	5.92
40.00	5.90	5.90	5.91	5.90	5.90	5.91	5.91	5.91	5.91	5.92	5.92
41.00	5.91	5.91	5.91	5.91	5.90	5.91	5.91	5.91	5.91	5.91	5.92
42.00	5.90	5.90	5.91	5.91	5.91	5.90	5.90	5.91	5.91	5.91	5.92
43.00	5.90	5.90	5.90	5.90	5.91	5.90	5.90	5.90	5.91	5.91	5.92
44.00	5.90	5.90	5.90	5.90	5.90	5.90	5.90	5.91	5.91	5.91	5.91
45.00	5.90	5.90	5.90	5.90	5.90	5.90	5.90	5.91	5.91	5.90	5.91
46.00	5.90	5.90	5.90	5.90	5.90	5.90	5.90	5.91	5.90	5.90	5.91
47.00	5.90	5.90	5.90	5.90	5.90	5.91	5.90	5.91	5.91	5.90	5.91
48.00	5.90	5.90	5.91	5.90	5.90	5.91	5.90	5.91	5.90	5.91	5.91
49.00	5.90	5.90	5.91	5.90	5.90	5.90	5.90	5.91	5.91	5.90	5.91
50.00	5.90	5.90	5.91	5.90	5.90	5.91	5.91	5.91	5.91	5.90	5.91
51.00	5.90	5.90	5.90	5.90	5.90	5.90	5.91	5.91	5.91	5.91	5.92
52.00	5.91	5.90	5.91	5.91	5.91	5.91	5.91	5.91	5.91	5.91	5.91
53.00	5.91	5.91	5.91	5.92	5.91	5.91	5.91	5.92	5.91	5.91	5.92
54.00	5.91	5.91	5.92	5.92	5.92	5.91	5.92	5.92	5.92	5.92	5.92
55.00	5.92	5.93	5.92	5.92	5.92	5.92	5.92	5.92	5.93	5.92	5.93
56.00	5.93	5.93	5.93	5.93	5.92	5.93	5.93	5.93	5.93	5.93	5.93

Well 2, R = 2.8m Expt 1 2008

Date:	13-Jul	14-Jul	15-Jul	16-Jul	17-Jul	18-Jul	20-Jul	21-Jul	22-Jul	23-Jul	24-Jul
Beginning Time	14:37	14:44	14:45	15:25	15:23	15:39	11:52	17:41	17:59	19:21	19:25
End Time	15:18	15:36	15:32	16:16	16:04	14:32	12:52	18:20	18:43	20:10	20:07
Effective Time	14:57	15:10	15:08	15:50	15:43	15:05	12:22	18:00	18:21	19:45	19:46
57.00	5.93	5.93	5.93	5.93	5.94	5.93	5.94	5.94	5.94	5.93	5.94
58.00	5.94	5.94	5.94	5.94	5.94	5.94	5.94	5.95	5.95	5.94	5.95
59.00	5.95	5.95	5.95	5.94	5.95	5.95	5.95	5.96	5.96	5.95	5.95
60.00	5.96	5.95	5.96	5.95	5.96	5.96	5.96	5.96	5.96	5.96	5.96
61.00	5.97	5.97	5.97	5.96	5.97	5.97	5.97	5.97	5.97	5.97	5.97
62.00	5.97	5.97	5.97	5.97	5.97	5.98	5.97	5.98	5.97	5.97	5.97

Well 2, R = 2.8m Expt 1 2008

Date:	25-Jul	27-Jul	28-Jul	29-Jul	30-Jul	31-Jul	01-Aug	03-Aug	04-Aug	05-Aug	06-Aug
Beginning Time	18:25	16:04	18:56	18:26	19:07	18:22	18:50	14:44	16:16	18:14	18:20
End Time	19:14	16:57	19:57	19:32	20:30	19:16	19:34	15:26	17:10	19:14	19:17
Effective Time	18:49	16:30	19:26	18:59	19:48	8:49	19:12	15:05	16:43	18:44	18:48
Depth [m]	T [°C]	T [°C]	T [°C]	T [°C]	T [°C]	T [°C]	T [°C]	T [°C]	T [°C]	T [°C]	T [°C]
0.00	25.69	30.57	27.96	23.99	27.90	26.54	30.48	20.62	20.13	27.64	28.33
0.33	20.72	21.56	20.19	19.93	20.78	20.31	21.12	19.43	19.03	19.60	21.44
0.67	16.92	18.10	17.12	17.02	17.66	17.31	17.62	17.83	17.14	17.24	17.96
1.00	14.56	15.46	14.72	14.75	15.08	15.08	15.65	15.59	15.08	15.61	16.23
1.33	12.34	13.21	12.64	12.76	13.12	13.03	13.54	13.54	13.39	13.65	14.35
1.67	10.83	11.51	10.95	10.84	11.48	11.41	11.76	11.80	11.50	11.84	12.14
2.00	9.47	9.88	9.46	9.37	9.73	9.71	10.06	10.17	9.86	10.36	10.80
2.33	7.97	8.42	8.12	8.15	8.31	8.49	8.60	8.70	8.53	8.76	9.30
2.67	7.03	7.31	7.11	6.97	7.30	7.37	7.47	7.48	7.37	7.52	8.01
3.00	6.28	6.51	6.36	6.86	6.56	6.58	6.68	6.71	6.71	6.89	7.15
3.33	5.89	6.01	6.03	6.33	6.10	6.15	6.20	6.27	6.25	6.39	6.50
3.67	5.74	5.77	5.77	5.97	5.86	5.88	5.92	5.98	5.99	6.05	6.20
4.00	5.72	5.69	5.72	5.74	5.76	5.79	5.81	5.85	5.88	5.97	6.04
4.33	5.76	5.70	5.74	5.77	5.84	5.79	5.80	5.82	5.86	5.95	5.97
4.67	5.83	5.77	5.83	5.88	5.96	5.86	5.87	5.87	5.92	5.98	5.98
5.00	5.91	5.86	5.91	5.95	6.03	5.96	5.97	5.98	5.99	6.04	6.03
5.33	6.00	5.97	6.00	6.05	6.16	6.06	6.06	6.06	6.09	6.14	6.07
5.67	6.17	6.11	6.15	6.18	6.26	6.18	6.15	6.18	6.20	6.23	6.18
6.00	6.25	6.23	6.27	6.28	6.35	6.27	6.26	6.28	6.30	6.32	6.26

Well 2, R = 2.8m Expt 1 2008

Date:	25-Jul	27-Jul	28-Jul	29-Jul	30-Jul	31-Jul	01-Aug	03-Aug	04-Aug	05-Aug	06-Aug
Beginning Time	18:25	16:04	18:56	18:26	19:07	18:22	18:50	14:44	16:16	18:14	18:20
End Time	19:14	16:57	19:57	19:32	20:30	19:16	19:34	15:26	17:10	19:14	19:17
Effective Time	18:49	16:30	19:26	18:59	19:48	8:49	19:12	15:05	16:43	18:44	18:48
Depth [m]	T [°C]	T [°C]	T [°C]	T [°C]	T [°C]	T [°C]	T [°C]	T [°C]	T [°C]	T [°C]	T [°C]
6.33	6.31	6.31	6.36	6.36	6.40	6.36	6.34	6.34	6.36	6.35	6.35
6.67	6.38	6.38	6.42	6.43	6.46	6.41	6.42	6.42	6.42	6.42	6.40
7.00	6.44	6.46	6.47	6.46	6.49	6.46	6.46	6.47	6.47	6.46	6.46
7.33	6.46	6.48	6.49	6.49	6.49	6.49	6.50	6.50	6.51	6.49	6.50
7.67	6.50	6.50	6.51	6.51	6.52	6.51	6.52	6.52	6.54	6.51	6.52
8.00	6.50	6.51	6.51	6.52	6.53	6.52	6.53	6.53	6.54	6.53	6.53
8.33	6.50	6.52	6.51	6.52	6.51	6.53	6.53	6.54	6.54	6.53	6.54
8.67	6.50	6.51	6.51	6.51	6.50	6.52	6.52	6.53	6.53	6.53	6.54
9.00	6.49	6.50	6.50	6.50	6.48	6.50	6.51	6.51	6.52	6.51	6.53
9.33	6.48	6.48	6.48	6.48	6.48	6.48	6.49	6.50	6.50	6.50	6.51
9.67	6.46	6.46	6.45	6.45	6.46	6.47	6.47	6.48	6.47	6.48	6.50
10.00	6.42	6.44	6.42	6.43	6.43	6.44	6.44	6.44	6.45	6.45	6.47
11.00	6.33	6.35	6.34	6.33	6.33	6.34	6.35	6.35	6.35	6.36	6.38
12.00	6.24	6.25	6.23	6.23	6.25	6.25	6.26	6.26	6.25	6.28	6.29
13.00	6.15	6.16	6.15	6.15	6.16	6.16	6.16	6.17	6.18	6.21	6.22
14.00	6.10	6.10	6.10	6.10	6.11	6.14	6.16	6.14	6.15	6.19	6.20
15.00	6.10	6.09	6.10	6.12	6.12	6.14	6.29	6.19	6.21	6.24	6.25
16.00	6.14	6.15	6.21	6.26	6.25	6.29	6.41	6.32	6.36	6.36	6.36
17.00	6.18	6.24	6.28	6.31	6.36	6.39	6.43	6.43	6.45	6.46	6.46

Well 2, R = 2.8m Expt 1 2008

Date:	25-Jul	27-Jul	28-Jul	29-Jul	30-Jul	31-Jul	01-Aug	03-Aug	04-Aug	05-Aug	06-Aug
Beginning Time	18:25	16:04	18:56	18:26	19:07	18:22	18:50	14:44	16:16	18:14	18:20
End Time	19:14	16:57	19:57	19:32	20:30	19:16	19:34	15:26	17:10	19:14	19:17
Effective Time	18:49	16:30	19:26	18:59	19:48	8:49	19:12	15:05	16:43	18:44	18:48
18.00	6.21	6.27	6.31	6.34	6.37	6.41	6.42	6.45	6.46	6.47	6.48
19.00	6.19	6.26	6.30	6.32	6.36	6.38	6.40	6.44	6.45	6.46	6.46
20.00	6.18	6.25	6.29	6.30	6.35	6.37	6.34	6.43	6.43	6.44	6.45
21.00	6.15	6.22	6.23	6.24	6.28	6.29	6.31	6.38	6.37	6.39	6.40
22.00	6.14	6.19	6.21	6.22	6.26	6.27	6.30	6.34	6.35	6.36	6.38
23.00	6.13	6.17	6.20	6.22	6.25	6.24	6.27	6.32	6.33	6.35	6.35
24.00	6.11	6.14	6.18	6.20	6.22	6.25	6.27	6.29	6.31	6.31	6.32
25.00	6.11	6.15	6.18	6.21	6.23	6.26	6.27	6.30	6.31	6.32	6.32
26.00	6.10	6.14	6.17	6.19	6.22	6.24	6.28	6.30	6.31	6.33	6.33
27.00	6.10	6.15	6.18	6.20	6.23	6.27	6.39	6.32	6.35	6.35	6.35
28.00	6.17	6.23	6.28	6.33	6.35	6.39	6.44	6.45	6.47	6.47	6.44
29.00	6.17	6.26	6.28	6.31	6.36	6.38	6.33	6.45	6.46	6.47	6.48
30.00	6.12	6.18	6.20	6.22	6.26	6.28	6.33	6.34	6.35	6.37	6.39
31.00	6.06	6.11	6.11	6.13	6.15	6.18	6.22	6.24	6.25	6.27	6.29
32.00	6.01	6.05	6.05	6.06	6.09	6.10	6.14	6.17	6.15	6.18	6.22
33.00	5.98	6.00	6.01	6.01	6.03	6.05	6.07	6.08	6.10	6.11	6.14
34.00	5.96	5.97	5.97	5.99	6.00	6.01	6.04	6.05	6.05	6.08	6.09
35.00	5.95	5.95	5.96	5.97	5.98	5.99	6.00	6.02	6.03	6.04	6.05
36.00	5.94	5.96	5.96	5.97	5.98	5.99	6.00	6.01	6.03	6.03	6.05
37.00	5.94	5.95	5.96	5.96	5.98	5.98	5.99	6.01	6.02	6.03	6.04

Well 2, R = 2.8m Expt 1 2008

Date:	25-Jul	27-Jul	28-Jul	29-Jul	30-Jul	31-Jul	01-Aug	03-Aug	04-Aug	05-Aug	06-Aug
Beginning Time	18:25	16:04	18:56	18:26	19:07	18:22	18:50	14:44	16:16	18:14	18:20
End Time	19:14	16:57	19:57	19:32	20:30	19:16	19:34	15:26	17:10	19:14	19:17
Effective Time	18:49	16:30	19:26	18:59	19:48	8:49	19:12	15:05	16:43	18:44	18:48
38.00	5.93	5.93	5.94	5.95	5.96	5.97	5.99	6.00	6.00	6.02	6.03
39.00	5.93	5.94	5.94	5.94	5.95	5.96	5.97	5.99	6.00	6.01	6.02
40.00	5.92	5.93	5.94	5.94	5.95	5.96	5.97	5.99	5.99	6.01	6.01
41.00	5.92	5.93	5.94	5.94	5.95	5.96	5.97	5.99	5.99	6.00	6.01
42.00	5.92	5.92	5.93	5.94	5.95	5.96	5.96	5.98	5.99	6.00	6.00
43.00	5.92	5.93	5.93	5.94	5.95	5.95	5.96	5.98	5.98	5.99	6.00
44.00	5.91	5.92	5.93	5.94	5.94	5.94	5.96	5.96	5.98	5.99	6.00
45.00	5.91	5.92	5.92	5.93	5.94	5.94	5.96	5.96	5.97	5.98	5.99
46.00	5.91	5.92	5.92	5.93	5.93	5.93	5.95	5.95	5.96	5.97	5.98
47.00	5.91	5.91	5.92	5.92	5.93	5.93	5.94	5.95	5.96	5.96	5.98
48.00	5.91	5.91	5.92	5.92	5.93	5.93	5.94	5.95	5.96	5.96	5.97
49.00	5.91	5.91	5.92	5.92	5.92	5.93	5.93	5.94	5.96	5.96	5.97
50.00	5.91	5.91	5.92	5.92	5.92	5.93	5.93	5.95	5.95	5.96	5.97
51.00	5.91	5.92	5.92	5.92	5.92	5.93	5.94	5.94	5.95	5.96	5.96
52.00	5.91	5.92	5.92	5.92	5.93	5.93	5.94	5.94	5.95	5.95	5.96
53.00	5.92	5.92	5.92	5.92	5.93	5.93	5.93	5.94	5.95	5.95	5.96
54.00	5.92	5.92	5.92	5.92	5.93	5.93	5.93	5.94	5.95	5.95	5.96
55.00	5.92	5.93	5.93	5.93	5.93	5.93	5.93	5.94	5.95	5.95	5.96
56.00	5.93	5.93	5.93	5.93	5.93	5.94	5.94	5.95	5.95	5.96	5.96
57.00	5.93	5.94	5.93	5.94	5.94	5.94	5.94	5.95	5.95	5.96	5.96

Well 2, R = 2.8m Expt 1 2008

Date:	25-Jul	27-Jul	28-Jul	29-Jul	30-Jul	31-Jul	01-Aug	03-Aug	04-Aug	05-Aug	06-Aug
Beginning Time	18:25	16:04	18:56	18:26	19:07	18:22	18:50	14:44	16:16	18:14	18:20
End Time	19:14	16:57	19:57	19:32	20:30	19:16	19:34	15:26	17:10	19:14	19:17
Effective Time	18:49	16:30	19:26	18:59	19:48	8:49	19:12	15:05	16:43	18:44	18:48
58.00	5.95	5.94	5.94	5.95	5.95	5.95	5.94	5.96	5.96	5.96	5.96
59.00	5.95	5.95	5.95	5.95	5.96	5.96	5.95	5.96	5.96	5.97	5.97
60.00	5.96	5.96	5.96	5.96	5.96	5.96	5.96	5.97	5.97	5.97	5.97
61.00	5.97	5.96	5.97	5.96	5.96	5.97	5.97	5.97	5.97	5.97	5.97
62.00	5.97	5.97	5.98	5.97	5.97	5.98	5.98	5.98	5.98	5.98	5.98

Well 2, R = 2.8m	Expt 1	2008	
Date:	07-Aug	08-Aug	10-Aug
Beginning Time	21:25	18:40	16:55
End Time	22:24	19:32	17:45
Effective Time	21:54	19:06	17:20
Depth [m]	T [°C]	T [°C]	T [°C]
0.00	25.33	29.97	28.31
0.33	23.28	21.07	21.00
0.67	18.50	17.80	17.89
1.00	16.30	15.65	15.84
1.33	14.59	14.07	13.95
1.67	12.62	12.19	12.14
2.00	10.86	10.57	10.47
2.33	9.41	9.01	9.03
2.67	8.08	7.75	7.85
3.00	7.24	7.09	7.04
3.33	6.55	6.56	6.52
3.67	6.28	6.24	6.27
4.00	6.05	6.09	6.04
4.33	5.98	6.01	5.98
4.67	5.99	6.01	6.00
5.00	6.03	6.05	6.01
5.33	6.10	6.11	6.14
5.67	6.19	6.20	6.26
6.00	6.28	6.30	6.30

Well 2, R = 2.8m	Expt 1	2008	
Date:	07-Aug	08-Aug	10-Aug
Beginning Time	21:25	18:40	16:55
End Time	22:24	19:32	17:45
Effective Time	21:54	19:06	17:20
Depth [m]	T [°C]	T [°C]	T [°C]
6.33	6.36	6.37	6.37
6.67	6.42	6.46	6.49
7.00	6.48	6.50	6.52
7.33	6.52	6.53	6.55
7.67	6.53	6.54	6.56
8.00	6.54	6.55	6.57
8.33	6.55	6.56	6.56
8.67	6.55	6.55	6.56
9.00	6.54	6.54	6.56
9.33	6.53	6.51	6.52
9.67	6.50	6.50	6.51
10.00	6.48	6.47	6.48
11.00	6.40	6.38	6.40
12.00	6.29	6.29	6.30
13.00	6.22	6.22	6.23
14.00	6.20	6.21	6.22
15.00	6.26	6.27	6.29
16.00	6.35	6.32	6.41
17.00	6.44	6.44	6.45

Well 2, R = 2.8m	Expt 1	2008	
Date:	07-Aug	08-Aug	10-Aug
Beginning Time	21:25	18:40	16:55
End Time	22:24	19:32	17:45
Effective Time	21:54	19:06	17:20
Depth [m]	T [°C]	T [°C]	T [°C]
18.00	6.47	6.46	6.46
19.00	6.46	6.47	6.46
20.00	6.47	6.46	6.45
21.00	6.42	6.42	6.41
22.00	6.40	6.38	6.38
23.00	6.36	6.36	6.36
24.00	6.33	6.33	6.33
25.00	6.33	6.33	6.33
26.00	6.34	6.34	6.34
27.00	6.36	6.37	6.37
28.00	6.45	6.44	6.43
29.00	6.46	6.45	6.44
30.00	6.38	6.38	6.37
31.00	6.30	6.30	6.30
32.00	6.22	6.23	6.24
33.00	6.15	6.15	6.16
34.00	6.10	6.10	6.12
35.00	6.07	6.06	6.09
36.00	6.06	6.06	6.08

Well 2, R = 2.8m	Expt 1	2008	
Date:	07-Aug	08-Aug	10-Aug
Beginning Time	21:25	18:40	16:55
End Time	22:24	19:32	17:45
Effective Time	21:54	19:06	17:20
Depth [m]	T [°C]	T [°C]	T [°C]
37.00	6.05	6.05	6.07
38.00	6.04	6.04	6.06
39.00	6.02	6.03	6.05
40.00	6.02	6.03	6.04
41.00	6.02	6.02	6.04
42.00	6.02	6.02	6.03
43.00	6.01	6.01	6.03
44.00	6.00	6.01	6.02
45.00	6.00	6.00	6.02
46.00	5.99	5.99	6.00
47.00	5.98	5.98	6.00
48.00	5.98	5.99	6.00
49.00	5.97	5.98	6.00
50.00	5.97	5.98	5.99
51.00	5.97	5.97	5.98
52.00	5.96	5.97	5.98
53.00	5.96	5.97	5.99
54.00	5.96	5.96	5.97
55.00	5.96	5.96	5.97

Well 2, R = 2.8m Expt 1 2008

Date:	07-Aug	08-Aug	10-Aug
Beginning Time	21:25	18:40	16:55
End Time	22:24	19:32	17:45
Effective Time	21:54	19:06	17:20
Depth [m]	T [°C]	T [°C]	T [°C]
56.00	5.96	5.96	5.98
57.00	5.96	5.96	5.98
58.00	5.97	5.97	5.98
59.00	5.97	5.97	5.98
60.00	5.98	5.98	5.98
61.00	5.98	5.98	5.99
62.00	5.98	5.98	5.99

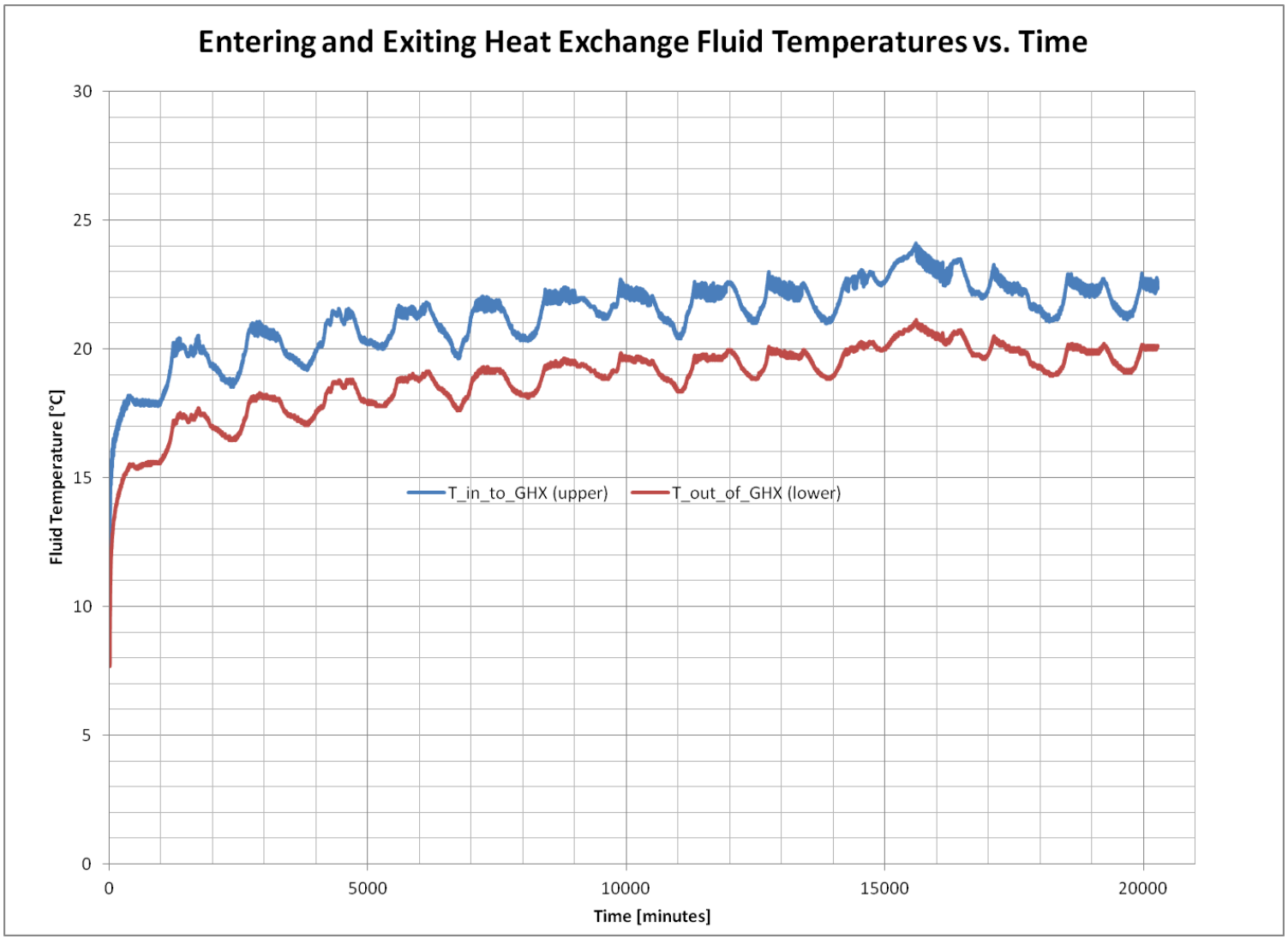

Figure 85 Measurements from the 3-Wire RTD adjacent to the HPU – July 2008 Experiment.

Table 18 Nearer Well Temperature Data, Experiment 2

Well 1, R = 1.4m Expt 2 2008

Date:	07-Sep	08-Sep	09-Sep	10-Sep	11-Sep	12-Sep	14-Sep	15-Sep	16-Sep	17-Sep	18-Sep
Beginning Time	11:40	12:25	17:50	17:22	18:00	16:12	17:23	19:00	17:10	17:15	17:03
End Time	12:55	13:01	18:28	18:00	18:40	16:52	18:01	19:35	17:58	18:25	18:15
Effective Time	12:17	12:43	18:09	17:41	18:20	16:32	17:42	19:17	17:34	17:50	17:39
Depth [m]	T [°C]	T [°C]	T [°C]	T [°C]	T [°C]	T [°C]	T [°C]	T [°C]	T [°C]	T [°C]	T [°C]
0.00	14.52	14.04	21.34	21.95	22.69	28.90	22.56	25.97	23.25	18.50	27.87
0.33	14.41	13.92	14.78	15.01	15.65	16.70	15.89	17.01	16.01	15.15	16.48
0.67	14.91	14.38	14.73	14.74	14.91	14.98	15.12	15.00	15.02	14.96	14.82
1.00	14.85	14.35	14.82	14.81	14.82	14.77	14.77	14.75	14.74	14.71	14.60
1.33	14.85	14.37	14.51	14.50	14.47	14.51	14.34	14.42	14.29	14.30	14.24
1.67	13.95	13.84	13.58	13.67	13.61	13.71	13.71	13.78	13.47	13.56	13.51
2.00	12.54	13.78	12.36	12.43	12.36	12.59	12.58	12.76	12.41	12.57	12.51
2.33	11.46	12.54	11.25	11.31	11.28	11.59	11.61	11.79	11.52	11.70	11.70
2.67	10.18	11.34	9.98	10.10	10.02	10.20	10.46	10.69	10.36	10.54	10.51
3.00	9.06	9.04	8.99	9.06	9.02	9.24	9.40	9.52	9.42	9.60	9.60
3.33	8.17	8.27	8.17	8.27	8.31	8.52	8.51	8.68	8.56	8.77	8.88
3.67	7.62	7.72	7.61	7.69	7.69	7.88	8.00	8.07	7.96	8.13	8.22
4.00	7.18	7.25	7.18	7.24	7.24	7.41	7.47	7.58	7.49	7.66	7.98
4.33	6.89	6.97	6.90	6.94	7.00	7.14	7.12	7.00	7.22	7.35	7.34
4.67	6.73	6.77	6.73	6.82	6.82	6.88	6.96	6.85	6.97	7.08	7.15
5.00	6.66	6.67	6.66	6.70	6.70	6.77	6.80	6.77	6.86	6.92	7.01
5.33	6.62	6.63	6.63	6.65	6.66	6.72	6.72	6.74	6.80	6.83	6.91
5.67	6.62	6.63	6.63	6.64	6.65	6.67	6.69	6.73	6.77	6.80	6.86

Well 1, R = 1.4m Expt 2 2008

Date:	07-Sep	08-Sep	09-Sep	10-Sep	11-Sep	12-Sep	14-Sep	15-Sep	16-Sep	17-Sep	18-Sep
Beginning Time	11:40	12:25	17:50	17:22	18:00	16:12	17:23	19:00	17:10	17:15	17:03
End Time	12:55	13:01	18:28	18:00	18:40	16:52	18:01	19:35	17:58	18:25	18:15
Effective Time	12:17	12:43	18:09	17:41	18:20	16:32	17:42	19:17	17:34	17:50	17:39

Depth [m]	T [°C]	T [°C]	T [°C]	T [°C]	T [°C]	T [°C]	T [°C]	T [°C]	T [°C]	T [°C]	T [°C]
6.00	6.65	6.65	6.66	6.65	6.66	6.67	6.70	6.74	6.77	6.80	6.86
6.33	6.69	6.68	6.69	6.68	6.70	6.70	6.72	6.77	6.78	6.81	6.85
6.67	6.73	6.72	6.72	6.72	6.72	6.72	6.75	6.79	6.81	6.84	6.87
7.00	6.76	6.74	6.75	6.74	6.75	6.75	6.77	6.82	6.83	6.85	6.89
7.33	6.79	6.78	6.79	6.76	6.78	6.78	6.80	6.85	6.85	6.89	6.92
7.67	6.82	6.81	6.81	6.79	6.80	6.81	6.83	6.86	6.87	6.91	6.94
8.00	6.84	6.84	6.84	6.82	6.83	6.83	6.85	6.89	6.90	6.94	6.97
8.33	6.85	6.85	6.84	6.84	6.84	6.84	6.88	6.92	6.82	6.96	6.99
8.67	6.86	6.87	6.86	6.86	6.86	6.86	6.90	6.93	6.93	6.97	7.00
9.00	6.87	6.87	6.86	6.86	6.86	6.86	6.91	6.93	6.95	6.98	7.01
9.33	6.87	6.87	6.86	6.85	6.86	6.86	6.91	6.94	6.96	6.99	7.02
9.67	6.86	6.86	6.85	6.85	6.86	6.86	6.91	6.94	6.95	6.99	7.02
10.00	6.86	6.86	6.85	6.85	6.85	6.85	6.90	6.93	6.94	6.98	7.02
11.00	6.83	6.82	6.81	6.81	6.81	6.82	6.86	6.90	6.94	6.96	7.01
12.00	6.79	6.79	6.77	6.77	6.78	6.79	6.84	6.87	6.92	6.96	7.00
13.00	6.75	6.74	6.74	6.73	6.74	6.74	6.80	6.86	6.89	6.94	6.99
14.00	6.72	6.70	6.68	6.68	6.70	6.72	6.77	6.84	6.86	6.91	6.97
15.00	6.62	6.61	6.60	6.59	6.61	6.65	6.72	6.79	6.86	6.92	7.02
16.00	6.53	6.53	6.54	6.57	6.63	6.68	6.89	6.93	7.07	7.17	7.17

Well 1, R = 1.4m Expt 2 2008

Date:	07-Sep	08-Sep	09-Sep	10-Sep	11-Sep	12-Sep	14-Sep	15-Sep	16-Sep	17-Sep	18-Sep
Beginning Time	11:40	12:25	17:50	17:22	18:00	16:12	17:23	19:00	17:10	17:15	17:03
End Time	12:55	13:01	18:28	18:00	18:40	16:52	18:01	19:35	17:58	18:25	18:15
Effective Time	12:17	12:43	18:09	17:41	18:20	16:32	17:42	19:17	17:34	17:50	17:39
17.00	6.50	6.49	6.53	6.62	6.72	6.82	7.05	7.16	7.27	7.36	7.41
18.00	6.48	6.48	6.55	6.67	6.82	6.95	7.29	7.40	7.46	7.55	7.69
19.00	6.47	6.47	6.51	6.63	6.75	6.91	7.17	7.32	7.39	7.47	7.55
20.00	6.45	6.44	6.46	6.53	6.62	6.74	6.93	7.10	7.22	7.23	7.36
21.00	6.43	6.42	6.44	6.50	6.57	6.68	6.84	6.96	7.03	7.09	7.18
22.00	6.40	6.39	6.43	6.48	6.55	6.64	6.80	6.87	6.91	7.00	7.07
23.00	6.36	6.36	6.40	6.45	6.52	6.60	6.76	6.82	6.86	6.94	6.99
24.00	6.34	6.33	6.37	6.43	6.49	6.56	6.75	6.81	6.84	6.91	6.96
25.00	6.32	6.32	6.33	6.38	6.45	6.51	6.67	6.75	6.81	6.84	6.89
26.00	6.29	6.29	6.30	6.35	6.40	6.45	6.57	6.64	6.71	6.75	6.81
27.00	6.26	6.26	6.26	6.29	6.33	6.39	6.50	6.56	6.62	6.67	6.72
28.00	6.23	6.22	6.23	6.26	6.31	6.36	6.49	6.55	6.62	6.69	6.75
29.00	6.22	6.21	6.21	6.23	6.28	6.34	6.47	6.54	6.59	6.65	6.71
30.00	6.22	6.22	6.21	6.23	6.26	6.31	6.44	6.50	6.53	6.61	6.66
31.00	6.24	6.24	6.23	6.24	6.26	6.29	6.38	6.44	6.46	6.50	6.54
32.00	6.27	6.26	6.26	6.26	6.27	6.28	6.35	6.40	6.41	6.43	6.48
33.00	6.28	6.28	6.27	6.27	6.27	6.28	6.33	6.35	6.38	6.41	6.44
34.00	6.29	6.28	6.28	6.27	6.28	6.28	6.31	6.32	6.34	6.37	6.40
35.00	6.28	6.26	6.27	6.26	6.28	6.27	6.30	6.31	6.35	6.36	6.39
36.00	6.27	6.26	6.26	6.26	6.27	6.28	6.31	6.33	6.34	6.39	6.41

Well 1, R = 1.4m Expt 2 2008

Date:	07-Sep	08-Sep	09-Sep	10-Sep	11-Sep	12-Sep	14-Sep	15-Sep	16-Sep	17-Sep	18-Sep
Beginning Time	11:40	12:25	17:50	17:22	18:00	16:12	17:23	19:00	17:10	17:15	17:03
End Time	12:55	13:01	18:28	18:00	18:40	16:52	18:01	19:35	17:58	18:25	18:15
Effective Time	12:17	12:43	18:09	17:41	18:20	16:32	17:42	19:17	17:34	17:50	17:39
37.00	6.26	6.26	6.25	6.25	6.25	6.27	6.29	6.31	6.34	6.37	6.40
38.00	6.25	6.25	6.24	6.24	6.24	6.25	6.27	6.30	6.31	6.33	6.35
39.00	6.24	6.23	6.23	6.23	6.23	6.23	6.25	6.26	6.28	6.30	6.32
40.00	6.22	6.22	6.21	6.21	6.21	6.21	6.24	6.26	6.27	6.28	6.31
41.00	6.21	6.21	6.20	6.20	6.20	6.20	6.21	6.24	6.25	6.27	6.30
42.00	6.20	6.20	6.19	6.19	6.19	6.19	6.20	6.22	6.24	6.26	6.28
43.00	6.20	6.19	6.19	6.19	6.18	6.19	6.20	6.22	6.23	6.25	6.25
44.00	6.20	6.19	6.18	6.18	6.18	6.19	6.20	6.20	6.22	6.23	6.25
45.00	6.19	6.19	6.18	6.18	6.18	6.18	6.20	6.20	6.21	6.23	6.23
46.00	6.19	6.19	6.18	6.18	6.18	6.18	6.19	6.20	6.20	6.21	6.22
47.00	6.17	6.18	6.17	6.18	6.18	6.17	6.18	6.18	6.20	6.20	6.21
48.00	6.17	6.17	6.17	6.17	6.17	6.17	6.18	6.18	6.19	6.20	6.20
49.00	6.16	6.17	6.16	6.16	6.16	6.16	6.17	6.18	6.18	6.19	6.20
50.00	6.16	6.16	6.16	6.16	6.15	6.15	6.16	6.17	6.17	6.18	6.18
51.00	6.15	6.15	6.15	6.15	6.15	6.15	6.15	6.16	6.16	6.16	6.16
52.00	6.15	6.15	6.15	6.14	6.14	6.14	6.13	6.15	6.15	6.16	6.15
53.00	6.14	6.13	6.13	6.13	6.13	6.13	6.13	6.14	6.14	6.15	6.15
54.00	6.13	6.13	6.13	6.13	6.13	6.13	6.13	6.13	6.14	6.14	6.14
55.00	6.12	6.12	6.12	6.12	6.12	6.12	6.12	6.12	6.13	6.13	6.13
56.00	6.12	6.12	6.12	6.12	6.12	6.12	6.12	6.12	6.12	6.12	6.13

Well 1, R = 1.4m Expt 2 2008

Date:	07-Sep	08-Sep	09-Sep	10-Sep	11-Sep	12-Sep	14-Sep	15-Sep	16-Sep	17-Sep	18-Sep
Beginning Time	11:40	12:25	17:50	17:22	18:00	16:12	17:23	19:00	17:10	17:15	17:03
End Time	12:55	13:01	18:28	18:00	18:40	16:52	18:01	19:35	17:58	18:25	18:15
Effective Time	12:17	12:43	18:09	17:41	18:20	16:32	17:42	19:17	17:34	17:50	17:39
57.00	6.11	6.11	6.11	6.11	6.11	6.11	6.11	6.11	6.11	6.11	6.13
58.00	6.10	6.10	6.10	6.10	6.10	6.10	6.10	6.10	6.11	6.10	6.11
59.00	6.09	6.09	6.09	6.09	6.09	6.09	6.09	6.09	6.10	6.10	6.10
60.00	6.08	6.08	6.08	6.08	6.08	6.08	6.08	6.08	6.08	6.08	6.09
61.00	6.07	6.07	6.06	6.07	6.07	6.07	6.07	6.07	6.08	6.07	6.08

Well 1, R = 1.4m	Expt 2	2008	
Date:	19-Sep	21-Sep	24-Sep
Beginning Time	17:32	20:36	19:05
End Time	17:46	21:28	20:06
Effective Time	17:39	21:02	19:35
Depth [m]	T [°C]	T [°C]	T [°C]
0.00	X	22.02	21.09
0.33	X	17.08	16.18
0.67	X	14.92	15.28
1.00	X	14.63	14.81
1.33	X	14.15	14.25
1.67	X	13.47	13.51
2.00	X	12.55	12.57
2.33	X	11.60	11.76
2.67	X	10.59	10.83
3.00	X	9.74	9.86
3.33	X	8.91	9.09
3.67	X	8.31	8.53
4.00	X	7.85	8.04
4.33	X	7.49	7.64
4.67	X	7.20	7.37
5.00	7.00	7.11	7.20
5.33	6.92	6.99	7.12
5.67	6.88	6.94	7.06
6.00	6.88	6.94	7.04

Well 1, R = 1.4m	Expt 2	2008	
Date:	19-Sep	21-Sep	24-Sep
Beginning Time	17:32	20:36	19:05
End Time	17:46	21:28	20:06
Effective Time	17:39	21:02	19:35
Depth [m]	T [°C]	T [°C]	T [°C]
6.33	6.89	6.95	7.04
6.67	6.89	6.96	7.05
7.00	6.92	6.97	7.05
7.33	6.94	6.99	7.06
7.67	6.96	7.02	7.11
8.00	7.00	7.05	7.13
8.33	7.01	7.07	7.16
8.67	7.03	7.10	7.20
9.00	7.04	7.13	7.23
9.33	7.05	7.14	7.25
9.67	7.06	7.14	7.25
10.00	7.05	7.14	7.26
11.00	7.04	7.15	7.27
12.00	7.05	7.16	7.29
13.00	7.04	7.14	7.29
14.00	7.02	7.13	7.28
15.00	7.02	7.11	7.26
16.00	7.27	7.43	7.43
17.00	7.52	7.65	7.87

Well 1, R = 1.4m	Expt 2	2008	
Date:	19-Sep	21-Sep	24-Sep
Beginning Time	17:32	20:36	19:05
End Time	17:46	21:28	20:06
Effective Time	17:39	21:02	19:35
Depth [m]	T [°C]	T [°C]	T [°C]
18.00	7.78	7.91	8.12
19.00	7.65	7.75	8.06
20.00	7.43	7.57	7.73
21.00	7.27	7.38	7.52
22.00	7.12	7.21	7.34
23.00	7.02	7.12	7.26
24.00	7.00	7.12	7.24
25.00	6.95	7.05	7.21
26.00	6.80	6.94	7.08
27.00	6.78	6.89	7.02
28.00	6.79	6.89	7.02
29.00	6.76	6.87	6.98
30.00	6.71	6.78	6.92
31.00	6.59	6.66	6.90
32.00	6.51	6.58	6.78
33.00	6.48	6.55	6.70
34.00	6.42	6.51	6.64
35.00	6.41	6.47	6.58
36.00	6.45	6.50	6.55

Well 1, R = 1.4m	Expt 2	2008	
Date:	19-Sep	21-Sep	24-Sep
Beginning Time	17:32	20:36	19:05
End Time	17:46	21:28	20:06
Effective Time	17:39	21:02	19:35
Depth [m]	T [°C]	T [°C]	T [°C]
37.00	6.42	6.46	6.55
38.00	6.39	6.43	6.51
39.00	6.33	6.39	6.47
40.00	6.32	6.37	6.45
41.00	6.32	6.36	6.43
42.00	6.29	6.34	6.40
43.00	6.27	6.32	6.37
44.00	6.26	6.31	6.36
45.00	6.25	6.30	6.35
46.00	6.25	6.27	6.33
47.00	6.23	6.26	6.31
48.00	6.22	6.25	6.30
49.00	6.21	6.23	6.28
50.00	6.20	6.22	6.26
51.00	6.18	6.20	6.24
52.00	6.16	6.19	6.22
53.00	6.16	6.17	6.20
54.00	6.14	6.16	6.18
55.00	6.13	6.15	6.17

Well 1, R = 1.4m Expt 2 2008

Date:	19-Sep	21-Sep	24-Sep
Beginning Time	17:32	20:36	19:05
End Time	17:46	21:28	20:06
Effective Time	17:39	21:02	19:35

Depth [m]	T [°C]	T [°C]	T [°C]
56.00	6.13	6.14	6.15
57.00	6.12	6.13	6.15
58.00	6.10	6.12	6.14
59.00	6.10	6.11	6.13
60.00	6.09	6.09	6.11
61.00	6.08	6.08	6.09

Table 19 Farther Well Temperature Data, Experiment 2

Well 2, R = 2.8m Expt 2 2008

Date:	07-Sep	08-Sep	09-Sep	10-Sep	11-Sep	12-Sep	14-Sep	15-Sep	16-Sep	17-Sep	18-Sep
Beginning Time	11:40	12:25	17:50	17:22	18:00	16:12	17:23	19:00	17:10	17:15	17:03
End Time	12:55	13:01	18:28	18:00	18:40	16:52	18:01	19:35	17:58	18:25	18:15
Effective Time	12:17	12:43	18:09	17:41	18:20	16:32	17:42	19:17	17:34	17:50	17:39
Depth [m]	T [°C]	T [°C]	T [°C]	T [°C]	T [°C]	T [°C]	T [°C]	T [°C]	T [°C]	T [°C]	T [°C]
0.00	15.29	14.46	19.80	19.65	19.98	25.89	19.14	22.93	22.14	17.48	25.57
0.33	15.28	14.61	15.20	15.03	15.66	16.50	15.75	17.34	16.70	16.05	17.00
0.67	15.50	14.98	15.00	14.98	15.02	15.12	15.14	15.28	15.22	15.35	15.08
1.00	15.53	15.05	15.08	14.99	14.86	14.81	14.68	14.87	14.72	14.87	14.71
1.33	15.02	14.71	14.80	14.50	14.34	14.41	14.10	14.36	14.18	14.27	14.18
1.67	13.79	13.63	13.90	13.48	13.23	13.62	13.27	13.67	13.35	13.53	13.46
2.00	12.27	12.21	12.88	12.23	12.11	12.50	12.10	12.65	12.35	12.59	12.34
2.33	12.27	10.95	11.42	10.94	10.98	11.39	10.98	11.56	11.14	11.48	11.24
2.67	11.05	9.77	10.28	9.60	9.53	9.94	9.71	10.35	9.97	10.24	10.17
3.00	9.63	8.68	9.07	8.66	8.62	8.93	8.70	9.16	9.04	9.23	9.21
3.33	8.71	8.04	8.14	7.87	7.90	8.20	7.95	8.26	8.26	8.44	8.45
3.67	7.27	7.30	7.56	7.33	7.32	7.53	7.43	7.66	7.63	7.76	7.77
4.00	6.85	6.99	7.09	6.94	6.96	7.12	6.99	7.20	7.17	7.33	7.32
4.33	6.60	6.67	6.77	6.65	6.68	6.78	6.77	6.89	6.86	6.93	6.96
4.67	6.45	6.52	6.54	6.53	6.55	6.65	6.58	6.68	6.67	6.69	6.74
5.00	6.38	6.43	6.45	6.45	6.46	6.53	6.51	6.58	6.54	6.58	6.49
5.33	6.37	6.43	6.41	6.42	6.43	6.49	6.46	6.52	6.49	6.51	6.55
5.67	6.39	6.40	6.40	6.43	6.45	6.48	6.46	6.48	6.48	6.49	6.54

Well 2, R = 2.8m Expt 2 2008

Date:	07-Sep	08-Sep	09-Sep	10-Sep	11-Sep	12-Sep	14-Sep	15-Sep	16-Sep	17-Sep	18-Sep
Beginning Time	11:40	12:25	17:50	17:22	18:00	16:12	17:23	19:00	17:10	17:15	17:03
End Time	12:55	13:01	18:28	18:00	18:40	16:52	18:01	19:35	17:58	18:25	18:15
Effective Time	12:17	12:43	18:09	17:41	18:20	16:32	17:42	19:17	17:34	17:50	17:39
Depth [m]	T [°C]	T [°C]	T [°C]	T [°C]	T [°C]	T [°C]	T [°C]	T [°C]	T [°C]	T [°C]	T [°C]
6.00	6.44	6.43	6.41	6.45	6.46	6.48	6.47	6.48	6.50	6.49	6.52
6.33	6.47	6.47	6.46	6.48	6.49	6.50	6.50	6.50	6.50	6.50	6.53
6.67	6.51	6.51	6.50	6.52	6.52	6.52	6.53	6.52	6.53	6.53	6.55
7.00	6.55	6.56	6.53	6.55	6.53	6.55	6.56	6.53	6.56	6.57	6.57
7.33	6.58	6.56	6.58	6.58	6.59	6.58	6.59	6.58	6.58	6.59	6.59
7.67	6.61	6.58	6.60	6.61	6.61	6.61	6.61	6.60	6.60	6.61	6.61
8.00	6.62	6.63	6.62	6.62	6.62	6.62	6.63	6.62	6.62	6.62	6.62
8.33	6.63	6.63	6.63	6.63	6.63	6.63	6.64	6.63	6.63	6.63	6.62
8.67	6.63	6.64	6.64	6.63	6.63	6.63	6.64	6.64	6.64	6.64	6.63
9.00	6.63	6.63	6.63	6.63	6.63	6.63	6.63	6.63	6.64	6.63	6.64
9.33	6.62	6.63	6.62	6.62	6.62	6.63	6.62	6.63	6.63	6.63	6.63
9.67	6.60	6.62	6.61	6.60	6.60	6.60	6.61	6.62	6.61	6.62	6.62
10.00	6.59	6.59	6.60	6.59	6.59	6.58	6.59	6.60	6.59	6.60	6.61
11.00	6.52	6.51	6.53	6.52	6.53	6.53	6.52	6.54	6.55	6.55	6.55
12.00	6.44	6.45	6.46	6.45	6.46	6.46	6.45	6.48	6.47	6.47	6.48
13.00	6.38	6.39	6.39	6.40	6.40	6.41	6.40	6.42	6.40	6.42	6.42
14.00	6.36	6.36	6.37	6.37	6.37	6.36	6.38	6.38	6.38	6.38	6.40
15.00	6.36	6.36	6.36	6.35	6.35	6.34	6.36	6.36	6.36	6.37	6.38
16.00	6.35	6.35	6.34	6.34	6.34	6.34	6.35	6.36	6.38	6.39	6.39

Well 2, R = 2.8m Expt 2 2008

Date:	07-Sep	08-Sep	09-Sep	10-Sep	11-Sep	12-Sep	14-Sep	15-Sep	16-Sep	17-Sep	18-Sep
Beginning Time	11:40	12:25	17:50	17:22	18:00	16:12	17:23	19:00	17:10	17:15	17:03
End Time	12:55	13:01	18:28	18:00	18:40	16:52	18:01	19:35	17:58	18:25	18:15
Effective Time	12:17	12:43	18:09	17:41	18:20	16:32	17:42	19:17	17:34	17:50	17:39
17.00	6.35	6.35	6.34	6.34	6.34	6.34	6.37	6.38	6.41	6.43	6.44
18.00	6.34	6.34	6.34	6.34	6.33	6.34	6.37	6.40	6.41	6.44	6.46
19.00	6.33	6.33	6.33	6.33	6.32	6.33	6.36	6.38	6.39	6.42	6.45
20.00	6.33	6.32	6.33	6.32	6.32	6.32	6.34	6.37	6.37	6.41	6.45
21.00	6.30	6.30	6.30	6.30	6.30	6.31	6.32	6.34	6.34	6.36	6.40
22.00	6.29	6.29	6.29	6.28	6.29	6.30	6.31	6.33	6.34	6.36	6.39
23.00	6.28	6.28	6.28	6.27	6.27	6.28	6.29	6.31	6.32	6.34	6.37
24.00	6.26	6.26	6.25	6.26	6.25	6.26	6.27	6.29	6.30	6.31	6.33
25.00	6.25	6.25	6.25	6.24	6.25	6.24	6.26	6.27	6.29	6.30	6.32
26.00	6.25	6.24	6.24	6.23	6.23	6.24	6.27	6.26	6.27	6.28	6.30
27.00	6.23	6.23	6.23	6.22	6.22	6.22	6.23	6.24	6.25	6.27	6.28
28.00	6.23	6.21	6.22	6.22	6.21	6.22	6.24	6.25	6.27	6.29	6.31
29.00	6.22	6.21	6.21	6.21	6.21	6.22	6.23	6.25	6.26	6.29	6.31
30.00	6.21	6.21	6.21	6.20	6.20	6.21	6.21	6.22	6.23	6.25	6.27
31.00	6.21	6.20	6.20	6.20	6.20	6.20	6.21	6.21	6.21	6.23	6.24
32.00	6.21	6.19	6.21	6.20	6.20	6.20	6.20	6.20	6.20	6.21	6.22
33.00	6.20	6.18	6.20	6.20	6.19	6.19	6.19	6.19	6.19	6.20	6.20
34.00	6.18	6.16	6.18	6.17	6.18	6.18	6.18	6.18	6.18	6.18	6.18
35.00	6.15	6.13	6.16	6.15	6.15	6.16	6.15	6.16	6.16	6.16	6.16
36.00	6.14	6.12	6.14	6.13	6.14	6.14	6.14	6.14	6.15	6.15	6.15

Well 2, R = 2.8m Expt 2 2008

Date:	07-Sep	08-Sep	09-Sep	10-Sep	11-Sep	12-Sep	14-Sep	15-Sep	16-Sep	17-Sep	18-Sep
Beginning Time	11:40	12:25	17:50	17:22	18:00	16:12	17:23	19:00	17:10	17:15	17:03
End Time	12:55	13:01	18:28	18:00	18:40	16:52	18:01	19:35	17:58	18:25	18:15
Effective Time	12:17	12:43	18:09	17:41	18:20	16:32	17:42	19:17	17:34	17:50	17:39
37.00	6.13	6.11	6.13	6.13	6.13	6.13	6.14	6.13	6.13	6.14	6.14
38.00	6.12	6.12	6.12	6.11	6.12	6.12	6.13	6.13	6.13	6.13	6.13
39.00	6.11	6.11	6.11	6.11	6.11	6.11	6.12	6.12	6.12	6.12	6.12
40.00	6.10	6.10	6.11	6.10	6.11	6.10	6.11	6.11	6.11	6.11	6.11
41.00	6.10	6.10	6.10	6.10	6.09	6.10	6.10	6.10	6.10	6.11	6.11
42.00	6.09	6.09	6.09	6.09	6.09	6.09	6.10	6.10	6.10	6.10	6.11
43.00	6.09	6.09	6.09	6.09	6.09	6.09	6.10	6.09	6.10	6.10	6.10
44.00	6.09	6.09	6.09	6.09	6.09	6.08	6.09	6.09	6.09	6.10	6.10
45.00	6.08	6.08	6.08	6.08	6.08	6.08	6.09	6.09	6.09	6.09	6.09
46.00	6.08	6.07	6.08	6.08	6.08	6.08	6.09	6.08	6.08	6.09	6.08
47.00	6.07	6.07	6.07	6.07	6.07	6.07	6.08	6.08	6.08	6.09	6.08
48.00	6.07	6.07	6.07	6.07	6.07	6.07	6.08	6.08	6.08	6.08	6.08
49.00	6.07	6.07	6.07	6.07	6.07	6.07	6.08	6.08	6.08	6.08	6.08
50.00	6.07	6.07	6.06	6.07	6.07	6.07	6.07	6.07	6.08	6.08	6.08
51.00	6.07	6.06	6.06	6.07	6.06	6.07	6.07	6.07	6.07	6.07	6.07
52.00	6.07	6.06	6.06	6.06	6.06	6.07	6.07	6.06	6.07	6.07	6.07
53.00	6.06	6.05	6.06	6.06	6.06	6.06	6.07	6.06	6.06	6.07	6.06
54.00	6.05	6.05	6.05	6.05	6.06	6.05	6.06	6.06	6.06	6.06	6.06
55.00	6.05	6.05	6.05	6.05	6.05	6.05	6.06	6.06	6.06	6.06	6.06
56.00	6.04	6.05	6.05	6.05	6.05	6.05	6.06	6.06	6.06	6.05	6.06

Well 2, R = 2.8m Expt 2 2008

Date:	07-Sep	08-Sep	09-Sep	10-Sep	11-Sep	12-Sep	14-Sep	15-Sep	16-Sep	17-Sep	18-Sep
Beginning Time	11:40	12:25	17:50	17:22	18:00	16:12	17:23	19:00	17:10	17:15	17:03
End Time	12:55	13:01	18:28	18:00	18:40	16:52	18:01	19:35	17:58	18:25	18:15
Effective Time	12:17	12:43	18:09	17:41	18:20	16:32	17:42	19:17	17:34	17:50	17:39
57.00	6.04	6.04	6.04	6.05	6.05	6.05	6.05	6.05	6.05	6.05	6.06
58.00	6.04	6.04	6.04	6.05	6.04	6.05	6.05	6.05	6.05	6.05	6.05
59.00	6.03	6.04	6.04	6.04	6.04	6.04	6.04	6.04	6.04	6.05	6.04
60.00	6.03	6.03	6.03	6.03	6.04	6.04	6.04	6.04	6.04	6.04	6.04
61.00	6.02	6.03	6.03	6.03	6.03	6.03	6.03	6.03	6.04	6.04	6.04
62.00	6.03	6.02	6.03	6.03	6.03	6.03	6.03	6.03	6.03	6.03	6.04

Well 2, R = 2.8m	Expt 2	2008	
Date:	19-Sep	21-Sep	24-Sep
Beginning Time	17:32	20:36	19:05
End Time	17:46	21:28	20:06
Effective Time	17:39	21:02	19:35
Depth [m]	T [°C]	T [°C]	T [°C]
0.00	X	19.66	17.04
0.33	X	16.99	15.31
0.67	X	15.07	15.28
1.00	X	14.60	14.63
1.33	X	14.03	14.02
1.67	X	13.34	13.37
2.00	X	12.41	12.46
2.33	X	11.21	11.46
2.67	X	10.27	10.36
3.00	X	9.27	9.41
3.33	X	8.47	8.62
3.67	X	7.79	7.98
4.00	X	7.30	7.43
4.33	X	6.98	7.07
4.67	X	6.74	6.81
5.00	6.60	6.62	6.67
5.33	6.56	6.53	6.59
5.67	6.52	6.51	6.54
6.00	6.51	6.50	6.53

Well 1, R = 1.4m	Expt 2	2008	
Date:	19-Sep	21-Sep	24-Sep
Beginning Time	17:32	20:36	19:05
End Time	17:46	21:28	20:06
Effective Time	17:39	21:02	19:35
Depth [m]	T [°C]	T [°C]	T [°C]
6.33	6.53	6.52	6.52
6.67	6.55	6.54	6.54
7.00	6.55	6.57	6.58
7.33	6.61	6.59	6.59
7.67	6.63	6.61	6.61
8.00	6.64	6.62	6.63
8.33	6.64	6.64	6.64
8.67	6.64	6.64	6.65
9.00	6.64	6.64	6.65
9.33	6.63	6.63	6.64
9.67	6.62	6.62	6.63
10.00	6.60	6.61	6.62
11.00	6.54	6.54	6.56
12.00	6.48	6.48	6.50
13.00	6.42	6.42	6.43
14.00	6.39	6.39	6.40
15.00	6.38	6.39	6.42
16.00	6.42	6.45	6.53
17.00	6.48	6.53	6.63

Well 2, R = 2.8m	Expt 2	2008	
Date:	19-Sep	21-Sep	24-Sep
Beginning Time	17:32	20:36	19:05
End Time	17:46	21:28	20:06
Effective Time	17:39	21:02	19:35
Depth [m]	T [°C]	T [°C]	T [°C]
18.00	6.48	6.56	6.65
19.00	6.46	6.53	6.61
20.00	6.45	6.53	6.60
21.00	6.39	6.46	6.53
22.00	6.39	6.44	6.50
23.00	6.37	6.43	6.48
24.00	6.34	6.38	6.44
25.00	6.34	6.38	6.44
26.00	6.32	6.36	6.42
27.00	6.31	6.34	6.41
28.00	6.34	6.39	6.46
29.00	6.34	6.39	6.49
30.00	6.32	6.33	6.41
31.00	6.24	6.28	6.33
32.00	6.23	6.28	6.28
33.00	6.20	6.24	6.24
34.00	6.19	6.21	6.23
35.00	6.17	6.20	6.19
36.00	6.15	6.17	6.18

Well 1, R = 1.4m	Expt 2	2008	
Date:	19-Sep	21-Sep	24-Sep
Beginning Time	17:32	20:36	19:05
End Time	17:46	21:28	20:06
Effective Time	17:39	21:02	19:35
Depth [m]	T [°C]	T [°C]	T [°C]
37.00	6.14	6.16	6.18
38.00	6.13	6.14	6.16
39.00	6.13	6.13	6.15
40.00	6.12	6.12	6.15
41.00	6.11	6.12	6.14
42.00	6.11	6.11	6.13
43.00	6.11	6.11	6.13
44.00	6.10	6.11	6.13
45.00	6.09	6.10	6.11
46.00	6.09	6.09	6.11
47.00	6.08	6.09	6.10
48.00	6.08	6.09	6.10
49.00	6.08	6.09	6.10
50.00	6.07	6.08	6.10
51.00	6.07	6.08	6.09
52.00	6.07	6.07	6.09
53.00	6.07	6.07	6.08
54.00	6.07	6.07	6.07
55.00	6.06	6.06	6.07

Well 2, R = 2.8m	Expt 2	2008	
Date:	19-Sep	21-Sep	24-Sep
Beginning Time	17:32	20:36	19:05
End Time	17:46	21:28	20:06
Effective Time	17:39	21:02	19:35
Depth [m]	T [°C]	T [°C]	T [°C]
56.00	6.06	6.06	6.07
57.00	6.05	6.06	6.06
58.00	6.05	6.05	6.06
59.00	6.04	6.05	6.06
60.00	6.04	6.04	6.05
61.00	6.03	6.04	6.04
62.00	6.03	6.04	6.04

Heat Pump Shutdown Times

Heat pump shutdown occurred at 16:04 on July 27th for the first experiment and at 17:03 on September 18th for the second experiment.

The second experiment does not include a natural ground temperature recovery portion.

References

Abramowitz, M., & Stegunx, I. A. (1972). *Handbook of Mathematical Functions with Formulas, Graphs, and Mathematical Tables.* U.S. Department of Commerce.

Anderson, M. P., & Woessner, W. W. (1992). *Applied Groundwater Modeling.* San Diego: Academic Press.

ASHRAE. (2007). APPLICATIONS Handbook. Atlanta, Georgia: American Society of Heating, Refrigerating and Air-Conditioning Engineers.

Austin, W. A. (1998). *DEVELOPMENT OF AN IN SITU SYSTEM FOR MEASURING GROUND THERMAL PROPERTIES.* M.Sc. Thesis, Oklahoma State University.

Bennet, J., Claesson, J., & Hellström, G. (1987). *Multipole Method to Compute the Conductive Heat Flow to and between Pipes in A Composite Cylinder.* Report, University of Lund, Sweden, Department of Building and Mathematical Physics.

Bernier, M. A. (2001). Ground-Coupled Heat Pump System Simulation. *ASHRAE Transactions:Symposia , 107*, 605-616.

Bettess, P. (1992). *Infinite Elements.* Sunderland U.K.: Penshaw Press.

Carslaw, H. S. (1921). *Introduction to the Mathematical Theory of the Conduction of Heat in Solids* (2 ed.).

Carslaw, H. S., & Jaeger, J. C. (1959). *Conduction of Heat in Solids* (2 ed.). Oxford: Clarendon Press.

Çengel, Y. A., & Boles, M. A. (2002). *Thermodynamics: An Engineering Approach* (4 ed.). McGraw-Hill.

Chemical Engineering Research Information Center. (2011). Retrieved from http://www.cheric.org/research/kdb/hcprop/showprop.php?cmpid=817

Claesson, J., & Eskilson, P. (1988). Conductive heat Extraction to a Deep Borehole: Thermal analysis and Dimensioning Rules. *Energy , 13* (6), 509-527.

Deerman, J. D., & Kavanaugh, S. (1991). Simulation of Vertical U-Tube Ground-Coupled Heat Pump Systems Using the Cylindrical Heat Source Solution. *ASHRAE Transactions , 97* (1), 287-295.

Diao, N. R., Zeng, H. Y., & Fang, Z. H. (2004). Improvement in Modeling of Heat Transfer in Vertical Ground Heat Exchangers. *HVAC&R Research , 10* (4), 459-470.

Dickinson, J. S., Buik, N., Matthews, M. C., & Snijders, A. (2009). Aquifer thermal energy storage: theoretical and operational analysis. *Géotechnique , 59* (3), 249-260.

Domenico, P., & Schwartz, F. (1998). *Physical and Chemical Hydrogeology* (2 ed.).

Doughty, C., Hellström, G., Tzang, C. F., & Claesson, J. (1982). A Dimensionless Parameter Approach to the Thermal Behaviour of an Aquifer Thermal Energy Storage System. *Water Resources Research , 18* (3), 571-587.

Eckert, E. R., & Drake, R. (1972). *Analysis of heat and mass transfer.* McGraw-Hill.

Environment Canada. (2011). *National Climate Data and Infromation Archive*. Retrieved from www.climate.weatheroffice.gc.ca

Eskilson, P. (1987). *Thermal analysis of heat extraction boreholes.* Ph.D. Thesis, University of Lund, Department of Mathematical Physics, Lund, Sweden.

Eskilson, P. (1987). *Thermal analysis of heat extraction boreholes.* University of Lund, Sweden, Department of Mathematical Physics.

Eskilson, P., & Claesson, J. (1988). Simulation Model for Thermally Interacting Heat Extraction Boreholes. *Numerical Heat Transfer , 13*, 149-165.

Ferguson, G. A., & Woodbury, A. (2005). Thermal sustainability of groundwater-source cooling in Winnipeg, Manitoba. *Canadian Geotechnical Journal , 42*, 1-12.

Ferguson, G. (2004). *Groundwater and Heat Flow in Southern Manitoba: Implications to Water Supply and Thermal Energy.* Ph.D. Thesis, University of Manitoba.

Gehlin, S. (1998). *Thermal Response Test – In-Situ Measurement of Thermal Properties in Hard Rock.* Licentiate Thesis, Luleå University of Technology, Sweden.

Gehlin, S., & Hellström, G. (2003). Comparison of Four Models for Thermal Response Test Evaluation. *ASHRAE Transactions , 109* (1), 131-142.

GEO-SLOPE International, Ltd. (2007). *Geostudio 2007, Temp/W module [Computer Software]*. Retrieved from http://www.geo-slope.com/

GEO-SLOPE International, Ltd. (2008, March). *Thermal Modeling with TEMP/W 2007, An Engineering Methodology*. Retrieved from http://www.geo-slope.com/

Hellström, G. (1991). *Ground heat storage: Thermal analysis of duct storage systems.* Ph.D. Thesis, University of Lund, Sweden, Department of Mathematical Physics.

Incropera, F. P., & DeWitt, D. P. (2002). *Fundamentals of Heat and Mass Transfer* (5 ed.). Wiley.

Ingersoll, L. R. (1954). *Heat Conduction With Engineering, Geological, and Other Applications* (Revised ed.). Madison: Unviersity of Wisconsin press.

Kasubuchi, T. (1984). Heat conduction model of saturated soil and estimation of thermal conductivity of soil solid phase. *Journal of Soil Science* , 240–247.

Kavanaugh, S. (2010, August). Ground Heat Exchangers: Determining Thermal Resistance. *ASHRAE Journal* , 72-75.

Kelvin, S. W. (1882). *Mathematical and Physical Papers* (Vol. 2).

Klien, S., & al., e. (1988-1997). *FEHT – A Finite element heat transfer program.* University of Wisconsin, Solar Energy Laboratory, Madison.

Lamarche, L., & Beauchamp, B. (2007b). A new contribution to the finite line-source model for geothermal boreholes. *Energy and Buildings , 39* (2), 188–198.

Lamarche, L., & Beauchamp, B. (2007a). New solutions for the short-time analysis of geothermal vertical boreholes. *International Journal of Heat and Mass Transfer , 50*, 1408–1419.

Lamarche, L., Kajl, S., & Beauchamp, B. (2010). A review of methods to evaluate borehole thermal resistances in geothermal boreholes. *Geothermics , 39*, 187–200.

Nam, Y., & Ooka, R. (2010). Numerical simulation of ground heat and water transfer for groundwater heat pump system based on real-scale experiment. *Energy and Buildings* (42), 69–75.

Nam, Y., Ooka, R., & Hwang, S. (2008). Development of a numerical model to predict heat exchange rates for a ground-source heat pump system. *Energy and Buildings* (40), 2133–2140.

Paul, N. D. (1996). *The effect of grout thermal conductivity on vertical geothermal heat exchanger design and performance.* M.Sc. Thesis, South Dakota State University.

Remund, C. (1999). Borehole thermal resistance: Laboratory and field studies. *ASHRAE Transactions , 105* (1), 439-445.

Render, F. W. (1983). Hydrology. In A. Baracos, D. H. Shields, & B. H. Kjartanson (Eds.), *Geological Engineering Report for Urban Development of Winnipeg* (p. 76). Winnipeg, Manitoba, Canada.

Rottmayer, S. P., Beckman, W. A., & Mitchell, J. W. (1997). Simulation of a single vertical U-tube ground heat exchanger in an infinite medium. *ASHRAE Transactions: Symposia , 103* (2), 651–659.

Shonder, J. A., & Beck, J. V. (2000). *A New Method to Determine the Thermal Properties of Soil Formations from In Situ Field Tests.* Oak Ridge National Laboratories.

Spitler, J. D. (2005). Editorial: Ground-Source Heat Pump System Research—Past, Present, and Future. *HVAC&R Research , 11* (2), 165-167.

Sutton, M. G., Couvillion, R. J., Nutter, D. W., & Davis, R. K. (2002). An algorithm for approximating the performance of vertical bore heat exchangers installed in a stratified geological regime. *ASHRAE Transactions , 108* (2), 177-184.

Wang, H., Qi, C., Du, H., & Gu, J. (2010). Improved method and case study of thermal response test for borehole heat. *Renewable Energy , 35*, 727–733.

Xu, X., & Spitler, J. D. (2006). Modeling of Vertical Ground Loop Heat Exchangers with Variable Convective Resistance and Thermal Mass of the Fluid. *Proceedings of the 10th International Conference on Thermal Energy Storage-Ecostock 2006* .

Yang, H., Cui, P., & Fang, Z. (2010). Vertical-borehole ground-coupled heat pumps: A review of models and systems. *Applied Energy , 87*, 16-27.

Yang, H., Cui, P., & Fang, Z. (2010). Vertical-borehole ground-coupled heat pumps: A review of models and systems. *Applied Energy* (87), 16-27.

Yavuzturk, C. (1999). *MODELING OF VERTICAL GROUND LOOP HEAT EXCHANGERS FOR GROUND SOURCE HEAT PUMP SYSTEMS.* Ph.D. Thesis, Oklahoma State Univeristy.

Yavuzturk, C., & Spitler, J. D. (1999). A Short Time Step Response Factor Model for Vertical Ground Loop Heat Exchangers. *ASHRAE Transactions , 105* (2), 475-485.

Yavuzturk, C., & Spitler, J. D. (2001). Field Validation of a Short Time-Step Model for Vertical Ground Loop Heat Exchangers. *ASHRAE Transactions , 107* (1), 617-625.

Zeng, H., Diao, N., & Fang, Z. (2002). A finite line-source model for boreholes in geothermal heat exchangers. *Heat Transfer Asian Research , 37* (1), 558-567.